AD NUMBER: AD0902464

LIMITATION CHANGES

TO:

Approved for public release; distribution is unlimited.

FROM:

Distribution authorized to U.S. Government agencies only; Administrative/Operational Use; 31 DEC 1960. Other requests shall be referred to Office of Supersonic Transport Development (FAA), Washington, DC 20590.

AUTHORITY

FAA ltr dtd 26 Apr 1977

Report No. FAA-SS-72-13

SST Technology
Follow-On Program—Phase I
MECHANICAL AND METALLURGICAL CHARACTERISTICS OF TITANIUM ALLOY 6A1-4V

Fred L. Parkinson
W. F. Spurr

The Boeing Company
Commercial Airplane Group
P.O. Box 3707
Seattle, Washington 98124

D6-60213
July, 1972

FINAL REPORT
Task 1

Prepared for

FEDERAL AVIATION ADMINISTRATION
Supersonic Transport Office
800 Independence Avenue, S.W.
Washington, D.C. 20590

The contents of this report reflect the views of The Boeing Company, which is responsible for the facts and the accuracy of the data presented herein. The contents do not necessarily reflect the official views or policy of the Department of Transportation. This report does not constitute a standard, specification, or regulation.

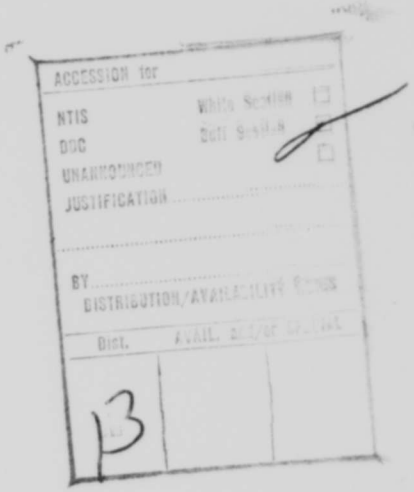

TECHNICAL REPORT STANDARD TITLE PAGE

1. Report No.	2. Government Accession No.	3. Recipient's Catalog No.
FAA-SS-72-13		

4. Title and Subtitle	5. Report Date
SST TECHNOLOGY FOLLOW-ON PROGRAM, PHASE I Mechanical and Metallurgical Characteristics of Titanium Alloy 6Al-4V	July 1972
	6. Performing Organization Code
	173p.

7. Author(s)	8. Performing Organization Report No.
F. L. Parkinson and W. F. Spurr (latter)	D6-60213

9. Performing Organization Name and Address	10. Work Unit No.
The Boeing Company Commercial Airplane Group P.O. Box 3707 Seattle, Washington 98124	
	11. Contract or Grant No. DOT-FA-SS-71-12

12. Sponsoring Agency Name and Address	13. Type of Report and Period Covered
Federal Aviation Administration Supersonic Transport Office 800 Independence Avenue, S.W. Washington, D. C. 20590	Final Report on Task 1
	14. Sponsoring Agency Code

15. Supplementary Notes

16. Abstract

Mechanical, fracture, and metallurgical tests of Ti-6Al-4V which were halted at the cancellation of the SST program were reinitiated under the DOT Technology Follow-On program. These test data, supplemented by earlier data generated by the SST program, provided a sufficient data base for quantitative analysis of the factors that control Ti-6Al-4V mechanical and fracture properties. Data for continuously rolled sheet, hand-mill sheet, plate, extrusions, bar, and forgings were analyzed by regression analyses to relate alloy composition, microstructure, and crystallographic texture to the properties of strength, fracture toughness, and stress-corrosion resistance. The major variables affecting properties were oxygen and aluminum contents, texture, and ordering of the alpha phase (formation of Ti_3Al).

17. Key Words		18. Distribution Statement
Ti-6Al-4V	Fracture toughness	"Approved for U.S. Government only. Transmittal of this document outside of U.S. Government must have prior approval of the Office of Supersonic Transport Development."
Sheet	Texture	
Plate	Stress corrosion	
Extrusions	Strength	
Bar and forgings	Crack growth rates	
Chemical composition	Beta processing	

19. Security Classif. (of this report)	20. Security Classif. (of this page)	21. No. of Pages	22. Price
Unclassified	Unclassified	165	

Form DOT F 1700.7 (8-69)

390 145

CONTENTS

CONTENTS (Continued)

FIGURES

FIGURES (Continued)

FIGURES (Concluded)

TABLES

TABLES (Concluded)

SYMBOLS AND NOMENCLATURE

CYS	0.2% offset compression yield strength
E_C	compression modulus of elasticity
E_T	tension modulus of elasticity
K_A	anisotropy factor, determined from X-ray diffraction pole figure
K_c	plane stress fracture toughness
K_{Ic}	plane strain fracture toughness
K_Q	mixed-mode fracture toughness (thick gage)
K_{scc}	threshold stress intensity level for stress corrosion in 3.5% NaCl (thin gage)
K_{Iscc}	threshold stress intensity level for stress corrosion in 3.5% NaCl (thick gage)
R	minimum to maximum stress ratio in a fatigue test
RA	percent reduction in area in a tension test
R/t	ratio of bend radius to material thickness in the formability test
TUS	ultimate tensile strength
TYS	0.2% offset tension yield strength
α	peripheral angle in pole figure
α_2	ordered phase (Ti_3Al) in titanium alloys with moderately high aluminum content
$\Delta 2a/\Delta N$	crack growth rate (crack extension per cycle) in a fatigue test
σ_g	maximum gross area stress
ϕ	radial angle in pole figure
ΔTYS	transverse minus longitudinal yield strength
MR	microstructural rating (where 0 = alpha-beta type and 10 = transformed beta type)

1.0 INTRODUCTION

Ti-6Al-4V alloy was selected in 1965 (ref. 1) as the primary structural material for construction of the SST. The selection led to numerous developmental studies to characterize the various mill forms of Ti-6Al-4V with respect to design properties and metallurgical characteristics. Wide ranges in design properties were observed and were qualitatively related to alloy composition, microstructure, and crystallographic texture. The developmental studies conducted on each mill form including sheet, plate, extrusions, and bar and forgings were summarized in four associated documents (refs. 2, 3, 4, and 5). The documents summarize the development effort prior to the SST program cancellation, March 1971.

This document describes additional tests and analyses conducted to complete the titanium technology development initiated under the SST program.

The additional test data described here for Ti-6Al-4V sheet, plate, extrusions, and bar and forgings were used to supplement the earlier data so that a more quantitative analysis could be implemented. Each alloy form is discussed individually, with the major emphasis placed on sheet and plate.

The titanium technology generated under both the SST program and the DOT technology follow-on effort will be used as a basis for the preparation of new titanium mill product specifications. These new specifications, to be developed during phase II of the DOT program, will provide titanium mill products with superior mechanical and fracture characteristics.

2.0 CHARACTERIZATION TESTING

Ti-6Al-4V continuously rolled sheet, hand-mill sheet, plate, extrusions, and bar and forgings were characterized for design properties and metallurgical characteristics. The major emphasis of detailed metallurgical evaluations was directed toward sheet and plate forms. Much of the metallurgical information is considered directly applicable to extrusions and bar and forging material.

2.1 SHEET

The basic Ti-6Al-4V sheet data generated on the SST program has been documented in a DOT report, FAA-SS-72-01 (ref. 2). The testing of Ti-6Al-4V sheet on this program continues much of the work which was in progress at the time of SST contract cancellation on both hand-mill and continuously rolled sheet. The continuously rolled sheet evaluated herein is limited to the special super ELI (extra-low interstitial) heat of Ti-6Al-4V. This material was procured especially for several high-toughness SST applications.

The hand-mill sheet testing includes further K_{scc} tests on material just received at SST contract cancellation as well as tests in technical areas that were not covered in depth in the previous report. Much testing was conducted on 3- by 12-in. blanks which were delivered to Boeing prior to the receipt of the larger sheet material for the actual SST prototype fabrication.

The testing includes K_c, K_{scc}, CYS, E_T, and crack growth rates Several test technique variables were evaluated including the effect of specimen width and salt water concentration on K_{scc}.

2.2 PLATE

The basic Ti-6Al-4V plate data generated on the SST program has been documented in a DOT report, FAA-SS-72-00 (ref. 3). The testing on Ti-6Al-4V beta-processed plate includes much of testing which was in progress at the time of the SST contract cancellation. The tests conducted herein include fracture toughness (including K_Q and valid K_{Ic}) tests, further stress-corrosion resistance (K_{Iscc}) tests on modified Ti-6Al-4V chemistry, effect of heat treatment on K_{Iscc}, and modulus of elasticity evaluation. The effect of a simulated diffusion bonding cycle on K_Q and K_{Iscc} was also determined.

2.3 EXTRUSION EVALUATION

The evaluations of Ti-6Al-4V extrusions conducted prior to SST cancellation were summarized in a DOT report, FAA-SS-72-06 (ref. 4). Many of the extrusion tests in progress at the time of cancellation were halted and were reinitiated under the DOT continued testing program described in this report. The mechanical and metallurgical data generated by these tests supplement the data previously developed and thereby provide a more statistical basis for quantitatively relating microstructure and alloy composition to properties. The characterization tests conducted included tension, compression, fracture toughness, and K_{Iscc}. The metallurgical analyses included microstructure, chemical composition, and crystallographic texture. Regression analyses were applied to the data to determine quantitatively the major factors controlling properties.

The extrusion samples evaluated were selected to provide data representative of all sizes, compositions, and processing involved in the production of SST prototype extrusions. Differences in processing were included in the analyses by the selection of samples from various extrusion producers. Five suppliers produced extrusions for the SST prototype program: Curtiss-Wright (C-W), Armco Steel Corp., Titanium Metals Corporation of America (Timet), Harvey Aluminum, Inc., and H. M. Harper Co.

2.4 BAR AND FORGING EVALUATION

Ti-6Al-4V bar and forging evaluations in support of the SST prototype program were summarized in an associated document, FAA-SS-72-04 (ref. 5). This evaluation covers many of the reinitiated tests that were halted at the time of SST cancellation plus additional tests that were initiated to provide a more representative data base. The mechanical, fracture, and metallurgical data generated by this evaluation supplement the data previously generated and thereby provide a more complete basis for quantitatively relating alloy composition, processing, microstructure, and texture to properties. Tension strength, fracture toughness, and K_{Iscc} were determined for various grain directions. Microstructures were characterized with respect to alpha-phase morphology and the crystallographic texture of the basal planes. Regression analyses were applied to the data using a computer (ref. 6) in an attempt to determine quantitatively the effects of each alloying element and texture on properties.

The samples of beta-processed bar evaluated were selected to provide data representative of typical sizes encountered in SST prototype construction. Cross-sectional areas ranged from 6 to 72 sq in. The majority of the samples evaluated were produced by Timet or Reactive Metals, Inc. (RMI).

2.5 TESTING PROCEDURES

In general standard, well-established testing procedures were used for property evaluation whenever possible. In some cases alternate or somewhat nonstandard procedures were employed because of lack of material or a need for comparison with previous tests, etc.

2.5.1 Tensile and Compression Testing

The bulk of the tensile testing was performed on a receiving inspection basis when the material was procured for SST prototype fabrication. Here, tests were performed as required per the Boeing material specification.

The detailed testing procedure followed that outlined in ASTM E8. Figures 1 and 2 show the specimen configurations used. The strain rate was consistently held within 0.003 to 0.007 in./in./min, using class B extensometers. Tensile properties obtained were ultimate tensile strength (TUS), 0.2% offset tension yield strength (TYS), % elongation in 2 in. or 4 diameters, reduction in area, and modulus of elasticity.

2.5.2 Fracture Toughness Testing

Several testing procedures were used in the evaluation of fracture toughness. The choice of specimen was generally related to the amount of material available, grain direction to be tested, and necessity of heat treatment.

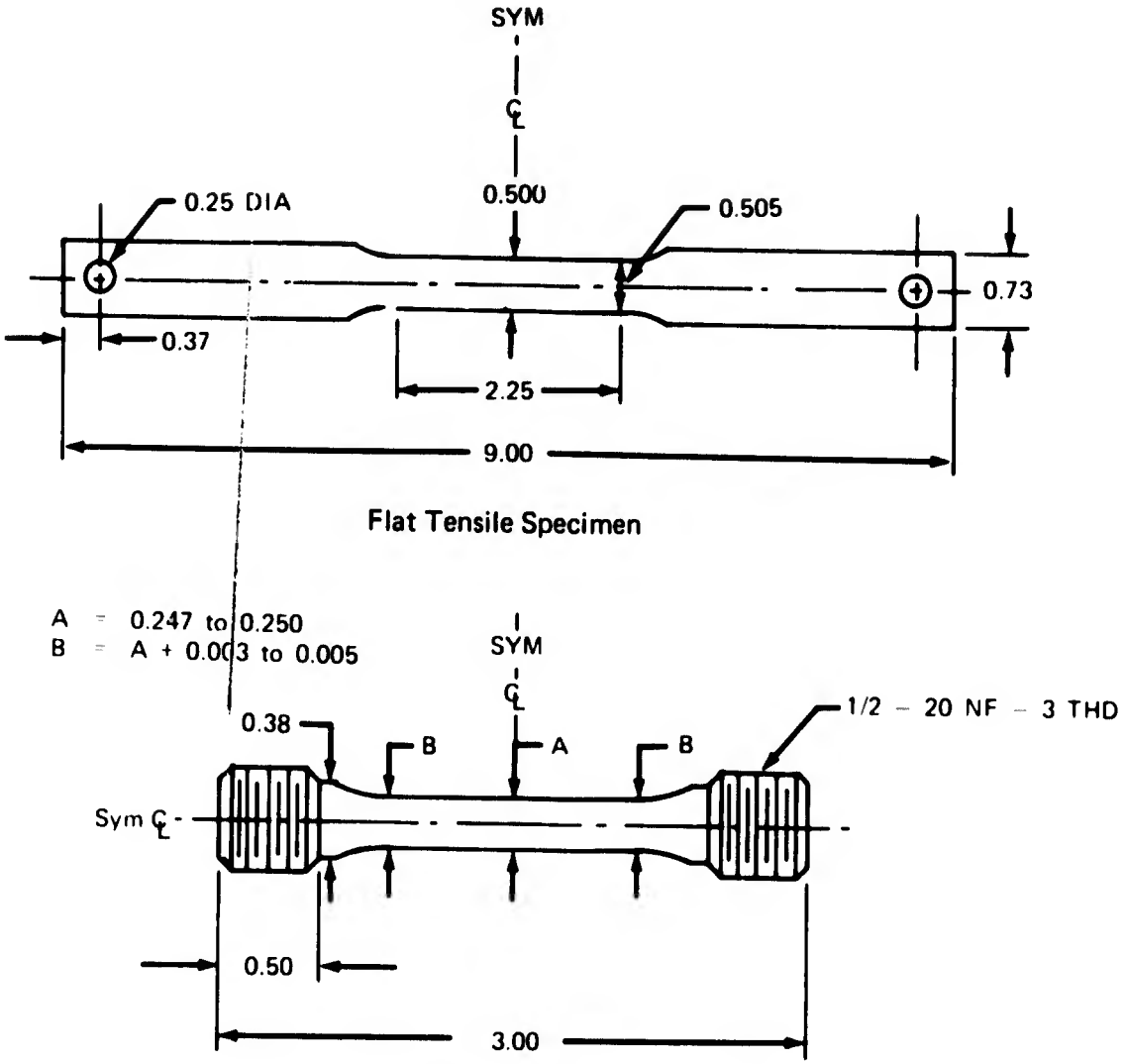

FIGURE 1.–TYPICAL TENSILE SPECIMENS

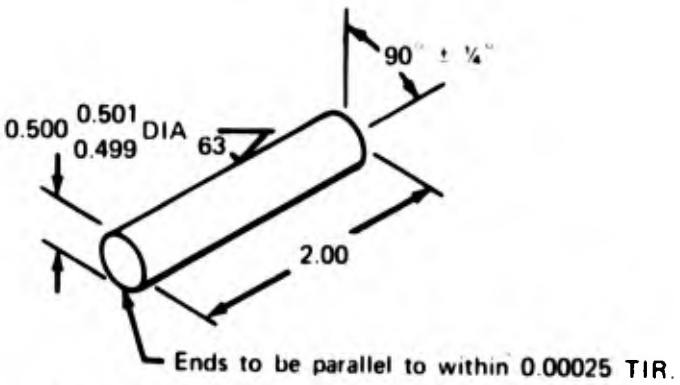

FIGURE 2.–COMPRESSION SPECIMEN CONFIGURATION

2.5.2.1 Notched Bend Specimen

It has been customary to limit the thickness of notched bend specimens to 0.480-in., since most of the Ti-6Al-4V plate data were collected at this gage in past years. This thickness was also very convenient, since 0.500-in. plate was usually used as a standard for evaluating effects of preferred orientation, heat treatment, and compositional variables. Also, 0.500-in.-thick (maximum) plate was close to covering most of the plate applications on the SST, at least in the preliminary design stages, at which point significant amounts of materials development were conducted. It is realized that 0.480-in. does not satisfy the ASTM requirements of $t \geq 2.5\ (K_{Ic}/TYS)^2$, but it was felt that it would be useful to distinguish between near-K_{Ic} conditions (i.e., 0.480 in.) and clearly mixed-mode conditions (K_c) for gages such as 0.050 and 0.125 in.

Figure 3 shows the standard four-point-loaded notched bend specimen and related formulas, and figure 4 shows the notch orientation code. A small number of valid K_{Ic} tests were conducted per ASTM E-399. These were performed by electron beam welding blocks of Ti-6Al-4V to the center test section in order to provide a 2.5-in.-thick compact tension specimen. Thinner specimens were also used. The specimen configuration is shown in figure 5 and an example of the welded 2.5-in.-thick specimen is shown in figure 6. The specimen was precracked by fatigue cycling in either a Sonntag SF-10-U fatigue machine with a cantilever bending fixture or in a Vibraphor resonant cycling fatigue machine with tensile loading. The fracture testing was conducted in tensile testing machines at room temperature in air. The gross area bending stress rate applied to the specimen was 1000 psi/sec. Load deflection curves were taken for each specimen, with the load P_5 (5% secant load) used for the calculation of the fracture toughness value K_Q or K_{Ic}.

2.5.2.2 Center-Notched Panels

Center-notched panels (CNP) were used for sheet materials (< 0.188-in. thick). Figure 7 shows a 12- by 36-in. CNP, although other panel sizes were also used. In many cases 12- by 36-in. panels were fabricated by electron beam welding 3- by 12-in. pieces to 16.5- by 12-in. panels. An example of this is shown in figure 8. The size of the panel was dictated by the amount of material available, as well as the requirement that the ratio of net area stress to yield strength be < 0.8. The total crack length (2a) was kept at one-third the panel width. For these conditions, the panel width W must obey the following:

$$W \geq 5.91\ (K_c/TYS)^2$$

The term K_c mixed-mode or plane stress fracture toughness is used here, as thicknesses were normally much less than those required for K_{Ic}. In this regard, a 12-in.-wide panel would be valid for K_c determinations up to 185 ksi$\sqrt{\text{in.}}$ for a yield strength of 130 ksi.

The center-notched panels are tension-tension fatigue cycled to grow the fatigue crack from either 0.5 in. or 2.0 in. to 4.2 in. After fatigue cycling, the panels are fracture tested in room temperature air at a stress rate of 1000 psi/sec. K_c is calculated from the following equation:

FORMULAS

K_{IE} = P_5 α stress intensity factor (critical)

$$\alpha = \frac{L}{BW^{3/2}} \left[\left(\frac{1}{1-\mu^2} \right) \left(34.7 \frac{a}{W} - 55.2 \left(\frac{a}{w} \right)^2 + 196 \left(\frac{a}{w} \right)^3 \right) \right]^{1/2}$$

$$G_{iE} = K_{IE}^2 \left(\frac{1-\mu^2}{E} \right)$$

P_5 = intersection of load-deflection curve and line drawn from origin with slope offset 5% from linear portion of load-deflection curve

E = modulus of elasticity (assumed = 16.0×10^3 ksi)

μ = Poisson's ratio (assumed = 0.33)

σ_N = net area stress $\frac{Mc}{I}$ where $M = \frac{LP_5}{2}$ and $I = \frac{B(W-a)^3}{12}$

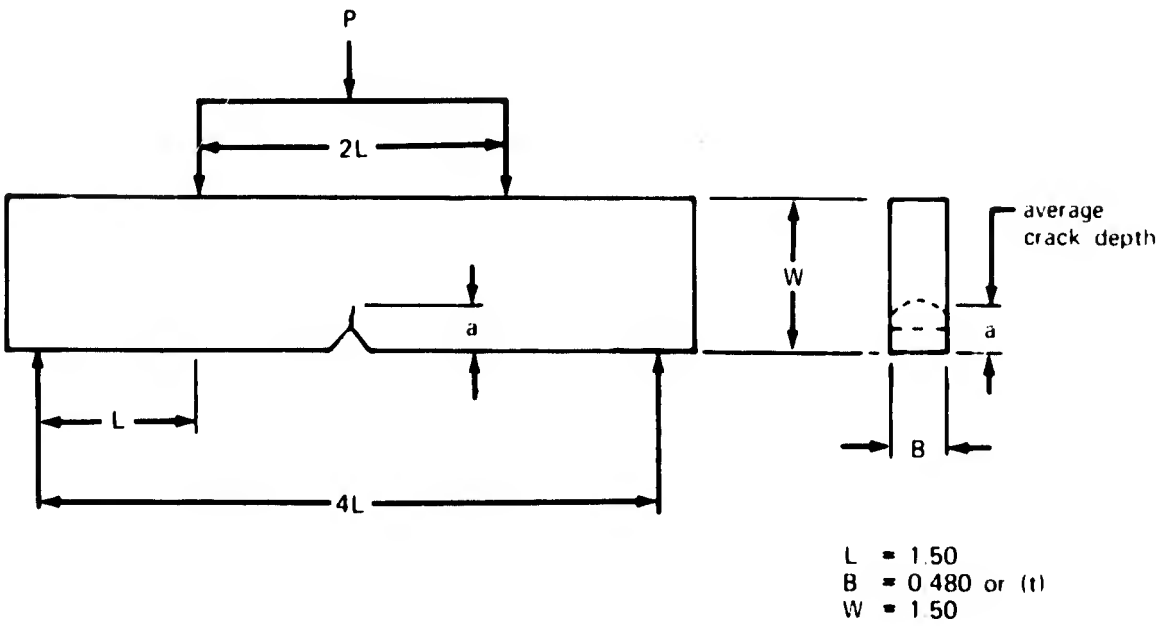

FIGURE 3.—FOUR-POINT-LOADED NOTCHED BEND SPECIMEN

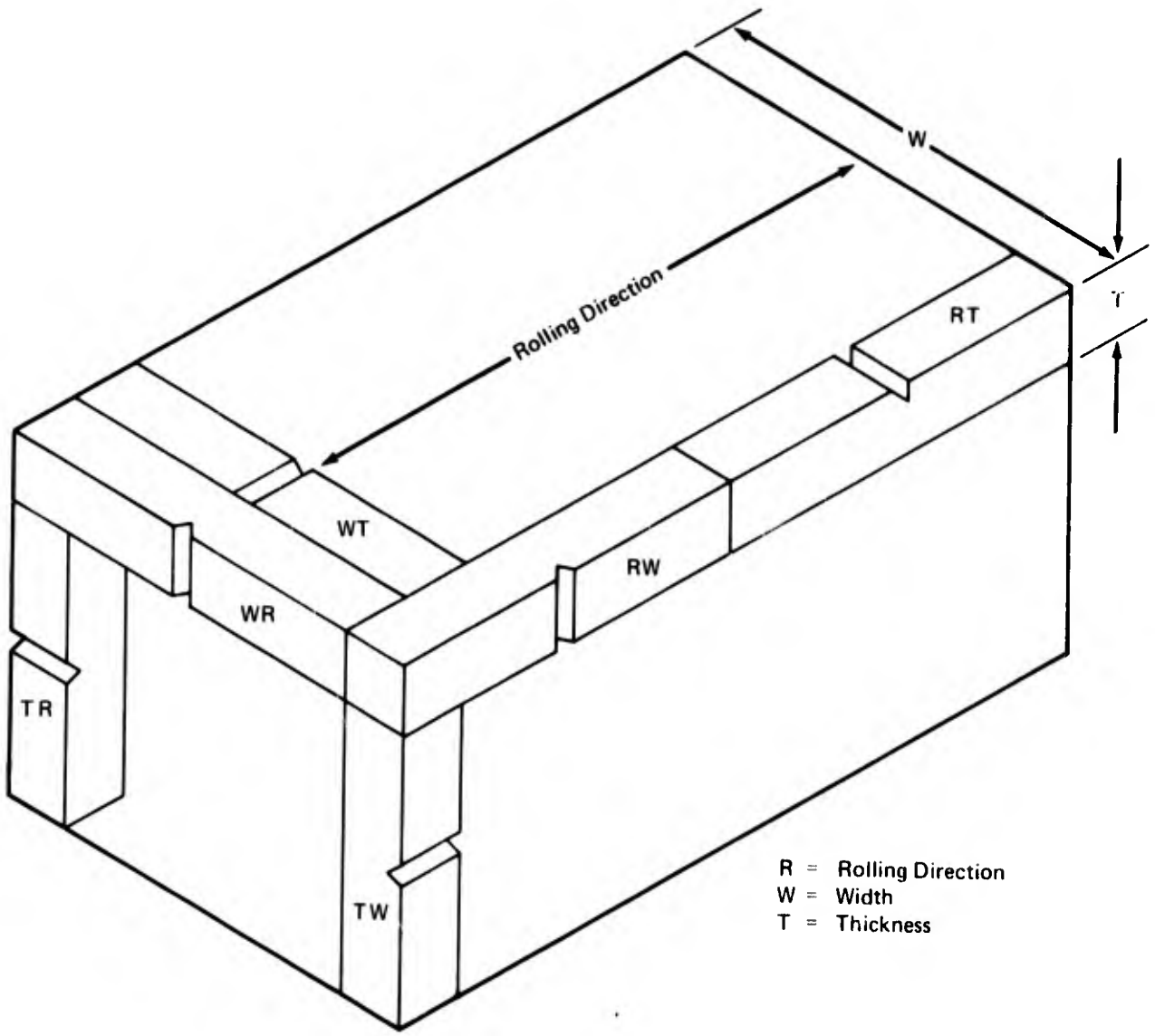

FIGURE 4.—NOTCH ORIENTATION CODE FOR NOTCHED BEND SPECIMENS

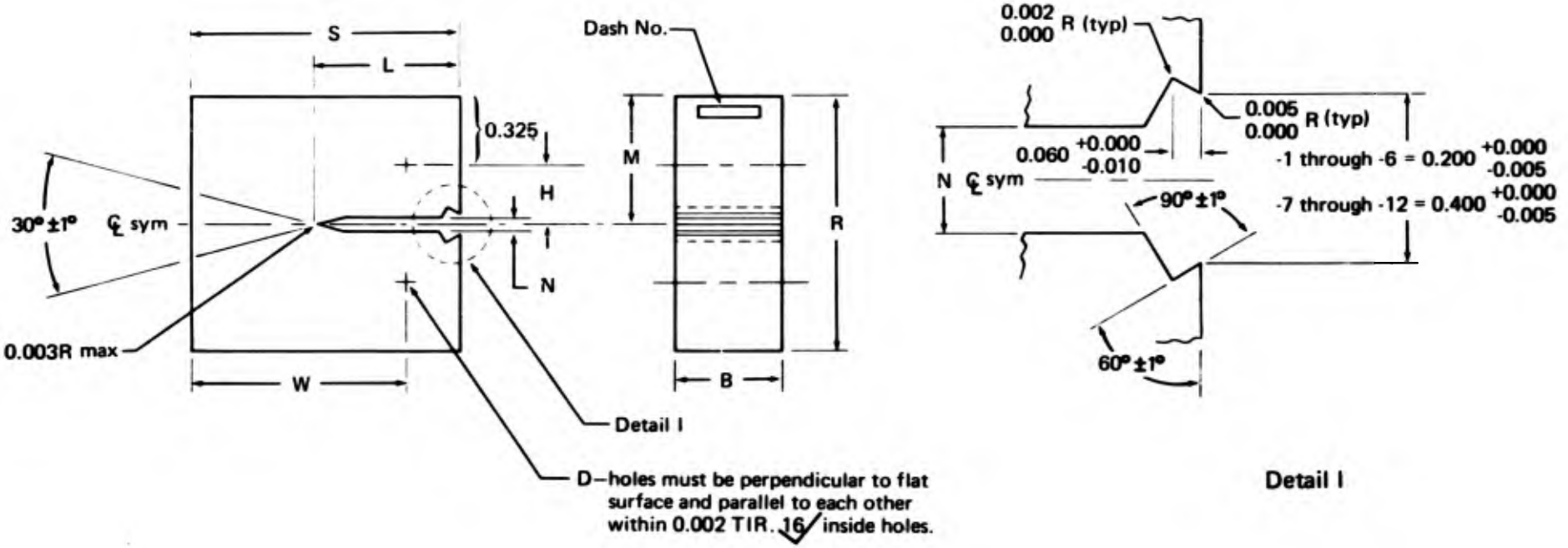

Dash No.	B ±0.010	L ±0.01	W ±0.002	D ±0.005	R ±0.010	S ±0.005	H ±0.005	N ±0.01	M ±0.005
-1	0.25	0.29	0.500	0.125	0.60	0.625	0.138	0.03	0.300
-2	0.50	0.64	1.000	0.250	1.20	1.250	0.275	0.06	0.600
-3	0.75	0.99	1.500	0.375	1.80	1.875	0.412	0.09	0.900
-4	1.00	1.32	2.000	0.500	2.40	2.500	0.550	0.12	1.200
-5	1.25	1.65	2.500	0.625	3.00	3.125	0.688	0.16	1.500
-6	1.50	1.98	3.000	0.750	3.60	3.750	0.825	0.19	1.800
-7	1.75	2.32	3.500	0.875	4.20	4.375	0.962	0.22	2.100
-8	2.00	2.65	4.000	1.000	4.80	5.000	1.100	0.25	2.400
-9	2.25	2.98	4.500	1.125	5.40	5.625	1.238	0.28	2.700
-10	2.50	3.31	5.000	1.250	6.00	6.250	1.375	0.31	3.000
-11	2.75	3.65	5.500	1.375	6.60	6.875	1.512	0.34	3.300
-12	3.00	3.98	6.000	1.500	7.20	7.500	1.650	0.38	3.600

Note: These specimens meet all of the ASTM requirements as noted in E399-70T, *Tentative Method of Test for Plane Strain Fracture Toughness of Metallic Materials*

32 all machined surfaces except as noted

Dimensions in inches

FIGURE 5.–COMPACT TENSION STRAIGHT-THROUGH-NOTCHED FRACTURE TOUGHNESS SPECIMEN

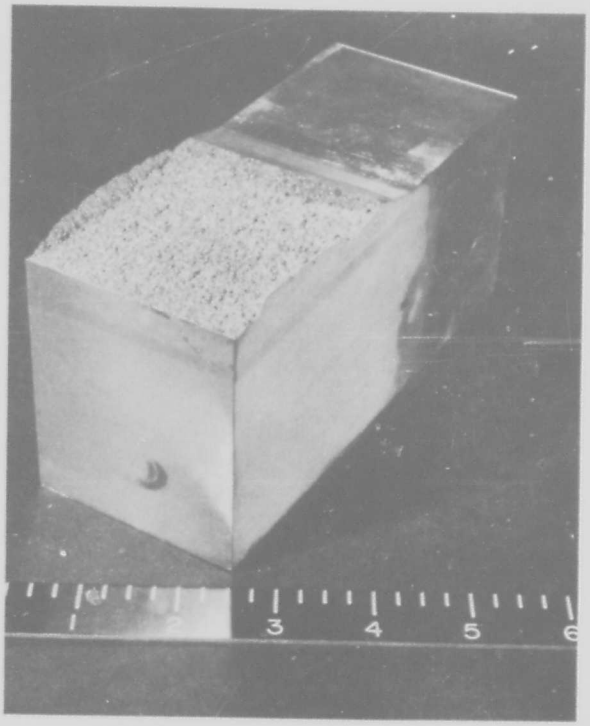

FIGURE 6.–WELDED COMPACT TENSION K_{Ic} SPECIMEN

$$K_c = \sigma_g \sqrt{\pi a} \left[\frac{W}{\pi a} \tan \frac{\pi a}{W} \right]^{1/2}$$

The last term here is the finite panel size correction factor and is 1.06 for a 12-in.-wide panel with 2a/W = 0.35. The calculation of K_c was based on maximum failure load and the initial fatigue crack length (a) prior to dynamic loading at 1000 psi/sec.

The fatigue crack growth procedures are discussed in section 2.5.4.

2.5.2.3 Single-Edge-Notched Specimen Tests

The single-edge-notched test specimen configuration is shown in figure 9. The value of K was calculated from the following equation:

$$K = \frac{Pa^{1/2}}{BW} Y$$

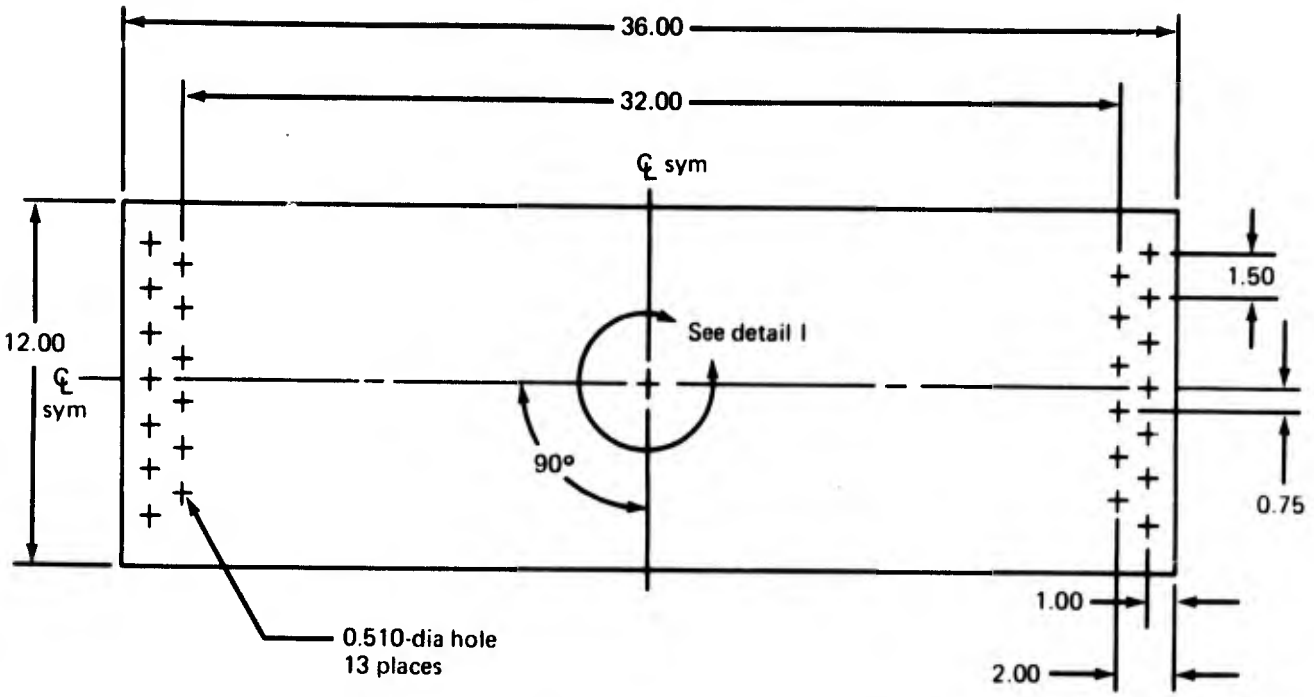

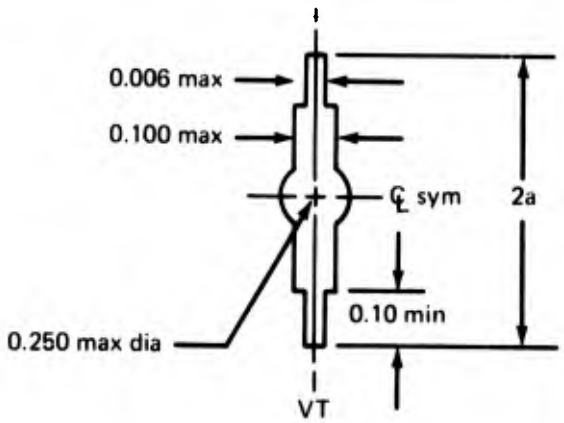

Detail I

Dimensions in inches

$$K = \sigma_g \sqrt{\pi a} \left[\frac{W}{\pi a} \tan \frac{\pi a}{W} \right]^{1/2}$$

FIGURE 7.–CENTER-NOTCHED PANEL

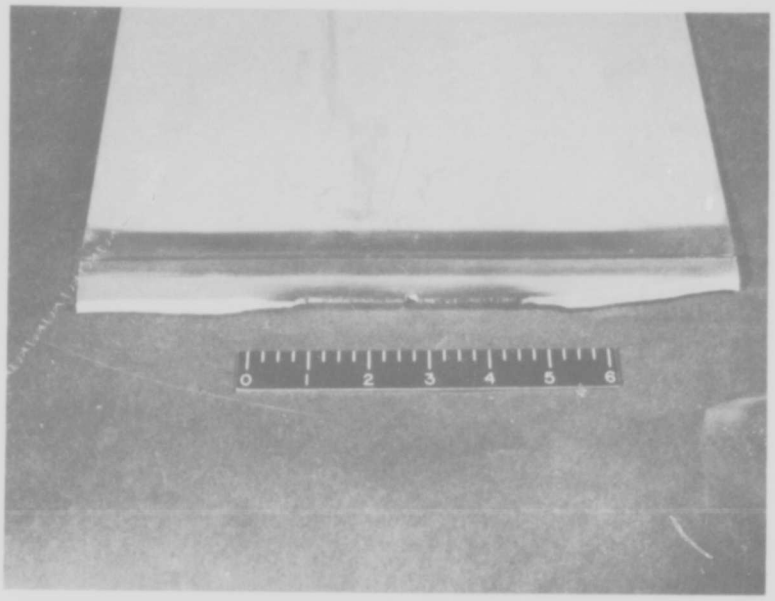

FIGURE 8.—12- BY 36-IN. CENTER-NOTCHED PANEL FABRICATED BY ELECTRON BEAM WELDING

where:

P = maximum load

a = crack length

B = specimen thickness

W = specimen width

$Y = 1.99 - 0.41\ (a/W) + 18.70\ (a/W)^2 - 38.48\ (a/W)^3 + 53.85\ (a/W)^4$

This equation is reported (ref. 2) to be accurate with 0.4% up to a/W values of 0.6. A 3.0-in.-wide specimen was generally used.

2.5.3 Stress-Corrosion Resistance

Stress-corrosion tests were conducted using the same specimens discussed in section 2.5.2 and a sustained loading technique in the environment of 3.5% NaCl aqueous solution. The stress intensity level is plotted versus time to failure and a curve is drawn to determine the threshold value at which no failure occurs. This value is defined as K_{scc} for thin sections and K_{Iscc} for thicker sections. No attempt is made to separate the two or to determine the cutoff gage for transition from K_{scc} to K_{Iscc}. The main interest is to determine the threshold stress intensity level that a material will sustain in 3.5% NaCl. Figure 10 shows a plot of sustained load K versus time and the resulting threshold value.

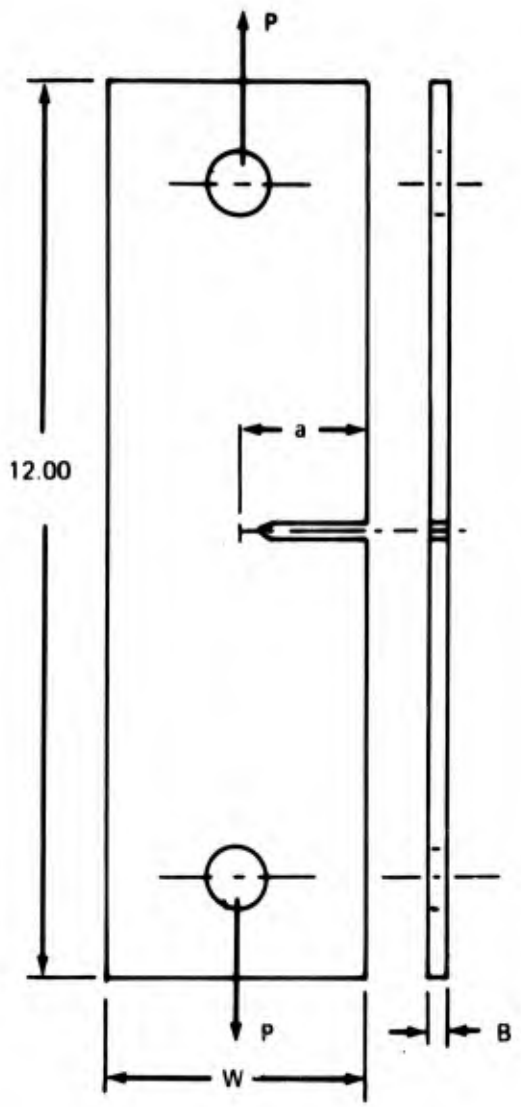

$$K = \frac{Pa^{1/2}}{BW} Y$$

Where: $Y = 1.99 - 0.41\left(\frac{a}{w}\right) + 18.70\left(\frac{a}{w}\right)^2 - 38.48\left(\frac{a}{w}\right)^3 + 53.85\left(\frac{a}{w}\right)^4$

Data from reference 2

Dimensions in inches

FIGURE 9.–SINGLE-EDGE-NOTCH SPECIMEN

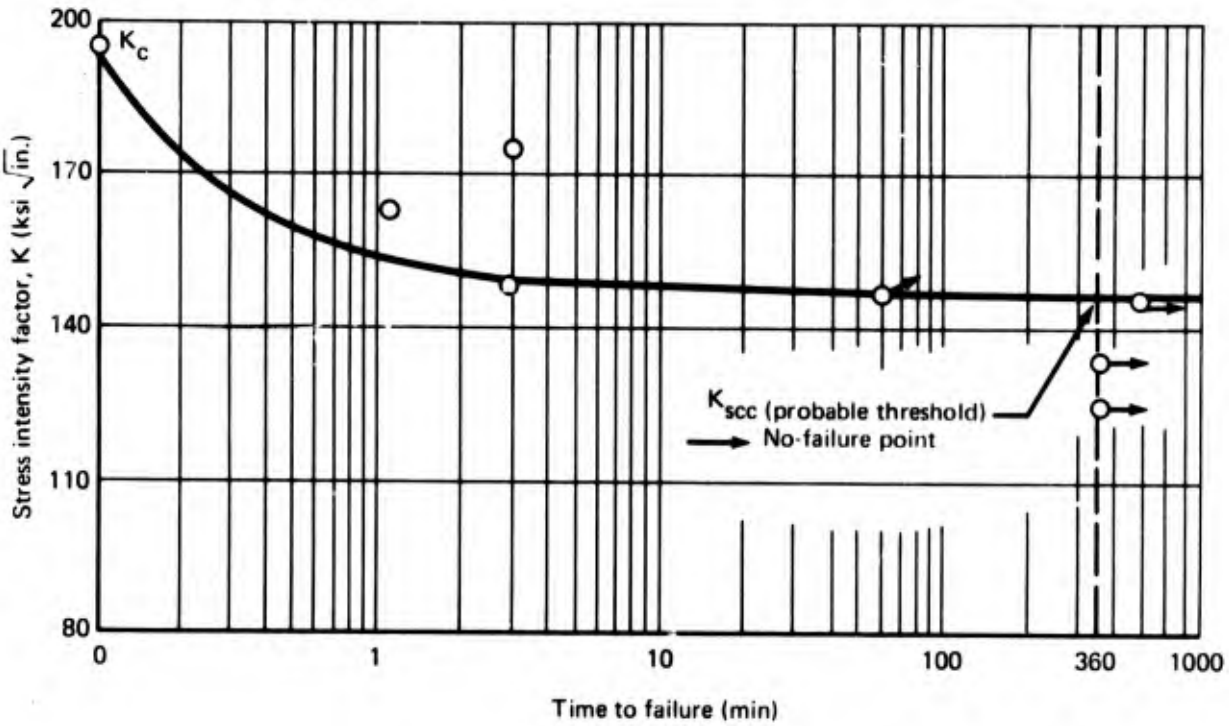

FIGURE 10.—TYPICAL SUSTAINED-LOADING CHARACTERISTICS OF TITANIUM SHEET IN SALT WATER

2.5.3.1 Single-Specimen Approach

To conserve material and lower overall testing costs, only one or two specimens were used per test. One specimen is fatigue cracked and sustained loaded for 60 minutes at a fairly low level. This level is preselected on the basis of what the anticipated threshold K will be. When the specimen does not fail, it is re-fatigue-cracked and reloaded at a higher K level. This process is repeated until failure occurs. The more accurately the threshold is known before the test, the smaller the spread will be between the highest "no-failure" K and the failure K. This results in a more accurate estimation of the actual threshold.

The maximum number of tests that can be conducted on a single specimen is related to the length the fatigue crack has grown between sustained loadings, the width of the specimen used, and the specimen validity requirements. The specimen was re-fatigue-cracked between sustained loadings to eliminate any chemical or electrochemical passivation effects at the crack tip, as well as to eliminate plastic yield zone effects on the stress-corrosion cracking mechanism. Here, the K level during fatigue cracking was kept at a lower level than the next sustained load. This prevented a large plastic yield zone from inhibiting stress-corrosion cracking. Past experience has shown that when the fatague K level is higher than the level used in the subsequent sustained load test, the "threshold" can be erroneously tested to be much higher than its actual value. To ensure no plastic zone effects, the length of the fatigue crack was usually kept at a minimum of $1/\pi\,(K_{fatigue}/TYS)^2$, which is twice the amount generally accepted as the radius of the plastic yield zone. The number of re-fatigue-cracking steps and hence the number of subsequent sustained loadings were restricted to keep the ratio of crack length to specimen width at generally 0.6 or less in the case of the single-edge-notched specimen and approximately 0.33 for the notched bend specimens. The center-notched panel ratio was generally kept to less than 0.5.

2.5.3.2 Effects of Time to Failure

For the above testing approach the standard time at which the specimens were held was 60 min. This was felt justified since 96% of the specimens that failed did so before 60 min. Figure 11 shows a plot of time to failure versus cumulative percent failure for 484 specimens.

2.5.3.3 Calculation of K_{scc} or K_{Iscc}

Most of the threshold values reported herein were determined using the highest no-failure and lowest failure loads. Using the one specimen and recracking approach there would be only one failure level. For example, if a specimen did not fail at a K of 40 but failed at a K of 50, an approach would be to simply call the threshold value 45, keeping in mind that the accuracy would be ± 5 ksi $\sqrt{\text{in}}$. A refinement of this approach was used that considered the time the specimen took to fail at the failure level. If, for example, a specimen did not fail at 40 but failed at 50 in 59 min the actual threshold would be closer to 50 than 40. By analyzing the shape of many failure curves a series of factors were developed to permit this refinement. The details of this procedure are given in appendix A.

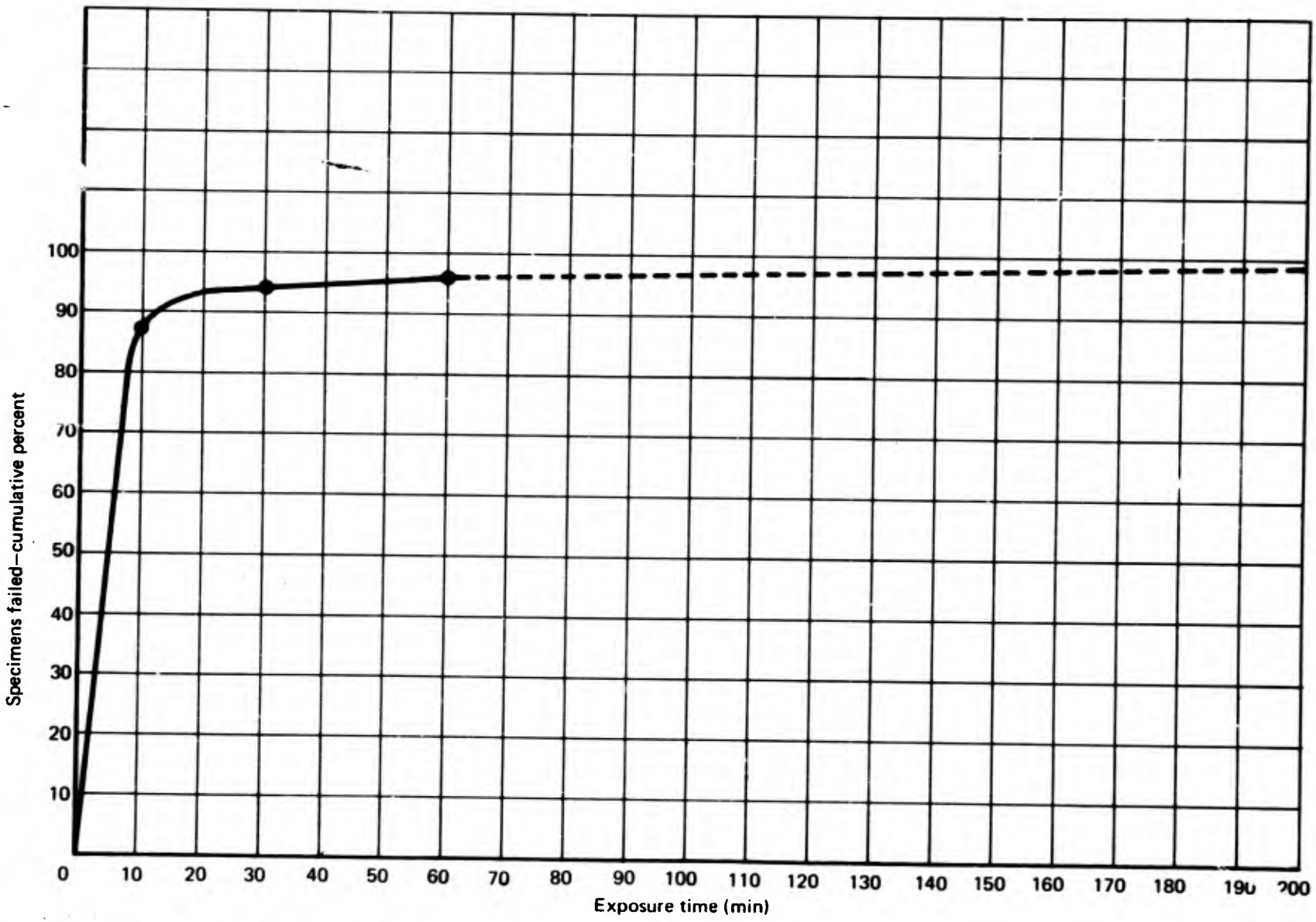

FIGURE 11.–PERCENT FAILED SPECIMENS VS TEST TIME–SUSTAINED-LOAD STRESS CORROSION

It is realized that this approach is slightly nonconservative, but it was felt that it was more desirable to obtain the best possible estimate of the actual threshold in order to study the interrelationship of such material parameters as composition, heat treatment, texture, etc., rather than a conservatively biased approach using, say, the highest no-failure K level.

2.5.4 Crack Growth Rates

Crack growth rates were determined from analysis of the growth of the fatigue crack for a measured number of cycles. Plexiglass buckling restraints were used during fatigue cracking to prevent the material in the region close to the center crack from cycling in and out of the plane of the panel. The fatigue crack growth data are gathered and plotted on a curve typically as shown in figure 12. The slope of the curve is then calculated for a number of crack lengths. Since the maximum gross area stress is known, the K level is calculated and the data replotted as maximum K level during fatigue versus crack extension per cycle (fig. 13). This rate ($\Delta 2a/\Delta N$) varies with the environment and the minimum/maximum stress ratio, R. The environments investigated were air (with the relative humidity noted), distilled water, and 3.5% aqueous salt water. The R ratios used were 0.05, 0.5, and 0.67.

2.5.5 Metallurgical Analysis

Several analytical techniques were developed in support of the SST titanium programs, with heavy emphasis on fundamental characterization of Ti-6Al-4V produced in various forms (sheet, plate, extrusions, bar, etc.) from various suppliers. Attempts were made to quantify the metallurgical variables based on relationships with actual mechanical property test data.

2.5.5.1 Optical Microscopy

Conventional light microscopy was used to assess basic metallurgical characteristics of the Ti-6Al-4V plate. Krolls 2% HF etch was used as the etchant. Photomicrographs were taken at 500X for detailed microstructure analysis and at much lower magnifications (5X-11X) to evaluate the size and shape of the prior beta grains. Optical photomicrographs were taken of the microstructure as viewed from the longitudinal, transverse, and short transverse directions.

2.5.5.2 Preferred Orientation

A quantitative computerized pole figure analysis for determining the preferred orientation in titanium alloys has been developed and modified over the past 4 years by Olsen (ref. 7), and the following provides a brief description of the procedure. X-ray diffraction data are obtained using a modified Siemens texture goniometer that is precisely aligned. Approximately 700 data points are taken as shown in figure 14. A computer program analyzes the data, subtracting for background and correcting for defocusing, and then plots a pole figure, as shown in figure 15. This pole figure gives the iso-intensity lines of poles* for a given crystallographic plane in terms of "times random intensity." This random intensity can be likened to taking all the data from a preferred titanium sample and spreading the data evenly over the entire pole figure. This results in an average or a "random" intensity. The pole figure, then, is a contour map showing the alignment of given planes.

---

*Poles are the projection points onto a sphere of the normal to the crystallographic plane as represented on two-dimensional space.

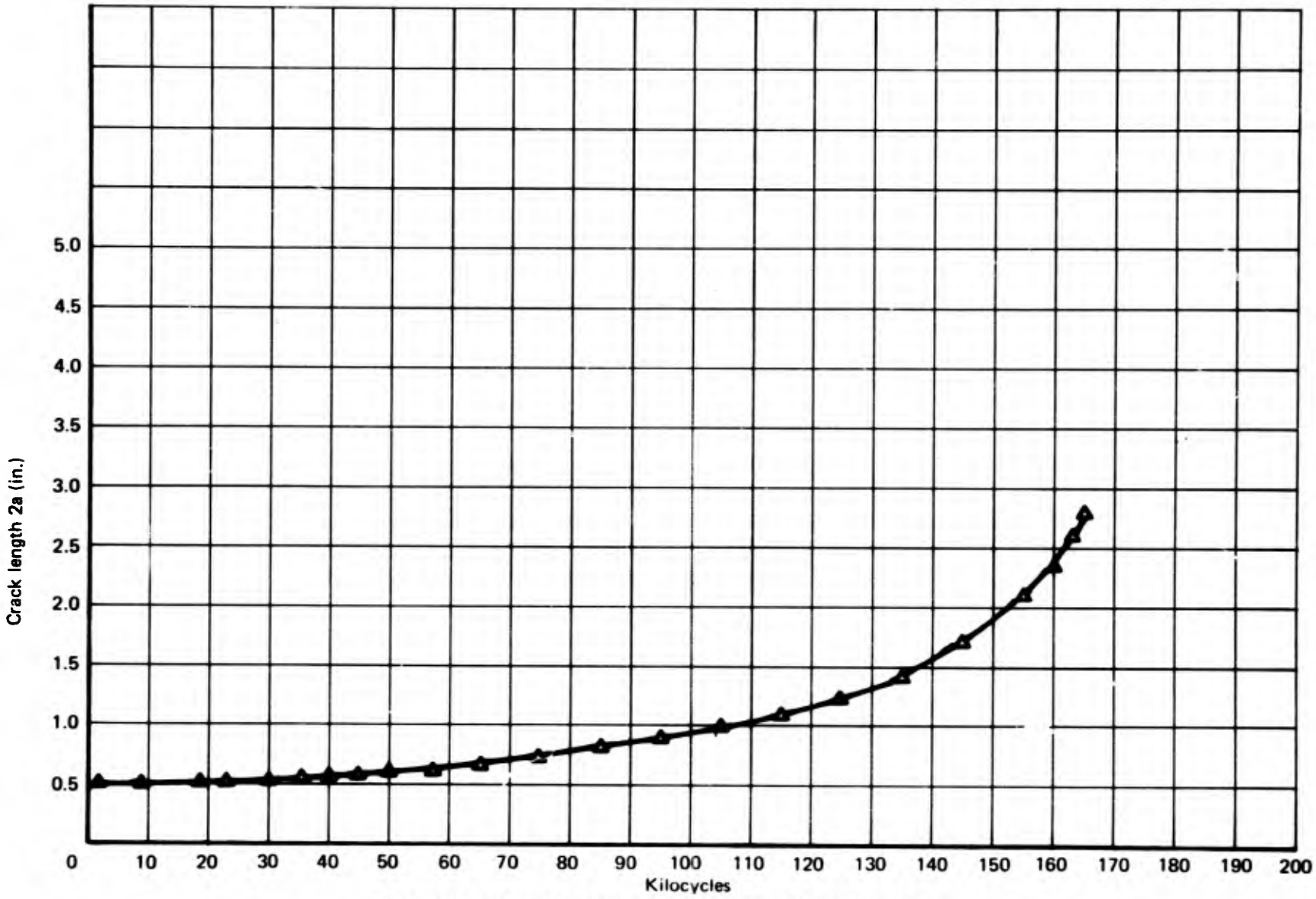

FIGURE 12.–CRACK LENGTH VS FATIGUE CYCLES

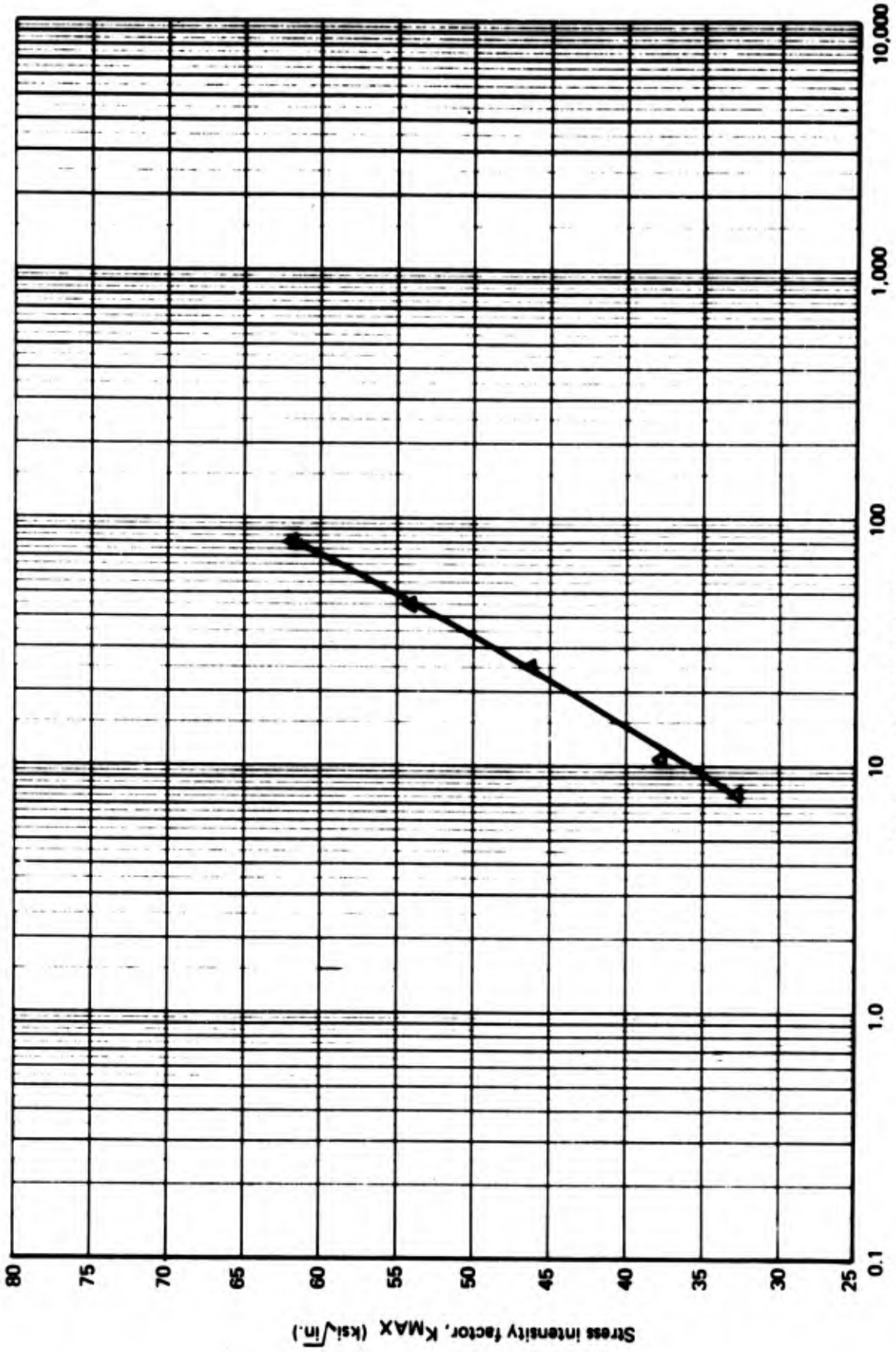

FIGURE 13.–STRESS INTENSITY VS CRACK GROWTH RATE

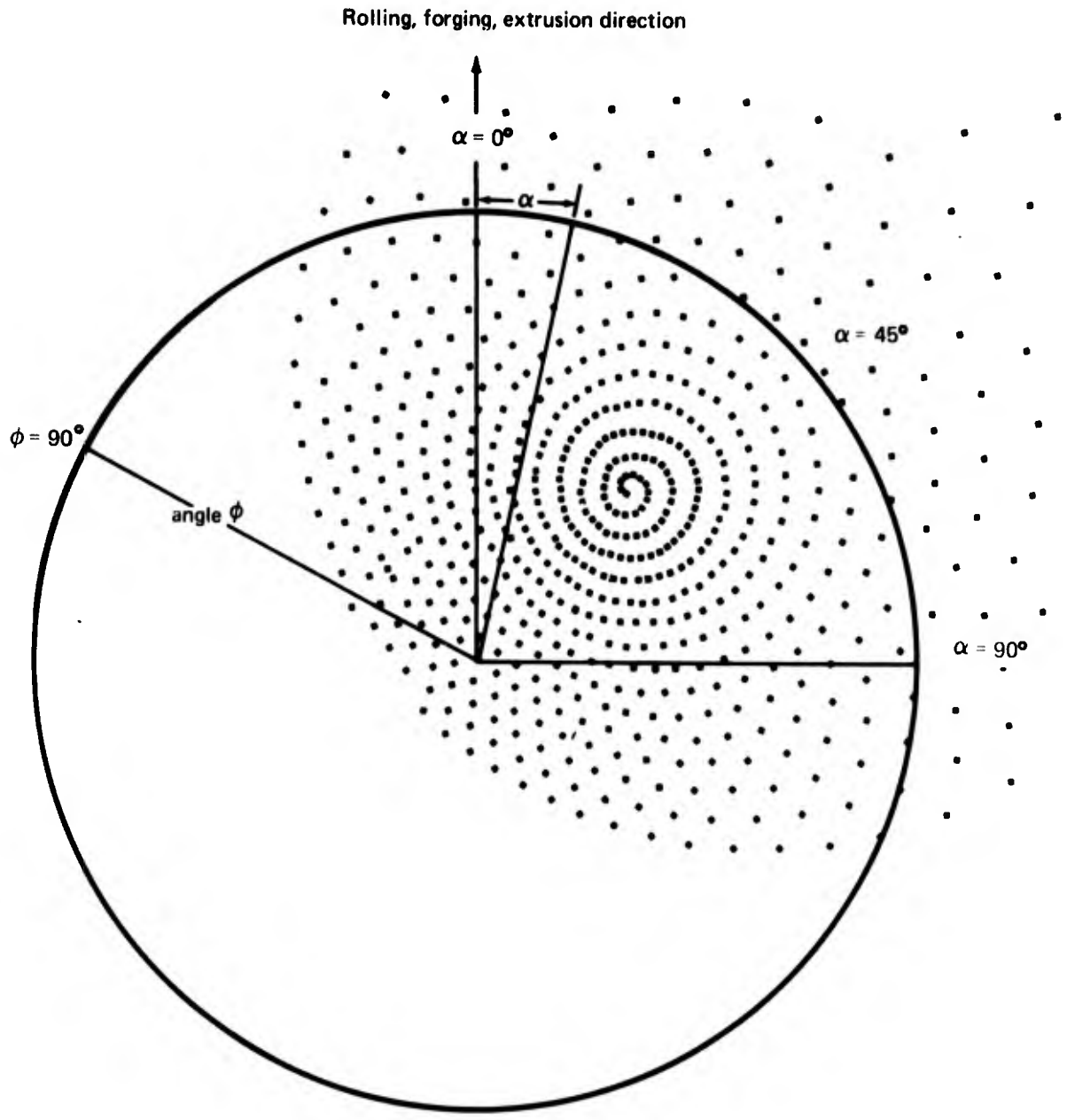

FIGURE 14.–METHOD OF COLLECTING POLE FIGURE DATA

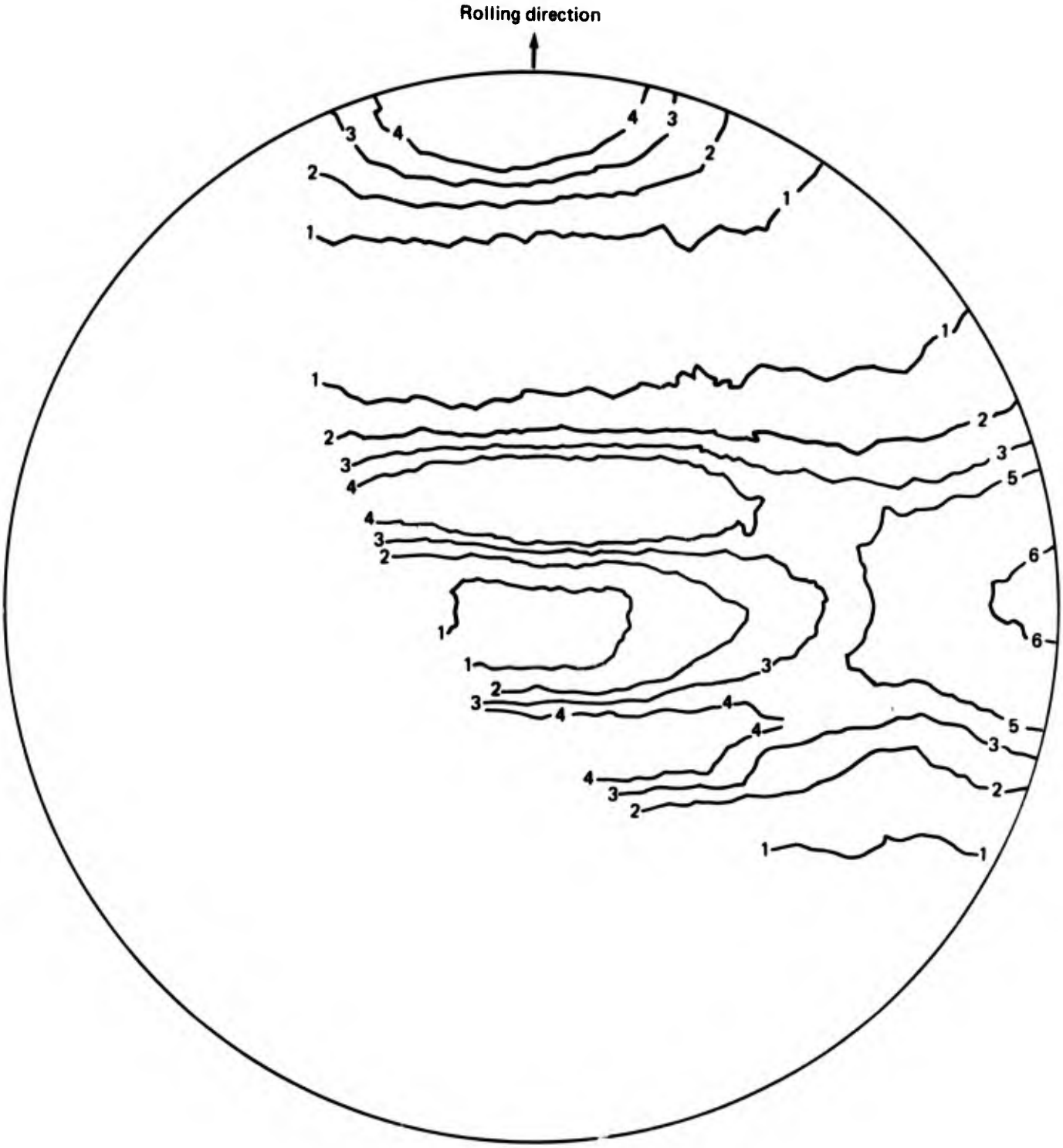

Contour lines	1	2	3	4	5	6
Times random intensity	0.5	1.0	1.5	2.0	4.0	8.0

$K_A = 46$

FIGURE 15.--POLE FIGURE SHOWING BASAL (0002)α PLANES AT TIMES RANDOM INTENSITY

The pole figure was further quantified by calculating an anisotropic factor, K_A, which is basically a measure of the number of basal planes perpendicular to the transverse direction minus the planes perpendicular to the longitudinal grain direction. It can be given by the following equation:

$$K_A = \sum_{\alpha,\phi=0}^{90^\circ} I_T \sin\phi \sin\alpha - \sum_{\alpha,\phi=0}^{90^\circ} I_L \sin\phi \cos\alpha$$

where:

I_T = intensity of basal planes perpendicular to transverse grain direction

I_L = intensity of basal planes perpendicular to longitudinal grain direction

ϕ, α = angles defined per figure 14

The data are integrated over ϕ and α from 0° to 90° by the computer and a single K_A value obtained. A high positive value of K_A would indicate a large percentage of the basal planes perpendicular to the transverse direction. A low value would indicate relatively equal amounts of basal planes in the longitudinal and transverse direction, and a high negative K_A value would indicate a high percentage of planes perpendicular to the rolling direction.

2.5.5.3 Other Techniques

Several other relatively standard metallurgical analysis techniques were used, including transmission electron microscopy, electron fractography, and macrofractography.

Transmission electron microscopy was used mainly to delineate the microconstituents of the microstructure (alpha platelets, beta-phase continuity, massive alpha), including the determination of the ordered phase $Ti_3Al(\alpha_2)$. The formation of α_2 was quantified by rating the amount present on a scale from 0 (none) to 10 (very strong α_2). This technique was developed by Boyer (ref. 8), and the α_2 parameter was assigned on the basis of the examination of six selected grains (four equiaxed and two lamellar). Ordering in the lamellar grains or platelets was weighted more heavily than ordering in the equiaxed grains. This was done on the basis that with Al being an α stabilizer the grains with the higher Al would be less susceptible to reversion to β during processing and would be equiaxed in form. Thus the transformed β (α platelets) would presumably have less Al than the equiaxed α, so the presence of ordering within the platelet was considered more significant.

Electron fractography was used to evaluate the fracture faces of the tested specimens for fatigue striation configuration, amount and type of cleavage, and general description of ductile rupture. Low-magnification fractography was used to evaluate the overall general fatigue crack growth, stress corrosion, and ductile rupture regions. Photographs of the fracture faces are shown in appendix B.

3.0 RESULTS AND DISCUSSION

3.1 Ti-6Al-4V SHEET

The results and discussion in this section are presented mainly on hand-mill sheet; section 3.1.8 presents an evaluation of the properties of a heat of super ELI (extra-low interstitial) continuously rolled sheet. The hand-mill sheet properties evaluated include K_{scc}, K_c, CYS, and E_T. In addition, the effect of furnace cooling to promote α_2 formation on K_{scc} of highly textured sheet was evaluated. The K_{scc} of solution-treated-and-aged material (STA 1000°F) was also evaluated.

The effect of salt water content and specimen width on K_{scc} is also presented, as well as a correlation between the crack growth rates measured macroscopically and using a microstriation spacing technique.

3.1.1 K_{scc} of Ti-6Al-4V Hand-Mill Sheet

The K_{scc} of annealed hand-mill Ti-6Al-4V sheet was evaluated as a function of chemical, physical, and metallurgical parameters. Both longitudinal and transverse K_{scc} were tested. The following are the variables investigated:

• Chemical composition	Al, O_2, V, Fe, H_2
• Tensile strength directionality	Transverse minus longitudinal ultimate tensile strength
• Tensile yield strength directionality	Transverse minus longitudinal tensile yield strength
• Size	Length, width, and thickness
• Ordered phase (Ti_3Al) parameter	Quantitative ordering parameter measured per section 2.5.5.3
• Texture parameter	Preferred orientation using K_A anisotropy factor
• Metallographic analysis	Percent primary alpha Average primary alpha grain size Elongation of primary alpha phase: ratio of major to minor axis length of alpha phase.

Over 125 K_{scc} tests were conducted to obtain a statistical evaluation of the effects of the above parameters. A general evaluation of the data shows the extremely significant effect of both oxygen content and preferred orientation. The data ranged from very low to very high K_{scc} values (21 to 150 ksi $\sqrt{in.}$). Because of material limitations, the test specimen used was a 3- by 12-in. single-edge-notched specimen. As a result, the upper limit of the K_{scc} attainable from this specimen is approximately 100 ksi $\sqrt{in.}$ True values of K_{scc} would have been much higher (see sec. 3.1.10).

The K_{scc} values of 21-30 ksi $\sqrt{in.}$ were obtained for both grain directions. This is contrary to earlier testing in which the transverse K_{scc} was found to be lower than the longitudinal K_{scc}. Later testing (ref. 2) showed that both grain directions of Ti-6Al-4V hand-mill sheet could have this extremely low K_{scc} value. This was confirmed by the further tests conducted on this program. The interrelationship between the oxygen and texture effects is rather complicated. Low K_{scc} can result with high oxygen and low texture or with low oxygen and high texture. At very low oxygen content (super ELI Ti-6Al-4V in sections 3.1.7 and 3.1.8) and high textures, the effects of texture are present but the material has high stress-corrosion resistance. The texture was measured using both strength directionality measurements and X-ray diffraction, which resulted in a quantitative pole figure and its associated K_A value. Both techniques are useful. The strength directionality measurement (transverse minus longitudinal strengths) suffers from the inherent inaccuracy in subtracting two numbers. Also, in 30% of the material, the strength data from the lot was used rather than actual test data from the sheet tested for K_{scc}. The K_A factor provides a more direct measurement of basal plane alignment, and the quantitative relationship between K_A and K_{scc} is presented later in this section.

The K_{scc} data are presented in table 1 and the predominant effect of oxygen is demonstrated. For oxygen contents greater than 0.130%, the K_{scc} is very low. Many of the higher oxygen materials (0.15%-0.17%) had very low K_{scc} in both the longitudinal and transverse directions. However, in the range 0.125%-0.135% oxygen content, only that grain direction having the basal planes parallel to the cracking surface had these very low K_{scc} values of 21-30 ksi $\sqrt{in.}$ For this to occur, a longitudinal test specimen would require a highly negative K_A and a transverse specimen would require a highly positive K_A. The actual lowest K_{scc} of these very low values was not determined, since most of the first sustained loads on a specimen were at a K level of 25 ksi $\sqrt{in.}$ It is probable that some of the test values reported to be 21-22 ksi $\sqrt{in.}$ are actually 15-18 ksi $\sqrt{in.}$ Many low K_{scc} results were observed at or just below the oxygen level of 0.130%. This is the conventional ELI limit for oxygen. Thus, the specification ELI Ti-6Al-4V will not guarantee the elimination of these low K_{scc} values unless texture is controlled. Even with texture control, 0.130% oxygen seems to be high for a material in which a high confidence of high K_{scc} is required.

Besides oxygen and texture, another parameter which can be observed to be important in affecting K_{scc} is the ordering parameter for α_2. The formation of α_2 (Ti_3Al) was quantified as described in section 2.5.5.3. Although the effects of oxygen and texture mask some of the results, those materials with a high α_2 parameter (5-10) generally have poor K_{scc}. The effect in many cases seems to be lower longitudinal and transverse K_{scc} for all but the most severe texture. Previous tests (ref. 2) on continuously rolled sheet have shown that the formation of α_2 reduces only the direction in which the basal plane alignment is unfavorable for

TABLE 1.—CONDITION V Ti-6Al-4V SHEET K_{SCC} DATA

Material or spec code	Data source	Vendor[a]	Heat	K_{SCC} (ksi$\sqrt{in}$)		Chemical composition					α_2	ΔTYS (ksi)		ΔTUS (ksi)		Size (in.)			Raw K_{SCC} data[b]						K_A	Metallography		
																			Long			Trans				% Prim α	Avg grain size ($\times 10^{-4}$ in.)	Elong (mag/min)[c]
				Long	Trans	Al (%)	O_2 (%)	V (%)	Fe (%)	H_2 (ppm)		Lot	Sheet	Lot	Sheet	Gage	Width	Length	NF	F	T	NF	F	T				
20017	FM 972	R	295393	78	78	6.3	0.119	4.3	0.18	55		8.2	3.0			0.095	42	92	75	100	0	75	100	0	97	76	1.96	1
20025	FM 977	R	295406		84	6.3	0.116	4.2	0.17	35		3.0		2.0		0.075	40	88				80	100	1.4	1	66	2.86	1
20032 3	FM 979	T	K6036	30	56	6.3	0.140	4.1	0.15	70	3.7		1.2		3.9	0.187	43	87	25	50	1	50	66	5	57	47	3.54	3
20043	FM 977	R	295407	68	82	5.9	0.126	4.2	0.16	66	3.5		2.1			0.090	42	139	65	90	2	80	100	0	27	78	3.18	1
20044	FM 977	R	295407	76	82	5.9	0.126	4.2	0.16	45		4.4				0.085	42	141				80	100	0	48	76	2.62	1
20052 3	FM 979	T	K5410	22	85	5.8	0.130	3.9	0.10	60			2.5		-0.4	0.075	36	96		25	11	80			121	82	4.34	1
20056 1			K6009		35	6.2	0.140	4.2	0.14	80	6.9		4.2		5.0	0.106	43	77				25	50	5				
20057 1			K6027		21	6.3	0.140	4.3	0.19	90	8.3		2.5		1.7	0.106	43	77					25	5.3				
20059 1			K5815	40	30	6.3	0.130	4.3	0.14	40	10.0		4.7		1.8	0.187	43	87	25	50	15	25	50	2	63	72	3.06	3
23061 1			K6021	53	32	6.3	0.150	4.2	0.16	100	0.8		1.2		1.1	0.106	43	125	50	65	1.5	25	49	3	38	55	4.04	1
20062 10			K6008	53	33	6.2	0.130	4.1	0.10	100	5.5		2.9		2.0	0.106	43	125	50	65	1	25	50	3	1	37	3.48	1
20063 1			K6010	21	30	6.2	0.150	4.1	0.15	80	10.0		2.0		1.7	0.187	43	105		25	7	25	50	3.5	72	65	3.64	1
20068 8		T	K6011	54	30	6.2	0.140	4.1	0.16	80	4.3		8.0		7.1	0.187	43	125	50	69	1	25	50	1	21	47	3.70	1
20091 3		R	295373	86	35	6.3	0.131	4.3	0.18	43	2.8		9.2		5.6	0.095	42	126	80	100	2.5	25	50	5	56	77	3.02	1
20092 2		R	295373	85	55	6.3	0.131	4.3	0.18	51	0		6.6		0.4	0.095	42	142				50	65	3	42	59	3.58	4
20180		R	295406	82	82	6.3	0.120	4.2	0.17			2.0		1.2		0.080	36	96	80	100	0	80	100	0	29	86	2.04	1
20182	FM 979	R	295393	67	82	6.3	0.119	4.3	0.18	56	0.8	8.0				0.095			65	80	0	80	100	0	64	74	2.44	1
20193	FM 972	R	295407	78	53	5.9	0.123	4.2	0.16	30		3.0		3.3		0.187	39	64	75	100	0	50	80	2.5		70	2.76	1
20240 1	FM 979	T	K6835	33	33	6.0	0.140	4.3	0.12	75	7.0		3.2	3.2		0.187	43	105	25	50	4	25	49	3	84			
20249 1	FM 979	T	K5880	20	83	5.9	0.130	4.1	0.14	100	10.0		8.3		6.5	0.053	36	96		25	3	65	80	1	100	34	3.76	1
20274	FM 979	R	295429		67	6.2	0.141	4.2	0.17		4.8					0.072	48	144				65	80	0	34			
20284 4	FM 979	T	K6398	20	21	6.4	0.170	4.2	0.17	55	10.0		3.5	6.4		0.106				25	4		25	5	47	56	3.86	1
20293		R	295429	67	53	6.2	0.136	4.2	0.17	37	2.1	0.5				0.125			65	70	4.2	50	65	1.5	28	58	3.22	3
20328			295429	67	67	6.2	0.136	4.2	0.17	51	2.3	1.5				0.075	42	62	65	80	0	65	80	0	9	56	4.08	1
20333			295440	85	105	6.2	0.116	4.2	0.17	38	1.3	0.6				0.066			80			100			17			
20356			295429		82	6.2	0.123	4.2	0.17	52	0	4.5				0.072	44	120				80	100	0	9	70	3.22	1
20359 1	FM 979	T	K5883	37	21	5.8	0.130	4.1	0.12	60	10.0		8.6		2.0	0.132	36	96	24.5	50	10		25	6	167	79	7.50	5
20360 2	FM 979	T	K5502	30	21	5.9	0.140	4.0	0.09	60	9.0		4.5		1.1	0.095	36	96	25	50	2.5		24.7	8	49	80	3.54	1
20370	FM 972	R	295429	78	53	6.2	0.136	4.2	0.17	39		1.4	0.6	0.1	0.9				75	100	0	50	75	0	32			
20374	FM 972	R	295414	64	105	6.4	0.112	4.2	0.18	34	3.0	6.6				0.112	30	153	60	80	1.9	100			72	61	1.92	1
20614	FM 972	R	295429		30	6.2	0.136	4.2	0.17				10.3		5.3	0.050						25	50	2	84			

[a]R = Reactive Metals, Inc. (RMI)
T = Titanium Metals Corp. of America (Timet)

[b]NF = No failure
F = Failure
T = Time to failure in minutes

[c]Average ratio, major/minor axis of the primary alpha particles

TABLE 1.—CONTINUED

Material or spec code	Data source	Vendor[a]	Heat	K_{scc} (ksi$\sqrt{in.}$)		Chemical composition					α_2	ΔTYS (ksi)		ΔTUS (ksi)		Size (in.)			Raw K_{scc} data[b]						K_A	Metallography		
																			Long			Trans				% Prim α	Avg grain size ($\times 10^{-4}$ in.)	Elong (mg/mm)[c]
				Long	Trans	Al (%)	O_2 (%)	V (%)	Fe (%)	H_2 (ppm)		Lot	Sheet	Lot	Sheet	Gage	Width	Length	NF	F	T	NF	F	T				
20620		R	295440	82	82	6.2	0.122	4.2	0.17	50		≈1.7	-0.2		-0.3	0.063	27	116	80	90	1.7	80	98	0	63	58	3.08	3
20646			295451	101	105	6.0	0.116	4.0	0.16	23		-14.3				0.112	42	162	80			100			53	68	3.40	5
20736			295440	105	81	6.2	0.125	4.2	0.17	56	0	1.5				0.063	–	–				79	100	0	18	39	3.12	1
20753			295429	83	82	6.2	0.139	4.2	0.17	23		- 3.5				0.085	–	–				80	100	0	60			
20757			295429		82	6.2	0.136	4.2	0.17	58		- 5.8				0.085	–	–				80	98	0	67	66	1.84	1
20785			295440		105	6.2	0.120	4.2	0.17	48		0.5	-7.8		-4.8	0.065	36	96				100			71	52	2.14	1
69364	FM 963	R		78	21	6.3	0.140					4.0		1.0		0.090	–	–	75	100	0		25	6	59			
69465	FM 963		295473	102	35	6.3	0.131					8.7		5.1		0.095	42	126	100	115	0	25	50	6	131	43	2.36	5
69466	FM 963		295473	80	80	6.3	0.131					3.9		-0.8		0.095	42	142	75	100	2	75	100	2	25	80	2.36	1
69615	FM 963		295372	33	83	6.3	0.150					- 1.7		0.6		0.080	36	120	25	50	3	80	105	0	25	68	2.68	3
69741			295435		82	6.4	0.127	4.3	0.20	52		- 4.9				0.063	36	120				80	100	0	92	49	2.36	4
69884	Program	R	295394	78	87	6.3	0.145	4.2	0.17	46		1.2		0.4		0.063	36	120	75	100	0	85	100	0	6	67	3.36	1
69914			295414		82	6.4	0.112	4.2	0.18	24	0	- 5.8				0.075	42	174				80	100	0	67	63	2.20	1
69915			295414		82	6.4	0.126	4.2	0.18	31	3.6	0.6				0.105	44	217				80	100	0	1	71	2.36	3
69920			295414	67	82	6.4	0.112	4.2	0.18	59	0.7	- 3.3			-0.7	0.075	44	156	65	80	0	80	100	0	35	75	2.44	1
69921			295407		105	5.9	0.128	4.2	0.16				-1.4		-0.2	0.075						100			38	42	3.58	4
69926			295414		105	6.4	0.118	4.2	0.18				1.0		2.2	0.075						100			61	66	2.20	1
69939			295435		82	6.4	0.127	4.3	0.20	38		1.0	-2.5		3.7	0.103						80	100	0	39			
69954			295407	67	69	5.9	0.141	4.2	0.16	71		8.2	2.8		0.2	0.123	14	142	75	85	0.7	66	83	1.5	45	75	2.32	5
69956	Program	R	295407	80	29	5.9	0.128	4.2	0.16	24		3.8		2.3		0.183	10	117	75	100	2	25	35	8	108			
69961			295435		67	6.4	0.12	4.3	0.20	44	1.5		2.3		0.8	0.100	36	96				65	80	0	9	57	2.82	1
69963			295406	68	83	6.3	0.12	4.2	0.17			5.5		2.5					65	80	1.3	81	100	0	57	81	1.90	1
69964			295435		68	6.4	0.125	4.3	0.20	42		≈3.0				0.125	36	96				65	81	1.5	40	57	2.16	4
69965			295435		85	6.4	0.127	4.3	0.20	72		2.7	1.7		0.4	0.093						80			25	68	2.00	1
69988			295435	82	82	6.4	0.127	4.3	0.20	49	1.0	- 1.4	6.1		-3.4	0.080	36	96	80	99	0	80	100	0	83	69	2.38	1
71076 (E)	FM 963	R	295377	79	78	6.3	0.110	4.3	0.19				8.0		8.0	0.125			76	107	0	76	103	0	49			
71081 (I)	FM 963	R	295377	78	55	6.3	0.129	4.3	0.19		0.8		5.0		1.0	0.125			76	100	0	50	75	1.5	61	49	3.52	4
71480			295429		30	6.2	0.129	4.2	0.17	41		- 0.2				0.072	48	144				25	49	2	1	70	3.96	1
71622	FM 979	R	295406		87	6.3	0.121	4.2	0.17	38		1.6				0.075	44	234				80	100	0	3	62	3.42	5
71689	FM 977		295429		20	6.2	0.145	4.2	0.17	31	10.0	7.0	8.0		1.6	0.056							24.6	2.7	167	57	4.90	4
71701			294647	105	70	6.2	0.133	4.2	0.16	42	0	5.2	6.7		1.0	0.080	36	96	100			67	80	1.5	15	81	1.88	1

[a]R = Reactive Metals, Inc. (RMI)
T = Titanium Metals Corp. of America (Timet)

[b]NF = No failure
F = Failure
T = Time to failure in minutes

[c]Average ratio, major/minor axis of the primary alpha particles

TABLE 1.—Concluded

Material or spec code	Data source	Vendor	Heat	K_{scc} (ksi$\sqrt{in.}$)		Chemical composition					α_2	ΔTYS (ksi)		ΔTUS (ksi)		Size (in.)			Raw K_{scc} data						K_A	Metallography		
																			Long			Trans				% Prim α	Avg grain size (x 10^{-4} in.)	Elong (mg/min)[c]
				Long	Trans	Al (%)	O_2 (%)	V (%)	Fe (%)	H_2 (ppm)		Lot	Sheet	Lot	Sheet	Gage	Width	Length	NF	F	T	NF	F	T				
71842	FM 977		295406		90	6.3	0.118	4.2	0.17			-9.1		-0.1		0.075						80	100	0	-12	58	2.28	1
21009	RMI 19'	R	295078	110	85	6.1	0.131	3.9	0.11	63	0.3		- 0.1		-0.1	0.150	42	228							50			
21016	RMI 20'	R	310987	85	30	6.3	0.143	4.4	0.18	105	5.7		7.0		0.4	0.150	48	240							93			
S/N A5494	FM267 A1 to A4		D8839		132	5.9	0.100	4.0	0.07	70			0.7		0.9	0.040	36	96										
S/N A5583	FM 267 C1 to C4		D7152		147	6.0	0.100	4.1	0.10	70			1.1		-0.2	0.063	36	96							73			
S/N 7583	FM 267 M5 to M8		292616		64	6.3	0.132	4.3	0.17	50			- 0.9		-0.1	0.100	36	92										
G8080	FM 934		E8080	NF126	NF151	5.8	0.080	4.1	0.04	65			9.1		3.7	0.060	36	96							18			
S/N 8091	FM 267 T1 to T4		G1768		90	6.0	0.110	4.1	0.09	65			N/A		N/A	0.040	36	96							83			
S/N 8144	FM 883 1-1, 1-2		G1793	86	95	5.9	0.100	4.1	0.09	80			0.8		-1.5	0.080	36	96	85	90	0				9			
S/N 9233	FM 883 2-1, 2-2		292832	72	53	6.3	0.119	4.4	0.10	50			10.0		3.7	0.160	36	96	70	90	0	50	65	1.1				
S/N 9356	FM 448 5-8		301762		106	6.4	0.140	4.2	0.15	50			- 1.6		-2.3	0.050	36	94										
S/N 12177	FM 883 3-1, 3-2		G8106		102	6.0	0.110	4.0	0.06	60			5.6		0.3	0.125	36	96										
L3579	ST 315	T	K6658	48	30	6.4	0.17	4.2	0.14	60			3.7		2.1	0.150	–	–	40	55	11	25	35	11				
FM267 G-1		R	292661	106	35	6.3	0.120	4.2	0.14	45			4.6		1.0	0.125	36	96				30	40	12				
FM267 H-1			301620	100	53	6.3	0.100	4.2	0.17	50			2.2		1.0	0.150	36	96				45	60	12				
L4071		T	K7237	41	86	5.8	0.17	3.9	0.09	80			3.1		-3.1	0.063	–	–	35	50	6							
L3914			K7016	19	30	5.8	0.15	4.0	0.17	90			- 2.9		-4.7	0.056	–	–	15	25	6	25	35	12				
FM267 B-1			292343	96	49	6.2	0.120	4.2	0.12	84			9.5		3.3	0.063	36	120										
L3777			K7017	–	–	5.9	0.17	4.0	0.17	70		4.4		4.3		0.071	–	–										
L4010		T	K7018	–	–	5.9	0.15	3.9	0.17	70		7.6		4.9		0.112	–	–										

[a] R = Reactive Metals, Inc
T = Titanium Metals Corp. of America (Timet)

[b] NF = No failure
F = Failure
T = Time to failure in minutes

high stress-corrosion resistance. However, specimen 20359-1 had longitudinal and transverse K_{scc} values of 37 and 21 ksi $\sqrt{in.}$, respectively, with a $K_A = +167$ and an α_2 parameter measurement of 10.0. Here even though the longitudinal direction had a very favorable alignment of basal planes, the K_{scc} was very low due to the high amount of α_2. The oxygen content was 0.130%. A similar effect was found with specimen 20063-1, although in this case the oxygen content was very high at 0.150%. The sheets tested were in the duplex-annealed condition, which requires a 1725°F/70 min/air cool plus 1250°F/4 hr annealing cycle. The cooling rate from 1250°F is optional and as a result slow cooling from this temperature can result in α_2 formation if the aluminum content is high enough. High ordering was observed on aluminum contents as low as 5.8%-5.9%, although 6.2%-6.4% was more common for a high α_2 parameter. Past work (ref. 2) has shown that aluminum contents below 6.0% do not result in low stress-corrosion resistance, even though in isolated cases slight ordering was present. Two problems are inherent in interpreting the aluminum content too literally. First, the inaccuracy of the measurement itself is not insignificant and second, the aluminum contents reported in table 1 are the supplier values, which are generally measurements conducted on the ingot. Although aluminum content tends to be fairly homogeneous, variations in the ingot of ±0.2% are not uncommon. Also, only the bulk aluminum content is measured. The aluminum content in the alpha phase will be higher than the bulk analysis due to beta-phase rejection of aluminum. Statistical determination of the accuracy of the aluminum content on each specimen was not practical. Hence, for the present it can be stated that ordering in Ti-6Al-4V hand-mill sheet can result in low K_{scc} when the aluminum is in the 5.8%-6.4% range, although this does not mean that the K_{scc} would necessarily be low if the aluminum content were in this range and other parameters such as oxygen and texture were at favorable levels.

The effects on K_{scc} of all the parameters listed in table 1 were evaluated using a regression analysis technique. Here a large number of combinations of various independent variables (O_2, Al, ΔTYS, ordering parameter, V, etc.) were utilized to develop equations for K_{scc} as a function of these independent variables. Rather than present all the equations developed for all the combinations of variables, two procedures were used in presenting the data here. (The actual coefficients for all the equations are given in appendix C.) First, parameters which did not improve the overall correlation between K_{scc} and the more significant variables were emphasized less heavily. Second, those parameters which had a high standard deviation for the coefficient compared to the value of the coefficient itself were also de-emphasized. Although an equation relating K_{scc} to several important parameters is useful in predicting the K_{scc} from these variables, it is probably more useful to understand the effects of the various independent variables themselves. For example, if it is known that oxygen has a strongly negative effect on K_{scc}—say, 1000 ksi $\sqrt{in.}$/% O_2, then the quantitative effect of a 300-ppm reduction in oxygen would be to increase K_{scc} by 30 ksi $\sqrt{in.}$

The data are presented in terms of "strong" parameters and "weak" parameters with respect to the significance of their effect on K_{scc}. A strong parameter would have a relatively large effect on K_{scc} and the standard deviation of its coefficient would be relatively small in comparison to the coefficient. In some cases, the coefficient could be large—Fe, for example, at +400 ksi $\sqrt{in.}$/% Fe. Since the Fe content generally runs from 0.11% to 0.20%, this total variation of 0.09% would account for a 36 ksi $\sqrt{in.}$ variation in K_{scc}. However, if the standard deviation of the coefficient is, say, 800 ksi $\sqrt{in.}$/% Fe one has little confidence in either the magnitude or the direction (positive or negative) of the Fe effect. This lack of confidence

stems from inaccuracy in the chemical composition data for iron and/or the fact that a very narrow range of this variable was considered. This type of result is far different from the case where the coefficient is quite small but the standard deviation of the coefficient is a low percentage of the coefficient. Here the result is to know confidently that there is little effect of this parameter on K_{scc}.

3.1.1.1 Strong Parameters

- Oxygen

  The oxygen content was the strongest consistent parameter, with the coefficient highly negative in the range of -720 to -1215 ksi $\sqrt{in.}$/% O_2. In all cases the standard deviation was higher than the coefficient, but past experience (refs. 2 and 3) has shown the oxygen content to be a very significant parameter. Also the single correlation coefficient was very high (0.65) for most equations. This single correlation coefficient is a measure of the explained variation in K_{scc} due only to oxygen and indicates that there is a high dependence of K_{scc} on oxygen. The reason for the high standard deviation on the coefficient for oxygen was the inaccuracy in the analysis technique for oxygen in titanium. Although the techniques used were the best presently available (neutron activation analysis at Boeing and vacuum fusion by the suppliers), the accuracy is still probably ±0.020% at best. Since the total range investigated was only 0.11% to 0.17%, this inaccuracy represents a significant portion of the range. However, the coefficient of approximately 800-1000 (negative) seems quite reasonable since K_{scc} reductions of 56 to 70 ksi $\sqrt{in.}$ have been observed for increases of oxygen from 0.10% to 0.17%.

  For these reasons, it was felt that oxygen must be considered a strong parameter and included in any equation for K_{scc}.

- Ordered phase formation

  The formation of the ordered phase Ti_3Al (α_2) consistently yielded a negative coefficient which had a very low standard deviation. This standard deviation was only approximately 5% of the coefficient using the quantitative ordering parameter described in section 2.5.5.3 and as a result the α_2 effect can be quite precisely determined. The average coefficient was -2.1 ksi $\sqrt{in.}$ per ordering parameter unit. Since the ordering parameter is defined as 0-10 with 0 being very good (no ordering at all) and 10 being very bad (severe ordering), the variation in K_{scc} due to ordering alone is 21 ksi $\sqrt{in.}$ This is a significant effect indeed.

- Texture

  The effect of texture was measured using two different parameters, K_A (pole figure anisotropy factor) and ΔTYS (transverse minus longitudinal yield strength). In both cases the effects of texture were to significantly lower the K_{scc} when the basal planes were aligned perpendicular to the applied stress (parallel to the crack).

For the yield strength parameter the average coefficient was 2.3 ksi $\sqrt{in.}$ per ksi ΔTYS and for K_A the average coefficient was 0.125 ksi $\sqrt{in.}$ per unit of K_A. Both K_A and ΔTYS can be either positive or negative depending upon the texture, and as such the contributions to K_{scc} can be either positive or negative depending upon grain direction tested. For the transverse direction there is a negative effect and for the longitudinal direction there is a positive effect when either ΔTYS or K_A is increased (made more positive). The magnitude of the effect on K_{scc} of these two parameters is quite significant. Since K_A can vary from -90 to +170, this total range would have an effect of 260 x 0.125 or over 32 ksi $\sqrt{in.}$ Also, for ΔTYS the range is approximately -9.0 to +9.0 ksi. This total range would result in an effect of 18 x 2.3 or over 41 ksi $\sqrt{in.}$ for K_{scc}. In those equations where both ΔTYS and K_A were included, the actual coefficient for each of these parameters was less than those equations where only one of the parameters was used. This is expected, since both parameters measure texture and are quite dependent upon each other. However, the single correlation between these parameters which measures the explained variation in ΔTYS due to the variation in K_A was only 0.60. Although fairly high, this 0.60 value indicates that the two parameters do measure slightly different texture effects.

- Gage

Although the standard deviation for the coefficient for gage was somewhat larger than the coefficient, it is worthwhile to briefly mention the effect of gage on K_{scc} in discussing "strong" parameters. The average coefficient was -150 ksi $\sqrt{in.}$ per inch of gage. Since most of the material fell in the gage range of 0.050 to 0.150 in., this 0.100-in. increase in gage would result in a 15 ksi $\sqrt{in.}$ reduction in K_{scc}. Although no effect of K_c on gage in the range 0.040-0.160 in. has been observed in the past (ref. 2) it is possible that a slight changing of fracture failure mode toward plane strain conditions is occurring and resulting in a reduction in K_{scc}.

3.1.1.2 Weak Parameters

- Aluminum

The coeffient for aluminum showed somewhat mixed results. The values obtained for the coefficient in many cases were in the range of -2.0 to +4.3 with an average value of approximately 1.0 ksi $\sqrt{in.}$/% Al. However, in many of the later equations the values of the coefficient were quite high and always negative. Here the values ranged from -8 to -60 with the standard deviation varying from 30% to 130% of the value of the coefficient. The average coefficient for Al for all the equations developed in which the coefficient was negative was approximately -24 ksi $\sqrt{in.}$/% Al. A coefficient of -24 seems more appropriate than one in the range of -2.0 to +4.3 ksi $\sqrt{in.}$/% Al, since the formation of the ordered phase (Ti_3Al) depends upon the aluminum content and since aluminum is a known solid-solution-strengthening solute element. Past work (ref. 3) with Ti-6Al-4V plate has shown a significant negative correlation of K_{Iscc} with Al content, but this has not been observed in the case of Ti-6Al-4V sheet (ref. 2). If a coefficient of approximately -24 ksi $\sqrt{in.}$/% Al is used, the reduction in K_{scc} would be approximately 12 ksi $\sqrt{in.}$ since the aluminum range was generally from 5.9% to 6.4%.

The interdependence of the ordering parameter and the aluminum content was low (single correlation coefficient 0.02), indicating that in the range of aluminum contents investigated the formation of Ti_3Al is not related to the aluminum content but is probably controlled by the cooling rate through the $(\alpha + \alpha_2)$ region. This effect on K_{scc} is somewhat inconsistent with prior results on continuously rolled sheet (ref. 2) where material with aluminum contents of 6.0% and below did not result in low K_{scc} when slow cooled through the $(\alpha + \alpha_2)$ region, whereas material with 6.2%-6.3% Al did show this reduction. However, in this study, although the range of aluminum content was from 5.9%-6.4%, most of the data are at 6.2% and 6.3% Al. For this very small variation in aluminum, then, it might be expected that the cooling rate would be much more important than the aluminum content in the formation of Ti_3Al and hence in the reduction of K_{scc}. The material used in this program was duplex annealed at 1725° F and subsequently 1250° F with no requirement on the cooling rate from 1250° F. These data indicate that Ti-6Al-4V sheet should be cooled rapidly (air cooled) from 1250° F to prevent the formation of Ti_3Al.

- Metallographic characteristics

A very small effect on K_{scc} was observed as a result of the parameter measuring the amount that the primary alpha particle was elongated. Here the maximum-to-minimum-diameter ratio is measured with values generally in the range of 1 (equiaxed) to 4 (4/1 elongation). The coefficient was -0.29 ksi$\sqrt{\text{in.}}$ per elongation parameter, with a coefficient standard deviation of 0.16. Although the coefficient standard deviation is relatively small, the total range of this parameter is such as to make an overall effect of less than 2 ksi$\sqrt{\text{in.}}$ on K_{scc}. Hence, this parameter has been assumed to have no appreciable effect on K_{scc}. The effect of the average primary alpha grain size was also determined. These are the equiaxed alpha particles which have not transformed from beta to alpha during the most recent hot rolling or annealing operation. The average primary alpha grain size varied between 1.8 and 4.9 x 10^{-4} in. diameter. The coefficient was -6.48 ksi$\sqrt{\text{in.}}/10^{-4}$ in. with a standard deviation of 0.70 ksi$\sqrt{\text{in.}}/10^{-4}$ in. This indicates that for the maximum variation of 3.1 x 10^{-4} in. in grain size the reducing effect on K_{scc} would be 3.1 x 6.48 or 20.1 ksi$\sqrt{\text{in.}}$ This is a surprisingly strong effect, indicating that the grain size should be kept to a minimum. This grain size effect could be closely related to texture since a fine grain structure that had basal planes aligned both favorably and unfavorably for stress-corrosion cracking would result only in small crack extensions before the stress on the cracking plane $(10\bar{1}7)$ would be reduced. More quantitative work is needed to more fully investigate this effect, but it certainly appears that the primary alpha grain size is important with respect to K_{scc} of Ti-6Al-4V duplex-annealed sheet. The effect of the percent of primary alpha was similar to that of the primary alpha grain size, although the magnitude was lower. The percent of primary alpha was measured using standard linear analysis techniques and was found to vary between 37% and 86%. Figure 16 shows examples of high (80%) and low (37%) amounts of primary alpha. The coefficient and standard deviation were found to be -0.123 and 0.0025 ksi$\sqrt{\text{in.}}$ per percent primary alpha, respectively. Over the total variation of 49% this would cause a reduction in K_{scc} of 49 x 0.123 or 6.0 ksi$\sqrt{\text{in.}}$ This is a significant reduction, although less than the effect of primary alpha grain size.

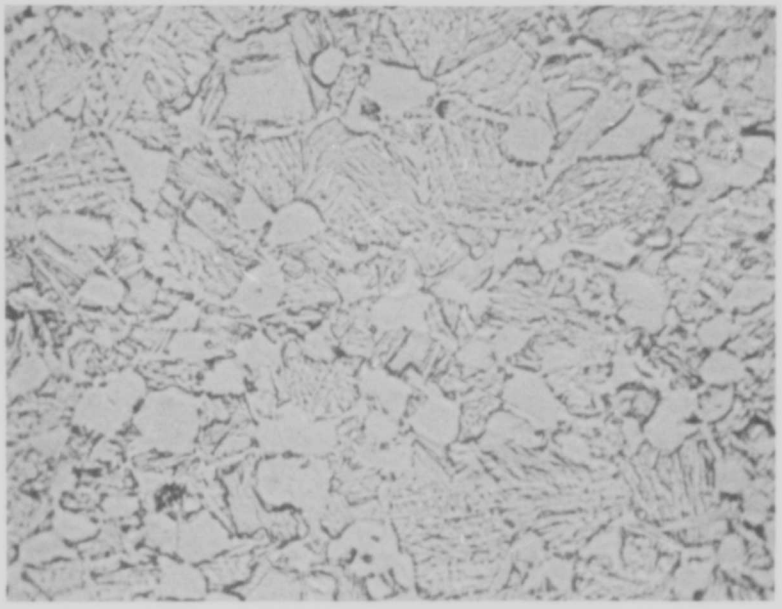

37% Primary Alpha–Specimen 20062

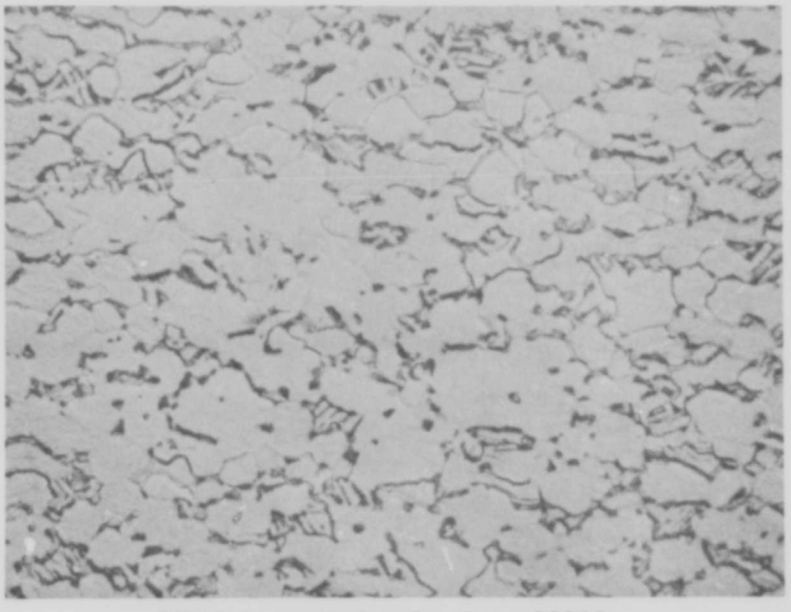

80% Primary Alpha–Specimen 20360

FIGURE 16.–MICROSTRUCTURE OF DUPLEX-ANNEALED Ti-6Al-4V SHEET SHOWING VARIATIONS IN PERCENT OF PRIMARY ALPHA (X 500)

- Other chemical effects

  In almost all cases examined the vanadium and iron coefficients had standard deviations far in excess of the coefficients themselves, and the coefficients varied between highly positive and highly negative values. This was a direct result of the small range in which these elements varied, especially for vanadium. Because of this no conclusion can be drawn on the effect of vanadium and iron on K_{scc}. The effect of hydrogen was to show a reduction in K_{scc} of -0.224 ksi$\sqrt{in.}$ per ppm H_2. The H_2 contents ranged from 24 to 100 ppm, which would result in a reduction of 76 x 0.224 or 17 ksi$\sqrt{in.}$ This seems a high reduction in light of past work (ref. 9) in which no reduction in K_{Iscc} was detected on beta-annealed low-oxygen Ti-6Al-4V plate when the H_2 contents were varied between 80 and 750 ppm. However, in this work on sheet the effect appears to be real since the standard deviation on the coefficient of 0.224 is only 0.00095 ksi$\sqrt{in.}$ per ppm H_2.

3.1.1.3 Regression Analysis Equations

In summary, the following two equations are presented for the longitudinal and transverse K_{scc} for Ti-6Al-4V hand-mill sheet:

- Transverse

$$K_{scc} = 321.9 - 22.8\,(Al) - 713\,(O_2) - 2.95\,(\alpha_2) - 2.73\,(\Delta TYS) - 0.224\,(H_2)$$

- Longitudinal

$$K_{scc} = 138.6 - 1.10\,(Al) - 363\,(O_2) - 5.64\,(\alpha_2) + 1.48\,(\Delta TYS)$$

where

Al = aluminum content in weight %

O_2 = oxygen content in weight %

H_2 = hydrogen content in parts per million

α_2 = ordering parameter

ΔTYS = transverse minus longitudinal yield strength (ksi)

3.1.2 Fracture Toughness, K_c, of Duplex-Annealed Sheet

The fracture toughness, K_c, of duplex-annealed Ti-6Al-4V sheet was determined on 16 lots of material in the thickness range of 0.056 to 0.150 in. Center-cracked panels 12 in. wide were fabricated from smaller 3- by 12-in. specimens by electron beam welding 12- by 16-in. extensions or handles to either side of the specimen. The interruption of the stress field at a distance of 1.5 in. on either side of the crack was considered negligible since the weld was continuous, defect free, and in general only 0.010-0.015 in. thicker than the material tested (see fig. 8). The results of the fracture testing are shown in table 2. Both the longitudinal and transverse grain directions were tested. Table 2 also includes the following:

TABLE 2.–FRACTURE TOUGHNESS, K_c, OF Ti-6Al-4V DUPLEX-ANNEALED SHEET (12- by 36-in. CENTER-CRACKED PANELS)

Specimen	Heat	Gage (in.)	ΔTUS (ksi)	ΔTYS (ksi)	Chemical composition					K_A	Metallography		α_2	K_c (ksi $\sqrt{in.}$)	
					Al (%)	O_2 (%)	V (%)	Fe (%)	H_2 (ppm)		% primary alpha	Avg α grain size (x 10^{-4} in.)		Long	Trans
20061 1	K6021	0 106	1 1	1.2	6.3	0.150	4.2	0.16	100	38	55	4.04	0 8		[a]71 5
20062 10	K6008	0.106	2 0	2 9	6.2	0.130	4.1	0.10	100	1	37	3 48	5 5		[a]107 9
20092 2	295373	0.095	0.4	6.6	6.3	0 131	4 3	0.18	51	42	59	3.58	0		175 4
20274	295429	0.072			6.2	0.141	4.2	0.17		34			4 8	148 9	
20293	295429	0.125		[b]0.5	6.2	0.136	4.2	0.17	37	28	58	3 22	2 1		137 1
20356	295429	0.072		[b]4.5	6.2	0.123	4.2	0.17	52	9	70	3 22	0		174 0
20374	295414	0 112		[b]6.6	6.4	0.112	4.2	0.18	34	72	61	1 92	3.0		166 9
20614	295429	0.050	5.3	10.3	6.2	0.136	4.2	0.17		84				155 2	
20753	295429	0.085		[b]3.5	6.2	0.139	4.2	0.17	23	60				175 3	
69914	295414	0.075		[b]5.8	6.4	0.112	4.2	0.18	24	67	63	2 20	0	170 2	182 0
69915	295414	0.105		[b]0.6	6.4	0 126	4.2	0.18	31	1	71	2 36	3 6	163 7	172 8
69961	295435	0.100	0.8	2.3	6.4	0.12	4.3	0 20	44	9	57	2 82	1 5	148 2	172 6
71689	295429	0.056	1.6	8.0	6.2	0.145	4.2	0 17	31	167	57	4 90	10 0	158 9	
L3579	K6658	0 150	2.1	3.7	6.4	0.17	4.2	0 14	60					167 2	
L3777	K7017	0.071	4.3	4.4	5.9	0.17	4.0	0 17	70					141 6	
L4010	K7018	0.112	4.9	7.6	5.9	0 15	3.9	0 17	70					144 0	

[a]Test panels were only 8 by 24 in.

[b]Average lot data

ΔTUS – difference between the transverse and longitudinal tensile strength

ΔTYS – difference between the transverse and longitudinal yield strength

Chemical composition (weight %) – Al, O_2, V, Fe, H_2 (ppm)

K_A – anisotropy factor per section 2.5.5.2

Metallography – percent primary alpha phase and average primary alpha grain size

α_2 formation – qualitative ordering parameter for Ti_3Al

With the exception of the two 8-in.-wide panels the K_c ranged from 137.1 to 182.0 ksi$\sqrt{in.}$. The average longitudinal K_c was 157.3 and the average transverse K_c was 168.7 ksi$\sqrt{in.}$. The tests were conducted to evaluate the effects on K_c of high and low amounts of both positive and negative directionality, variations in chemical composition, morphology changes, and the quantitative amount of α_2 formation. The effect of oxygen on the longitudinal K_c is shown in figure 17. There appears to be only a very slight trend of decreasing K_c with increasing O_2 content, although a 167 ksi$\sqrt{in.}$ value is obtained for a very high O_2 content of 0.17%. There is no apparent effect of the formation of the ordered phase, Ti_3Al, on K_c since the quantitative ordering parameter varies from 0 to 10 with little effect on K_c. This ordering parameter range is the maximum assigned as described in section 2.5.5.3. The effect of texture was evaluated by purposely testing the duplex-annealed Ti-6Al-4V sheet in a direction parallel to and perpendicular to the basal plane in heavily textured samples. Although K_{scc} is markedly affected by preferred orientation as described elsewhere (ref. 2) and in section 3.1.1, K_c is not affected in this manner. High toughness is

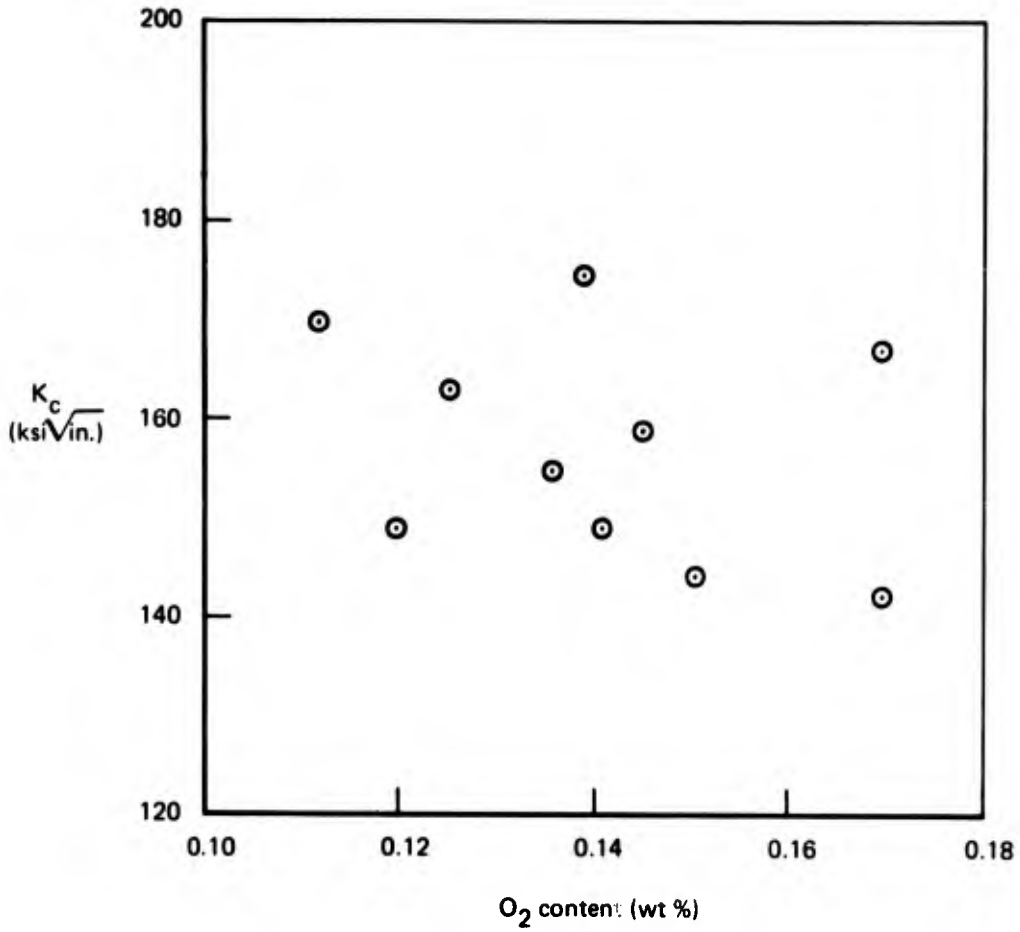

FIGURE 17.–EFFECT OF OXYGEN CONTENT ON THE K_c OF DUPLEX-ANNEALED Ti-6Al-4V SHEET– LONGITUDINAL DIRECTION

obtained in a direction perpendicular to the basal plane for both the longitudinal and transverse directions. If the fracture toughness is expected to be low perpendicular to the basal planes (as in K_{scc}) a sheet sample with a high positive K_A should show low K_c in the transverse direction and a sheet sample with a high negative K_A should show low K_c in the longitudinal direction. This, however, was not the case since high toughness (>150 ksi $\sqrt{in.}$) was obtained for both these cases. There was also little effect of either the percent of primary alpha phase or the average primary alpha grain size. It is conceivable that these parameters might show a statistical trend if more samples were evaluated, but no trends were observed for the 10 specimens evaluated.

Fatigue crack growth rates in 3.5% NaCl were obtained from two of the sheets used for determination of K_c. Both longitudinal and transverse directions were tested on two sheets, 20614 and 69914, with very high positive and very high negative texture (K_A values), respectively. The results of these tests are shown in figures 18 and 19. The texture of sheet 20614 is shown in figure 20. The high propensity of basal planes aligned perpendicular to the transverse direction results in higher crack growth rates in that direction compared to the longitudinal. This holds for both R = 0.05 and 0.67. The oxygen content is 0.136% for this material. A pole figure is also given for sheet 69914 in figure 21 showing the negative texture ($K_A = -67$). The crack growth rates shown in figure 19 for this material show little basic difference (if anything, a slightly higher rate) in the transverse direction. This would be contrary to what might be expected. However, the oxygen content is 0.112% for this material. Prior data (ref. 2) and the data presented in sections 3.1.7 and 3.1.8 have shown that when the oxygen content is low the effect of texture on crack growth rates in salt water is minimized. This is the case with these hand-mill sheets tested. Although the actual oxygen content for this minimizing effect would vary with texture, above 0.13% the texture effect is pronounced and at or about 0.11% the texture effect is minimized with respect to crack growth rates in 3.5% NaCl solution.

3.1.3 Compression Yield Strength of Ti-6Al-4V Hand-Mill Sheet

Since considerable directionality in CYS has been observed in textured continuously rolled sheet, longitudinal and transverse compression tests were conducted on 14 selected hand-mill sheets. These materials have widely varying textures due to variations in the hot rolling procedures. Some sheets had a large proportion of basal planes perpendicular to the transverse direction (high positive K_A) and others had the opposite texture (high negative K_A). Tests were also conducted on sheets with nominally balanced textures ($K_A \pm 20$). Figure 22 shows an example of a high positive K_A type texture and figure 23 shows an example of a high negative K_A type texture. The results of the compression testing are given in table 3 with some accompanying tensile data. Figure 24 shows the relationship between K_A and ΔCYS (the difference between the transverse and longitudinal compression yield strengths). This large increase in CYS in a direction perpendicular to the basal plane previously observed only in continuously rolled sheet is now appearing in hand-mill sheet. This is consistent with other texture-sensitive properties such as stress corrosion, tension yield strength, and modulus. With the most highly textured hand-mill sheet, texture has greater effect on CYS than on TYS.

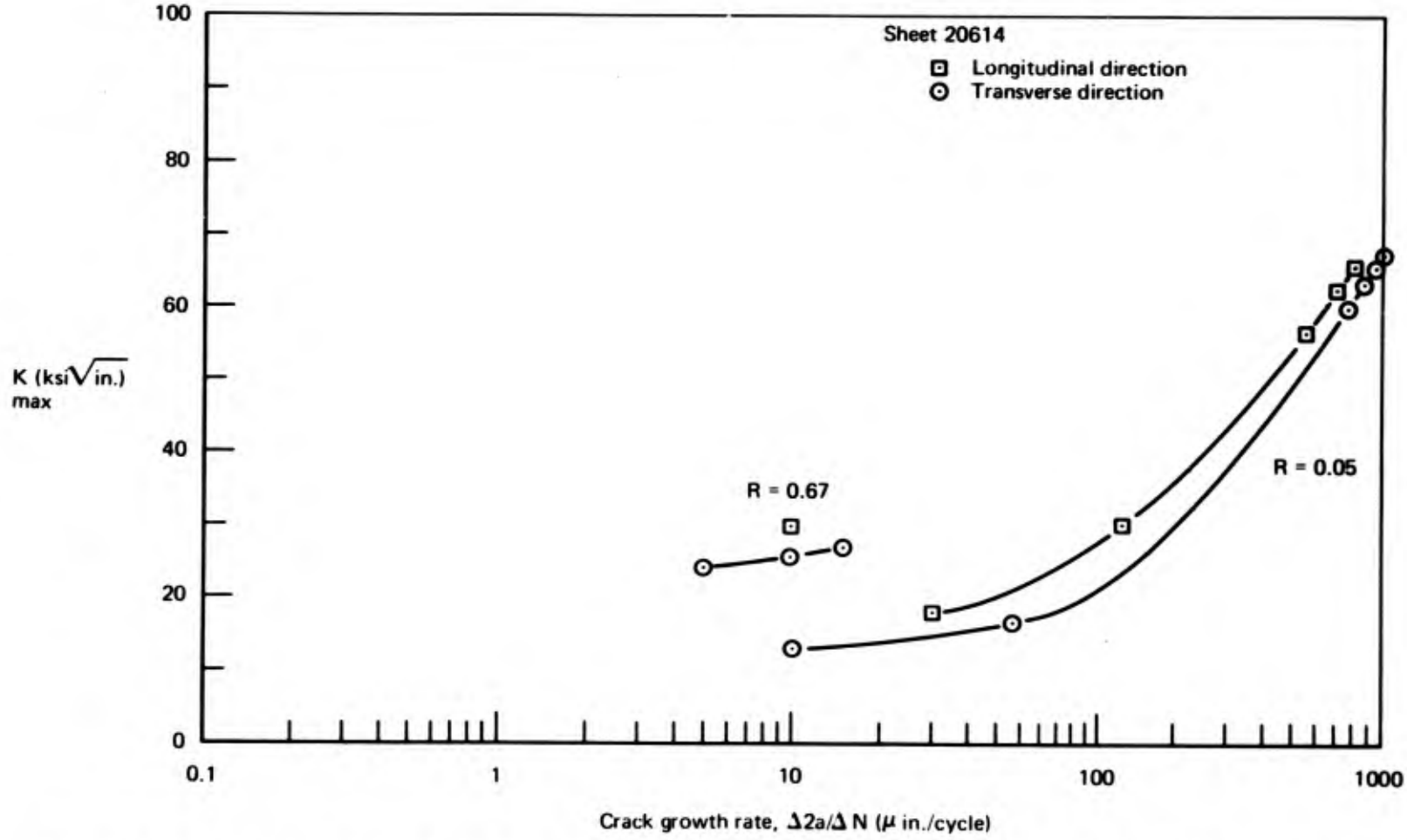

FIGURE 18.–FATIGUE CRACK GROWTH RATE FOR HIGH-POSITIVE-TEXTURED Ti-6Al-4V HAND-MILL SHEET

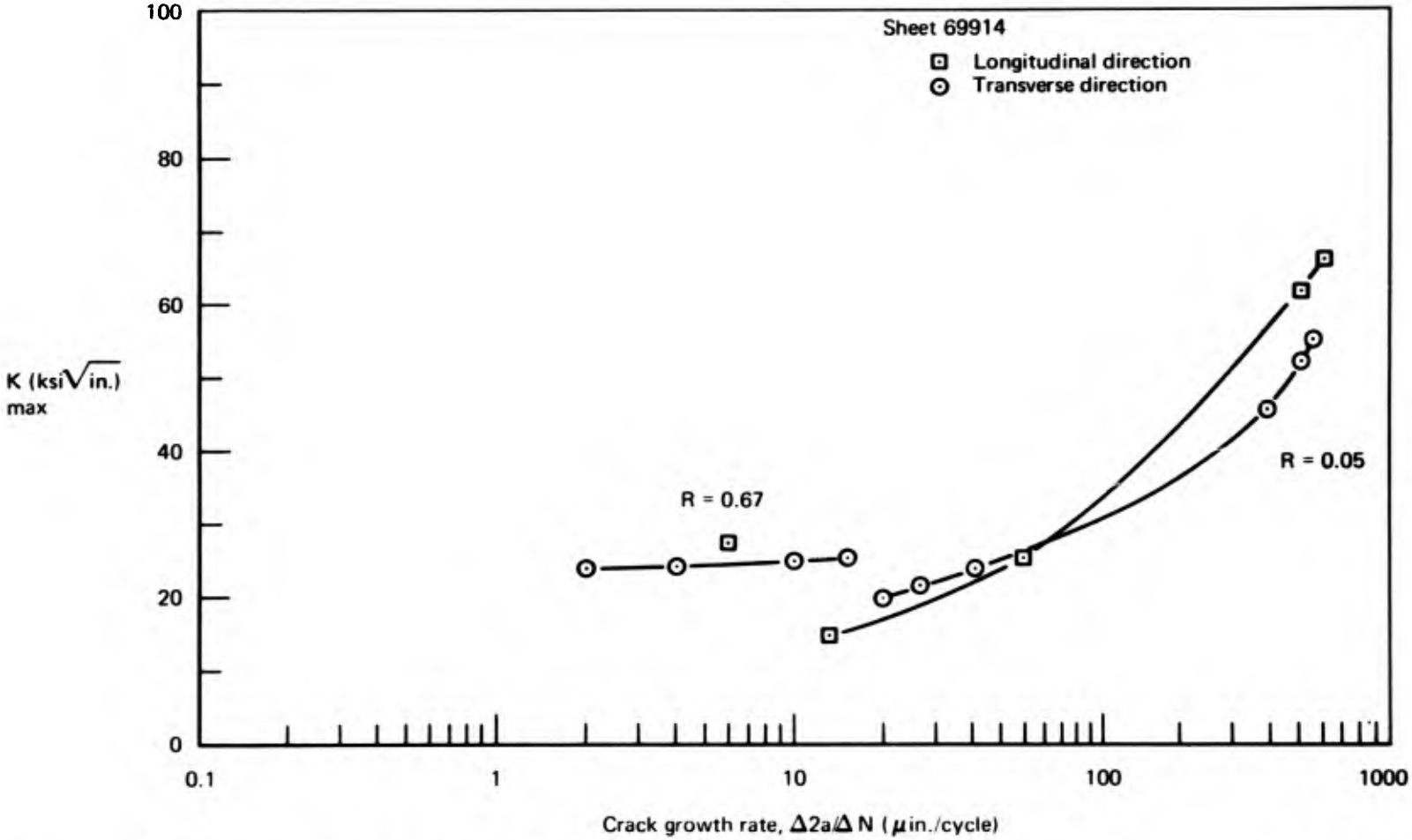

FIGURE 19.–FATIGUE CRACK GROWTH RATE FOR HIGH-NEGATIVE-TEXTURED Ti-6Al-4V HAND-MILL SHEET

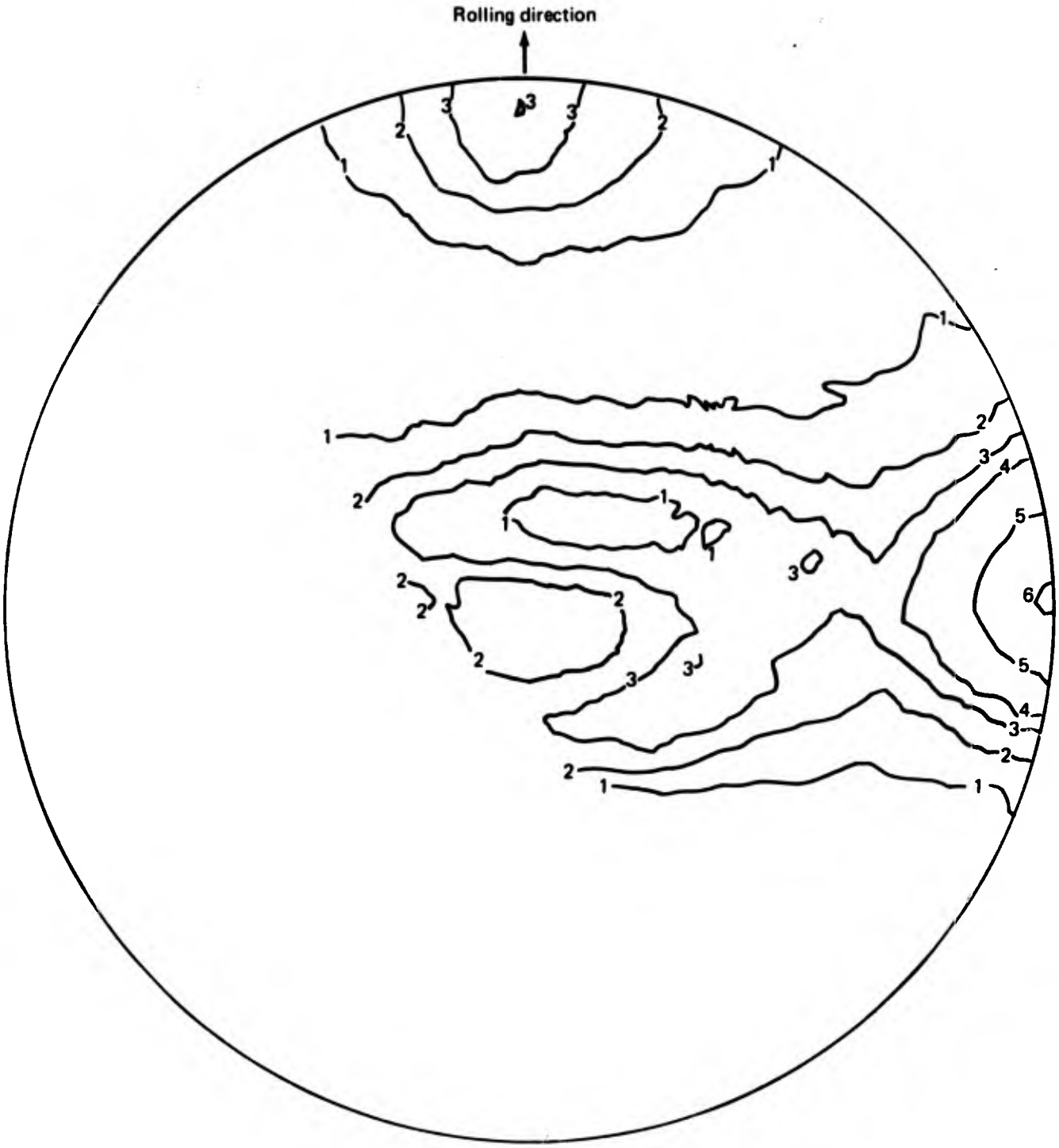

Contour lines	1	2	3	4	5	6
Times random intensity	0.5	1.0	1.5	2.0	4.0	8.0

$K_A = 57$

FIGURE 20.–BASAL PLANE POLE FIGURE FOR HIGH-POSITIVE-TEXTURED HAND-MILL Ti-6Al-4V SHEET 20614

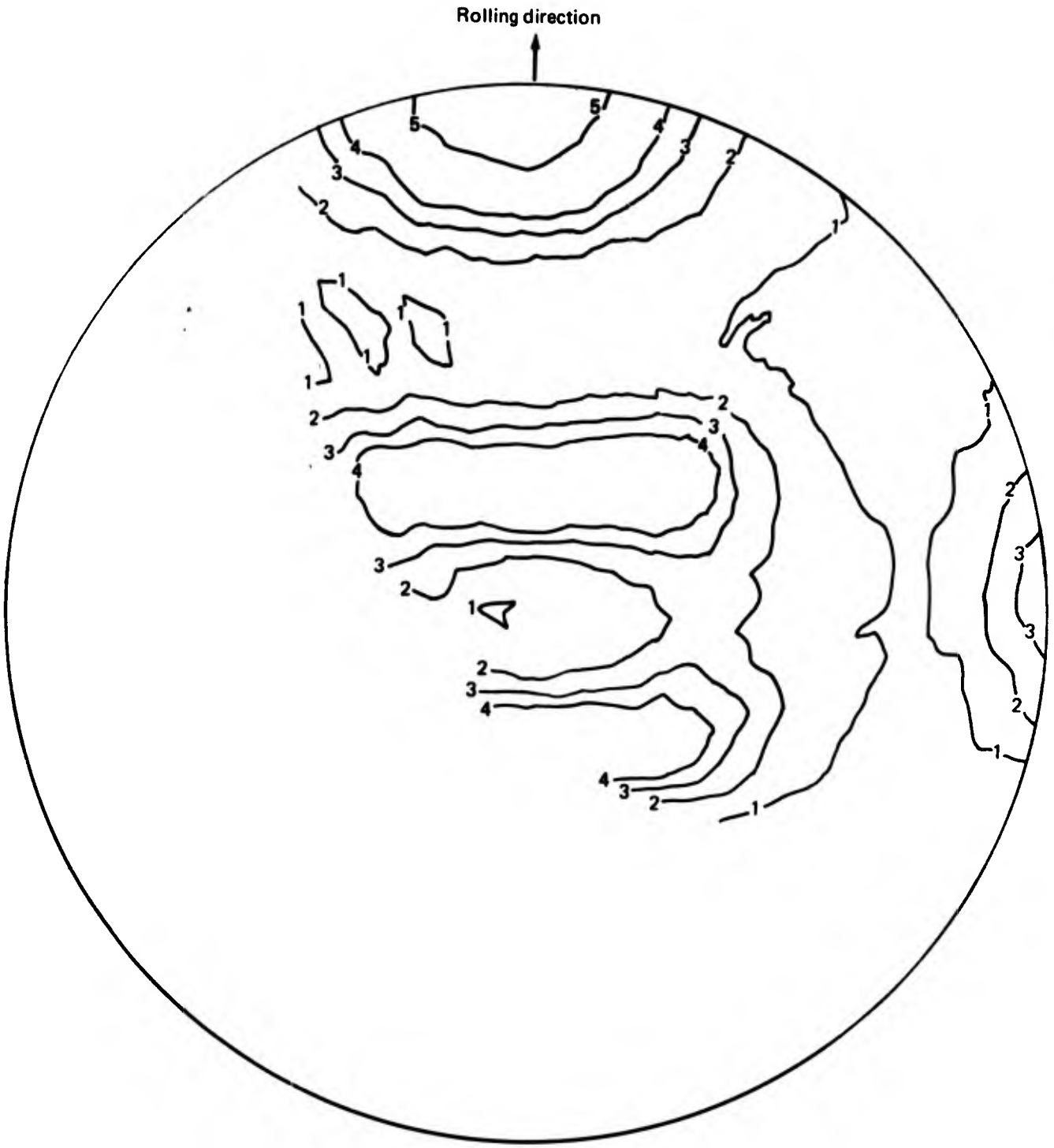

Contour lines	1	2	3	4	5	6
Times random intensity	0.5	1.0	1.5	2.0	4.0	8.0

$K_A = -29$

FIGURE 21.—BASAL PLANE POLE FIGURE FOR HIGH-NEGATIVE-TEXTURED HAND-MILL SHEET 69914

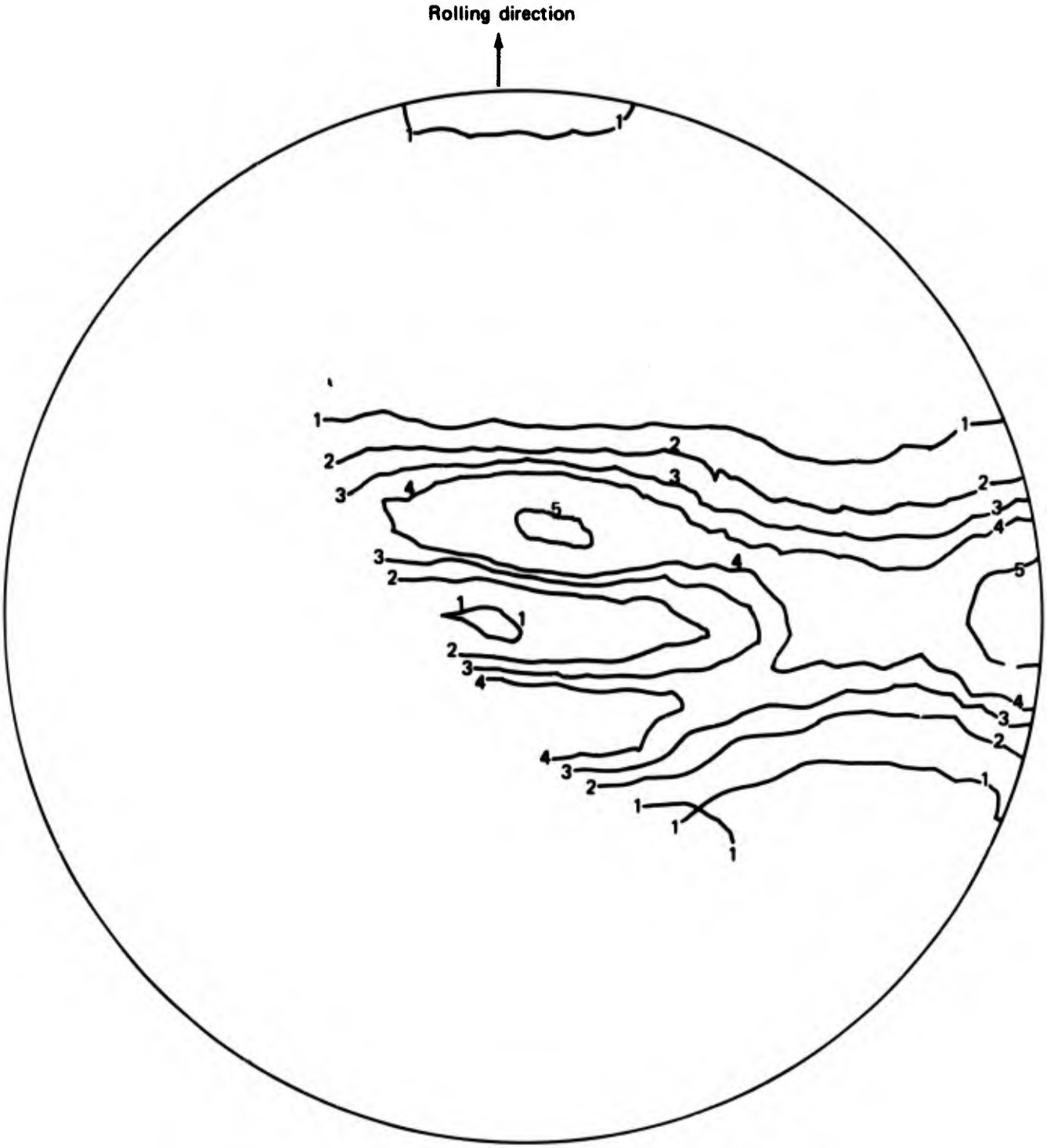

Contour lines	1	2	3	4	5	6
Times random intensity	0.5	1.0	1.5	2.0	4.0	8.0

$K_A = 63$

FIGURE 22.–EXAMPLE OF HIGH POSITIVE K_A TEXTURE IN HAND-MILL Ti-6Al-4V SHEET

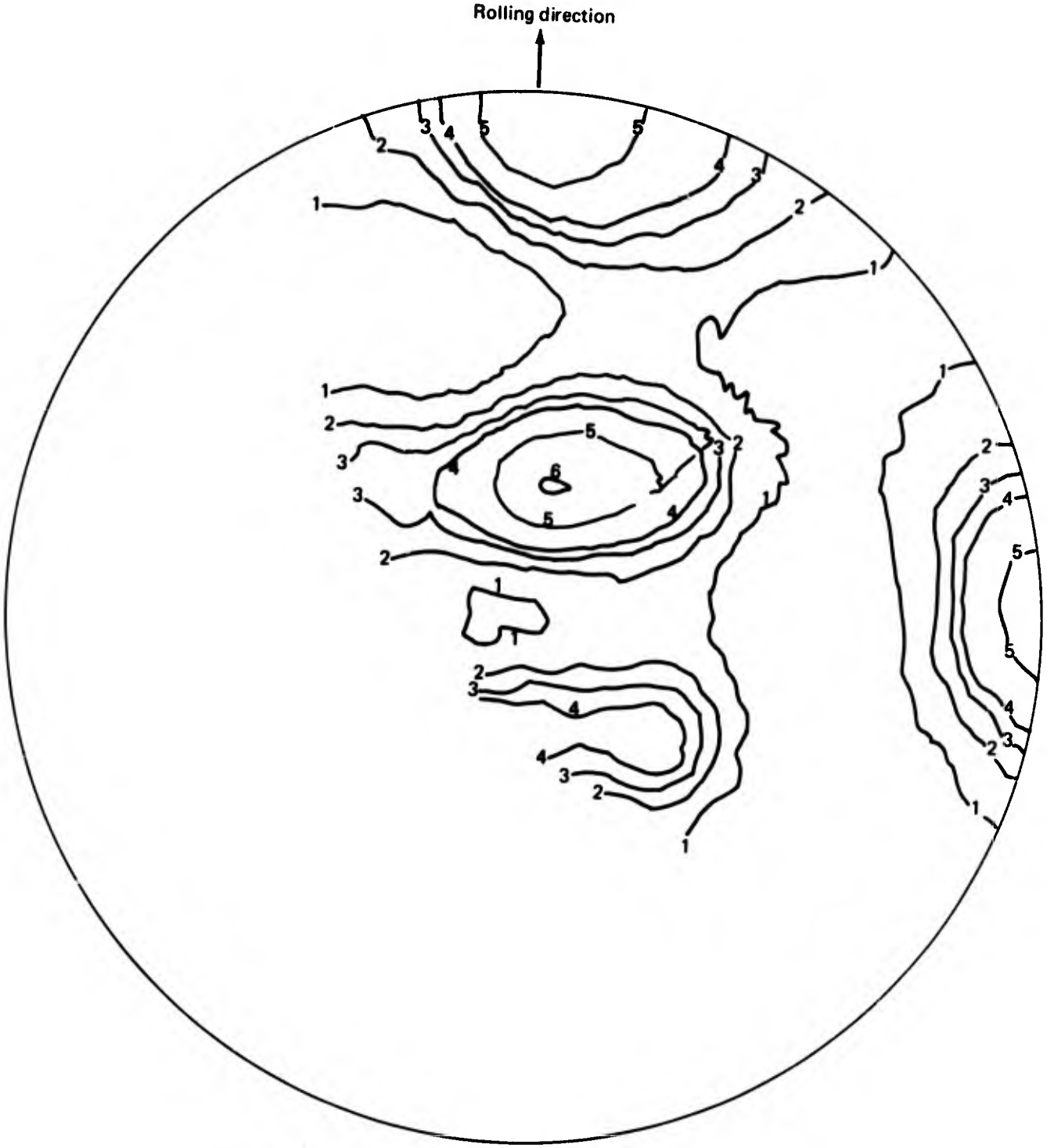

Contour lines	1	2	3	4	5	6
Times random intensity	0.5	1.0	1.5	2.0	4.0	8.0

$K_A = -63$

FIGURE 23.—EXAMPLE OF HIGH-NEGATIVE K_A TEXTURE IN HAND-MILL Ti-Al-4V SHEET

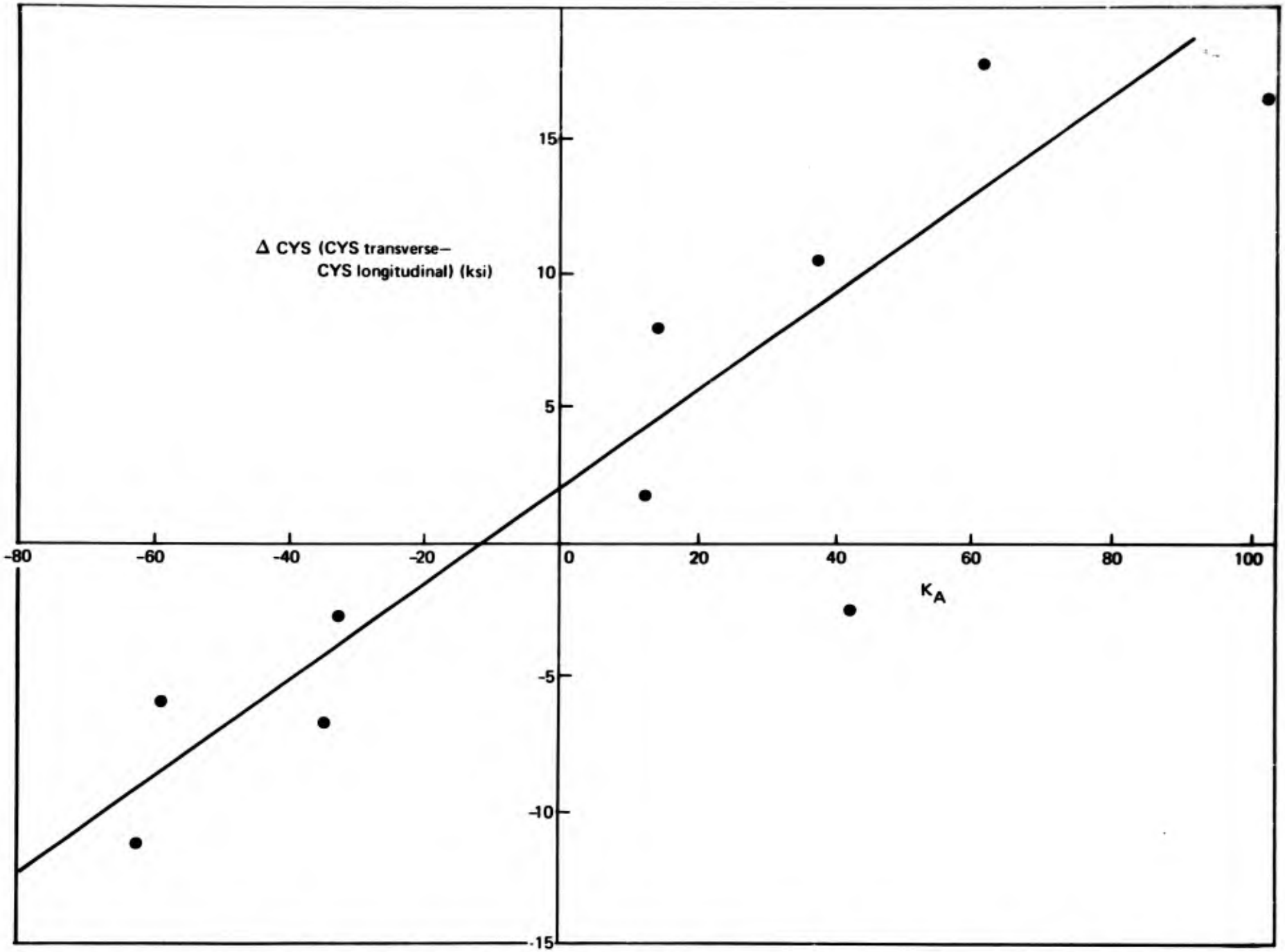

FIGURE 24.–EFFECT OF ANISOTROPY FACTOR, K_A, ON DIFFERENCE BETWEEN TRANSVERSE AND LONGITUDINAL COMPRESSION YIELD STRENGH, ΔCYS

TABLE 3.– COMPRESSION YIELD STRENGTH DATA FOR HAND-MILL SHEET

Specimen	Direction	TUS (ksi)	TYS (ksi)	Elong (%)	E_T (x 10^6 psi)	CYS (ksi)	E_C (x 10^6 psi)	T-L TYS (ksi)	T-L CYS (ksi)	K_A Old	K_A New
FM944	L					144.4	16.0				
	T					140.0	17.3		-4.4		
FM963	L					135.5	17.2				
	T					136.4	16.0		0.9		
20052-3	L					138.2	17.1				
	T					132.7	15.9	-2.5	-5.7	-59	-121
20056	L					140.3	16.8				
	T					141.1	16.3	4.2	0.8		
20249	L					152.9	18.5				
	T					149.2	18.3	-8.3	-3.7	-33	-100
69988	T	147.8	132.9	17	17.6	148.2	16.8				
	L	148.6	139.0	18	18.3	146.5	17.2	-6.1	-1.7		-83
20061-1	L					156.8	16.8				
	T					154.3	17.1	1.2	-2.5	42	38
20062-10	L					148.2	17.6				
	T					140.2	17.6	2.9	-8.0	13	
20068-8	L					143.8	17.1				
	T					145.7	16.1	8.0	1.9	12	
20359-1	L					138.0	16.2				
	T					154.3	17.2	8.6	16.3	102	
310487	L					138.5	15.1				
	T					156.4	16.1	7.0	17.9	61	
20032-3	L					151.5	17.2				
	T					140.3	17.3	-1.2	-11.2	-63	
20091	L	144.9	141.1	17	18.7	144.8	16.7				
	T	144.9	134.8	17	18.2	155.4	19.6	6.3	10.6	37	
69920	L	139.3	128.6	19	16.2	142.9	17.1				
	T	138.7	132.0	18	16.7	136.1	17.8	-3.3	-6.8		-35

3.1.4 Modulus of Elasticity

The tension modulus of elasticity for Ti-6Al-4V sheet was obtained from a large number of receiving inspection tensile test curves of load versus deflection. This value for E_T was then correlated with such other available parameters as tensile yield strength, chemical composition, grain direction, and heat treatment. Although the inherent inaccuracies in obtaining modulus data from tensile curves are well understood, it was felt that useful information could be obtained statistically by using large numbers of data. Data were gathered for Ti-6Al-4V sheet for both the longitudinal and transverse grain directions for the following heat treatments.

Condition I – mill annealed, 1350°-1450° F/2-4 hr

Condition III – STA 1000° F, 1725° F/15 min/water quench + 1000° F/4 hr

Condition IV – STA 1250° F, 1725° F/15 min/water quench + 1250° F/4 hr

Condition IC – continuously annealed, 1600° F/5 min/FC* + 1100° F/5 min/FC*

Condition V – duplex annealed, 1725° F/15 min/air cool + 1250° F/4 hr

The data are shown in tables 4 through 8 for the above heat treatment conditions. For the hand-mill sheet (cross rolled) the E_T was found to be always higher than 16.0×10^6 psi. As expected, the data scatter was fairly high but the standard deviation was within the $0.2\text{-}1.0 \times 10^6$-psi range. The effect of texture can be seen in the continuously rolled sheet (table 8) and to a lesser extent in the annealed conditions for the hand-mill sheet (tables 4 and 5). Here the abundance of basal planes perpendicular to the transverse direction results in a high (17.4×10^6-psi mean) E_T transverse compared to the low (15.3×10^6-psi mean) E_T for the longitudinal direction for continuously rolled sheet. The effect of texture is demonstrated by a regression analysis (ref. 6) in which E_T is determined as a function of tensile yield strength. The following equations were developed for continuously rolled sheet (units are 10^6 psi for E_T and 10^3 psi for TYS):

- Longitudinal direction

$$E_T = 7.42 + 0.061\ (TYS)$$

- Transverse direction

$$E_T = 4.68 + 0.092\ (TYS)$$

These equations would necessarily include the effects not only of texture but also of other factors such as chemical composition, thermal cycle, microstructure, etc., that might affect both the TYS and E_T. The effect of chemical composition was examined by developing

*Rapid furnace cool

TABLE 4.—E_T DATA FOR CONDITION I Ti-6Al-4V SHEET

	TUS (ksi)	TYS (ksi)	Elong (%)	RA[a] (%)	E_T (x 10^6 psi)	Chemical composition (wt %)						
						O_2	N_2	H_2	C	Al	V	Fe
Longitudinal direction												
Column mean	144.7	138.2	11.0	0.0	16.1	0.135	0.0172	0.0060	0.023	6.21	3.87	0.12
Column standard deviation	3.7	4.5	2.2	0.0	0.7	0.024	0.0050	0.0019	0.015	0.25	0.22	0.02
Number of non-zero data	43	43	43	0	43	41	41	35	41	41	41	41
Maximum value in data	157.0	148.8	14.0	0.0	17.6	0.178	0.0200	0.0104	0.065	6.50	4.40	0.17
Minimum (non-zero) value	138.4	128.9	1.0	*0.0	14.7	0.097	0.0057	0.0044	0.005	5.60	3.60	.09
Number of heat-lots	15											
Transverse direction												
Column mean	145.7	140.5	11.4	0.0	16.6	0.136	0.0172	0.0061	0.023	6.21	3.88	0.12
Column standard deviation	5.5	5.7	1.3	0.0	0.8	0.025	0.0049	0.0019	0.015	0.25	0.22	0.02
Number of non-zero data	44	44	44	0	44	42	42	36	42	42	42	42
Maximum value in data	162.0	157.1	14.0	0.0	19.1	0.179	0.0200	0.0104	0.065	65.0	4.40	0.19
Minimum (non-zero) value	139.4	132.1	8.0	*0.0	14.9	0.097	0.0057	0.0044	0.005	5.60	3.60	0.09
Number of heat-lots	16											

[a]Reduction in area

TABLE 5.—E_T DATA FOR CONDITION V Ti-6Al-4V SHEET

	TUS (ksi)	TYS (ksi)	Elong (%)	RA[a] (%)	E_T (x 10^6 psi)	Chemical composition (wt %)						
						O_2	N_2	H_2	C	Al	V	Fe
Longitudinal direction												
Column mean	145.8	138.3	13.4	0.0	16.4	0.137	0.0132	0.0068	0.026	5.99	4.16	0.14
Column standard deviation	5.8	6.6	1.2	0.0	0.7	0.014	0.0048	0.0018	0.008	0.28	0.16	0.04
Number of non zero data	56	56	56	0	56	50	48	50	50	50	50	50
Maximum value in data	156.0	150.2	16.0	0.0	18.3	0.170	0.0200	0.0093	0.052	6.50	4.50	0.21
Minimum (non-zero) value	136.0	122.5	11.0	*0.0	15.1	0.108	0.0060	0.0020	0.020	5.10	3.70	0.08
Number of heat-lots	29											
Transverse direction												
Column mean	147.4	140.5	13.4	0.0	16.7	0.137	0.0131	0.0067	0.026	6.00	4.16	0.14
Column standard deviation	6.3	6.7	1.3	0.0	0.7	0.014	0.0047	0.0018	0.008	0.28	0.16	0.04
Number of non zero data	55	55	55	0	55	49	47	49	49	49	49	49
Maximum value in data	159.2	154.4	16.0	0.0	19.1	0.170	0.0200	0.0093	0.052	6.50	4.50	0.21
Minimum (non-zero) value	136.0	123.5	10.0	*0.0	15.1	0.108	0.0060	0.0020	0.020	5.10	3.70	0.08
Number of heat-lots	29											

[a]Reduction in area

TABLE 6.—E_T DATA FOR CONDITION III Ti-6Al-4V SHEET

	TUS (ksi)	TYS (ksi)	Elong (%)	RA[a] (%)	E_T (x 10^6 psi)	Chemical composition (wt %)						
						O_2	N_2	H_2	C	Al	V	Fe
Longitudinal direction												
Column mean	174.1	164.7	9.5	0.0	17.4	0.094	0.0200	0.0071	0.007	5.99	3.6/3	0.10
Column standard deviation	3.2	2.8	3.5	0.0	0.3	0.011	*000	0.0011	0.004	0.11	0.0/9	0.01
Number of non zero data	2	2	2	0	2	2	2	2	2	2	2	2
Maximum value in data	176.4	166.7	12.0	0.0	17.6	0.102	0.0200	0.0079	0.010	6.07	3.7/0	0.11
Minimum (non-zero) value	171.9	162.7	7.0	*0.0	17.2	0.087	0.0200	0.0064	0.005	5.91	3.5/7	0.10
Number of heat-lots	2											
Transverse direction												
Column mean	169.7	161.8	9.0	0.0	17.1	0.094	0.0200	0.0071	0.007	59.9	3.6/3	0.10
Column standard deviation	0.4	3.8	0.0	0.0	0.8	0.011	*000	0.0011	0.004	0.11	0.0/9	0.01
Number of non zero data	2	2	2	0	2	2	2	2	2	2	2	2
Maximum value in data	170.0	164.5	9.0	0.0	17.7	0.102	0.0200	0.0079	0.010	6.07	3.7/0	0.11
Minimum (non-zero) value	169.5	159.1	9.0	*0.0	16.6	0.087	0.0200	0.0064	0.005	5.91	3.5/7	0.10
Number of heat-lots	2											

[a]Reduction in area

TABLE 7.—E_T DATA FOR CONDITION IV Ti-6Al-4V SHEET

	TUS (ksi)	TYS (ksi)	Elong (%)	RA[a] (%)	E_T (x 10^6 psi)	Chemical composition (wt %)						
						O_2	N_2	H_2	C	Al	V	Fe
Longitudinal direction												
Column mean	149.7	146.9	12.3	0.0	16.9	0.117	0.0200	0.0093	0.010	5.82	3.92	0.10
Column standard deviation	2.2	1.6	2.3	0.0	0.2	0.020	0.0000	0.0023	0.000	0.20	0.08	0.01
Number of non-zero data	3	3	3	0	3	3	3	3	3	3	3	3
Maximum value in data	151.1	148.2	15.0	0.0	17.2	0.129	0.0200	0.0119	0.010	6.05	3.98	0.10
Minimum (non-zero) value	147.2	145.1	11 0	*0.0	16.8	0.094	0.0200	0.0074	0.010	5.70	3.83	0.09
Number of heat-lots	3											
Transverse direction												
Column mean	148.6	145.1	13.7	0.0	16.9	0.117	0.0200	0.0093	0.010	5.82	3.92	0.10
Column standard deviation	1.9	1.8	3.1	0.0	0.6	0.020	0.0000	0.0023	0.000	0.20	0.08	0.01
Number of non-zero data	3	3	3	0	3	3	3	3	3	3	3	3
Maximum value in data	150.8	146.5	17.0	0.0	17.5	0.129	0.0200	0.0119	0.010	6.05	3.98	0.10
Minimum (non-zero) value	147.3	143.1	11.0	*0.0	16.3	0.094	0.0200	0.0074	0.010	5.70	3.83	0.09
Number of heat-lots	3											

[a]Reduction in area

TABLE 8.–E_T DATA FOR CONDITION IC Ti-6Al-4V SHEET

	TUS (ksi)	TYS (ksi)	Elong (%)	RA[a] (%)	E_T (x 10^6 psi)	Chemical composition (wt %)						
						O_2	N_2	H_2	C	Al	V	Fe
Longitudinal direction												
Column mean	146.5	129.9	11.0	0.0	15.3	0.138	0.0172	0.0067	0.016	6.13	3.94	0.11
Column standard deviation	7.3	8.6	1.6	0.0	0.9	0.021	0.0055	0.0015	0.012	0.46	0.48	0.03
Number of non zero data	38	38	38	0	38	38	37	38	38	37	38	34
Maximum value in data	165.2	144.3	14.0	0.0	17.1	0.168	0.0240	0.0121	0.075	6.68	6.58	0.18
Minimum (non-zero) value	126.7	110.1	7.0	*0.0	13.4	0.070	0.0042	0.0040	0.005	5.88	3.57	0.05
Number of heat-lots	18											
Transverse direction												
Column mean	147.0	138.4	11.3	0.0	17.4	0.137	0.0176	0.0064	0.014	6.16	3.90	0.11
Column standard deviation	7.9	7.5	1.1	0.0	1.0	0.022	0.0055	0.0011	0.013	0.49	0.53	0.01
Number of non zero data	30	30	30	0	30	30	30	30	30	30	30	28
Maximum value in data	153.8	145.8	13.0	0.0	18.5	0.167	0.0200	0.0090	0.075	6.68	6.58	0.14
Minimum (non-zero) value	128.5	119.4	8.0	*0.0	13.5	0.070	0.0042	0.0049	0.005	5.88	3.57	0.10
Number of heat-lots	12											

[a]Reduction in area

regression analysis equations of E_T, as a function of Al, O_2, V, and Fe contents. Most of the equations developed for Ti-6Al-4V sheet showed low correlation coefficients (R^2 = 0.10-0.35) and for this reason are not presented. However, the equations did generally show a positive effect of E_T for both aluminum and oxygen. The positive aluminum effect has been somewhat qualitatively developed in the past since the higher aluminum titanium alloys (e.g., Ti-8Al-1Mo-1V) have higher modulus than other alloys (Ti-6Al-4V, Ti-3Al-2.5V, and commercially pure titanium). A more quantitative relationship between E_T and chemical composition is presented in section 3.2.5 for Ti-6Al-4V plate.

The effect of heat treatment on E_T can be seen from tables 6 and 7 for condition III and IV sheet. Although there are very few data, the E_T for these higher strength heat treatments (especially condition III) is higher than the values for the annealed material. This is true in spite of the higher oxygen content for the annealed material (0.137%) compared to that for the heat-treated sheet (0.117%). Although more data would be needed to confirm this effect, the trend does appear to be real.

3.1.5 K_{scc} of Solution-Treated-and-Aged Ti-6Al-4V Sheet

To determine the interrelated effects of chemistry, preferred orientation, and heat treatment, seven samples of duplex-annealed Ti-6Al-4V sheet were heat treated and tested to determine K_{scc}. The solution treatment and aging cycle used was 1725°F/30 min/water quench + 1000°F/4 hr/air cool. This would result in tensile strengths of 165-175 ksi. Table 9 shows the results of this study. In all but two cases the reduction in K_{scc} for the heat-treated condition over the as-received duplex-annealed condition was approximately 40%. It is significant to point out that the K_{scc} of heat-treated sheet, which has low oxygen content and low directionality, is more than twice that of higher oxygen or more textured duplex-annealed sheet. On the other hand, the lowest K_{scc} for Ti-6Al-4V which we have encountered to date is on specimen 20284-4LT, which had a value of 11 ksi$\sqrt{\text{in}}$. This reduction was not observed, however, in two other specimens in which the value of K_{scc} for the heat-treated condition was virtually the same as for the duplex-annealed condition. In specimen

20182 the alignment of the basal planes is such that it favors high K_{scc} values for the transverse grain direction. This favorable alignment results in a high K_{scc} for this direction even after heat treatment. Specimen 310487 shows no decrease in K_{scc} in the heat-treated condition for the transverse direction. In this case the K_{scc} is already very low (30 ksi$\sqrt{in.}$) and no further reduction occurs.

TABLE 9.–K_{scc} OF SOLUTION-TREATED-AND-AGED Ti-6Al-4V HAND-MILL SHEET

Specimen	Heat	Grain direction	O_2 (%)	Al (%)	ΔTYS (ksi)		K_A new	K_{scc} (ksi$\sqrt{in.}$)		RA (%)	α_2 parameter duplex annealed
					Lot	Sheet		Duplex annealed (as-received)	Solution treated and aged		
20333-1L	295440	L	0.116	6.2	-0.6	–	-17	85	64	25	1.3
20333-2T	295440	T	0.116	6.2	-0.6	–	-17	105	62	41	1.3
20182-2TL	295393	L	0.119	6.3	-8.0	–	-64	67	41	39	0.8
20182-2T	295393	T	0.119	6.3	-8.0	–	-64	82	78	5	0.8
20284-4LT	K6398	T	0.17	6.4		-3.5	-47	21	11	48	10.0
310487 L	310487	L	0.143	6.3		7.0	63	85	58	43	5.7
310487 T	310487	T	0.143	6.3		7.0	63	30	31	-3	5.7

Note: Heat treatment 1725°F/30 min/water quench + 1000°F/4 hr/air cool.

The effect of α_2 (Ti_3Al) ordered phase formation can also be seen from these data. The high degree of ordering (α_2 parameter = 10) undoubtedly is a major contributing parameter to the K_{scc} of 11 ksi$\sqrt{in.}$ for specimen 20284-4LT. This low value is especially significant since the directionality factors would favor higher transverse K_{scc} (K_A = -47, TYS = -3.5). The low value is then a direct result of this severe ordering and the high oxygen content. The aluminum content of this specimen is 6.4%, which has been shown (ref. 2) to be well above that required for ordering which results in markedly reduced K_{scc} for Ti-6Al-4V sheet. In highly textured, continuously rolled Ti-6Al-4V sheet, aluminum contents of 6.2% and greater resulted in very low K_{scc} due to ordering whereas aluminum contents of 6.0% and less resulted in no ordering that produced low K_{scc}. The ordering parameters given are for the as-received condition (duplex annealed), but since the aging treatment of 1000° F/4 hr is also in the α_2 formation range similar amounts of ordering will also occur in the solution-treated-and-aged condition. The relatively high α_2 parameter (5.7) for specimen 310487 also contributes to the low K_{scc} (30-31 ksi$\sqrt{in.}$) for both the duplex-annealed and the solution-treated-and-aged material.

3.1.6 Effect of Furnace Cooling on K_{scc} of Hand-Mill Sheet

Past experience (ref. 2) has shown that when textured Ti-6Al-4V continuously rolled sheet is furnace cooled through the α_2 (Ti_3Al) region, a severe reduction in K_{scc} results in the direction perpendicular to the basal plane alignment. Because of this, seven examples of textured hand-mill sheet were thermally cycled as follows:

1350 F/1 hr/furnace cool at 100° F per hour to 600° F/air cool.

Four specimens with negative directionality (large amount of basal plane perpendicular to the rolling direction) were tested in the longitudinal direction and three specimens with positive directionality were tested in the transverse direction. The test results are shown in table 10. In all cases there was a marked decrease in K_{scc} after furnace cooling compared with the as-received or duplex-annealed condition. The effect of the ordering parameter is shown in figure 25. Although there is some scatter, the trend of increasing K_{scc} reduction with increasing α_2 parameter changes is evident. The results of the highly textured specimens are not surprising in light of past data. However, some of the results with nominally low directionality (ΔTYS ±2.0 ksi and K_A ±20) also had low K_{scc}. It is possible that the 6.2% aluminum promotes sufficient amounts of α_2 to result in this reduction, even with less than severe preferred orientation. Two specimens from the same heat, 295407, showed relatively high ordering parameters (4.2 and 6.7), although the reported aluminum content was 5.9. Since this chemical analysis was on the heat (ingot) it is conceivable that the actual value of the specimens tested could be 6.2%. This coupled with the moderate directionality (K_A = 45 and -27 for specimens S-3 and S-6) results in low K_{scc}.

TABLE 10.–K_{scc} OF FURNACE-COOLED Ti-6Al-4V DUPLEX-ANNEALED SHEET

Specimen	Sheet	Heat	Grain direction	O_2 (%)	Al (%)	ΔTYS (ksi)	K_A new	α_2		K_{scc} (ksi $\sqrt{in.}$)	
								As received	Furnace cooled	As received	Furnace cooled
S-1	69920	295414	L	0.112	6.4	-3.3	-35	0.7	5.3	67	46
S-2	69988	295435	L	0.127	6.4	-6.1	-83	1.0	7.7	82	31
S-3	20043	295407	L	0.126	5.9	-2.1	-27	3.5	4.2	68	46
S-4	20333	295440	L	0.116	6.2	-0.6	-17	1.3	3.5	85	29
S-5	20328	295429	T	0.136	6.2	1.5	9	2.3	5.5	67	44
S-6	69954	295407	T	0.141	5.9	2.8	45	1.0	6.7	69	31
S-7	20293	295429	T	0.136	6.2	0.5	28	2.1	5.8	53	22

Although further quantitative work is required, it appears that either lower aluminum contents than 6.2% must be used or that furnace cooling must be prohibited in order to preserve higher K_{scc} values for duplex-annealed hand-mill sheet. It is also possible that improving the preferred orientation would help. Techniques to develop a more random texture or a texture in which the basal planes are aligned parallel to the sheet surface should be considered.

3.1.7 Super ELI Hand-Mill Sheet

Tests were conducted on super ELI (extra-low interstitial) Ti-6Al-4V hand-mill sheet to obtain material property data on material with very low oxygen content. The sheet was in the mill-annealed condition and had the following chemical composition:

Heat	Lot	Size (in.)	Chemical composition (wt %)						
			O_2	Al	V	C	Fe	H_2	N_2
G8080	L1766	0.060x36x96	0.08	5.8	4.1	0.023	0.04	0.006	0.010

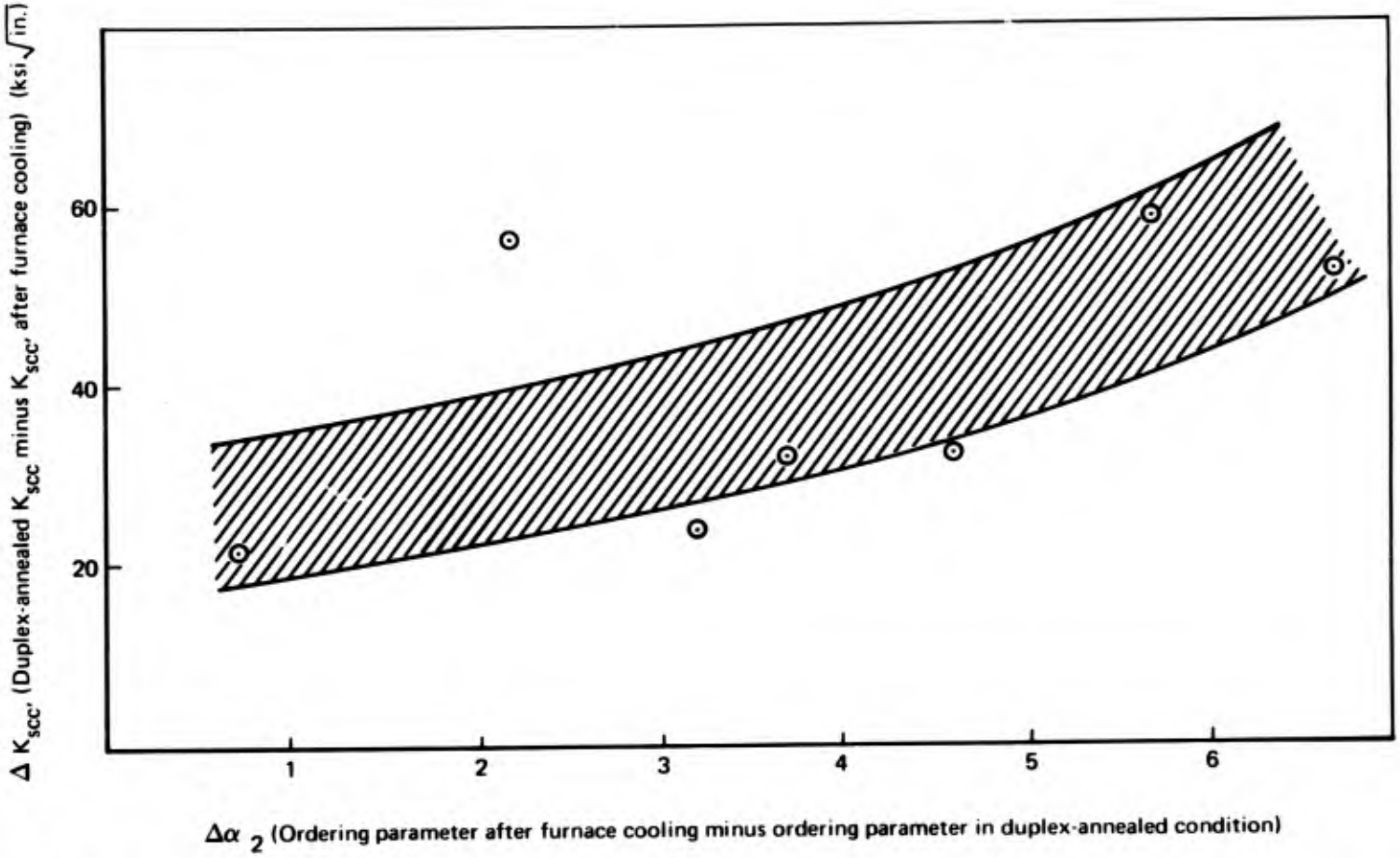

FIGURE 25.–EFFECT OF ORDERING PARAMETER ON THE REDUCTION IN K_{scc} OF FURNACE-COOLED OVER DUPLEX-ANNEALED Ti-6Al-4V SHEET

The tension and compression properties for both longitudinal and transverse directions are shown in table 11. The material shows a significant amount of property directionality, with the transverse direction having higher strengths and modulus than the longitudinal direction. Figure 26 shows the basal plane pole figure demonstrating the preponderance of basal planes aligned perpendicular to the transverse direction. K_A is 60. The increase in properties of the transverse direction over the longitudinal direction is 5.4 ksi for TUS, 8.1 ksi for TYS, and 10.9 ksi for CYS. The tension modulus is 2.7×10^6 psi and the compression modulus 1.5×10^6 psi higher for the transverse direction. It is interesting to note that the ductility as measured by percent elongation is not particularly high for both directions. This points out the relative insensitivity of percent elongation to material changes such as oxygen content and preferred orientation compared to the sensitivity of other properties. Fracture toughness and stress-corrosion tests were conducted on 18- by 36-in. center-cracked panels. These data are shown in table 12. As with earlier low chemistry (O_2 = 0.11, Al = 6.0) studies in continu-

TABLE 11.—TENSILE AND COMPRESSION PROPERTIES OF SUPER ELI HAND-MILL Ti-6Al-4V MILL-ANNEALED SHEET

Grain direction	TUS (ksi)	TYS (ksi)	Elongation in 2 in. (%)	E_T ($\times 10^6$ psi)	CYS (ksi)	E_C ($\times 10^6$ psi)
Longitudinal	133.7	129.4	12	15.6	139.2	17.3
Transverse	139.1	137.5	10	18.3	150.1	18.8

TABLE 12.—FRACTURE TOUGHNESS AND STRESS-CORROSION PROPERTIES OF SUPER ELI HAND-MILL Ti-6Al-4V MILL-ANNEALED SHEET

Specimen	Grain direction	K_c (ksi$\sqrt{\text{in.}}$)	Sustained K level in 3.5% NaCl (ksi$\sqrt{\text{in.}}$)
FM 934-1	Transverse	188.6	
FM 934-2	Transverse	214.0	151 no failure
FM 934-3	Transverse	199.1	151 no failure
		Avg 200.8	
FM 934-4	Longitudinal	157.0	
FM 934-5	Longitudinal	157.7	126 no failure
		Avg 157.3	

ously rolled sheet (ref. 2), the transverse grain direction is superior in fracture toughness even though basal plane alignment is perpendicular to this direction. This is contrasted to textured hand-mill sheet at O_2 contents of 0.14, in which the transverse direction had lower K_c than the longitudinal direction. Although no final K_{scc} was obtained from the center-cracked panel testing, the higher stress-corrosion resistance can be seen for the transverse direction from the data in table 12. Based on the K_{scc}/K_c ratios obtained for continuously rolled ELI sheet in section 3.1.8, the expected K_{scc} for the hand-mill ELI sheet would be:

- longitudinal direction 140-145 ksi$\sqrt{\text{in.}}$
- transverse direction 175-185 ksi$\sqrt{\text{in.}}$

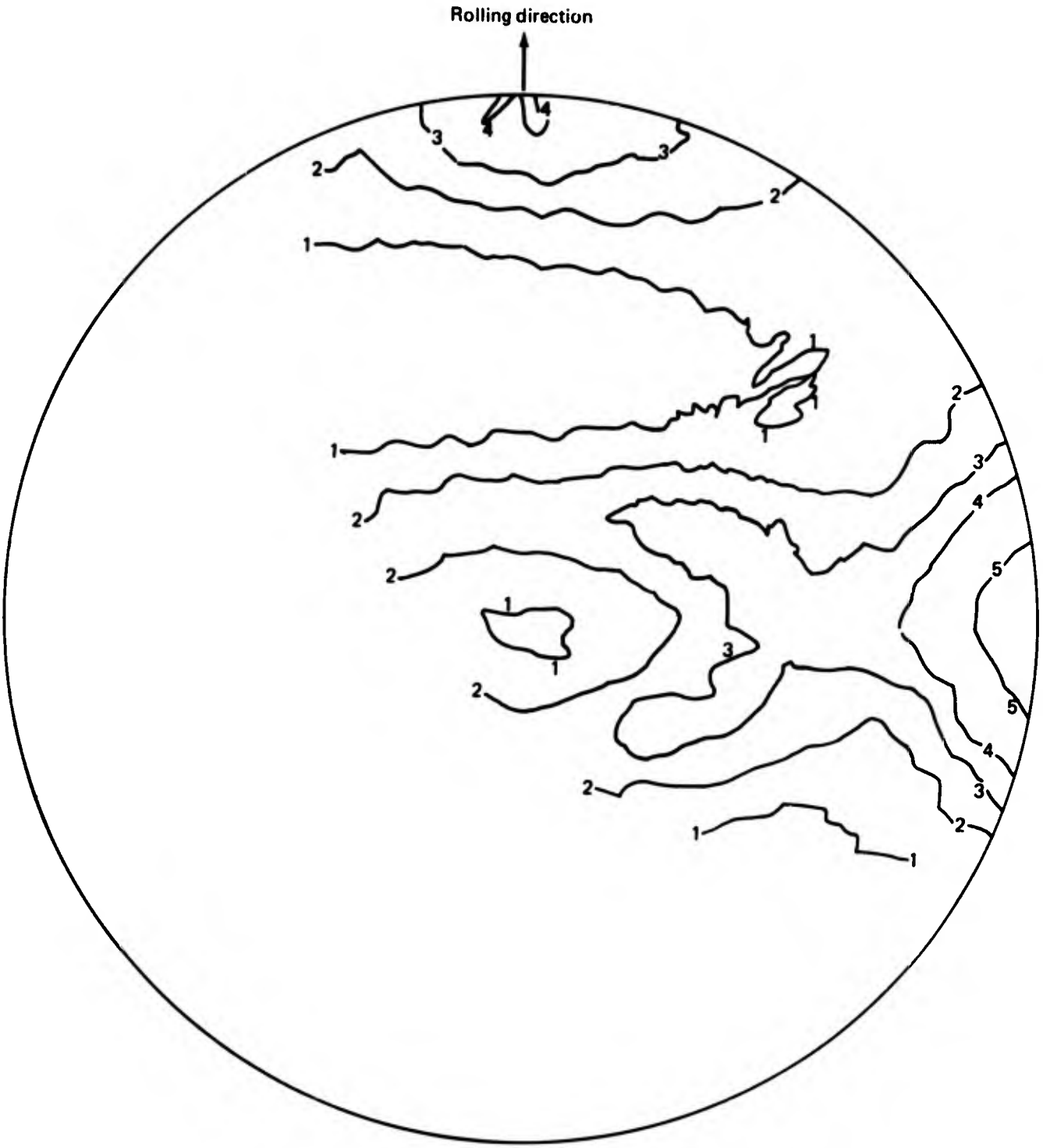

Contour lines	1	2	3	4	5	6
Times random intensity	0.5	1.0	1.5	2.0	4.0	8.0

$K_A = 51$

FIGURE 26.–BASAL PLANE POLE FIGURE FOR Ti-6Al-4V CONTINUOUSLY ROLLED SUPER ELI SHEET

GAGE: 0.062-0.063 WIDTH: 18.0
MANUFACTURER: TIMET
HEAT NO.: G8080
σ_G: 25 KSI R: 0.05
CYCLE RATE: 120 CPM
TEMP: 73-76°F REL. HUM.: NOTED %
ENVIRONMENT: NOTED
BUCKLING RESTRAINED

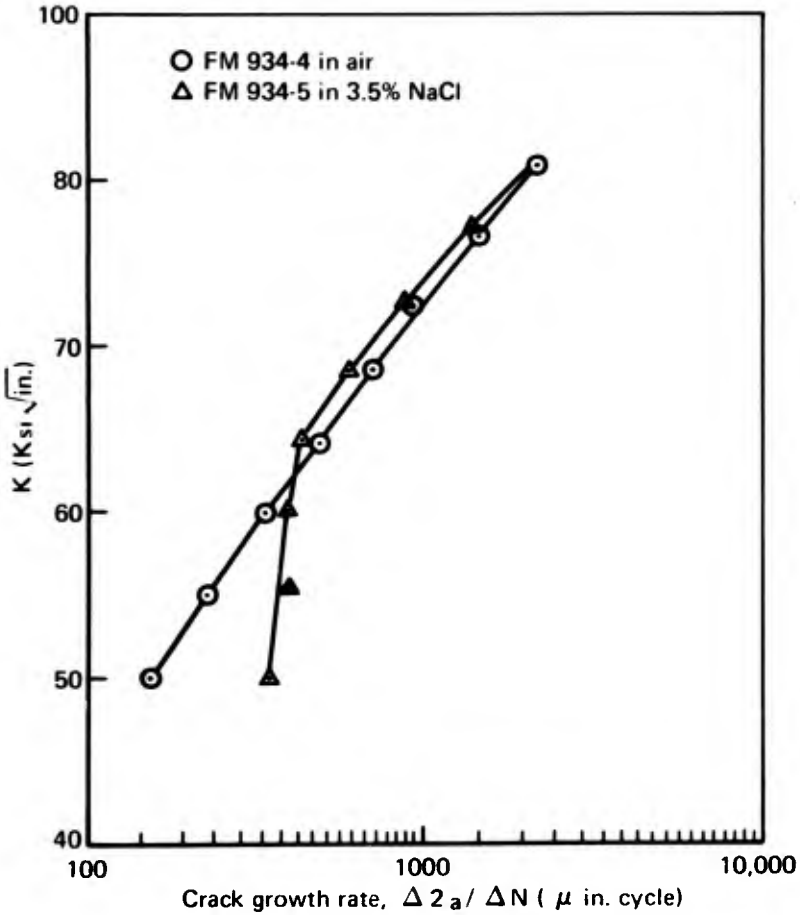

FIGURE 27.–CRACK GROWTH RATE OF SUPER ELI HAND-MILL Ti-6Al-4V SHEET–LONGITUDINAL DIRECTION

GAGE: 0.063-0.064 WIDTH: 18.0
MANUFACTURER: TIMET
HEAT NO.: G8080
σ_G: KSI R: .05
CYCLE RATE: 120 CPM
TEMP.: 72-78°F REL. HUM.: NOTED %
BUCKLING RESTRAINED

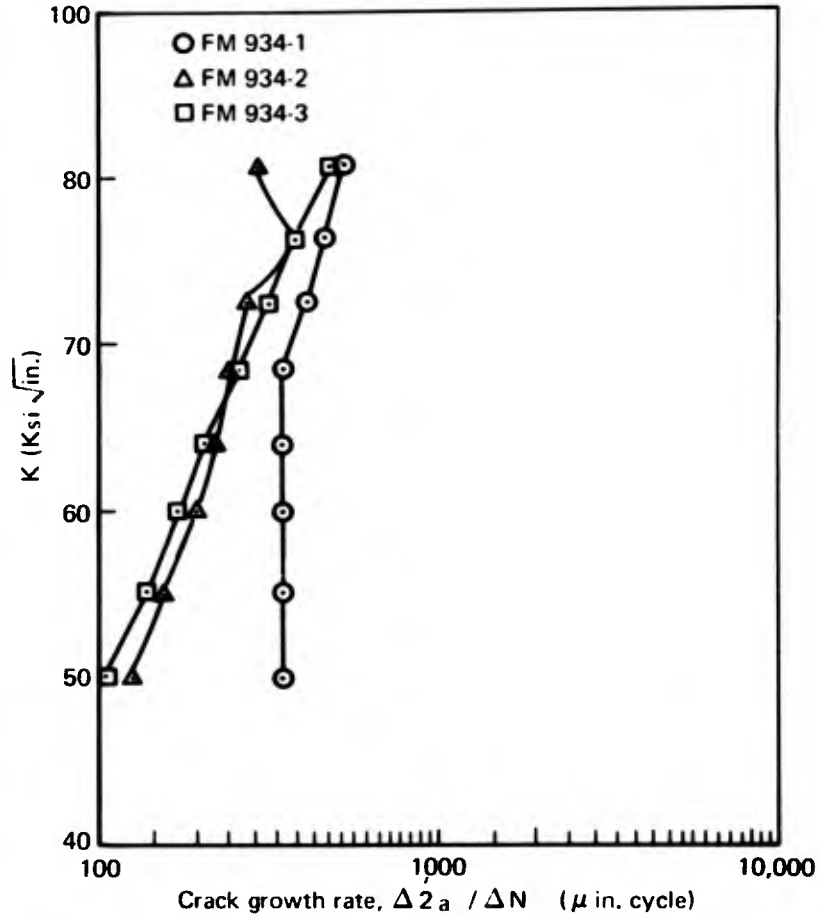

FIGURE 28.–CRACK GROWTH RATE OF SUPER ELI HAND-MILL Ti-6Al-4V SHEET–TRANSVERSE DIRECTION

Fatigue crack growth rate data for an R = 0.05 in air, distilled water, and 3.5% NaCl are shown in figures 27 and 28 for the longitudinal and transverse directions, respectively. As with fracture toughness, the crack growth rates are superior for the transverse direction to those for the longitudinal direction. The rate in air at a stress intensity level of 50 ksi $\sqrt{in.}$ is 100 μin./cycle for the transverse direction compared to 150 μin./cycle for the longitudinal. A very significant point for both directions is that the difference between the crack growth rates in 3.5% NaCl for the longitudinal and transverse directions is very low. This is markedly different for textured material with higher oxygen contents, where these rates are as much as 5-10 times greater when the stress is applied perpendicular to the basal planes (parallel to the transverse direction) than when it is applied parallel to the basal planes.

3.1.8 Super ELI Continuously Rolled Ti-6Al-4V Sheet

Tests were conducted on a special heat of Ti-6Al-4V having very low oxygen content which was continuously rolled to several gages. The material tested had the following chemical composition:

Heat	Lot	Trace	Size (in.)	Chemical composition (wt %)						
				O_2	Al	V	Fe	C	N_2	H_2
K6338	T4773	20374	0.063x42x145	0.07	6.0	4.1	0.02	0.022	0.011	0.003

The tensile properties were tested at the front and back end of the long coil from which the above sheet was cut and are given in table 13. The tensile property directionality can be

TABLE 13.– TENSILE PROPERTIES OF SUPER ELI CONTINUOUSLY ROLLED Ti-6Al-4V SHEET

Position in coil	Grain direction	TUS (ksi)	TYS (ksi)	Elongation in 2 in. (%)
Front	Longitudinal	126.8	107.7	13.0
Front	Transverse	128.4	117.0	12.5
Back	Longitudinal	126.8	109.4	13.5
Back	Transverse	128.4	117.0	12.5

seen from these data, where the ΔTYS is 9.0 ksi. Figure 29 gives the basal plane pole figure which explains this yield strength directionality. Although modulus of elasticity was not measured, the transverse direction would be expected to be approximately 2.0 x 10^6 psi higher than the longitudinal direction. The fracture toughness and stress-corrosion resistance were measured using 24- by 42-in. center-cracked panels. These data are presented in table 14. As with the low-oxygen hand-mill sheet discussed in section 3.1.7 and also higher oxygen continuously rolled sheet (ref. 2), the transverse grain direction has both higher K_c and stress-corrosion resistance than the longitudinal direction even though there is an apparent unfavorable alignment of basal planes. As table 14 shows, the material is very immune to stress corrosion since the K_{scc}/K_c ratio is greater than 0.9. In fact the transverse test did not fail in 3.5% NaCl at 110% of K_c. At this time this somewhat anomalous behavior can be attributed to scatter since it is reasonable that the K_c of the panel loaded in 3.5% NaCl could

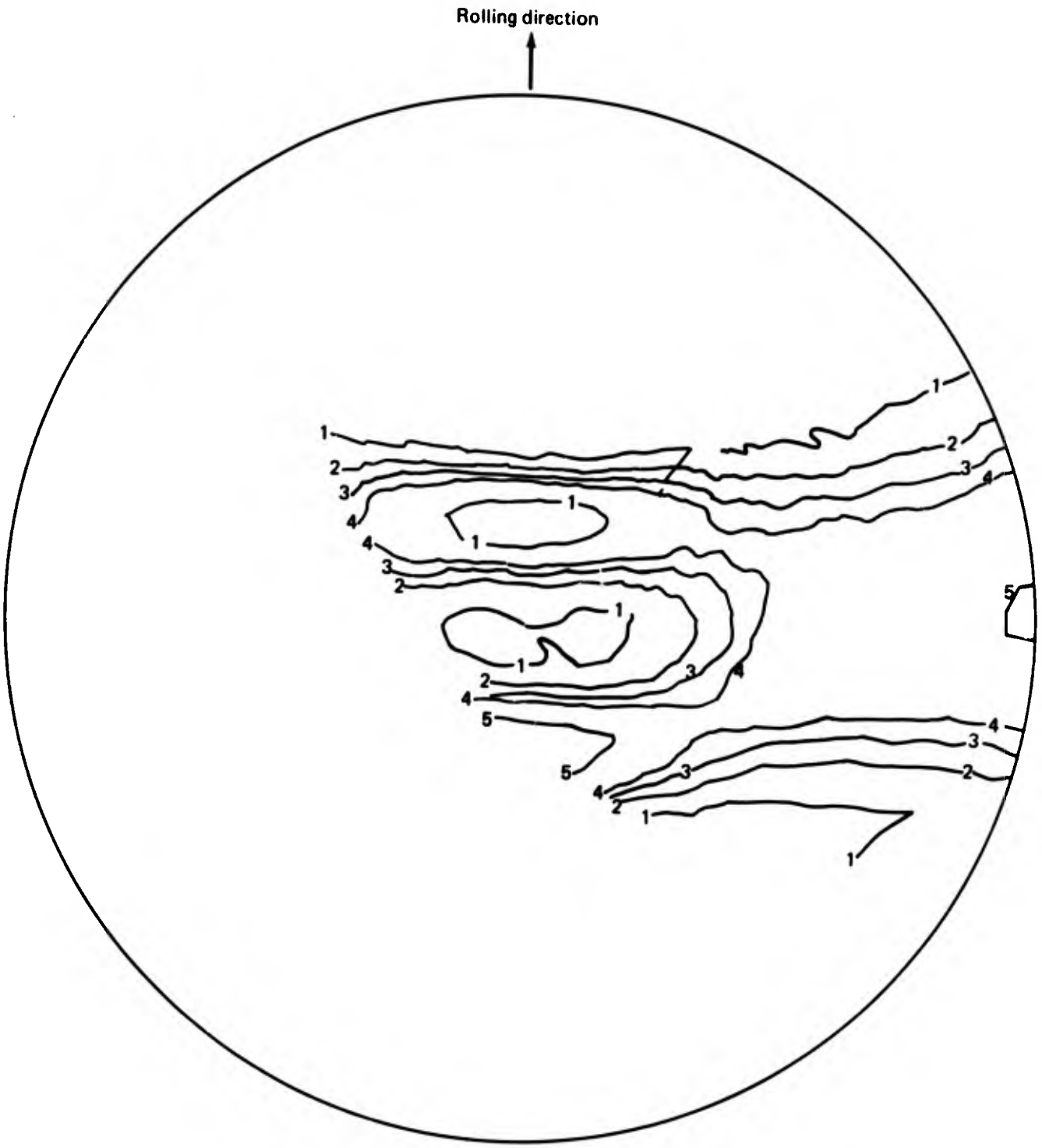

Contour lines	1	2	3	4	5	6
Times random intensity	0.5	1.0	1.5	2.0	4.0	8.0

$K_A = 111$

FIGURE 29.–BASAL PLANE (0002) POLE FIGURE FOR SUPER ELI CONTINUOUSLY ROLLED Ti-6Al-4V SHEET

have been 10% higher or 220 ksi $\sqrt{in}$. The crack growth rates at R = 0.05, 0.5, and 0.65, for air, distilled water, and 3.5% NaCl for both the longitudinal and the transverse direction are given in figure 30. The growth rates in 3.5% NaCl are quite similar for both directions, which is contrary to past data (ref. 2) on higher oxygen continuously rolled sheet. Generally the transverse direction has significantly higher rates in salt water.

TABLE 14.–FRACTURE TOUGHNESS AND STRESS-CORROSION RESISTANCE OF SUPER ELI CONTINUOUSLY ROLLED Ti-6Al-4V SHEET

Specimen	Grain direction	K_c (ksi $\sqrt{in.}$)	Sustained K level in 3.5% NaCl (ksi $\sqrt{in.}$)
ST-310-3	Longitudinal	177.0	
ST310-4	Longitudinal		No failure 159 Failure 177 (50 sec)
ST-310-1	Transverse	199.4	
ST-310-2	Transverse		No failure at 180, 200, 219 Failure at 239 (40 sec)

To evaluate the effect of furnace cooling through the α_2 region, two 3- by 12-in. single-edge-notched specimens were tested to determine K_{scc} after the following thermal cycle:

1350° F/1 hr/furnace cool at 150° F per hour to 600° F/air cool

The results are shown in table 15. The K_{scc} is approximately 92 ksi $\sqrt{in.}$, which demonstrates the immunity of this low-chemistry material to stress corrosion after furnace cooling.

TABLE 15.–SUSTAINED LOAD DATA FOR FURNACE-COOLED CONTINUOUSLY ROLLED SUPER ELI Ti-6Al-4V SHEET IN 3.5% NaCl

Specimen[a]	Grain direction	Sustained load K level in 3.5% NaCl (ksi $\sqrt{in.}$)	Results
FM 416-1	Transverse	85	No failure
		95	Failure (0 min)
FM 416-2	Transverse	90	No failure
		95	No failure

[a]Single-edge-notched specimen, 3- by 12 in.

The actual K_{scc} as tested on a wider panel would be much higher, since the 3-in.-wide single-edge notch becomes invalid at K levels greater than 80-90 ksi $\sqrt{in.}$ (see sec. 3.1.10). Although these tests do not demonstrate that the K_{scc} after furnace cooling is as high as that of the as-received condition (K_{scc} = 200 ksi $\sqrt{in.}$), the value is greater than 92 ksi $\sqrt{in.}$ and probably is much higher. This compares to a K_{scc} of 25 ksi $\sqrt{in.}$ for similar sheet with oxygen content of 0.13% and aluminum content of 6.3%. The super ELI sheet was examined for presence of α_2 (Ti_3Al) using thin-foil transmission electron microscopy, and no evidence of this phase was found. Figure 31 shows the similarity in optical microstructure for this material before and after furnace cooling, and figure 32 shows the preferred orientation after this thermal cycle. No difference is observed between this texture and that of the as-received material (fig. 29).

Specimen 405-1, super ELI, condition IC
Environment—air
Grain direction—transverse

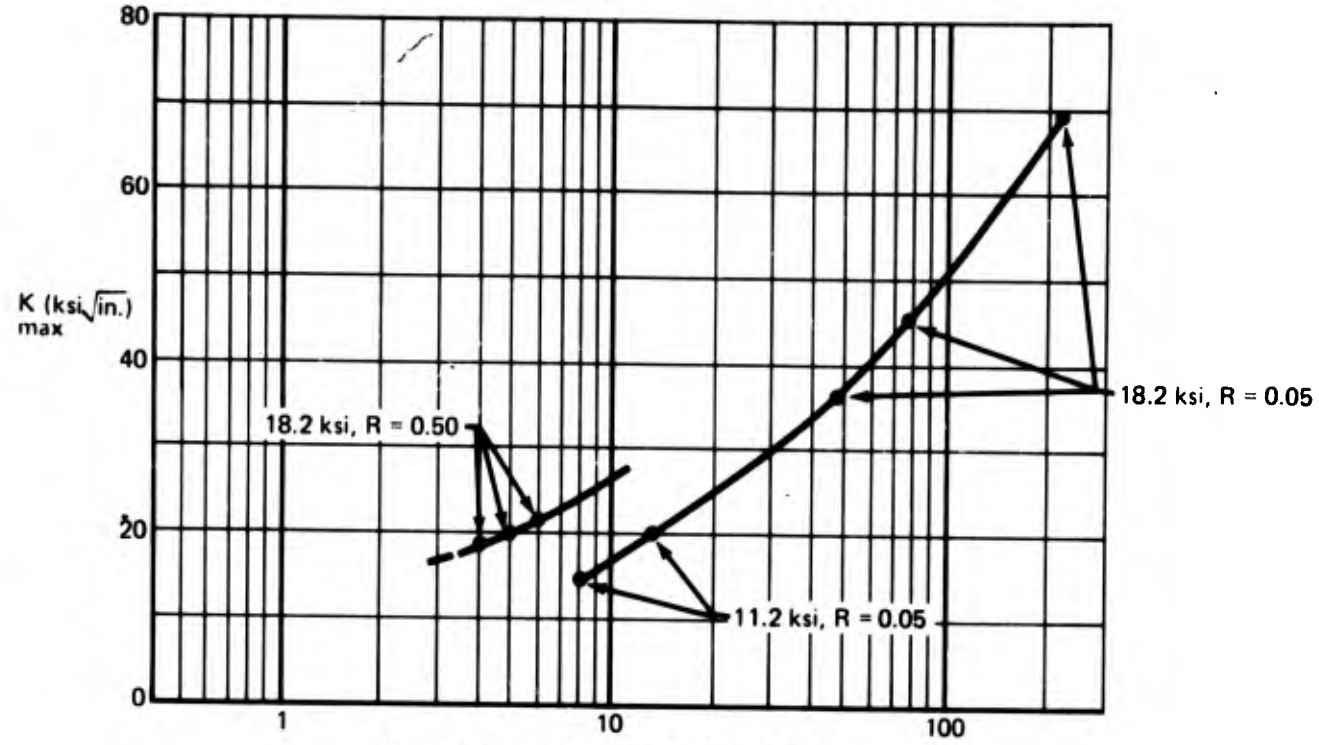

Specimen 405-3
Environment—air
Grain direction—longitudinal

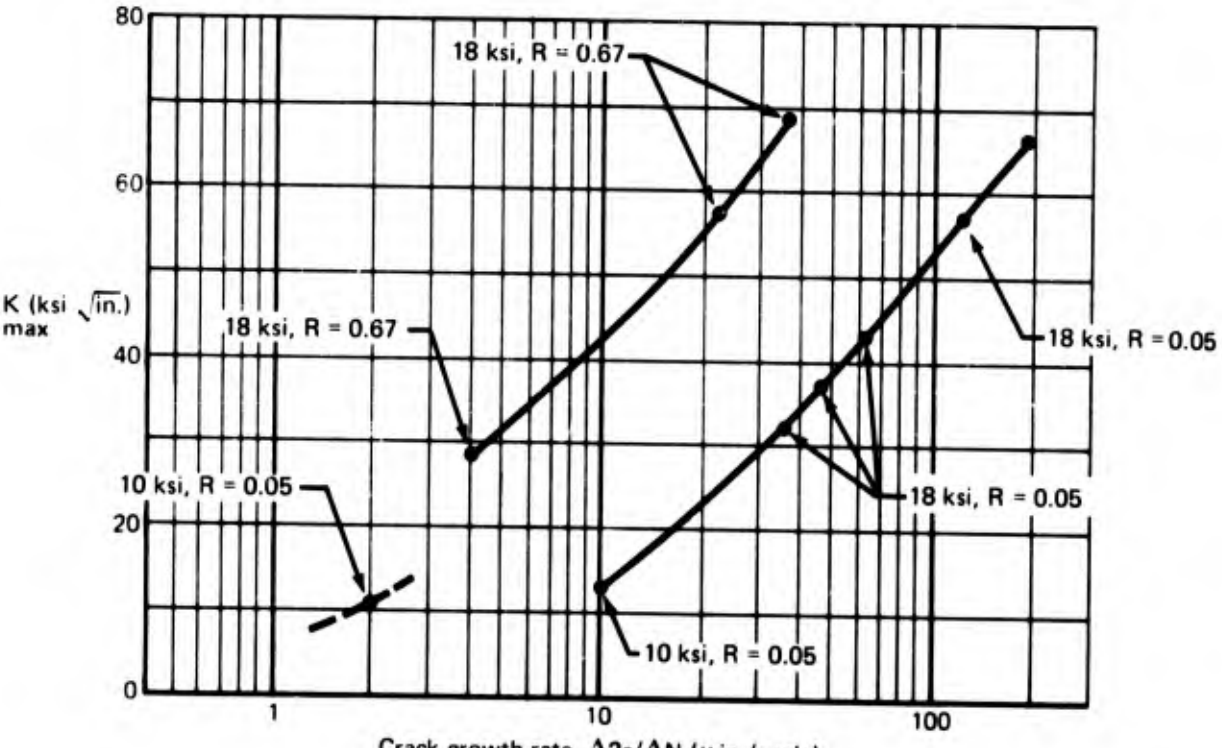

FIGURE 30.–CRACK GROWTH RATES FOR SUPER ELI CONTINUOUSLY ROLLED Ti-6Al-4V SHEET, HEAT K6338

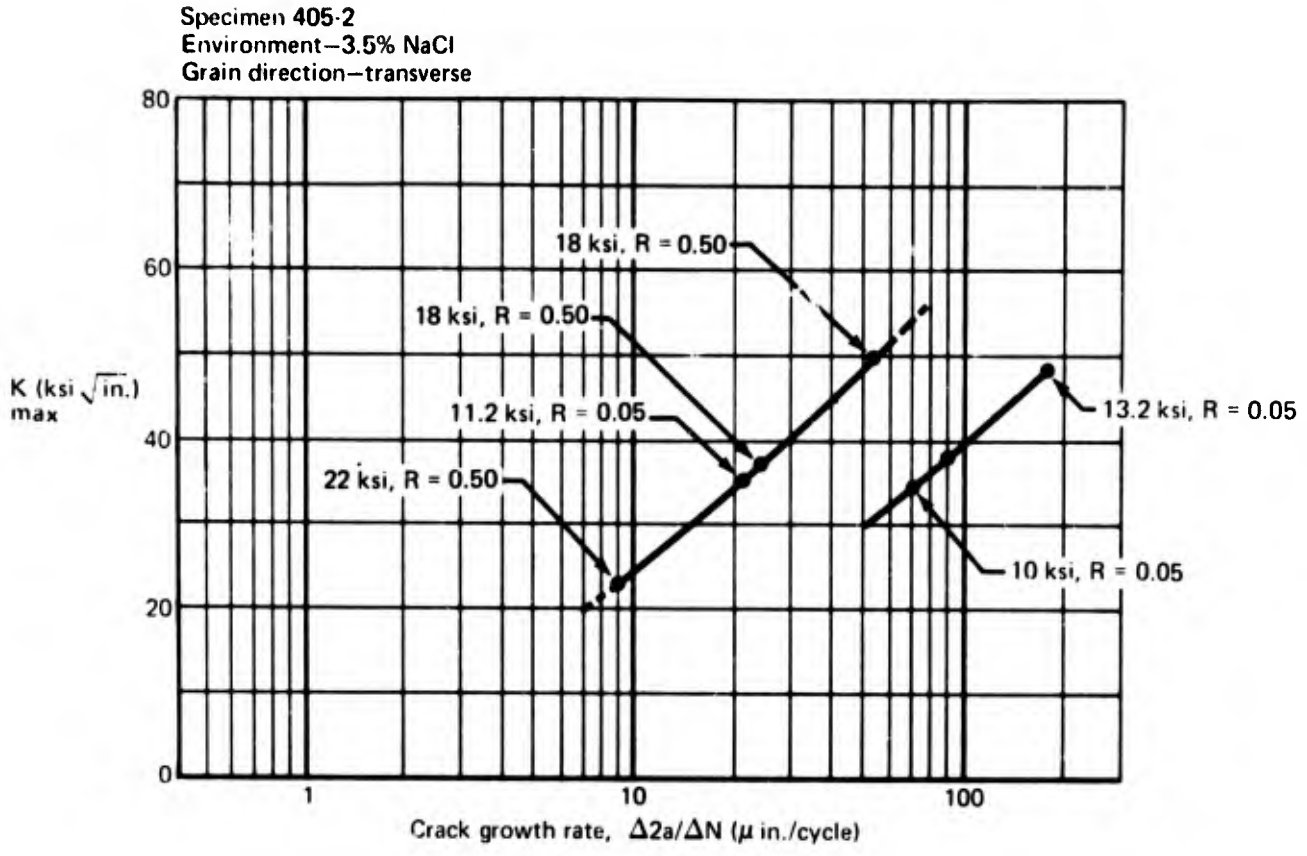

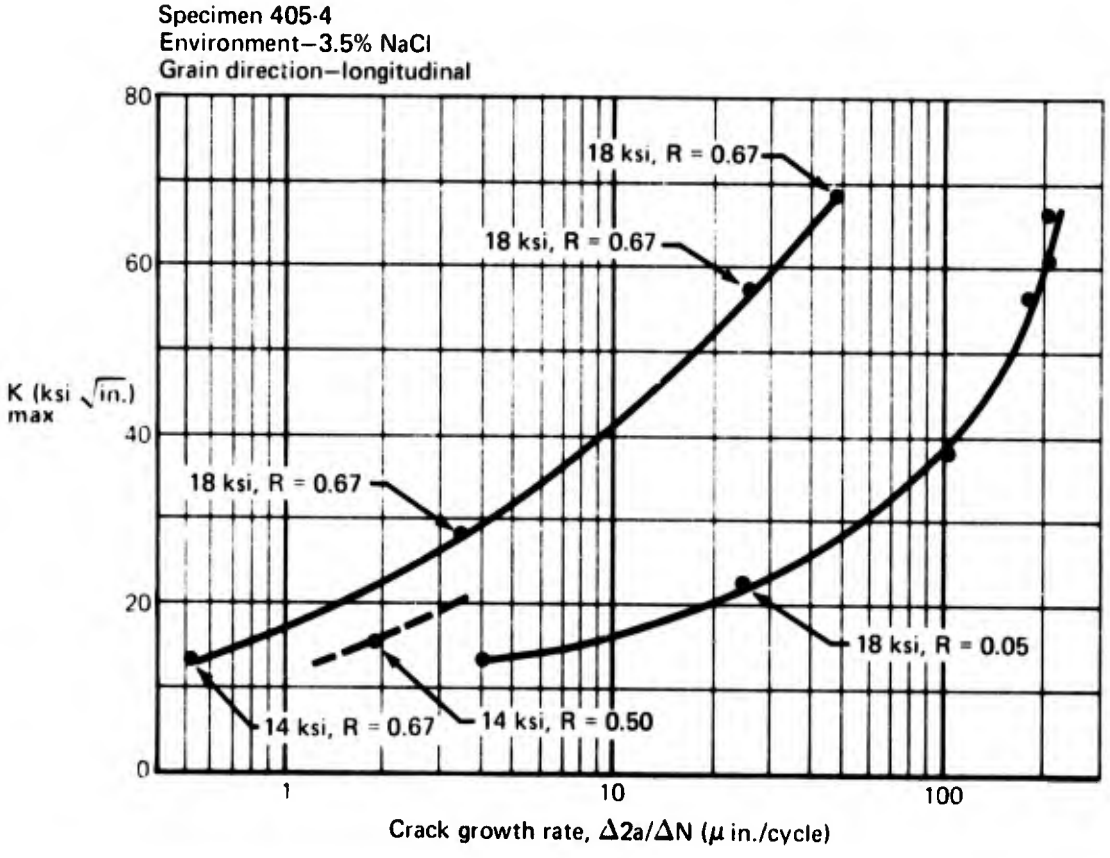

FIGURE 30.—CONCLUDED

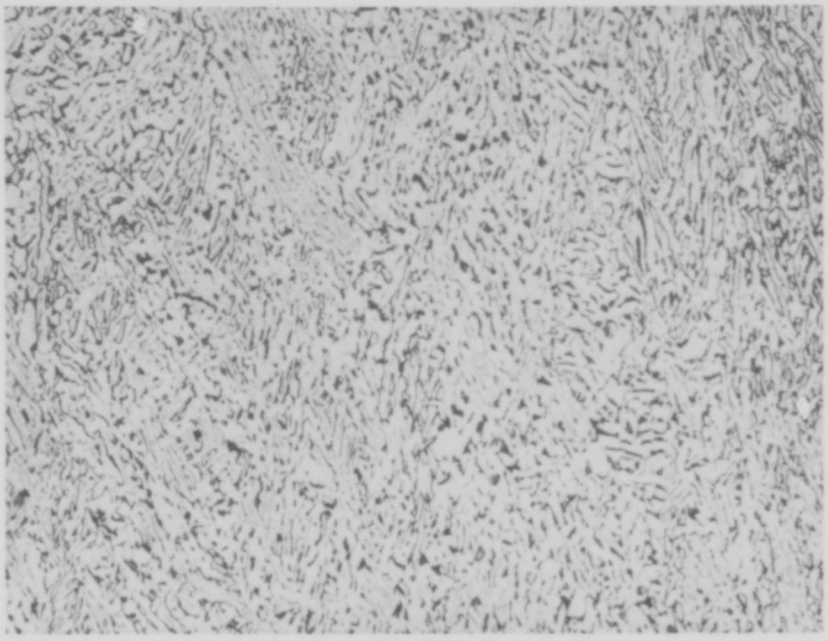

As Received

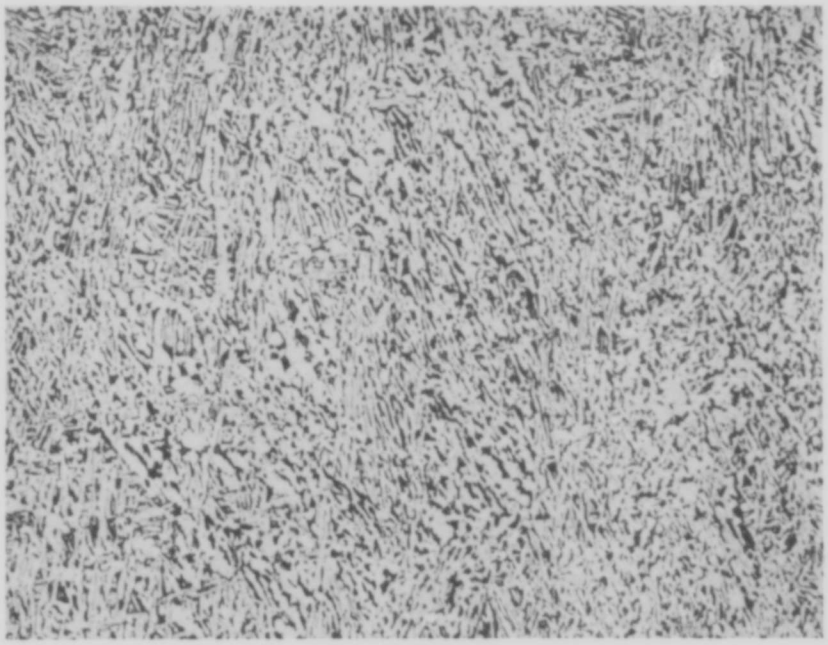

After 1350° F/1 hr/Furnace Cool To 600° F at 150° F/hr.

FIGURE 31.—OPTICAL MICROSTRUCTURE FOR SUPER ELI CONTINUOUSLY ROLLED Ti-6Al-4V SHEET BEFORE AND AFTER COOLING FROM 1350° F (X500)

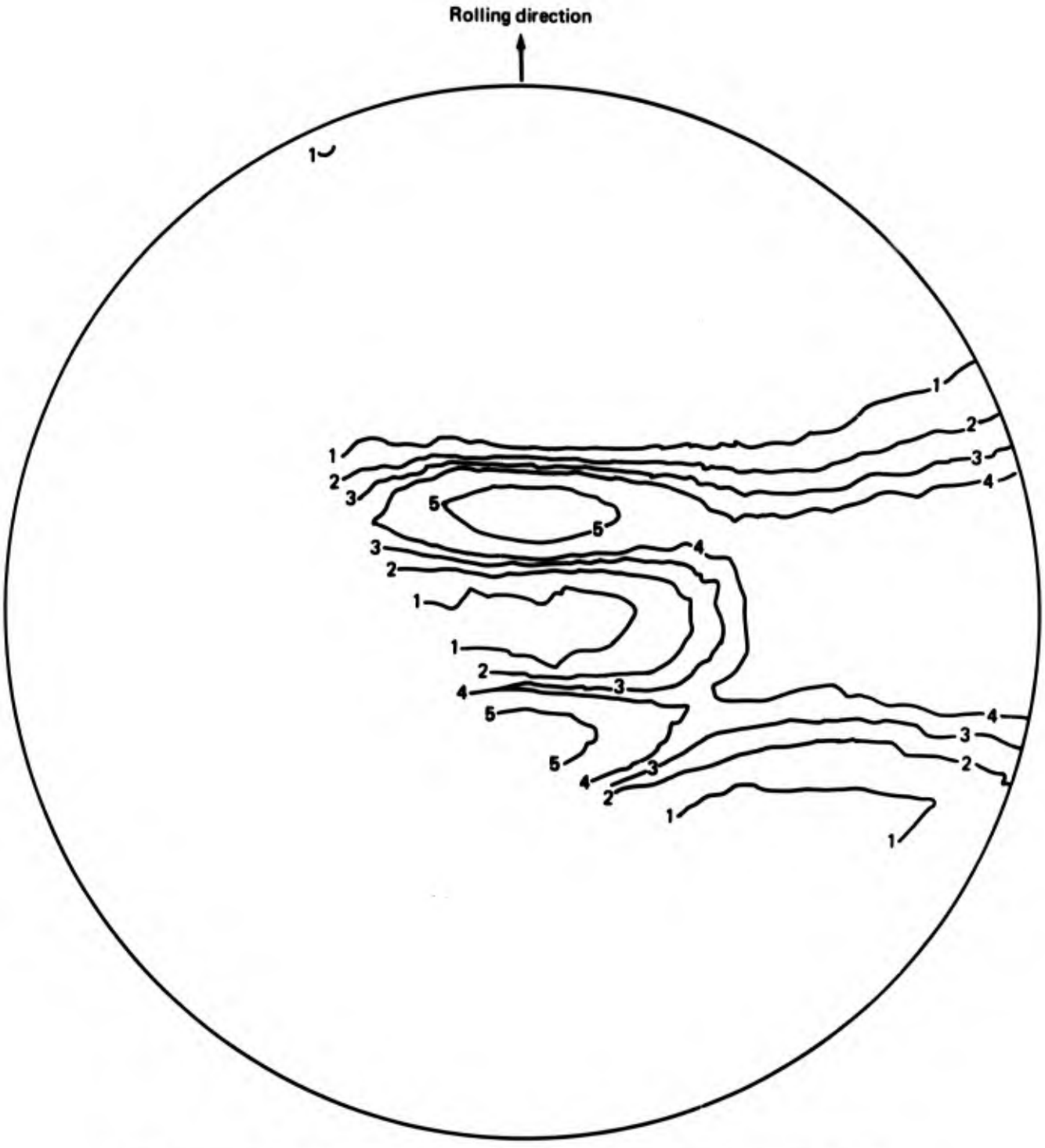

Contour lines	1	2	3	4	5	6
Times random intensity	0.5	1.0	1.5	2.0	4.0	8.0

$K_A = 115$

FIGURE 32.–BASAL PLANE (0002) POLE FIGURE FOR SUPER ELI CONTINUOUSLY ROLLED Ti-6Al-4V SHEET AFTER FURNACE COOLING AT 150°F/HR FROM 1350°F TO 600°F

In summary, the super ELI continuously rolled sheet is very tough and is not susceptible to K_{scc} degradation due to α_2 formation after furnace cooling. The strengths are, of course, lower than for the higher chemistry material, but the ultimate tensile strength would probably support a design "A" allowable of 115-120 ksi.

3.1.9 Effect of Salt Water Concentration on K_{scc}

The effect of various salt water concentrations on the K_{scc} of a highly susceptible Ti-6Al-4V sheet was determined by sustained loading precracked specimens in salt water with NaCl concentrations of 3.5%, 0.35%, 0.035%, and 0.0035%. Tests were also conducted on distilled water and on rain water collected from the Duwamish River in Seattle, Washington. The tests were conducted on sheet 21016, heat 310487, in which the K_{scc} (3.5% NaCl) had been determined to be approximately 35 ksi $\sqrt{in}$. The results are shown in table 16 and plotted in figure 33. For this susceptible material the K_{scc} is markedly influenced by the percentage of NaCl in the sustained load aqueous environment.

TABLE 16.–SUSTAINED LOAD DATA FOR Ti-6Al-4V SHEET IN VARIOUS SALT WATER ENVIRONMENTS

Specimen	Environment	Sustained load K level (ksi$\sqrt{in}$)[a]	K_{scc} (ksi$\sqrt{in}$)
FM 986-1 -2	3.5%Nacl	NF 35,F (0.85) F 40 (5)	37
-3 -4 -7	0.35%Nacl	NF 35 NF 35, F43.5 (5.5) F 50 (7)	38
-5 -6	0.035% Nacl	NF 50, F65 (0) NF 35, F 55 (6)	52
-7 -3 -8	0.0035% Nacl	NF 35 NF 50,F65 (0.11) NF 55, F60 (6)	57
-9	Seattle rain water	NF 50, F65 (10.5)	57
-10	Distilled water	NF 63, F66 (5)	64

[a]NF - No failure after 60 min
F - Failure (time to failure in minutes)

Two effects at the extreme ends of the concentrations investigated were observed. At the high NaCl levels, the 0.35% level results in the same low K_{scc} (37 ksi $\sqrt{in}$.) as the conventional sea water standard of 3.5%. However, at the 1000 to 1 dilution of 0.0035% NaCl the K_{scc} was similar to the distilled water test result (57 ksi $\sqrt{in}$.). The 100 to 1 dilution (0.035%) produced an intermediate K_{scc} of 52 ksi $\sqrt{in}$. Although no K_c tests were conducted on the 3-in.-wide single-edge-notched specimen, prior tests (ref. 2) on this same sheet of material had given a K_c of 90 ksi $\sqrt{in}$. for a 12-in.-wide center-cracked panel test. The ratio of K_c (3-in. single-edge notch) to K_c (12-in. center notch) is approximately 0.8 (sec. 3.1.10). This would give a K_c of 72 ksi $\sqrt{in}$. for the same 3-in.-wide specimen used for the salt water tests. Although this value is an approximation of K_c, there appears to be a reduction of only 10% (64 versus 72 ksi $\sqrt{in}$.) over K_c for sustained loading of this material in distilled water.

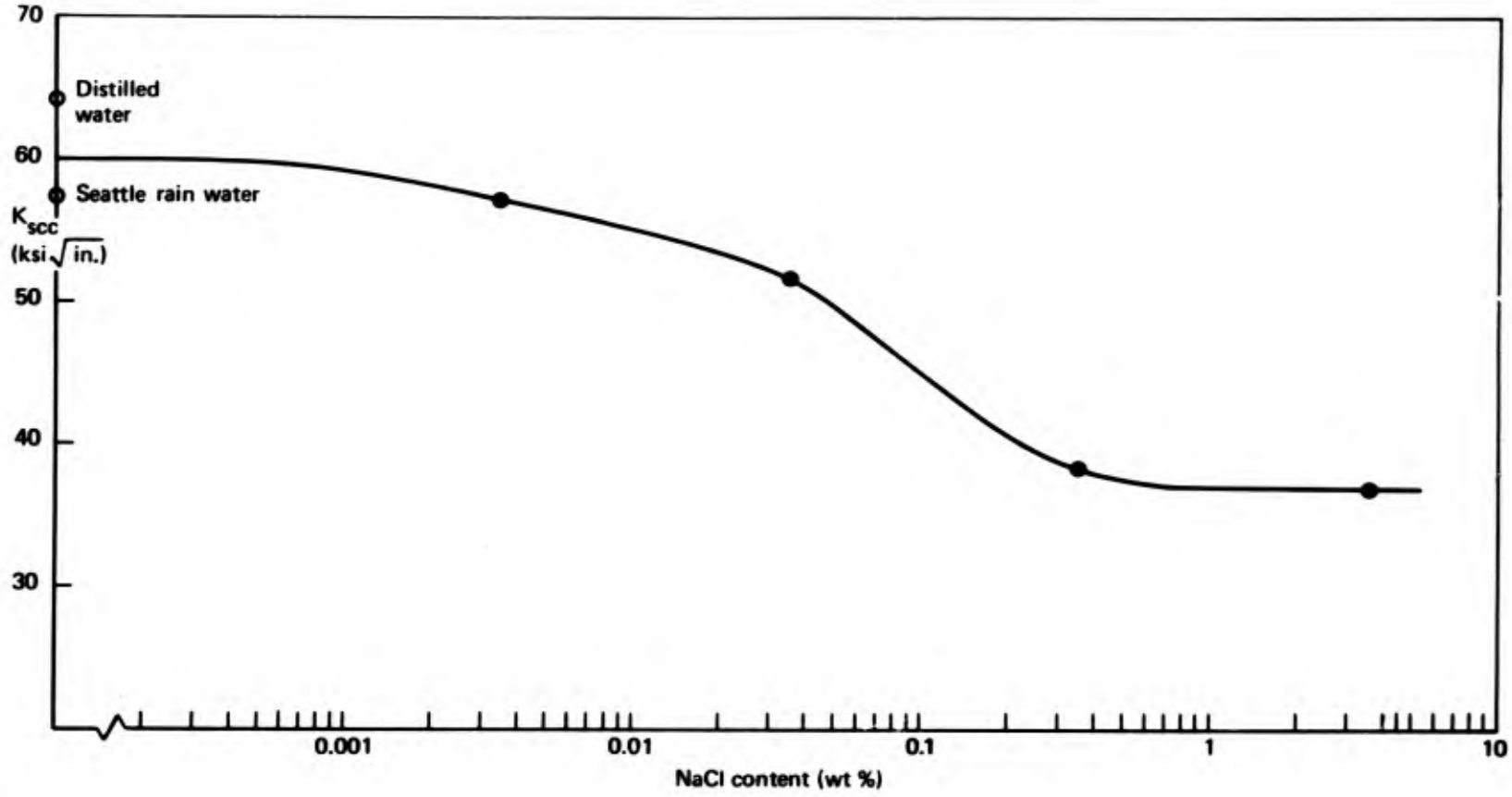

FIGURE 33.– EFFECT OF SALT WATER COMPOSITION ON K_{scc} OF HAND-MILL Ti-6Al-4V SHEET (S/N 21016)

The fracture failure modes were determined using electron microscopy replication techniques and are shown in figure 34. Although there were cleavage zones present in all of the specimens tested in salt water, the amount of cleavage generally increased as the NaCl percentage increased. There was no evidence at all of cleavage in the distilled water tests. It is interesting to note that although the reduction in K_{scc} of the 0.0035% NaCl test over the distilled water test was only 7 ksi$\sqrt{in}$. there was evidence of cleavage in the former test.

3.1.10 Effect of Width of Test Specimens on K_{scc} Results

To determine the effect of specimen width on K_{scc} results, three sheets of material were tested using the single-edge-notched specimen with widths varying from 1 to 6 in. The three sheets selected had varying degrees of susceptibility to NaCl content so that this effect could also be examined. These data are given in table 17 and plotted in figure 35. As expected, the largest difference between the 3-in. single-edge-notched and 12-in. center-cracked panels was obtained for the least susceptible material. For a K_{scc} of 72 ksi$\sqrt{in}$. determined on the single-edge-notched specimen, the value for the 12-in. panel was 130 ksi$\sqrt{in}$. This results in a significant amount of built-in conservatism for the higher K_{scc} values reported using the 3-in.-wide specimen (sec. 3.1.1). Only in one out of the three cases was the K_{scc} of the 6-in.-wide single-edge-notched specimen equal to that of the 12-in.-wide panel. This is somewhat surprising since a single-edge-notched specimen of width W has exactly the same crack configuration, loading system, and stress state as a center-cracked panel of width 2W. This result was also observed in previous dynamic tests where both K_c and a dynamic test to failure in salt water (K_{salt}) were determined for various widths of single-edge-cracked specimens. Figure 36 shows the results of these tests. Again, the wider (5 in.) specimens had lower values than the 12-in.-wide center-cracked panel.

3.1.11 Comparison of Macro and Micro Crack Growth Rates

The correlation between macro and micro crack growth rates was determined using typical data gathered by actual crack length measurement during cycling and striation spacing obtained using electron microscopy replication techniques. Several center-notched panels were evaluated which had been fatigue cracked in air and in 3.5% NaCl at R values of 0.05 and 0.67. The panels evaluated, with detailed descriptions, are shown in table 18. Figure 37 shows an example of a curve for panel FM 292-32, which was cycled in air at 120 cpm at an R value of 0.67. Appendix D shows the curves for all the other panels evaluated. Figure 38 shows photographs of the striations obtained using the replication technique. The correlation in general was excellent for virtually all the R values and environments investigated, for both the beta-annealed plate and the hand-mill and continuously rolled sheet. Since there are numerous regions of ductile tearing surrounding the regions of fatigue striations, the replication technique often overestimates the total number of cycles. This occurs because a larger number of cycles would be required for the crack to propagate by fatigue than are required for ductile rupture. The total cycles are obtained by summing over the entire crack length, assuming that the entire crack propagated by fatigue growth. However, although there is this possibility of total cycles being overestimated, it was not observed during this test. Also the difference between the acicular microstructure (beta-annealed plate) and the other mixed acicular plus equiaxed primary alpha (sheet) microstructure did not prevent the good correlation between the two methods.

3.5% NaCl

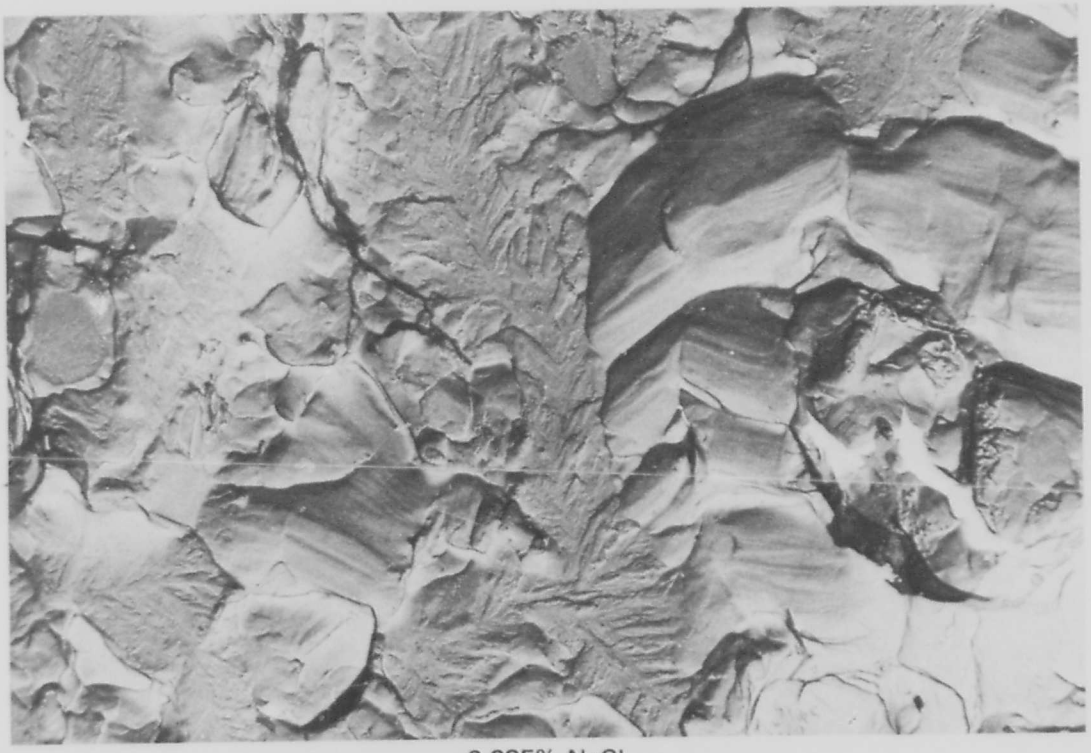

0.035% NaCl

FIGURE 34.–FRACTURE FACES OF SUSTAINED LOAD TESTS OF Ti-6Al-4V SHEET (HEAT 310487) IN VARIOUS % NaCl (X4400)

0.0035% NaCl

Distilled Water

FIGURE 34.–CONCLUDED

TABLE 17.–EFFECT OF WIDTH ON K_{scc} OF Ti-6Al-4V SHEET–TRANSVERSE DIRECTION (12-IN.-LONG SINGLE-EDGE-NOTCHED SPECIMEN)

Specimen	Heat	Sheet	SEN width (in.)	K_{scc} (ksi$\sqrt{in.}$)
E-1, 2	295377	"E"	0.5	37
E-3			1.0	37
E-4			2.0	59
E-5			3.0	72
E-6			4.0	72
E-7			6.0	91
FM 963 E			12-in. CNP	130
I-1, 2	295377	I 71081	0.5	46
I-3			1.0	47
I-4			2.0	46
I-5			3.0	48
I-6			4.0	49
I-7			6.0	58
FM 963 I			12-in. CNP	58
3-1, 2	310487	20	0.5	25
3-3			1.0	32
3-4			2.0	37
3-5			3.0	37
3-6			4.0	37
3.7			6.0	42
FM 939 2, 3			12-in. CNP	52

3.1.12 Receiving Inspection Data

Receiving inspection property data obtained on the SST program for Ti-6Al-4V hand-mill sheet included TYS, TUS, percent elongation, thickness, and chemical composition (O_2, N_2, H_2, C, Al, V, and Fe). The basic data including property mean, standard deviation, and maximum and minimum values were presented in another DOT report (ref. 3). Further evaluation was conducted on this data using a computerized multiple regression analysis technique. Equations were developed for TUS, TYS, and percent elongation, as a function of gage, O_2, N_2, H_2, C, Al, V, and Fe. Data were analyzed for both the longitudinal and transverse directions. The equations developed were of the form:

$$\text{Property} = A+B(\text{gage}) + C(O_2) + D(N_2) + E(H_2) + F(C) + G(Al) + H(V) + K(Fe)$$

where gage is in inches and the alloying elements are in weight percent. The correlation coefficients A, B,...K were determined along with the standard deviation for these coefficients. If the coefficient for N_2, D, had a value of +200 but a standard deviation of, say, 500 the statistical significance of the coefficient is then very low. If the standard deviation of the coefficient was greater than the coefficient itself the variable was not used in the equation.

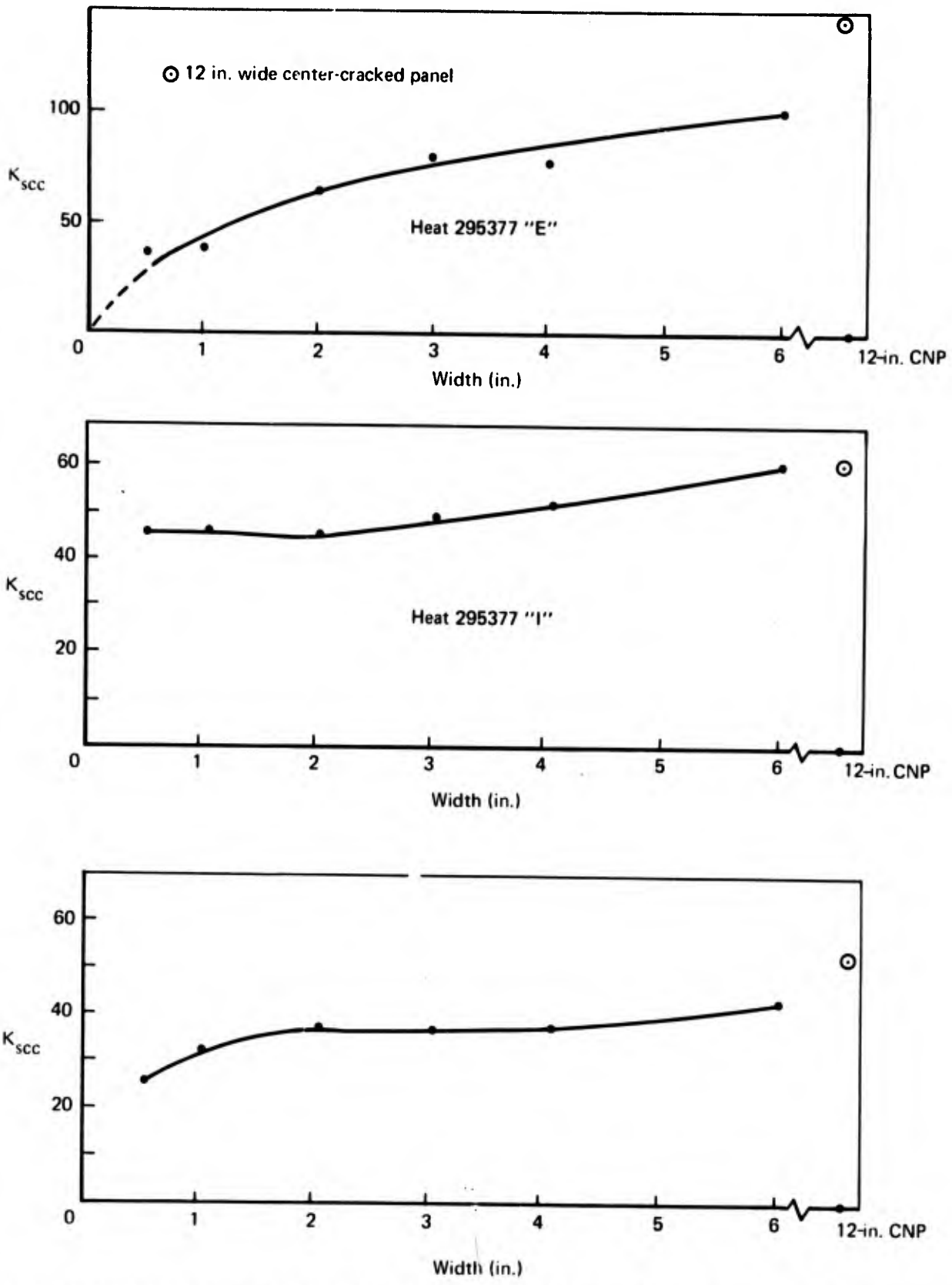

FIGURE 35.–EFFECT OF SINGLE-EDGE-NOTCHED SPECIMEN WIDTH ON K_{scc} OF Ti-6Al-4V SHEET

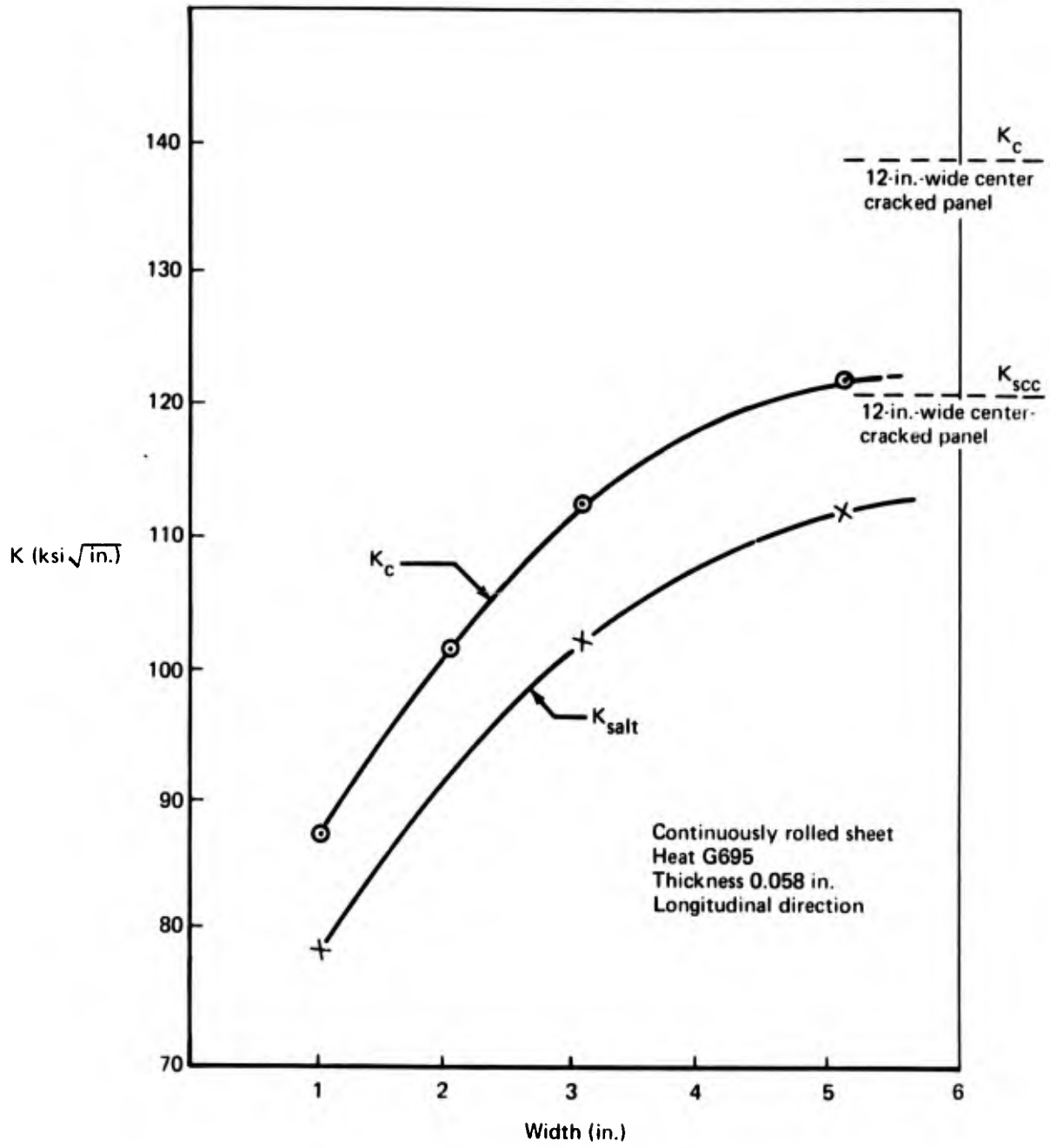

FIGURE 36.–EFFECT OF SINGLE-EDGE-NOTCHED SPECIMEN WIDTH ON K_c AND K_{SALT} OF Ti-6Al-4V SHEET

TABLE 18.—Ti-6Al-4V CENTER-NOTCHED PANELS USED FOR FATIGUE CRACK CORRELATION

Specimen	Sheet	Heat treatment	R	Cycling rate (cpm)	Environment	Crack length range	Correlation[a]
FM 883 -2-2	9233	Duplex-annealed sheet	0.05	120,30,10	3.5% NaCl	0.25-2.1	S
-4-1	12177	↓	0.67	120,30,10	3.5% NaCl	0.25-2.1	M
-5-D1	8841		0.05	120	Air	0.25-2.1	G
-5-B1	9233	Duplex-annealed sheet	0.67	120	Air	1.0 - 2.1	G
FM 891 -1	10809	Beta-annealed plate	0.05	120	Air	0.25 - 2.1	G
-2	10809	Beta-annealed plate	0.67	120	Air	1.0 - 2.1	S
-3	10809	Beta-annealed plate	0.05	120,30,10	3.5% NaCl	0.25 - 2.1	S
FM 292 -32	10685	Condition IC	0.67	120	Air	1.0 - 2.1	G

[a]Correlation between macro rates and striation spacing (see appendix D for curves)

G Good correlation
S Striation technique predicts slightly more cycles than measured crack technique
M Measured crack technique shows more cycles than striation technique

For a good correlation of variables one would desire the standard deviation to be approximately 10% or less of the coefficient. This would then result in knowing that, for a 95% confidence level, the coefficient was between 0.8 and 1.2 of the value given 90% of the time. Many of the coefficients had this quality of very low standard deviations. The multiple correlation coefficient, R, was also obtained with the parameter R^2 giving a measure of the explained variation in the dependent variable (i.e., the mechanical property) as a function of the independent variables selected. R^2 varied between values less than 0.20 to greater than 0.60, and although these lower values have little significance in actually predicting the value of the dependent variable from the independent variables used in the equations, the correlation coefficients with low standard deviation provide insight into the effect of the given independent variable. For example, if the coefficient for oxygen is +50 with a standard deviation of 5 in an equation for TUS, and R^2 is only 0.30 for the entire equation, the relationship between TUS and O_2 is still well known even though the total variation in TUS is not well explained by all the variables selected.

A major problem with any regression analysis technique lies with the accuracy and total variation of the input data. Although the accuracy of the chemical analyses used might be considered sufficient for a receiving inspection program, the techniques used in obtaining these data were not sufficiently accurate to provide high R^2 values and low correlation coefficient standard deviations. Also, many of the elements such as N_2, C, and V did not have sufficient range to provide for a sensitive analysis. A large amount of the data was also not normally distributed. All of these factors contribute to a reduction in the statistical significance of the regression analysis technique; however, much information is obtained from this approach.

Appendix E shows the results of the regression analysis for all the properties and independent variables (gage, chemical composition) evaluated. Almost all of the coefficients for N_2, H_2, and C had standard deviations larger than the coefficient. The following hand-mill sheet equations are presented for TUS, TYS, and percent elongation for both longitudinal and transverse directions using only those independent variables having coefficient standard deviations less than the coefficient (units are ksi, inches, and weight percent).

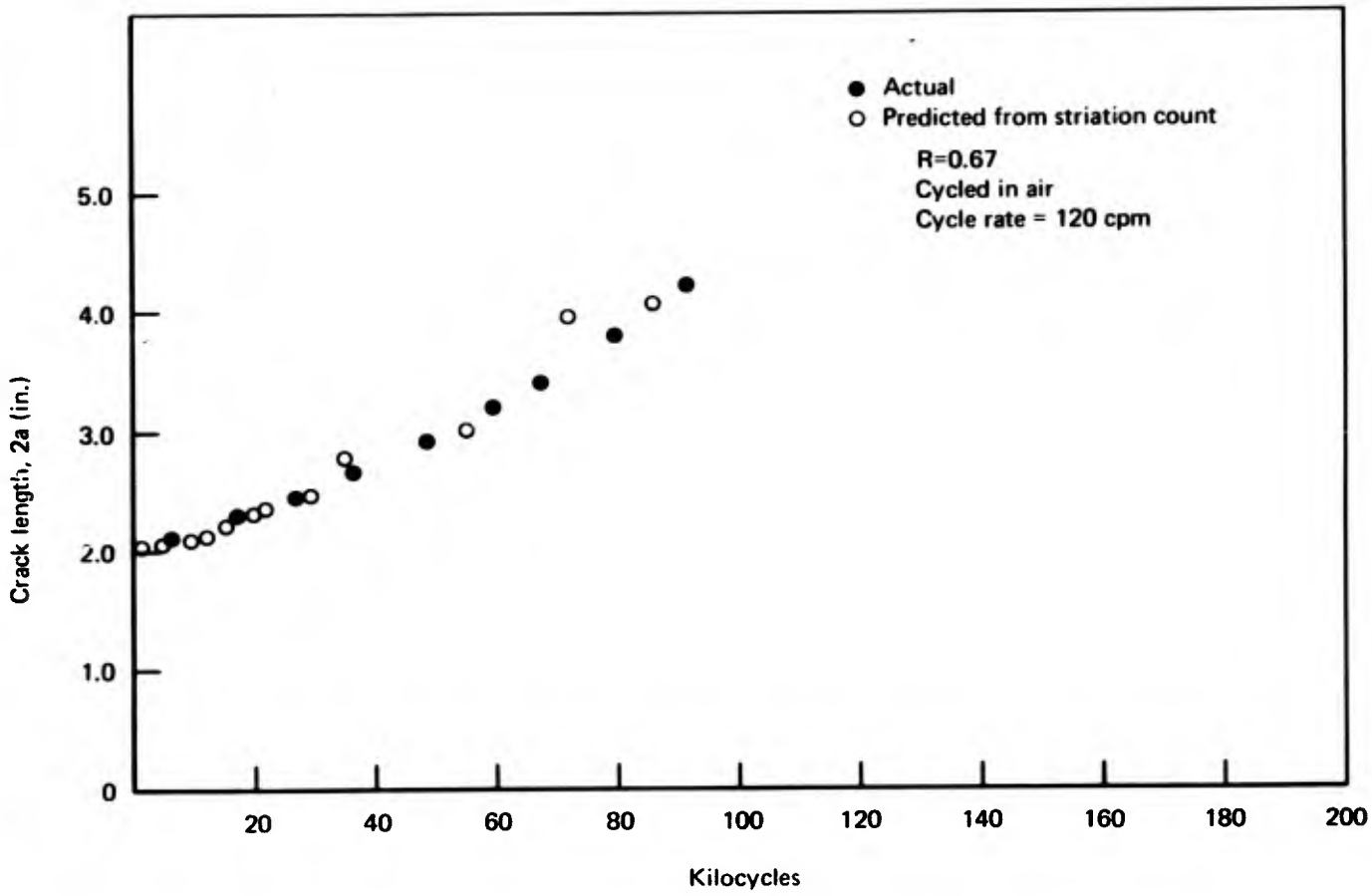

FIGURE 37.—COMPARISON OF CRACK LENGTH VS CYCLES FOR ACTUAL CRACK MEASUREMENT AND ELECTRON MICROSCOPY TECHNIQUE USING STRIATION SPACING

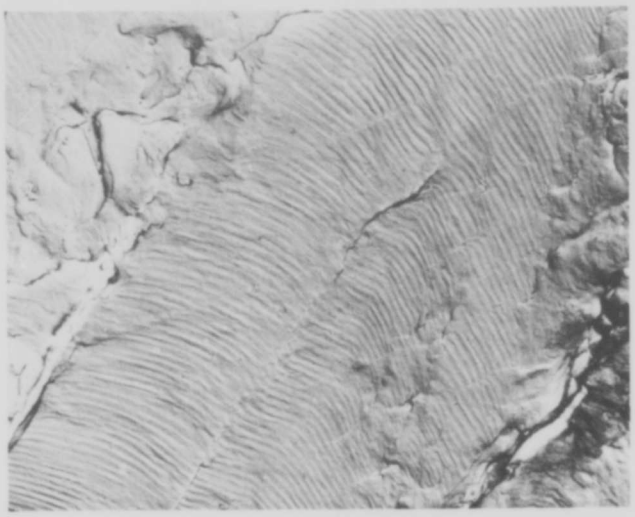

Panel FM 883-5B1, R=0.67, 120 cpm, air, a=1.18 in.

Panel FM 883-B1, R=0.67, 120 cpm, air, a=1.88 in.

FIGURE 38–FATIGUE CRACK STRIATION SPACING USING ELECTRON MICROSCOPY REPLICATION TECHNIQUE (X3400)

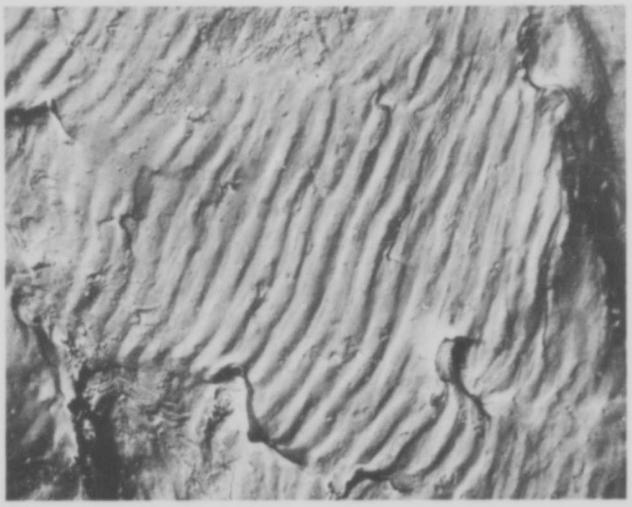

Panel FM 883-2-2, R=0.05, 120,30,10 cpm, 3.5% NaCl, a=0.26 in.

Panel FM 883-2-2, R=0.05, 120,30,10 cpm, 3.5% NaCl, a=0.31 in.

FIGURE 38.–CONCLUDED

TUS =

- Longitudinal: 137.1 - 45.4(gage) + 63.8(O_2) - 0.70(Al) + 4.80(V) + 9.55(Fe)
- Transverse: 124.8 + 24.1(gage) + 80.4(O_2) + 0.67(Al) + 0.76(V)

TYS =

- Longitudinal: 110.0 - 80.1(gage) + 49.2(O_2) - 0.437(Al) + 6.49(V) + 13.4(Fe)
- Transverse: 99.5 + 21.2(gage) + 85.7(O_2) + 261(C) + 1.25(Al) + 2.59(V)

Percent elongation =

- Longitudinal: 15.2 + 9.46(gage) + 7.90(O_2) - 0.372(Al) - 0.335(V) - 1.57(Fe)
- Transverse: 8.61 + 21.7(gage) + 9.36(O_2) + 0.071(Al) - 0.024(V) - 4.57(Fe)

As expected, the effect of gage on strength for the longitudinal direction is negative. However, for the transverse direction there appears to be the anomalous behavior of increased strength with increased gage. This is a result of the preferred orientation. The thicker sheet purchased for the SST was generally longer than the thinner sheet, as described elsewhere (ref. 3), and generally had a texture with a large number of basal planes aligned perpendicular to the transverse direction. This results in higher strengths in the transverse direction and in the equation shows up only as an effect of gage, since preferred orientation was not measured during receiving inspection. If the equations were determined using a factor which allowed for this effect (i.e., ΔTYS) the real effect of gage would be demonstrated.

The effect of oxygen was quite consistent with an average increase of 7 ksi per 0.1% increase in O_2, for both TUS and TYS and for both directions. Only one equation (transverse TYS) showed a carbon effect. The carbon content was very consistent and varied little between 0.020% and 0.022%. A slight increase of only 0.002% would result in a transverse TYS increase of 0.5 ksi, which shows the potent strengthening effect of the impurity element, C. The aluminum effect was mixed, the coefficients being negative for the longitudinal and positive for the transverse direction. However, the coefficients were quite small (0.4 to 1.2), and since the normal variation in aluminum content was from 5.8% to 6.3%, the variation in strength due to aluminum variations would be only (1.0 ksi/% Al) x (0.5% ΔAl) = 0.5 ksi. The effect of vanadium was more significant than that of aluminum, the average coefficient being +3.7 ksi/% V. In two cases there was a significant Fe effect, the average coefficient for the longitudinal TYS and TUS being +12.5 ksi/% Fe. The variation in Fe is generally 0.1%, which could account for over 1 ksi strength effect.

The ductility of hand-mill sheet was significantly affected by gage. Here the coefficients were +9.5% and +21.7% elongation per inch of gage increase for the longitudinal and transverse directions, respectively. This is as expected since for the thinner gages (especially below 0.035 in.) the inability of the material to deform plastically in the thickness direction results in very low percent reduction in area values and hence low percent elongation values. One quite surprising result is the increasing effect of oxygen on ductility. The coefficients are both positive (+7.90 and 9.36) for the longitudinal and transverse directions, respectively.

The answer probably lies in the fact that although the standard deviations for these coefficients are less than the coefficient, they are not significantly less (7.42 and 6.90) than the above respective coefficients. Using the longitudinal direction, for example, we can say with 95% confidence that 66% of the time the coefficient will be in the range of approximately 0 to 15 (±1 standard deviation). Although this range is still positive, it is wide and leads us to question the result from statistical considerations. Also, from a physical standpoint oxygen is known to be a strengthener, and generally increased strength means decreased ductility. Therefore, until further work confirms or rejects this effect few conclusions on the oxygen ductility effect can be made. The effect of the other variables (Al, V, and Fe) although statistically significant (low coefficient standard deviation) did not significantly contribute to ductility variations when the range of these independent variables are considered. The general ranges for these elements are 5.8%-6.3%, 3.9%-4.2%, and 0.10%-0.20% for Al, V, and Fe, respectively. This would result in only a 0.1%, 0.06%, and 0.3% variation in ductility for the three respective elements. Of these three, the 0.3% reduction in ductility due to Fe variations might be considered mildly significant. It must be realized that any of these equations only hold for the range of variables investigated, and extrapolation outside of this range could lead to large errors.

Appendix E also includes the coefficients obtained for the receiving inspection property data for continuously rolled sheet. However, because texture was not considered and because there were only 65 data compared to over 700 for hand-mill sheet, the standard deviations were almost always higher than the coefficients themselves. For this reason no trends or conclusions can be established from this analysis.

3.2 Ti-6Al-4V PLATE

Most of the Ti-6Al-4V plate evaluated was either beta rolled (as-received) or beta annealed. Some tests on alpha-plus-beta-rolled plate were conducted for comparison with the beta-processed plate. The properties evaluated include fracture toughness (both K_Q and K_{Ic}), K_{Iscc}, and E_T. The fracture properties of plate exposed to a typical diffusion bonding cycle were also examined. The K_{Iscc} of STA 1000° F and also preliminary data on a modified K_{Iscc} test are presented.

3.2.1 Fracture Toughness

3.2.1.1 Effect of Microstructure

The effect of microstructure on the fracture toughness of Ti-6Al-4V plate was evaluated using 0.48-in.-thick notched bend specimens. Two annealed plates were evaluated in both the alpha-plus-beta-worked condition (equiaxed primary alpha microstructure) and the beta-annealed condition (acicular or transformed beta microstructure). The material used was as follows:

Sheet	Heat	Plate thickness (in.)	Al (wt %)	O_2 (wt %)
7918	D7390	0.500	6.6	0.18
1486	292030	0.750	6.3	0.11

Both these plates were in the alpha-plus-beta-rolled and mill-annealed condition. The basal plane pole figures are shown in figures 39 and 40 for these plates. The results of the fracture testing are shown in table 19. The large increase in K_Q due to beta annealing can be seen for both the low- and high-oxygen-content material over the K_Q of the as-received material. This effect is more pronounced than the directionality effects for any one specimen. That is, the difference between the K_Q for the WR and RW directions is not as pronounced as this microstructural effect. Texture appears to have a slight effect on the alpha-plus-beta-worked specimens, since in plate 7918 the RW direction had a 25% increase in K_Q over the WR test direction.

The K_Q results for the low-oxygen-content plate (1486) are reported, although they are probably not meaningful. A typical load deflection curve for this material is shown in figure 41. The 5% secant load measurement, P_5, is approximately 40%-50% of the maximum load due to the rollover of the curve. Plate 7918 and all beta-annealed tests had P_5 of approximately 90% of the maximum load. Hence, these values of fracture toughness for as-received plate 1486 cannot be compared to the other results. The actual fracture toughness for plate 1486 is undoubtedly much higher than that for plate 7918 since the oxygen contents and yield strengths are much lower.

3.2.1.2 Valid K_{Ic} Test

K_{Ic} tests which met the validity requirements of ASTM E-399-70T were conducted on 0.6- and 1.0-in. beta-annealed plate by electron beam welding 2.5-in.-thick grip ends onto the plates. These 2.7- by 6.5- by 6.5-in. welded blocks were stress relieved and then fabricated into a 2.5-in.-thick compact tension specimen per ASTM E-399. Tests were also conducted on 0.48-in.-thick notched bend specimens for the same material. The test results are shown in table 20. The ratio of K_Q (0.480-in. notched bend) to K_{Ic} (ASTM compact tension) was 0.84-0.88 for all heats except K0759. The K_{Ic} for the beta-annealed plate was found to be 91-104 ksi $\sqrt{\text{in.}}$ for all the plates except heat K0759. This material had moderate oxygen content (0.146%) but had a very fine-grained fracture face characteristic of material worked in the alpha-plus-beta field. This type of fracture face has been generally associated with lower fracture toughness.

3.2.1.3 Fracture Toughness, K_Q of Beta-Processed Ti-6Al-4V Plate

Tests using 0.48-in. notched bend specimens were conducted to evaluate the effect of grain direction and heat treatment on the K_Q of beta-processed Ti-6Al-4V plate. Table 21 shows the K_Q results for both the WR and RW direction for beta-rolled and annealed plate. As with the K_{Iscc} for beta-rolled Ti-6Al-4V plate (ref. 3), the K_Q is lower in the transverse direction than in the longitudinal direction for relatively high-oxygen (0.15%-0.19%) material. There is an average reduction of 8.7 ksi $\sqrt{\text{in.}}$ for K_Q compared to the average reduction of 16.1 ksi $\sqrt{\text{in.}}$ for K_{Iscc}. As was shown in reference 3, the fracture toughness is less sensitive to grain direction than is stress-corrosion resistance. The effect of heat treatment on K_Q for beta-processed plate is shown in table 22. All solution-treated-and-overaged (STOA) treatments were lower than the beta-annealed K_Q test (specimen B-1, 108.2 ksi $\sqrt{\text{in.}}$), although the difference was only 4 ksi $\sqrt{\text{in.}}$ for the average STOA results. There was no consistent trend with respect to the difference between the beta-annealed and the beta-rolled condition, although differences for individual heats were observed.

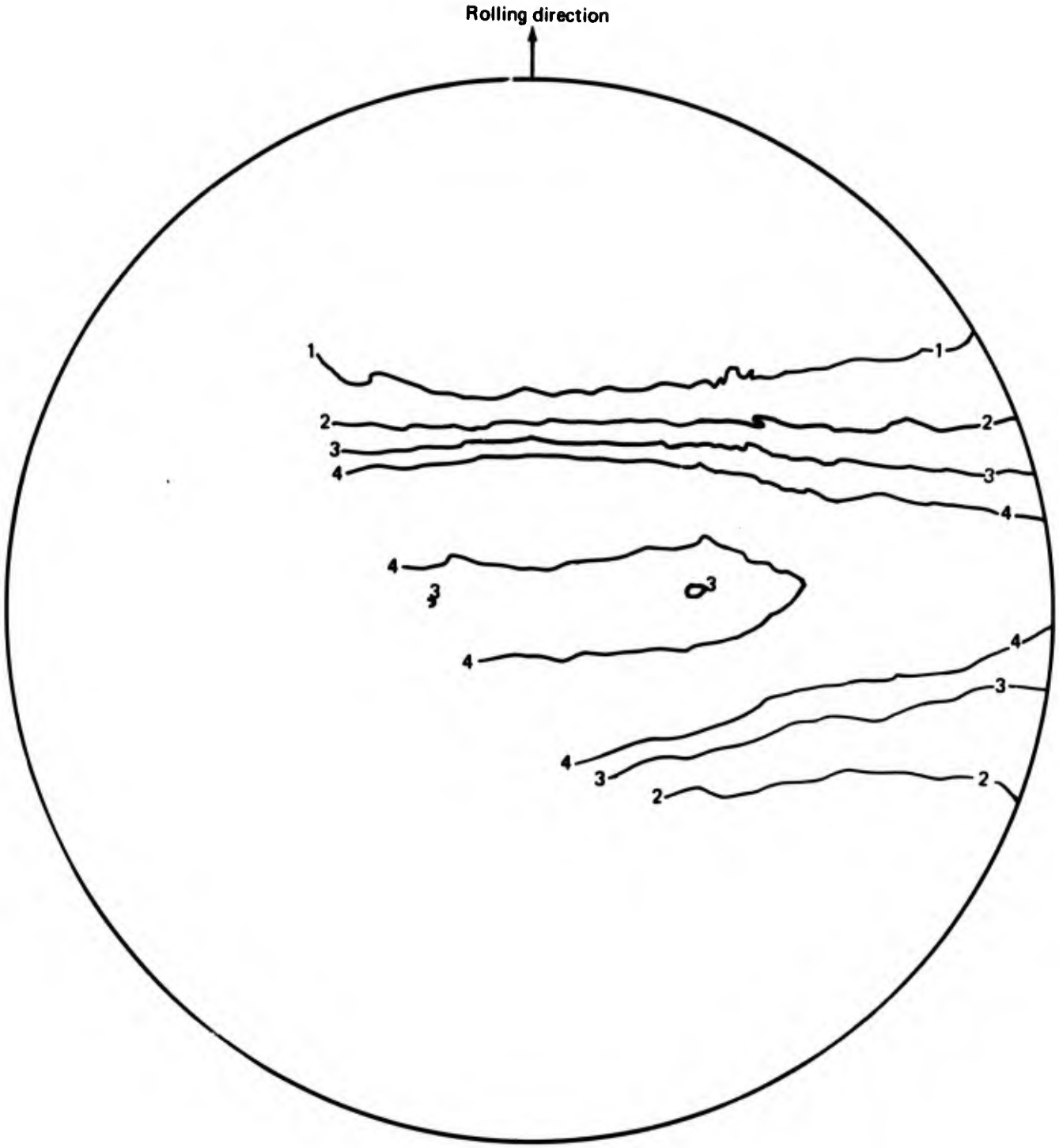

Contour lines	1	2	3	4	5	6
Times random intensity	0.5	1.0	1.5	2.0	4.0	8.0

$K_A = 100$

FIGURE 39.—BASAL PLANE POLE FIGURE FOR ALPHA-PLUS-BETA-WORKED Ti-6Al-4V PLATE 7918

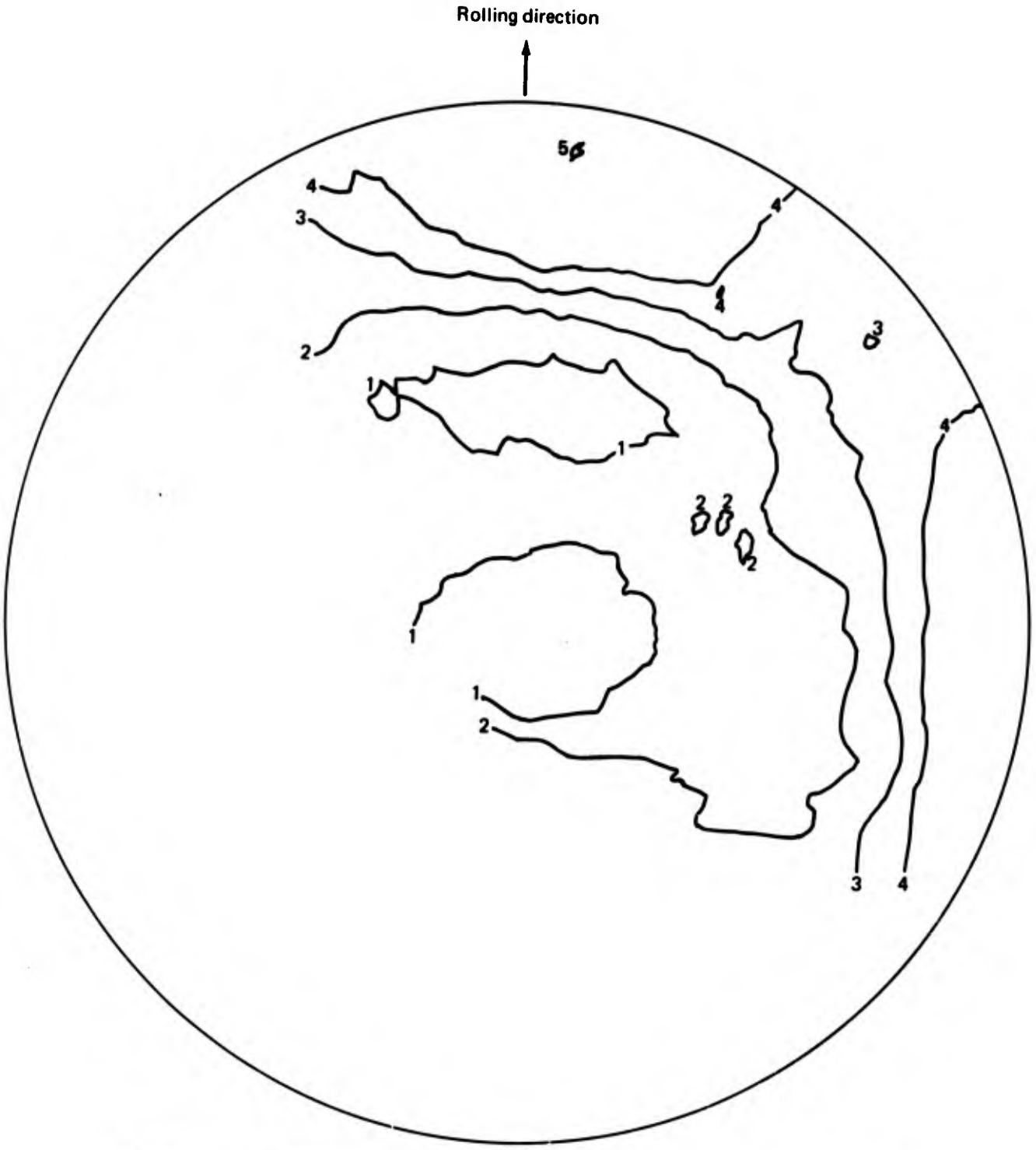

Contour lines	1	2	3	4	5	6
Times random intensity	0.5	1.0	1.5	2.0	4.0	8.0

$K_A = .17$

FIGURE 40.– BASAL PLANE POLE FIGURE FOR ALPHA-PLUS-BETA-WORKED Ti-6Al-4V PLATE 1486

TABLE 19.–FRACTURE TOUGHNESS OF ALPHA-PLUS-BETA-WORKED Ti-6Al-4V PLATE WITH AND WITHOUT A BETA ANNEAL

Specimen	Sheet	Heat treatment[a]	Grain direction	K_Q (ksi $\sqrt{in.}$)
ST 302 - B-1	7918	As received	WR	54.4
B-2	7918	As received	RW	68.5
ST 324 - DB-6	7918	As received plus beta anneal	WR	110.9
-11	7918	As received plus beta anneal	RW	93.2
ST 302 - B5	1486	As received	WR	43.4, retest 48.5[b]
-B6	1486	As received	RW	32.4, retest 52.5[b]
-A5	1486	As received plus beta anneal	WR	113.7
-B4	1486	As received plus beta anneal	RW	123.2

[a]As-received specimens are worked in the alpha-plus-beta field and mill annealed

[b]Not valid (see text)

TABLE 20.–K_{Ic} AND K_Q DATA FOR BETA-ANNEALED Ti-6Al-4V PLATE

Heat	Specimen	Plate thickness (in.)	O_2 (%)	Al (%)	K_Q 0.480-in. notched bend (ksi $\sqrt{in.}$)	K_{Ic} 2.5-in. compact tension per ASTM E399 (ksi $\sqrt{in.}$)
K7516		0.610	0.11	5.8	126.1	–
K7516	A	↓	↓	↓	98.1 (Avg 117.2)	102.1
K7516	B				121.9 (Avg 117.2)	104.3
K7516					122.6	–
295153	A	0.960	0.176	6.1	113.4	95.8
295153	B	0.960	0.176	6.1	115.4	[a]97.9
K0759	A	1.100	0.146	6.0	105.6	[ab]72.5
K0759	B	1.100	0.146	6.0	106.2	[b]67.5
K6087	A	1.000	0.15	6.3	108.6	91.2
K6087	B	1.000	0.15	6.3	103.7	91.4

[a]Fatigue crack does not extend completely to one corner

[b]Flat, fine-grained fracture not typical of beta-annealed Ti-6Al-4V

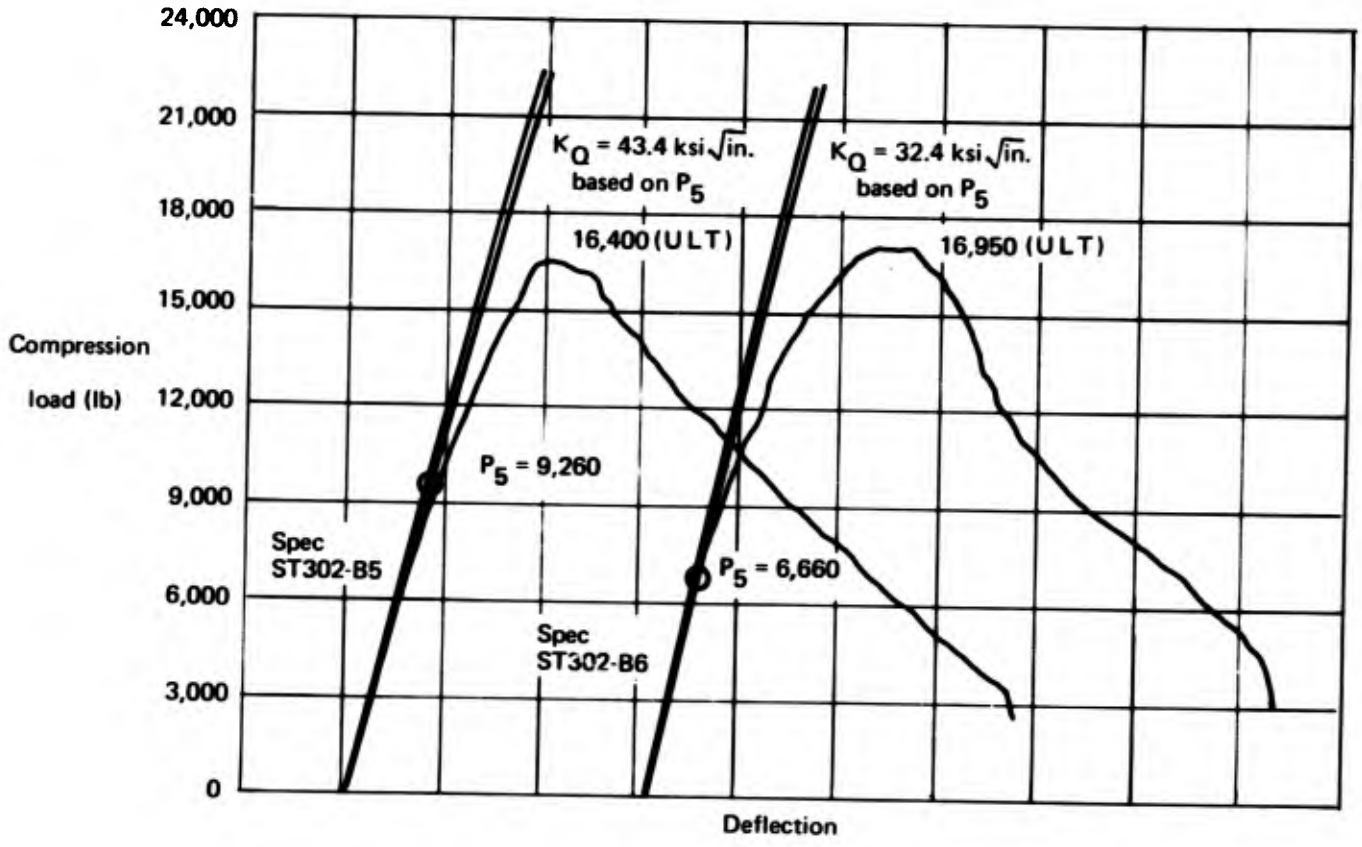

FIGURE 41.—LOAD-DEFLECTION CURVE FOR K_Q TESTS ON AS-RECEIVED PLATE 1486

TABLE 21.–EFFECT OF GRAIN DIRECTION ON K_Q OF BETA-ROLLED Ti-6Al-4V PLATE

Specimen	K_Q (ksi$\sqrt{in.}$)	Grain direction	Sheet	O_2 (%)	Al (%)	Trans-long K_Q (ksi$\sqrt{in.}$)	Trans-long K_{Iscc}[a] (ksi$\sqrt{in.}$)
FM961-3L	119.4	RW	14114	0.171	6.5	-18.2	-17
-3T	101.2	WR					
-4L	111.8	RW	14112	0.176	6.2	- 4.8	-19
-4T	107.0	WR					
-7L	116.6	RW	20103	0.15	6.3	- 9.6	- 0
-7T	107.0	WR					
-10L	121.3	RW	20113	0.19	6.4	-19.6	-19
-10T	101.7	WR					
-16L	99.6	RW	20111	0.180	6.1	+ 1.7	-31
-16T	101.3	WR					
-18L	112.0	RW	20114	0.176	6.6	- 2.0	-11
-18T	110.0	WR					

[a]Data from reference 3

TABLE 22.–EFFECT OF HEAT TREATMENT ON K_Q OF BETA-PROCESSED Ti-6Al-4V PLATE–WR DIRECTION

Specimen	Heat treatment[a]	O_2 (%)	Al (%)	K_Q (ksi$\sqrt{in.}$)	Heat
H-1B	STOA 1300°F	0.175	6.1	102.5	295153
H-2B	STOA 1400°F			99.9	295153
H-3B	Beta STOA 1300°F			101.3	295153
H-4B	Beta STOA 1400°F			106.7	295153
A-2	Beta rolled and annealed	0.189	6.5	110.0	295304
A-2B	Beta annealed			117.1	295304
N-1	Beta rolled and annealed	0.20	6.4	101.2	K5336
N-1B	Beta annealed			91.5	K5336
X-2	Beta rolled and annealed	0.13	6.3	120.3	K5816
X-2B	Beta annealed			108.5	K5816
B-1	As Beta rolled	0.175	6.1	108.2	295153
416-5	Beta-annealed			120.1	2304
-6	Ti-8Al-1Mo-1V			112.6	
A-1	Beta annealed	0.20	6.0	97.6	K5365
-2		0.15	6.3	103.4	K6003
-3		0.13	6.3	111.9	K3237
-4		0.165	6.6	116.7	295074
-5		0.11	6.3	113.7	292030

[a]STOA Solution treated and aged at the given temperature
Beta annealed–1900° F/30 min/AC + 1350° F/2 hr/AC

3.2.2 K_{Iscc} of Ti-6Al-4V Plate

The basic K_{Iscc} Ti-6Al-4V plate evaluation was conducted during the SST program and reported in depth in reference 3. Further tests were conducted to determine the effects of grain direction on beta-processed plate, and these results are shown in table 23. Three heats had very high oxygen (0.171%-0.20%) and aluminum (6.4%-6.6%) contents with significant amounts of K_{Iscc} directionality in the as-received (beta-rolled) condition. After beta annealing the K_{Iscc} was less directional, but the longitudinal K_{Iscc} was reduced. Two of the three heats showed a slight increase in the transverse K_{Iscc} due to beta annealing. The increase in K_{Iscc} due to beta annealing was much more marked for the lower oxygen (0.131%) material, heat K5957. Here the K_{Iscc} was 80-90 ksi$\sqrt{in.}$ after beta annealing compared to 45-55 ksi$\sqrt{in.}$ for the beta-rolled condition for the WR and RW grain directions, respectively.

TABLE 23.– EFFECT OF GRAIN DIRECTION ON K_{Iscc} OF BETA-PROCESSED Ti-6Al-4V PLATE

Specimen	Heat	O_2 (%)	Al (%)	Grain direction	Beta-annealed K_{Iscc} (ksi$\sqrt{in.}$)	Beta-rolled K_{Iscc} (ksi$\sqrt{in.}$)
ST-302 -E-1	K5336	0.20	6.4	WR	39	35
-E-2				RW	39	65
-E-3	304009	0.171	6.5	WR	41	36
-E-4				RW	41	53
-E-5	295154	0.176	6.6	WR	39	45
-E-6				RW	53	55
-E-7	K5957	0.131	6.3	WR	80	45
-E-8				RW	90	53

The effect of beta annealing Ti-6Al-4V with an equiaxed primary alpha microstructure can be seen in table 24. For heat 292030 (0.1142% O_2), the K_{Iscc} is 82 ksi$\sqrt{in.}$ after beta annealing compared to 51 ksi$\sqrt{in.}$ for the alpha-beta-rolled material. The texture for the beta-annealed condition for this material is shown in figure 42. The improvement in K_{Iscc} for the higher oxygen material (heat D7390) is shown in table 24. The K_{Iscc} after beta annealing is more than twice that of the alpha-beta-worked material. However, the difference between the WR and RW grain directions after beta annealing is much larger than expected.

To investigate the effect of thermal cycles, two highly textured pieces of Ti-6Al-4V were exposed to temperatures from 1730° to 1900° F and both furnace cooled and air cooled. The anisotropy factors for these treatments are shown in table 25. In general for both materials, the K_A remained very large (70-117) after exposure to 1730° to 1800° F for both furnace cooling and air cooling. This is a result of the growth of existing primary alpha at temperature as the beta transforms to alpha. No significant change is observed up to these temperatures compared to the as-received texture. This is shown in the pole figures presented

Contour lines	1	2	3	4	5	6
Times random intensity	0.5	1.0	1.5	2.0	4.0	8.0

$K_A = -35$

FIGURE 42.–BASAL PLANE POLE FIGURE FOR Ti-6Al-4V PLATE 1486 AFTER BETA ANNEALING

TABLE 24.–EFFECT OF MICROSTRUCTURE AND GRAIN DIRECTION ON ALPHA-PLUS-BETA AND BETA-PROCESSED PLATE

Specimen	Heat	O_2 (%)	Al (%)	Grain direction	Heat treatment	K_{Iscc}(ksi$\sqrt{in.}$)
ST-302 -F-1	292030	0.1142	6.3	WR	$\alpha+\beta$ I	51
-F-2				RW	$\alpha+\beta$ I	51
-F-3	292030	0.1142	6.3	WR	β I	82
-F-4				RW	β I	82
-F-5	07390	0.180	6.2	WR	$\alpha+\beta$ I	16
-F-6				RW	$\alpha+\beta$ I	31
-F-7	07390	0.180	6.2	RW	β I	38
-F-8				RW	β I	63

[a] $\alpha+\beta$ I Rolled in the alpha-plus-beta field and mill annealed
β I Beta annealed

TABLE 25.–ANISOTROPY FACTOR, K_A, FOR HIGHLY TEXTURED Ti-6Al-4V EXPOSED TO 1730°-1900°F

Material	Temperature (%)	Anisotropy factor, K_A	
		Aircooled	Furnace cooled
7918	1758	78	98
	1783	86	97
	1808	75	70
	1833	21	5
	1883	4	2
7918	1900	1	
	As received–no thermal cycle, K_A = 109		
310487	1730	116	117
	1770	81	95
	1795	86	98
	1815	-74	11
	1870	-72	-85
310487	1900	-56	
	As received–no thermal cycle, K_A = 113		

in figures 43 through 45. However, at temperatures from 1815° to 1900° F the texture reverts from strong basal plane peaks in the transverse direction to strong peaks in the longitudinal direction. This is not consistent with tests conducted in the past (ref. 3), as the K_A tends to be very low after beta annealing, and not -70 to -85 as demonstrated with material 310487. The difference in K_A values for the two materials after exposure to temperatures above 1800° F may be exaggerating the actual texture, since strong peaks are observed in the longitudinal direction for material 7918 even though the K_A is very close to zero. This effect is shown in figures 46 and 47. It is very hard to explain the effect of grain direction on the K_{Iscc} of 7918 (table 24), since the longitudinal K_{Iscc} is 63 ksi$\sqrt{in.}$ in the RW direction compared to 38 ksi$\sqrt{in.}$ for the transverse direction after a beta anneal. This occurs in spite of a high concentration of basal planes in the longitudinal direction. There is a wide variation in mill processing parameters which gives rise to a wide range of textures for both alpha-beta working and beta working. The effect of a beta-annealing treatment is complicated by these prior textures, especially with respect to effect on K_{Iscc}. More work needs to be done in this area.

The effect of aluminum on K_{Iscc} was briefly examined by testing two special heats of Ti-6Al-4V having very low aluminum content. These test results, along with beta-annealed Ti-8Al-1Mo-1V K_{Iscc} results, are shown in table 26. Using the following equation for K_{Iscc} from reference 3:

$$K_{Iscc}\ (\text{ksi}\sqrt{\text{in.}}) = 171 - 320(O_2) + 60(\text{Fe}) - 16(\text{Al}) + 1.4\text{MR}^*$$

TABLE 26.—K_{Iscc} OF BETA-ANNEALED LOW-ALUMINUM Ti-6Al-4V AND BETA-ANNEALED Ti-8Al-1Mo-1V

Specimen	Heat	Chemical composition (wt %)					Sustained load data[a] (ksi$\sqrt{in.}$)	K_{Iscc} (ksi$\sqrt{in.}$)	
		O_2	Al	Fe	C	N		Test data	Calculated[b]
I5-7A -7B	I5 I5	0.105	5.3	0.06	0.04	0.039	NF 70, F 75 (35 sec) NF 75, F 80 (25 sec)	73	84
I6-7A -7B	I6 I6	0.170	5.4	0.08	0.06	0.042	F 50 (3 min) NF 40, F 45 (3 min)	42	63
FM416-3 -4	[c]291870	0.131	7.4	0.05	0.05	0.0047	NF 20, F 40.9 (5 min) NF 37, F 50 (4 min)	38	42

[a]NF No failure in 60 min

[b]Calculated from equation; see text

[c]Ti-8Al-1Mo-1V

the K_{Iscc} values for these two low-aluminum materials were calculated to be 63 ksi$\sqrt{in.}$ for the I6 heat and 84 ksi$\sqrt{in.}$ for the I5 heat. Since these are 21 and 11 ksi$\sqrt{in.}$ higher than the test results of the I6 and I5 heats, respectively, it appears that the above equation overestimates the positive effect of low aluminum content. This is not surprising, since the equation is based on data from material having aluminum contents between 5.8% and 6.6%. As an approximation of the high aluminum region, the K_{Iscc} result of the Ti-8Al-1Mo-1V (7.4% Al) was calculated and found to be 42 ksi$\sqrt{in.}$ using an MR of 20 for beta annealing. This approximation appears to agree closely with the actual test result of 38 ksi$\sqrt{in.}$ assuming that the error in equating 4V to 1V plus 1Mo is small. On an approximation basis this would appear to hold, since the elements V and Mo do not appear in the equation.

*Microstructure rating (0 = bad, 20 = good; beta anneal = 20)

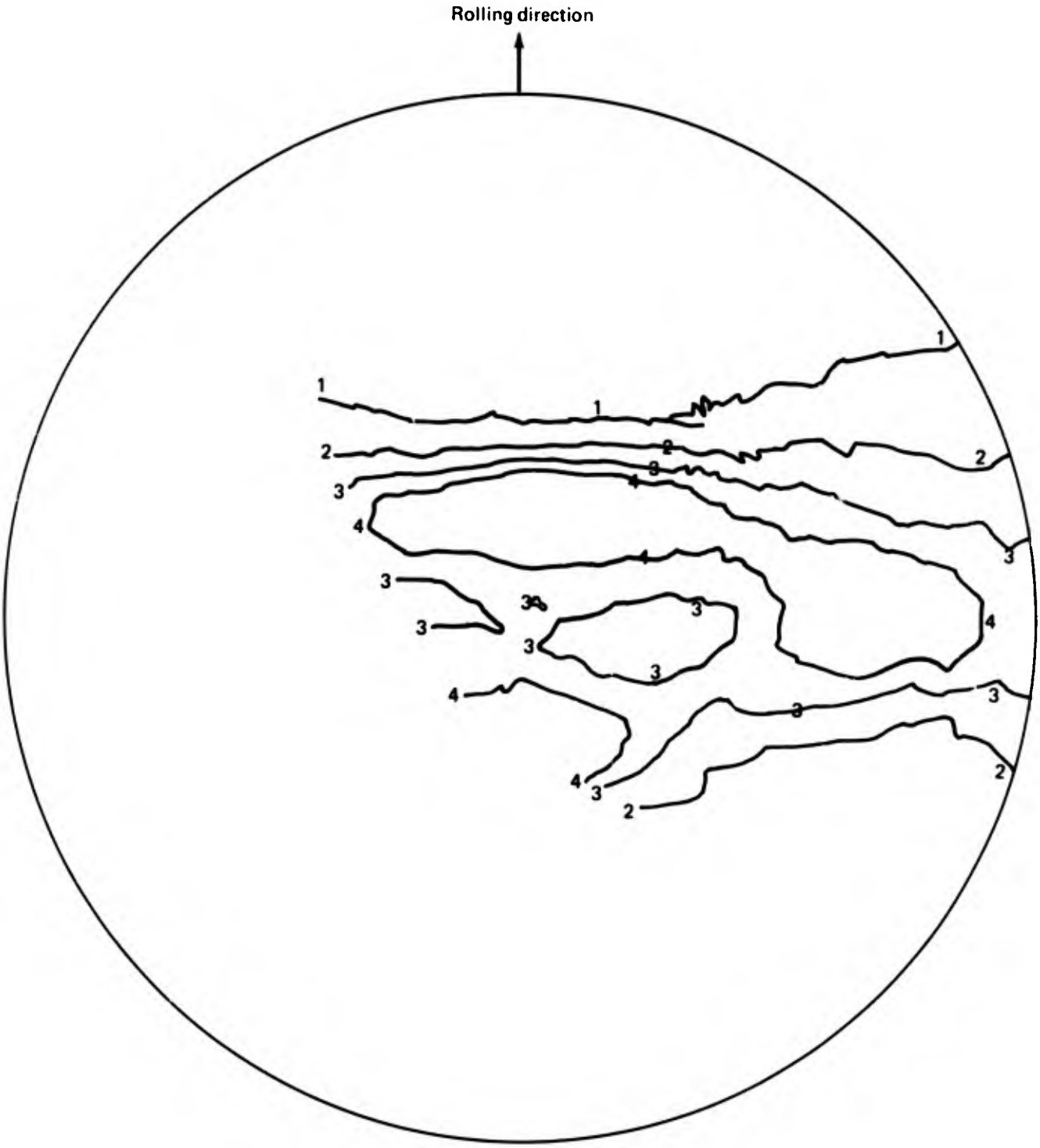

Contour lines	1	2	3	4	5	6
Times random intensity	0.5	1.0	1.5	2.0	4.0	8.0

K_A=78

FIGURE 43.–BASAL PLANE POLE FIGURE FOR Ti-6Al-4V PLATE 7918 AFTER AIR COOLING FROM 1758°

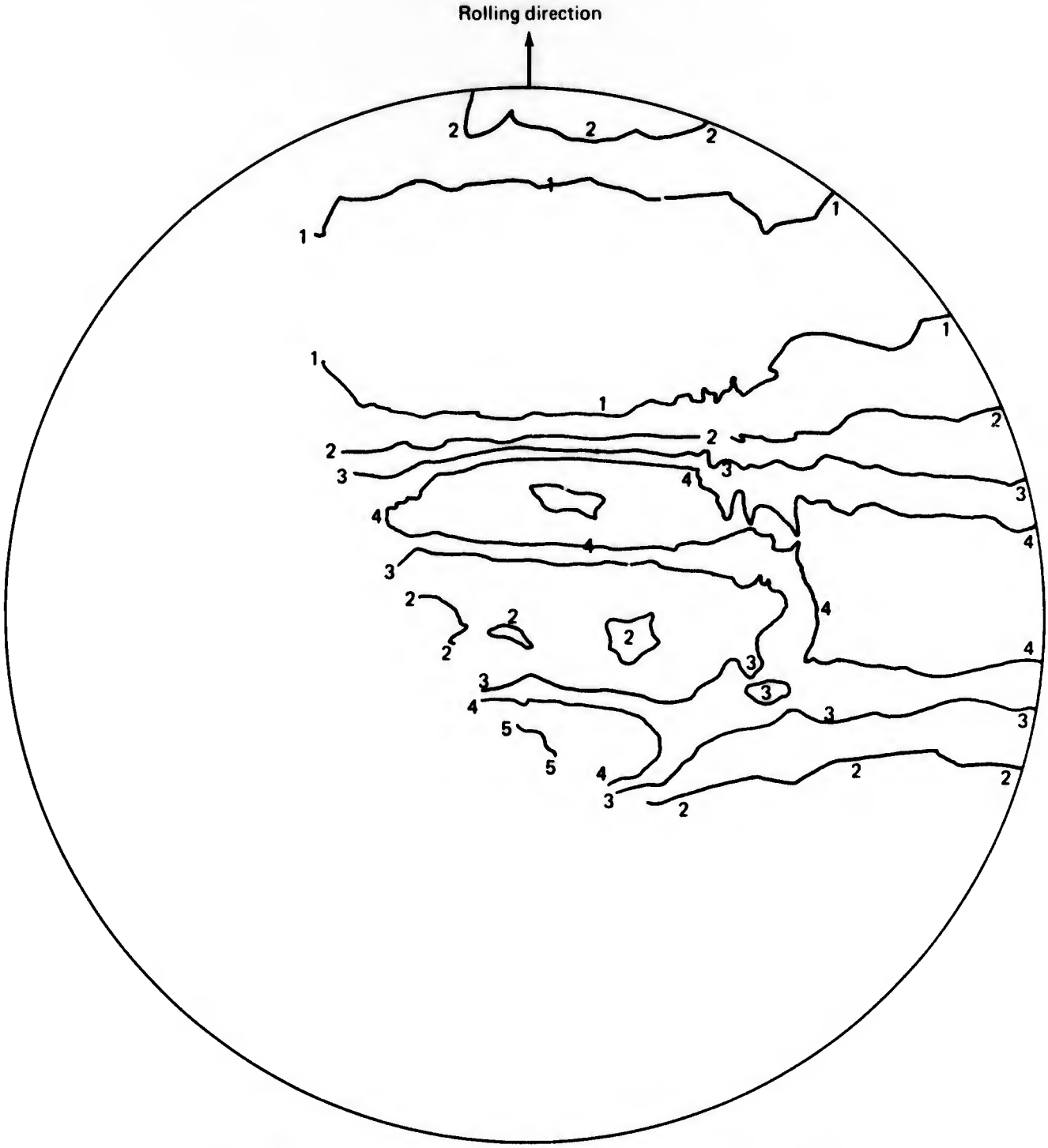

Contour lines	1	2	3	4	5	6
Times random intensity	0.5	1.0	1.5	2.0	4.0	8.0

$K_A = 75$

FIGURE 44.—BASAL PLANE POLE FIGURE FOR Ti-6Al-4V PLATE 7918 AFTER AIR COOLING FROM 1808° F

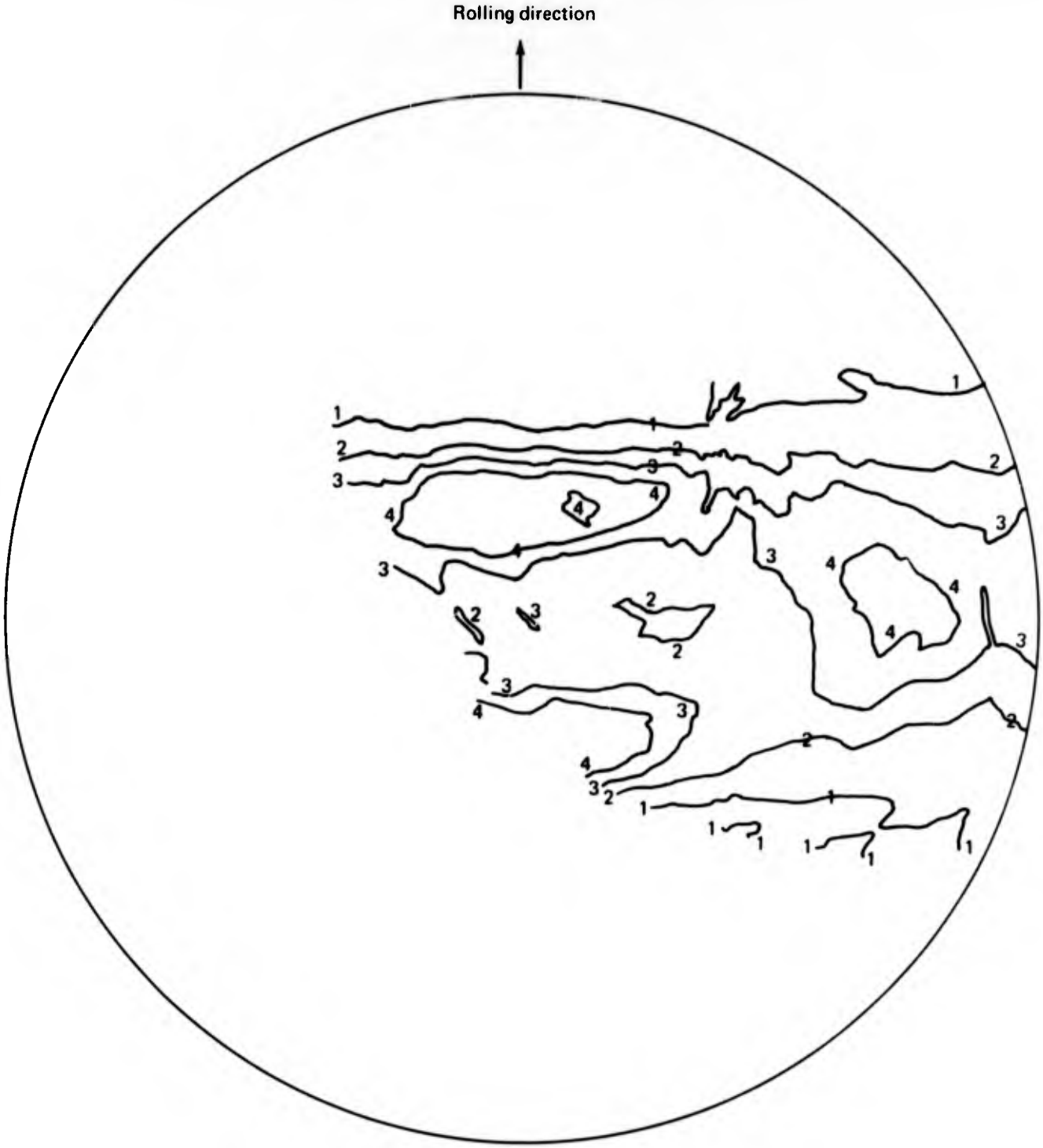

Contour lines	1	2	3	4	5	6
Times random intensity	0.5	1.0	1.5	2.0	4.0	8.0

$K_A = 70$

FIGURE 45.—BASAL PLANE POLE FIGURE FOR Ti-6Al-4V PLATE 7918 AFTER FURNACE COOLING FROM 1808° F

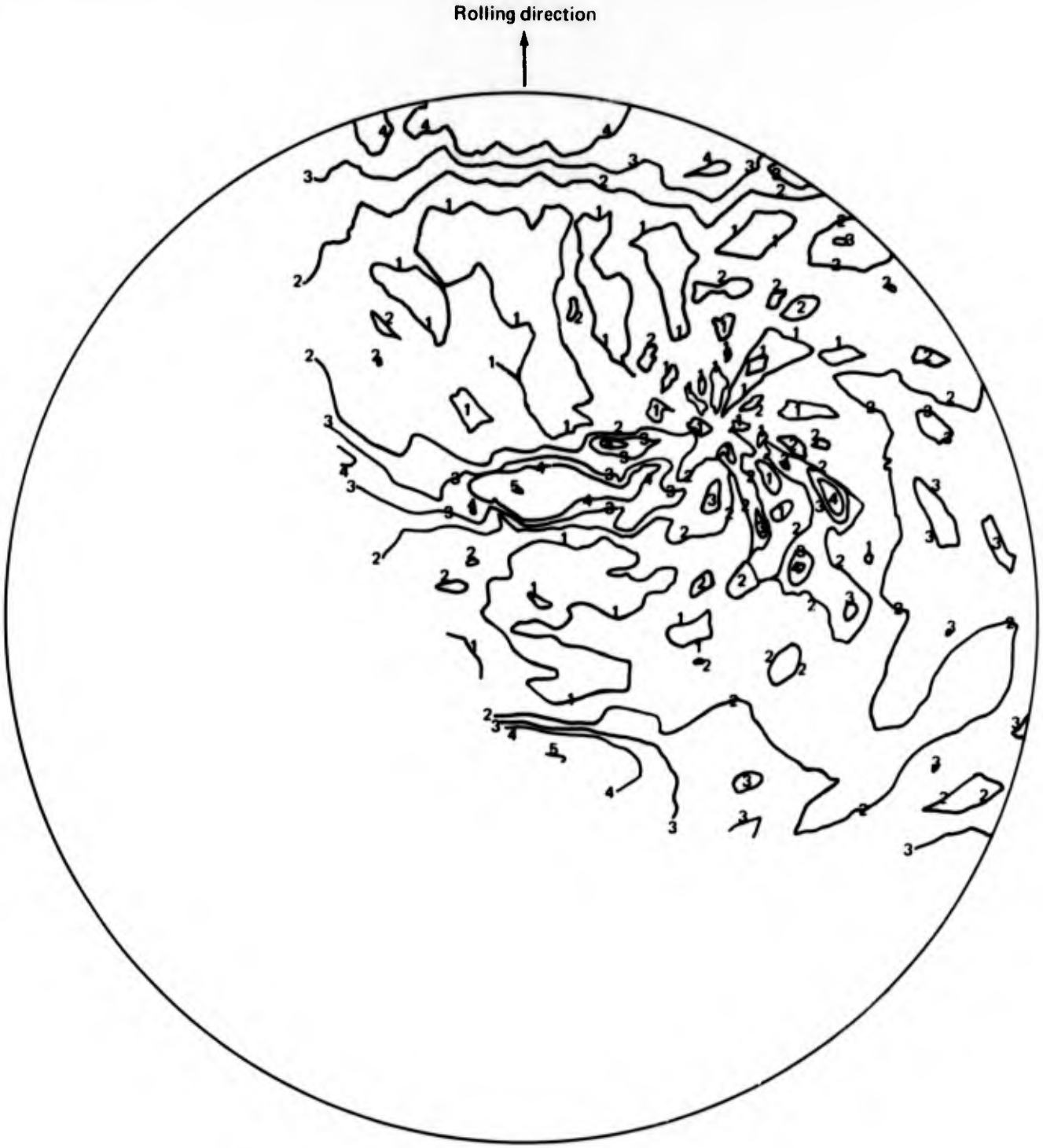

Contour lines	1	2	3	4	5	6
Times random intensity	0.5	1.0	1.5	2.0	4.0	8.0

$K_A = 1.3$

FIGURE 46.–BASAL PLANE POLE FIGURE FOR Ti-6Al-4V PLATE 791S AFTER BETA ANNEALING

Contour lines	1	2	3	4	5	6
Times random intensity	0.5	1.0	1.5	2.0	4.0	8.0

$K_A = -56$

FIGURE 47.– BASAL PLANE POLE FIGURE FOR Ti-6Al-4V SHEET 310487 AFTER BETA ANNEALING

K_{Iscc} tests were also conducted on a lower oxygen heat of Ti-6Al-4V which had been beta processed by the supplier. The material had the following chemistry:

Heat	Thickness (in.)	Chemical composition (wt %)						
		C	Fe	N_2	Al	V	H_2	O_2
K7516	0.590	0.022	0.16	0.012	5.8	4.0	0.006	0.11

The material had an acicular microstructure typical of material heated above the transus, and the texture showed strong peaks in the longitudinal direction (fig. 48). This material was tested for K_{Iscc} in both the longitudinal and transverse grain directions, with resulting values of 38-42 ksi$\sqrt{in}$. for both directions. This was considerably below what was expected for Ti-6Al-4V plate having 0.11% oxygen. The texture shown in figure 48 would explain the lower longitudinal values, since there is a strong alignment of basal planes perpendicular to the rolling direction. However, there is a lack of basal planes perpendicular to the transverse direction, and therefore the lower K_{Iscc} in this direction does not appear to be a result of texture. The chemical composition was checked and the above supplier data were confirmed with the exception of aluminum. Two values of aluminum, 6.20% and 6.04%, were determined on the actual plates. No other chemical variation or foreign elements were found. Electron microscopy was used to determine the presence of α_2 (Ti_3Al), and very strong ordering was found. The ordering parameter on a scale of 0 (good) to 10 (bad) was 10 which is as strong a rating as has been observed in Ti-6Al-4V. This ordered phase has been demonstrated to reduce the stress-corrosion resistance in a wide variety of Ti-6Al-4V mill products such as plate (ref. 3), continuously rolled sheet (ref. 2), and hand-mill sheet (sec. 3.1.1). Although no ordering parameters were determined, past work (refs. 3 and 10) on a wide variety of plate having low oxygen has shown higher values of K_{Iscc} than 38-42 ksi$\sqrt{in}$. It is possible, however, that these plates were less ordered than the plate evaluated here (heat K7516). Recent work by Wingert (ref. 11) has shown that increasing oxygen retards the formation of Ti_3Al. Hence, it is possible that the lower oxygen (0.11%) in this heat is promoting ordering with a resultant K_{Iscc} decrease. These results must be considered preliminary at this time and more work is needed to quantitatively determine the interrelationship between ordering, chemistry, texture, and stress-corrosion resistance.

As a further test on the effect of oxygen on K_{Iscc}, a 1.0-in.-thick Ti-6Al-4V plate having an oxygen content of 0.06% was beta annealed and tested to determine K_{Iscc}. This material was tested as 0.950-in. four-point-loaded, notched bend specimens. The resulting K_{Iscc} was found to be 87 ksi$\sqrt{in}$. This demonstrates that excellent stress-corrosion resistance can be achieved for very low oxygen (super ELI) Ti-6Al-4V plate.

3.2.3 Receiving Inspection Data for Beta-Processed Ti-6Al-4V Plate

Receiving inspection data were analyzed using the computerized regression analysis techniques described in 3.1.12. All the coefficients for the equations for Ti-6Al-4V beta-processed plate are given in appendix E. The following equations for TUS, TYS, percent elongation, and K_{salt} were developed using only those coefficients whose standard deviation was less than the coefficient itself.

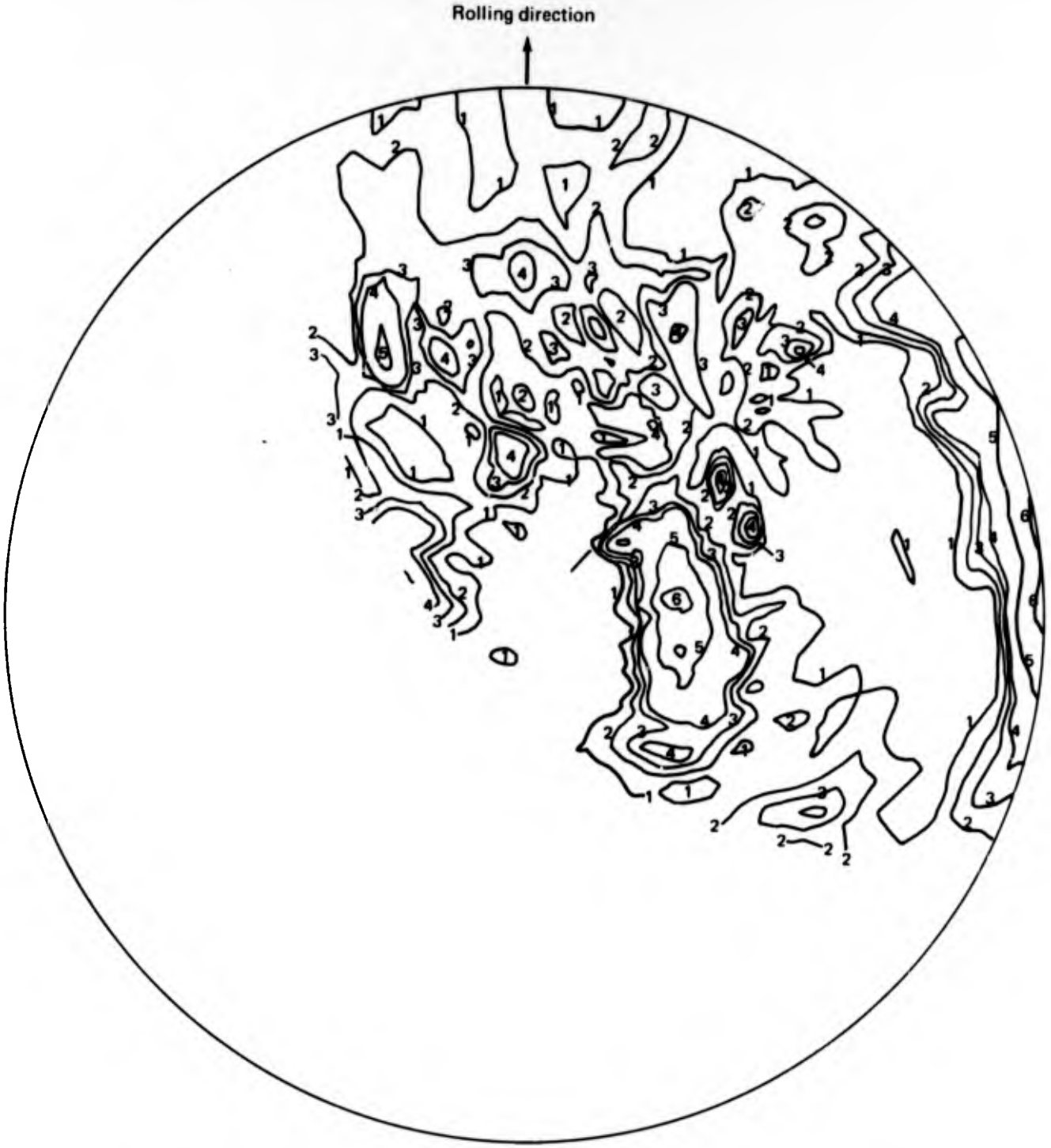

Contour lines	1	2	3	4	5	6
Times random intensity	0.5	1.0	1.5	2.0	4.0	8.0

$K_A = 51$

FIGURE 48. – BASAL PLANE POLE FIGURE FOR Ti-6Al-4V HEAT K7516

K_{salt} (transverse) =

- 148.4 + 9.79(gage) - 279(O_2) - 22.5(Al) + 22.6(V) + 135(Fe)

TUS =

- Longitudinal: 135.8 - 4.70(gage) + 102(O_2) + 1.64(Al) + 0.21(V)
- Transverse: 148.0 - 4.58(gage) + 97.1(O_2) - 1.90(Al) - 1.07(V)

TYS =

- Longitudinal: 119.7 - 6.94(gage) + 87.9(O_2) + 0.533(Al) - 0.43(V) + 38.9(Fe)
- Transverse: 164.9 - 6.48(gage) + 72.6(O_2) - 4.90(Al) - 2.54(V)

Percent elongation =

- Longitudinal: 14.4 - 0.651(gage) - 0.254(V) - 11.8(Fe)
- Transverse: 22.5 - 0.904(gage) - 0.896(Al) - 1.01(V) - 6.85(Fe)

The negative effect of oxygen and aluminum on K_{salt} is quite significant since the variation in these elements over the general range encountered would account for a 27.9 ksi $\sqrt{in.}$ and an 11.2 ksi $\sqrt{in.}$ reduction for a 0.1% and 0.5% variation in oxygen and aluminum, respectively.

The positive effect of the beta-stabilizing elements V and Fe can also be seen. Here an increase in K_{salt} associated with the range in V and Fe found would be 6.8 ksi $\sqrt{in.}$ (0.3% V) and 13.5 ksi $\sqrt{in.}$ (0.1% Fe), respectively. The effect of gage is also significant since a 1-in. increase in gage would result in a 10-ksi $\sqrt{in.}$ increase in K_{salt}. This has been observed in the past (ref. 5) where very thick (8-18 in.) Ti-6Al-4V has had excellent fracture toughness and stress-corrosion resistance. Generally this can be attributed to the lower strength effect with gage, as shown in the TUS and TYS equations. Here a 5- to 7-ksi reduction in strength occurs with an increase of 1 in. in thickness. The positive effect of oxygen on strength is also shown, with the coefficients ranging between 70 and 102 ksi per percent O_2. The Al and V strengthening effects are mixed, with both positive and negative coefficients obtained for both these elements. However, considering the range of Al and V the total maximum effect is less than 1 ksi in all but one case. The strengthening effect of Fe is shown only for the longitudinal TYS, where the coefficient is approximately 40. Here the total range of Fe encountered (0.1%) would result in a 4.0-ksi strength increase.

The significant effect of gage on ductility can be seen from the equations. Reductions of 0.5% to 1.0% elongation values would result for each inch of increased gage. The Al and V effects are both negative, but considering the little variation in these parameters the effect on the percent elongation is only 0.3%-0.5%. Iron shows a mildly significant negative effect, with a 0.7%-1.2% reduction for a 0.1% range.

3.2.4 Fracture Toughness and Stress-Corrosion Resistance of STA 1000° F Ti-6Al-4V Plate

Ti-6Al-4V plates which had previously been tested in the annealed condition for K_Q and K_{Iscc} were tested after the following heat treatment:

1725° F/30 min/water quench + 1000° F/4 hr/air cool

Two heats of material were tested for K_Q in this heat-treatment condition, both with and without a prior beta anneal. The material which was not beta annealed had an equiaxed alpha microstructure typical of material worked in the alpha-plus-beta region. The K_Q values are shown in table 27. The difference between the fracture toughness of the beta-annealed material and the material worked in the alpha-plus-beta field is rather significant. The beta-annealed samples had 50%-90% higher toughness values. The effect of oxygen on the beta-annealed samples can be seen, since the K_Q for material containing 0.18% oxygen was 84.5 ksi$\sqrt{in.}$ compared to 110.8 ksi$\sqrt{in.}$ for 0.114% oxygen. This oxygen effect was not observed with the alpha-plus-beta worked STA 1000 F specimens. The toughness of the beta-annealed STA 1000° F material was very high—approximately 80%-90% of that of the annealed material.

TABLE 27.—FRACTURE TOUGHNESS, K_Q, OF STA Ti-6Al-4V PLATE

Specimen	Sheet	Plate thickness (in.)	Test thickness (in.)	Heat treatment [a]	O_2 (%)	Al (%)	K_Q (ksi$\sqrt{in.}$)
ST302-C-1	7918	0.50	0.480	$\alpha+\beta$ STA 1000	0.180	6.4	58.2
C-2	7918	0.50	0.480	β STA 1000	0.180	6.4	84.5
C-3	1486	1.00	0.480	$\alpha+\beta$ STA 1000	0.114	6.3	58.2
C-4	1486	1.00	0.480	β STA 1000	0.114	6.3	110.8

[a] $\alpha+\beta$ STA 1000°F, worked in the $\alpha+\beta$ field, then STA 1000°F
β STA 1000°F, beta annealed, then STA 1000°F

The results of the K_{Iscc} tests on STA 1000° F material are shown in table 28, along with the corresponding results for annealed material. For the three lower oxygen beta-annealed specimens (8506, P2, and 1486) there was an average reduction of 36% of the K_{Iscc} of the STA 1000° F over the beta-annealed condition. With the higher oxygen (0.15%-0.19%) specimens the difference between the two conditions was much less, with two test results showing somewhat higher values in the STA 1000° F condition. It should be pointed out that the beta-rolled (BR) condition does not have an optimum microstructure and texture. Past experience (ref. 3) has shown large differences in beta-rolled and beta-annealed structures with respect to K_{Iscc}. In summary these tests show that material having a good microstructure and texture (i.e., beta annealed) as well as low oxygen will have reasonably high K_{Iscc} (45 to 60 ksi$\sqrt{in.}$) in the STA 1000° F condition. This may provide material for applications requiring reasonably high strengths with good stress-corrosion resistance.

TABLE 28.–K_{Iscc} DATA FOR Ti-6Al-4V SOLUTION TREATED AND AGED AT 1000° F–WR ORIENTATION

Specimen	Heat	Sheet or lot	Heat treatment[a]	O_2 (%)	Al (%)	K_{Iscc} (ksi$\sqrt{in.}$)	
						Annealed	STA 1000°F
8506	E2205	8506	βI	0.11		78	46
P2	K5957	L2504	βI	0.14	6.3	73	43
7918			α+β	0.18	6.2	16	26
1486			βI	0.11		82	61
68316-2	295243	01	R	0.177	6.6	35	32
1944C	K5417	1944	βR	0.19	6.2	35	33
2054	K4400	2054	βR	0.19	6.2	35	32
25021B	K6003	2502	βI	0.15	6.3	35	41
W	K2701	L2022	βR	0.15	6.4	44	52

[a]Heat treatment– α+β Alpha + beta rolled + STA 1000° F

βI Beta annealed 1900° F/30 min/AC + 1350° F/2 hr/AC

βR Rolled near the beta transus + 1350°-1450° F/2-4 hr/ (not optimum beta structure)

3.2.5 Modulus of Elasticity

As was done for Ti-6Al-4V sheet, the modulus of elasticity of Ti-6Al-4V beta-processed plate was determined from tensile test curves of load versus deflection. The results of these tests for both the longitudinal and transverse directions are shown in table 29. The mean values for E_T were 16.9 and 17.1 x 10^6 psi for the longitudinal and transverse grain directions, respectively. However, the standard deviation was quite large, at 1.1-1.4 x 10^6 psi. This was due in part to the wide variation in chemical composition (oxygen 0.112%-0.210%, aluminum 5.8%-6.5%) and resulted in a wide range of other properties (ref. 3). Although some variation in texture has been observed, beta-processed plate tends to be much less textured than alpha-plus-beta worked sheet. This is demonstrated in table 29, where the moduli for both the longitudinal and transverse directions are virtually identical. The effect of chemical composition was determined using a regression analysis technique. The following are the equations developed for both the longitudinal and transverse directions (units are 10^6 psi for E_T and weight percent for chemical composition):

- Transverse

$$E_T = -5.38 + 7.40(O_2) + 3.42(Al) + 0.737(V) - 18.4(Fe)$$

- Longitudinal

$$E_T = -5.75 + 18.8(O_2) + 4.57(Al) - 1.99(V) - 3.90(Fe)$$

TABLE 29.—E_T DATA FOR CONDITION I BETA-PROCESSED Ti-6Al-4V PLATE

	TUS (ksi)	TYS (ksi)	Elong (%)	RA[a] (%)	E_T (x 10^6 psi)	Chemical composition (wt %)						
						O_2	N_2	H_2	C	Al	V	Fe
Longitudinal direction												
Column mean	145.4	134.6	10.5	0.0	16.9	0.163	0.0173	0.0075	0.016	6.27	4.06	0.16
Column standard deviation	8.0	6.7	1.4	0.0	1.4	0.031	0.0036	0.0025	0.008	0.21	0.22	0.03
Number of non-zero data	31	31	31	0	31	29	29	27	28	29	29	29
Maximum value in data	168.2	154.7	12.5	0.0	20.2	0.216	0.0200	0.0115	0.040	6.50	4.40	0.20
Minimum (non-zero) value	134.7	126.4	6.5	*0.0	14.7	0.112	0.0100	0.0030	0.005	5.85	3.50	0.10
Number of heat-lots	25											
Transverse direction												
Column mean	146.4	135.1	10.4	0.0	17.1	0.160	0.0176	0.0078	0.016	6.26	4.06	0.16
Column standard deviation	8.2	7.3	1.6	0.0	1.1	0.031	0.0036	0.0024	0.008	0.20	0.23	0.03
Number of non-zero data	29	29	29	0	29	27	27	25	26	27	27	27
Maximum value in data	171.9	159.8	13.0	0.0	19.3	0.216	0.0200	0.0115	0.040	6.50	4.40	0.20
Minimum (non-zero) value	134.5	124.6	6.0	*0.0	15.1	0.112	0.0100	0.0030	0.005	5.85	3.50	0.10
Number of heat-lots	25											

[a]Reduction in area

The positive effects of oxygen and aluminum can be seen from these equations. The negative effect of the strong beta stabilizer Fe is also shown. This is somewhat consistent with the more highly beta-stabilized titanium alloys (e.g., Beta III) which have lower moduli than the alpha-plus-beta alloys. Vanadium shows a mixed result, although for the transverse direction the effect is also negative. This seems to be more consistent with the beta-stabilizing effect. These equations must be considered somewhat preliminary at this time due to the scatter in the data. However, the general trend appears to be real.

3.2.6 Effect of Diffusion Bonding on K_{Iscc} and K_Q of Ti-6Al-4V Plate

The effect of a typical high-temperature diffusion bonding cycle on the K_Q and K_{Iscc} properties of Ti-6Al-4V plate was determined by exposing material as follows:

1750° F/2 hr/furnace cool at 150° F per hour to 600° F

Two heats of material (sheets 7918 and 1486) which had been rolled in the alpha-plus-beta field with a subsequent mill anneal (1350°-1450° F for 2-4 hr) were exposed to this simulated diffusion bonding cycle. The material was tested both with and without a prior beta anneal (1900° F/30 min/air cool + 1350° F/2 hr/air cool). The resulting textures from these thermal cycles are shown in figures 49 through 55 and figure 42. The results of the stress-corrosion tests are shown in table 30. As expected, the beta-annealed material had much higher K_{Iscc} than the alpha-plus-beta worked material: 82 ksi$\sqrt{in.}$ versus 51 ksi$\sqrt{in.}$ for the low-oxygen (0.11%) sheet 1486, and 38 to 63 ksi$\sqrt{in.}$ versus 16 to 38 ksi $\sqrt{in.}$ for the high-oxygen (0.18%) sheet 7918. The strong texture in sheet 7918 results in K_{Iscc} directionality in the as-received condition. However, the beta-annealed condition also retains K_{Iscc} directionality but at a much higher level of K_{Iscc} than the as-received material. Plate 1486 has a texture in both the as-received and beta-annealed conditions which results in no K_{Iscc} directionality. It should be noted that the beta-annealed condition for this plate is quite textured, with a K_A value of -35. In spite of this, there is no difference between the K_{Iscc} results of the WR and RW directions. The effect of the diffusion bonding can be seen from the data in table 30.

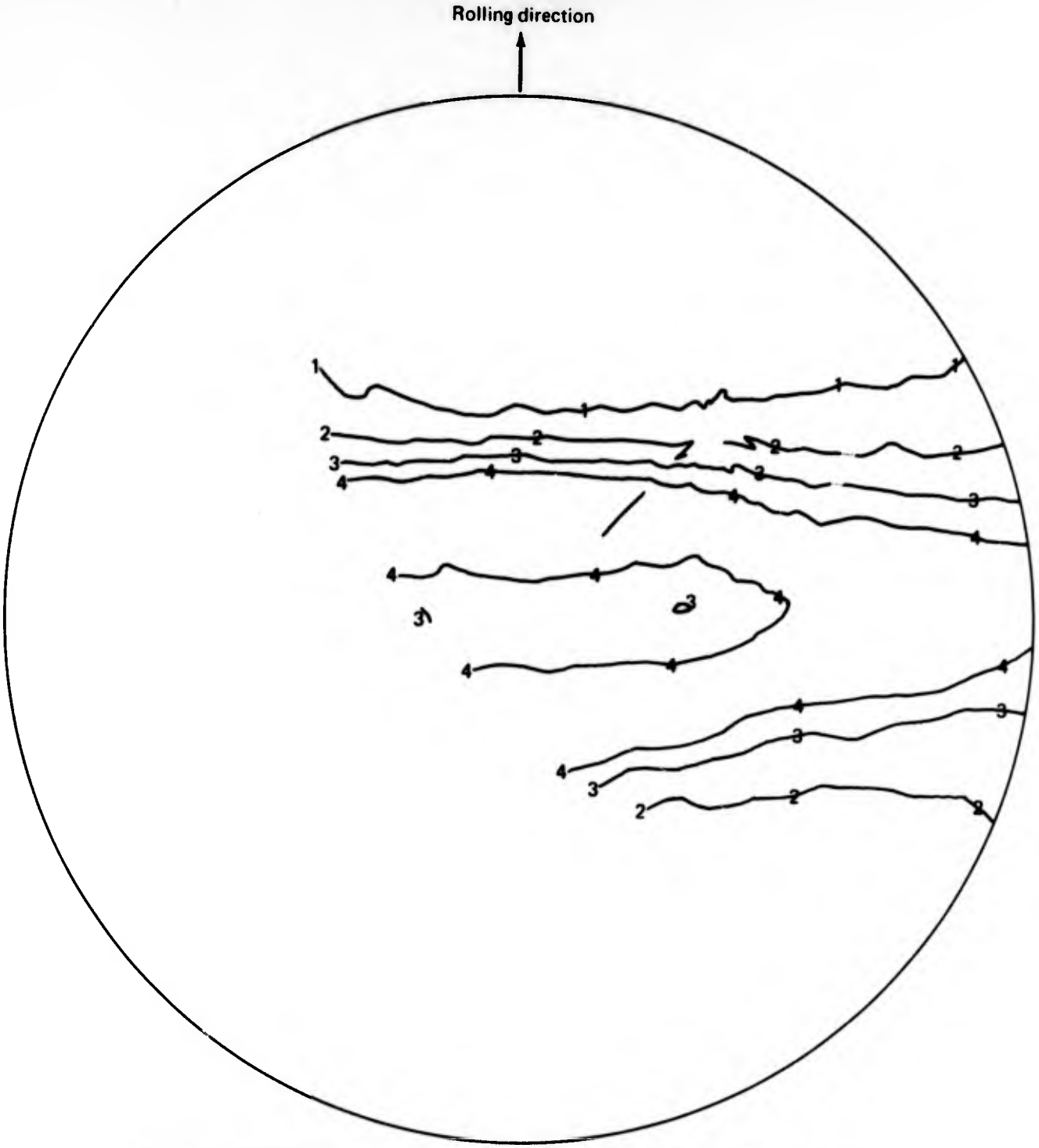

Contour lines	1	2	3	4	5	6
Times random intensity	0.5	1.0	1.5	2.0	4.0	8.0

$K_A = 100$

FIGURE 49.—BASAL PLANE POLE FIGURE FOR Ti-6Al-4V PLATE 7918 AS-RECEIVED

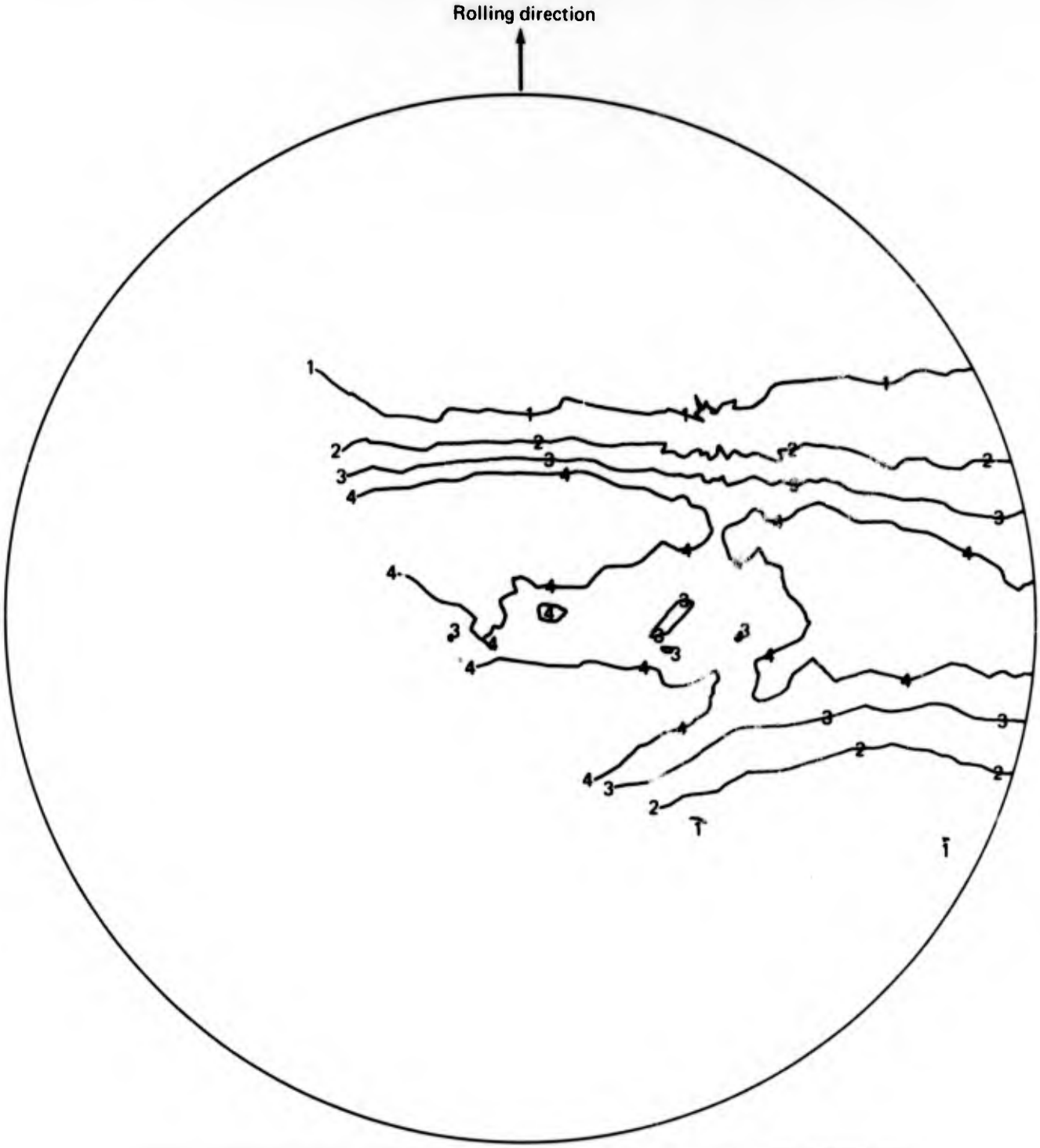

Contour lines	1	2	3	4	5	6
Times random intensity	0.5	1.0	1.5	2.0	4.0	8.0

$K_A = 90$

FIGURE 50.—BASAL PLANE POLE FIGURE FOR Ti-6Al-4V PLATE 7918 AFTER THE DIFFUSION BONDING CYCLE

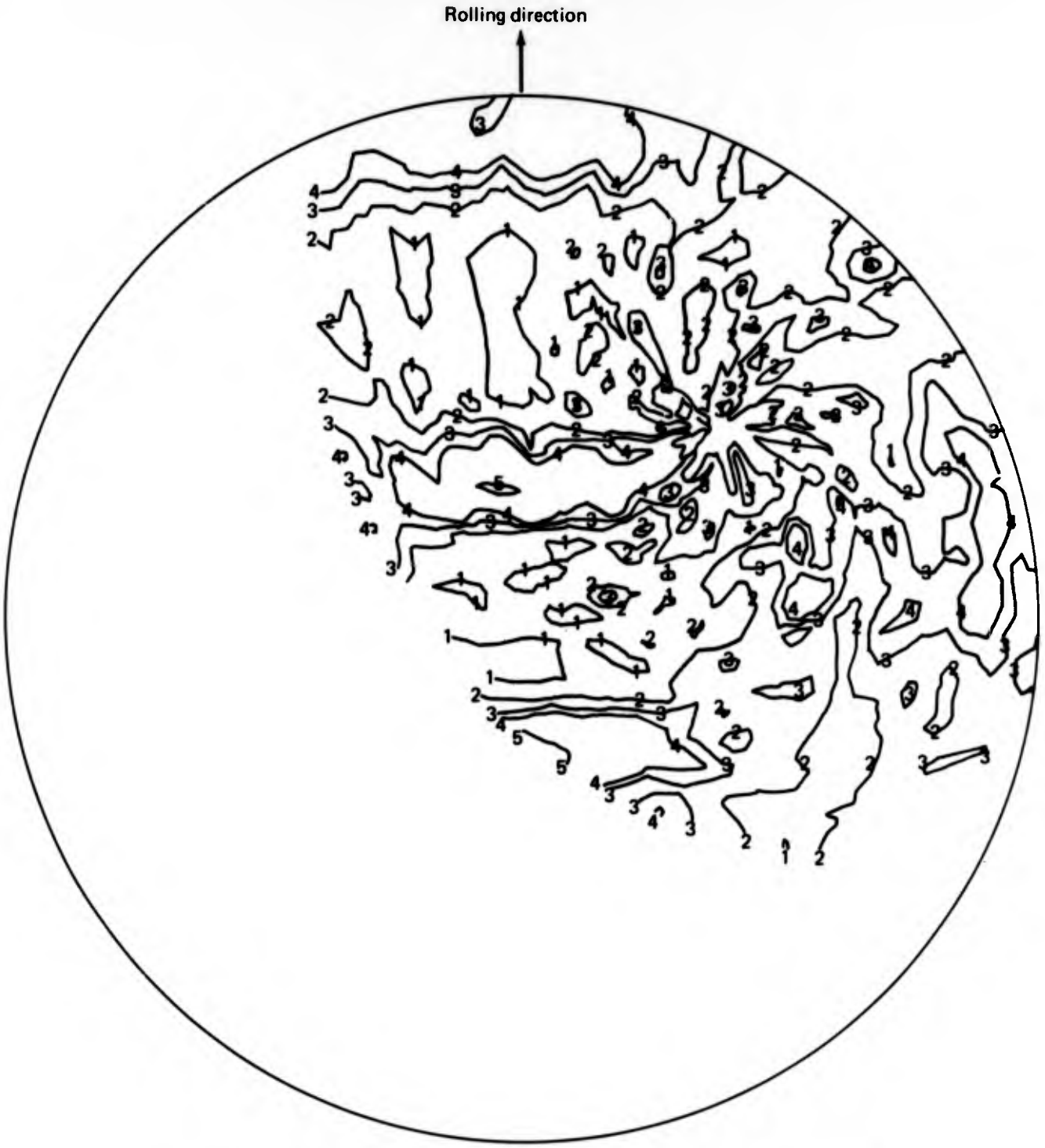

Contour lines	1	2	3	4	5	6
Times random intensity	0.5	1.0	1.5	2.0	4.0	8.0

$K_A = 12$

FIGURE 51.–BASAL PLANE POLE FIGURE FOR Ti-6Al-4V PLATE 7918 AFTER BETA ANNEALING

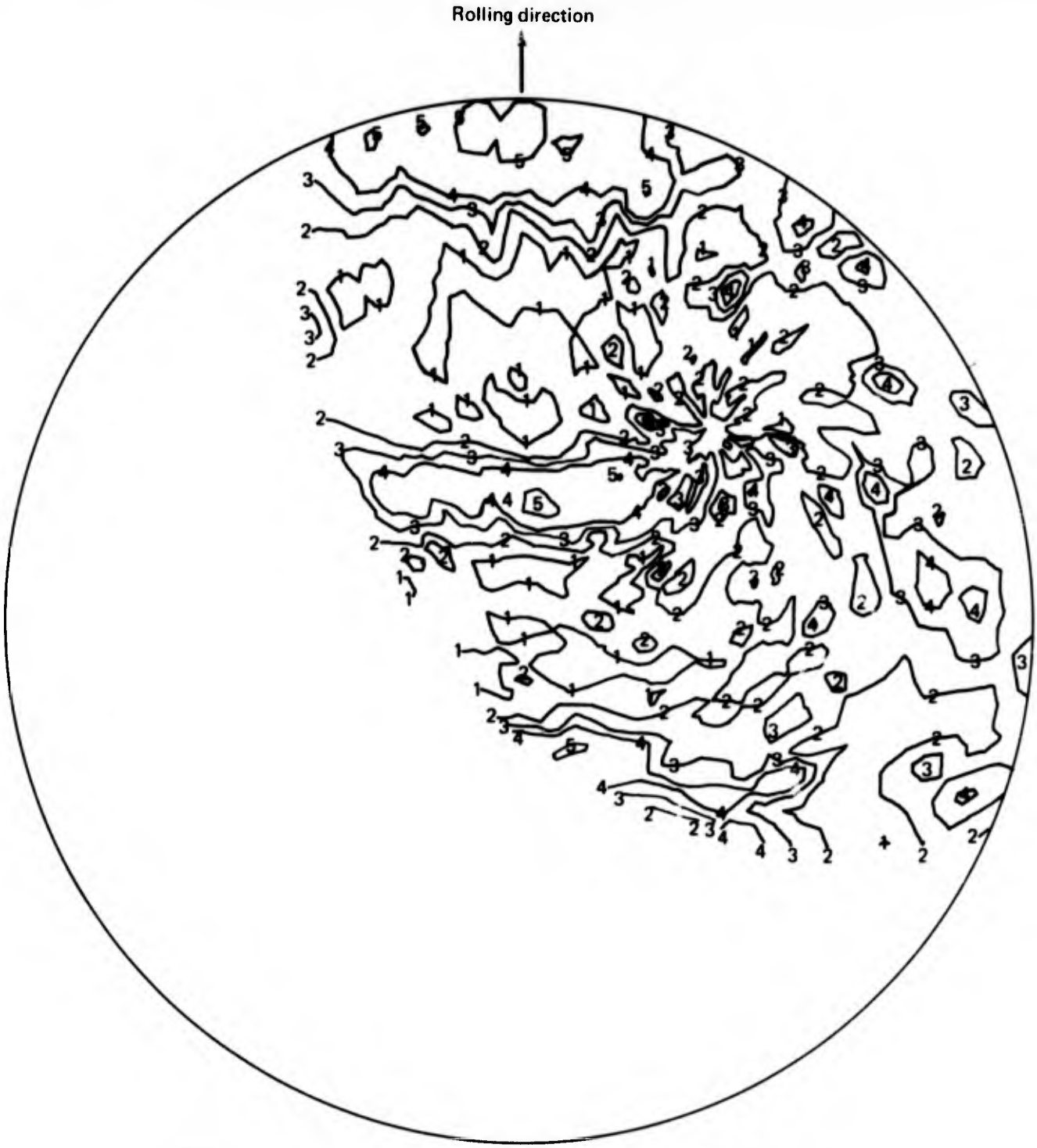

Contour lines	1	2	3	4	5	6
Times random intensity	0.5	1.0	1.5	2.0	4.0	8.0

$K_A = -14$

FIGURE 52.–BASAL PLANE POLE FIGURE FOR Ti-6Al-4V PLATE 7918 AFTER BETA ANNEALING AND DIFFUSION BONDING CYCLE

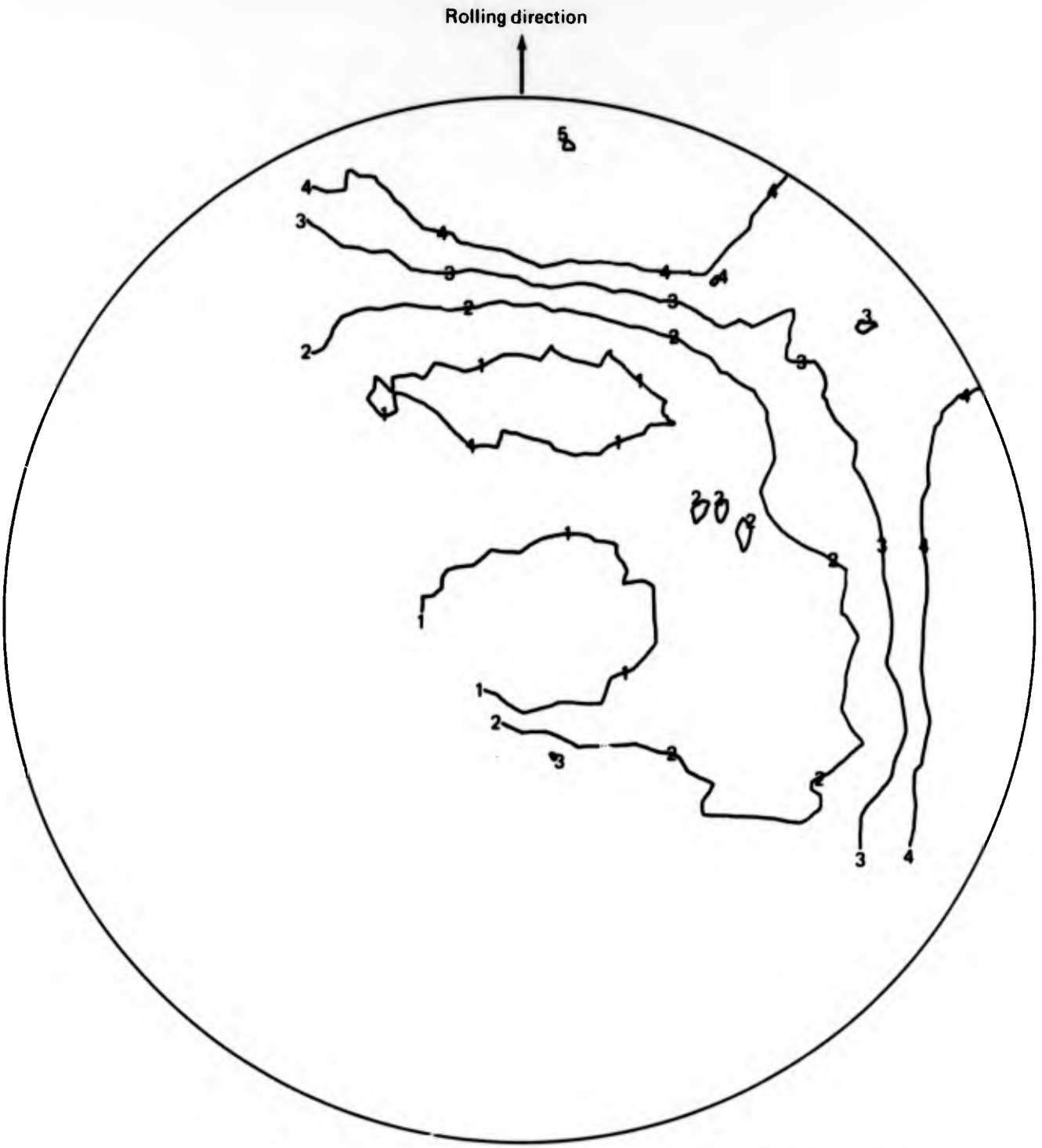

Contour lines	1	2	3	4	5	6
Times random intensity	0.5	1.0	1.5	2.0	4.0	8.0

$K_A = -17$

FIGURE 53.–BASAL PLANE POLE FIGURE FOR Ti-6Al-4V PLATE 1486 AS-RECEIVED

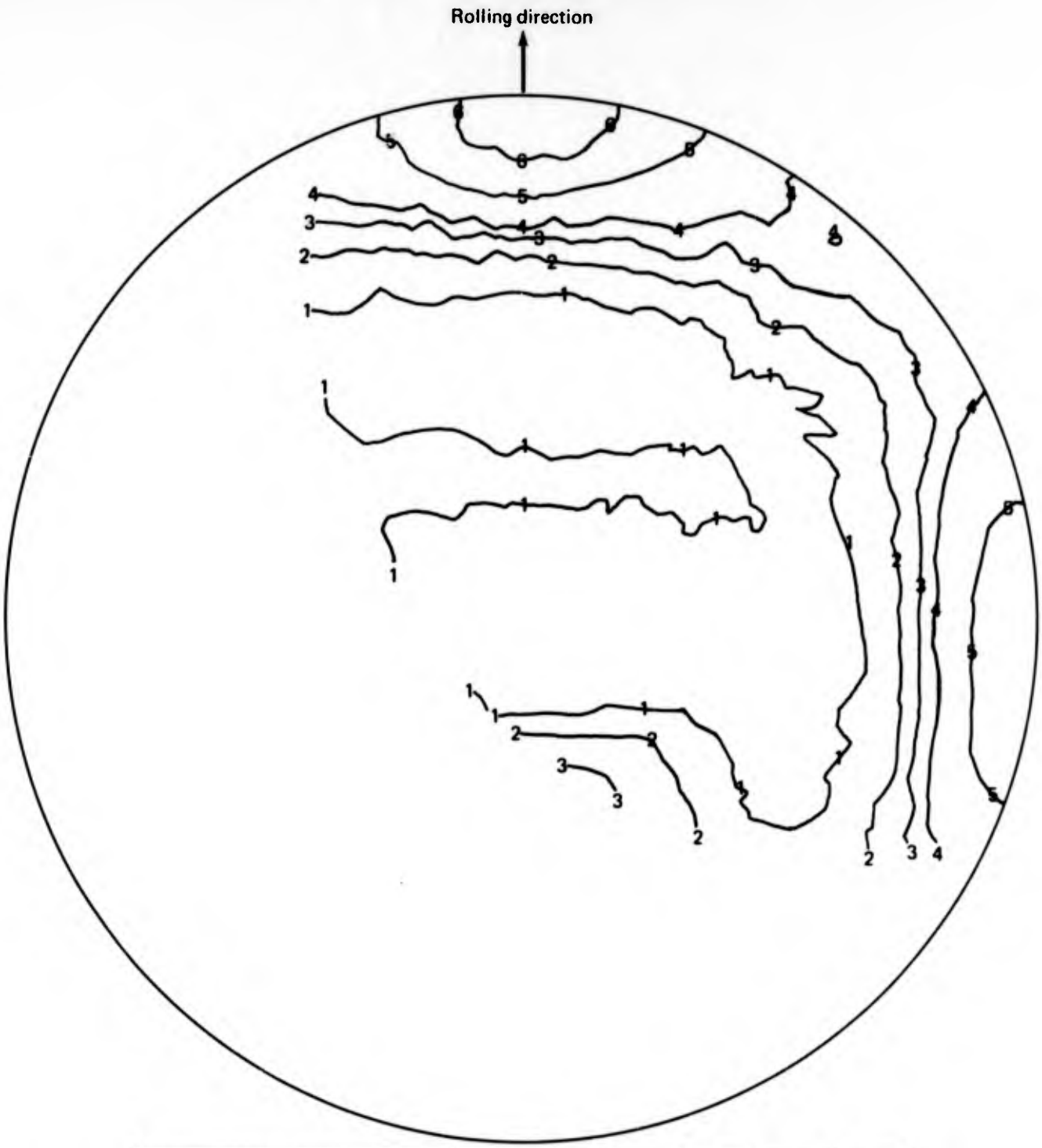

Contour lines	1	2	3	4	5	6
Times random intensity	0.5	1.0	1.5	2.0	4.0	8.0

$K_A = -66$

FIGURE 54.—BASAL PLANE POLE FIGURE FOR Ti-6Al-4V PLATE 1486 AFTER THE DIFFUSION BONDING CYCLE

Contour lines	1	2	3	4	5	6
Times random intensity	0.5	1.0	1.5	2.0	4.0	8.0

$K_A = -63$

FIGURE 55.– BASAL PLANE POLE FIGURE FOR Ti-6Al-4V PLATE 1486 AFTER BETA ANNEALING AND THE DIFFUSION BONDING CYCLE

TABLE 30.–EFFECT OF DIFFUSION-BONDING CYCLES ON K_{Iscc} OF MILL-ANNEALED AND BETA-MILL-ANNEALED Ti-6Al-4V

Specimen	Sheet	Grain direction	Thermal cycle	K_{Iscc} (ksi$\sqrt{in.}$)	Time to failure (min)
DB-18	1486	WR	As received + diffusion bonding	44	
DB-3	1486	RW		<40	11
DB-8	7918	WR		28	
DB-13	7918	RW		40	
DB-20	1486	WR	Beta annealed + diffusion bonding	<70	3.5
DB-5	1486	RW		<60	3.5
DB-10	7918	WR		<35	8
DB-15	7918	RW		<40	7
	1486	WR	As received	51	
	1486	RW	As received	51	
	1486	WR	Beta annealed	82	
	1486	RW	Beta annealed	82	
	7918	WR	As received	16	
	7918	RW	As received	31	
	7918	WR	Beta annealed	38	
	7918	RW	Beta annealed	63	

The as-received (alpha-plus-beta-rolled) material has K_{Iscc} results which are mixed. For the low-oxygen plate 1486, the K_{Iscc} after diffusion bonding values are 44 ksi$\sqrt{in.}$ (WR direction) and < 40 ksi$\sqrt{in.}$ (RW direction) compared to 51 ksi$\sqrt{in.}$ for both directions in the as-received condition. The values for the high-oxygen plate 7918, however, were reversed, with the diffusion bonding treatment resulting in higher K_{Iscc} results (28 and 40 ksi$\sqrt{in.}$) compared to 16 and 31 ksi$\sqrt{in.}$ for the as-received condition for the WR and RW directions, respectively. The diffusion bonding cycle reduced the K_{Iscc} for the beta-annealed condition for both the low- and high-oxygen material. The actual K_{Iscc} was not precisely determined after diffusion bonding, as the specimens failed on the first loading. However, the failure K level for the beta-annealed plus diffusion bonding condition was in all cases lower than the beta-annealed treatment only. Photomicrographs for the four thermal treatments are shown in figure 56. The larger grains in the diffusion-bonded cycle are a result of the slow cooling cycle from 1750° F, where the primary alpha at temperatures grows at the expense of the beta as the temperature is lowered.

The effect of the simulated diffusion bonding cycles on K_Q is shown in table 31. For the as-received (alpha-plus-beta-rolled) material there is a large increase in K_Q after diffusion bonding compared to the as-received condition. The meaning of the as-received K_Q of plate 1486 is quite uncertain since the curves show gross rollover (see sec. 3.2.1), but the K_Q for the high-oxygen plate (7918) shows approximately a 70% increase over K_Q due to diffusion bonding. However, no general increase was observed for the beta-annealed specimens. Most of the specimens with the diffusion bond cycle showed a slight decrease of 2%-5% over the beta-annealed-only cycle. One condition (plate 7918, RW direction) did show a 27 ksi$\sqrt{in.}$ increase, however. In general there appears to be no basic difference in the K_Q of beta-annealed plate with and without a subsequent diffusion bonding cycle.

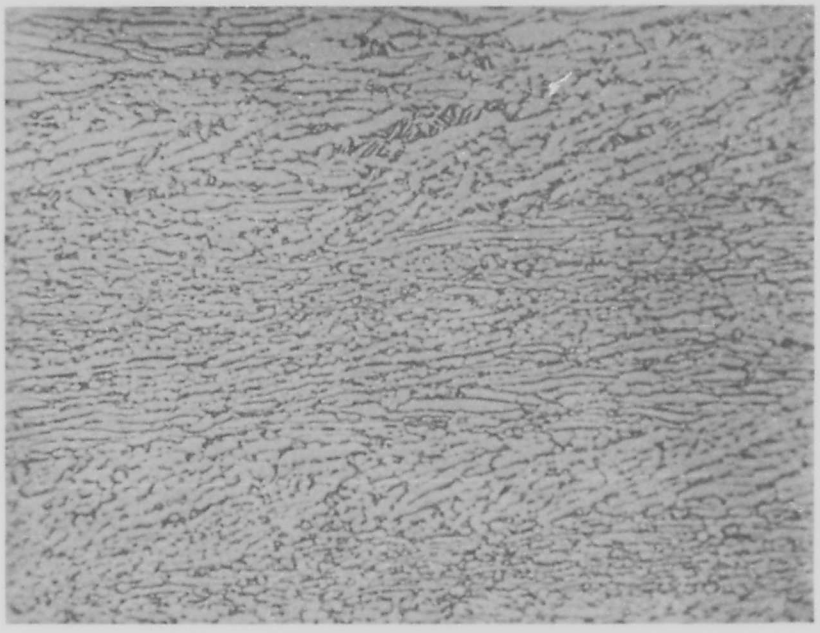

As Received

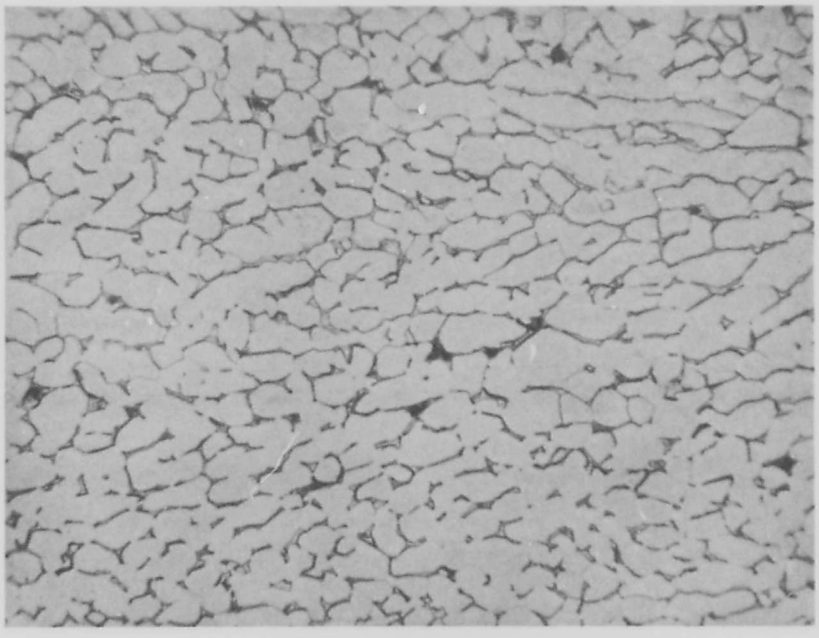

Diffusion-Bonded Cycle

FIGURE 56.–PHOTOMICROGRAPH OF Ti-6Al-4V PLATE 1486 TESTED TO DETERMINE EFFECT OF DIFFUSION BONDING CYCLE ON K_{Iscc} (X500)

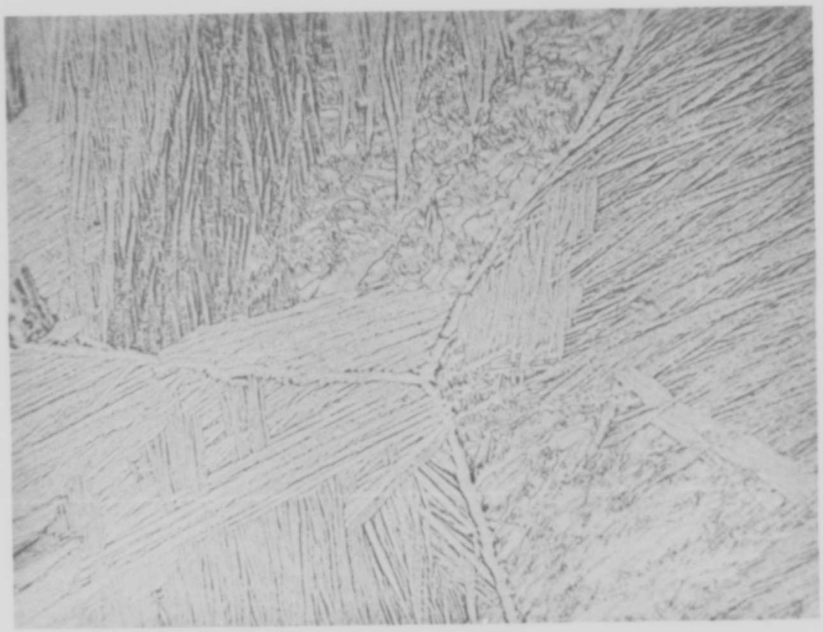

Beta Annealed

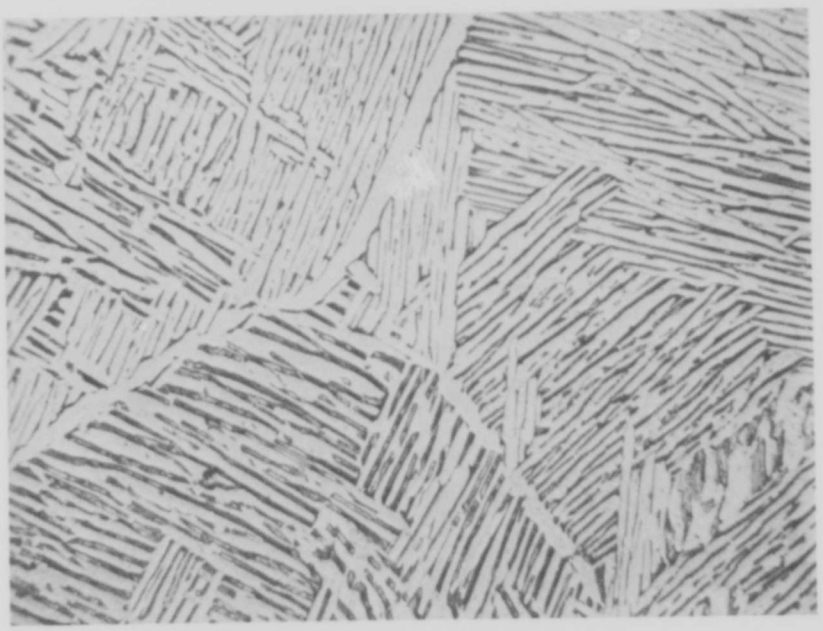

Beta Annealed Plus Diffusion-Bonding Cycle

FIGURE 56.–CONCLUDED

TABLE 31.–EFFECT OF DIFFUSION-BONDING CYCLE ON K_Q OF MILL-ANNEALED AND BETA-ANNEALED Ti-6Al-4V PLATE

Specimen	Sheet	Thermal cycle[a]	Grain direction	K_Q (ksi$\sqrt{in.}$)
DB-16	1486	AR	WR	48.5 (43.4)[b]
DB-1		AR	RW	52.5 (32.4)[b]
DB-17		AR + DB	WR	69.1
DB-2		AR + DB	RW	93.7
A-5		βI	WR	113.7
B-4		βI	RW	123.1
DB-19		βI + DB	WR	111.6
DB-4	1486	βI + DB	RW	123.0
B-1	7918	AR	WR	54.4
B-2		AR	RW	68.5
DB-7		AR + DB	WR	90.0
DB-12		AR + DB	RW	118.3
DB-6		βI	WR	110.9[c]
DB-11		βI	RW	93.2
DB-9		βI + DB	WR	105.1
DB-14	7918	βI + DB	RW	120.2

[a]AR As received
DB Diffusion bonding 1750° F/2 hr/furnace cooled at 150° F/hr to 600° F
βI Beta annealed 1900° F/30 min/air cooled + 1350° F/2 hr/air cooled

[b]Prior test points, see figure 40

[c]Fatigue crack length only 0.10 in.

An attempt was made using electron microscopy to evaluate the dislocation density of the plates with the various thermal cycles. In general the beta-annealed structure had the lowest number of dislocations, with the only areas of high density at the alpha/beta interface. The as-received condition contained the largest number of dislocations of the four treatments as a result of the mechanical deformation in the alpha-plus-beta field. The diffusion bond cycle material resulted in a significant elimination of the as-received dislocation structure, but was not as dislocation free as the beta-annealed condition. The beta-annealed plus diffusion bonding treatment had dislocation contents somewhere between those of the beta-annealed condition and the diffusion-bonded cycle. The elimination of the dislocation networks is probably at least partially the cause of the increase in K_Q for the equiaxed alpha (non-beta-annealed) material. It is difficult to conclude that this would be the cause of the increase in K_Q of the beta-annealed condition over the as-received condition because of the other changes such as texture and microstructure. However, one would expect some improvement in K_Q due to the more dislocation-free structure. It is hard to understand the reduction in K_{Iscc} of the diffusion-bonded plate 1486, since a dislocation-free material would be expected to have at least as high a stress-corrosion resistance as one with a heavier dislocation content. Conversely, it is possible that the more dislocation-free structure is the cause for the higher K_{Iscc} for plate 7918 in the diffusion-bonded condition over the as-received condition. Also, since the beta-annealed plates were more dislocation free than the beta-anneal plus diffusion bonded plates, the above argument might explain the higher K_{Iscc} results for the former. However, more work would be needed to confirm this.

3.2.7 Modified Stress-Corrosion Testing Procedure

A small number of tests were conducted to evaluate the possibility of modifying the sustained-load stress-corrosion testing procedure for possible material specification usage. The test used was based on a loading sequence in which a specimen was held at a first sustained K level in 3.5% NaCl for 20 min, then unloaded, recracked, and reloaded. In the modified procedure, instead of unloading and recracking the specimen, the load was increased (if there was no failure after 20 min) and held for 7 min at each of several increasing K levels. As long as there is no overload during the increasing of the stress intensity to the next level, there should be no exaggerated plastic yield zone effects. These effects have been observed in the past to retard stress corrosion and result in a higher K_{Iscc} than would have been obtained if the fatigue crack plastic zone was smaller. There is a possibility with this new test, however, that electrochemical passivation effects would prevent stress corrosion, resulting in higher measured threshold.

Five specimens were tested using this 20-min, 7-min, 7-min, ..., procedure and the results compared to those obtained with the 60-min sustained-load test with recracking between loadings. The results are shown in table 32. Except for the very low K_{Iscc} material (specimen ST-302 F-5), there is no basic disagreement between the two methods. Some of the variation in the results is caused by the slight difference in selected loads. There is one specimen (F-7) which did not fail at a K level of 35 ksi$\sqrt{\text{in.}}$ in the original test after 60 min but failed at this level in the modified test in 16 min. This can be attributed to general scatter in the test technique, material variability, and the fact that when a failure occurs at a long time (greater than approximately 10 min) the K level is very close to the threshold value. Although more testing is needed to confirm this procedure on a wider range of materials and heat-treat conditions, the technique does seem to have promise. At the very least the use of a 20-min sustained-load-type test as a specification "go/no go" test is justified to measure a minimum stress-corrosion resistance level. The disadvantage of using only a go/no go test is that the actual K_{Iscc} (or K_{scc}) cannot be determined. This precludes the measurement of the effect of material variables such as chemistry, heat treatment, and texture on K_{Iscc}. This favors the additional 7-min higher sustained-load-type testing in order to estimate the actual threshold value.

TABLE 32.–MODIFIED STRESS-CORROSION TEST PROCEDURE DATA

Specimen	Heat	Modified test procedure K level[a] (ksi$\sqrt{\text{in.}}$)					Old test procedure K level[a] (ksi$\sqrt{\text{in.}}$)			K_{Iscc}[b]
		First 20 min	Second 7 min	Third 7 min	Fourth 7 min	Fifth 7 min	First 60 min	Second 60 min	Third 60 min	
ST 302 F1	292030	NF 45.9	NF 55.0	F 64.1 (0)			NF 50	F 60 (0)		51
ST 302 F3	292030	NF 75.0	F 90 (1.5)				NF 80	F 90 (1)		82
ST 302 F5	D7390	NF 14.0	NF 17.0	NF 20.0	NF 23.0	F 26.0 (4)	NF 15	F 20 (1)		16
ST 302 F7	D7390	F 35.0 (16)					NF 35	F 45 (4)		38
ST 193 2054B	K4400	F 41.6 (12.5)					NF 25	NF 40	F 55 (1)	43

[a]NF No failure.
F Failure (time to failure in minutes).

[b]Using factor procedure outlined in section 2.5.5.

Tests were also conducted on three materials to very precisely determine the K_{Iscc} (K_{scc}) value and evaluate the time to failure at levels very close to the threshold values. Table 33 shows the results of these tests. For heat K7516 the no-failure K levels are, in ascending order, 31.2, 35.0, 36.9, 37.6, 39.0, 39.9, and 40.0 and the failure loads are 37.0, 39.0, 40.5, 41.6, 43.6, 44.0, and 46.4. There is an obvious overlap between no-failure and failure results in the range of K levels from 37.0 to 39.0, since in this range there are no-failure results higher than the failure results. This would indicate that the K_{Iscc} would be 38 ±1.5 ksi $\sqrt{in.}$ and also that there could be an error of 3 ksi $\sqrt{in.}$ if there were a no-failure test result of 40.0 ksi $\sqrt{in.}$ and this was used as the threshold value. There are many combinations of test results that could be used from the 14 data points in table 33 for heat K7516. They would all produce varying results for K_{Iscc}. Heat K6568 showed better consistency, since the no-failure data were 38.0, 39.0, 40.0, 40.0, 40.5, and 40.7, whereas the failure levels were 40.7, 40.9, 42.0, and 42.0. Taken arithmetically there is no overlap of the no-failure and failure data and one would predict the threshold level to 40.7 ±0.1 ksi $\sqrt{in.}$ This, of course, would be naive since this level of accuracy could not be maintained. However, the test does appear to be quite discriminating in its ability to determine the threshold. Similar accuracy was obtained with the single-edge-notched sheet specimens (heat 295377), for which the no-failure levels were 60.0, 65.0, and 68.0 and the failure levels were 69.0, 70.9, and 74.8. The difference between the sheet (SEN) and plate (NB) times to failure appear to be significant. Near the threshold level for the plate specimens the times to failure are relatively long (10-14 min), whereas on the sheet tests the time to failure was only 1 min at a K level of 1 ksi $\sqrt{in.}$ above the highest no-failure level.

TABLE 33.–MULTIPLE SPECIMEN STRESS-CORROSION TEST RESULTS

Specimen	Heat	Test[a]	Sustained load K levels[b] (ksi $\sqrt{in.}$)
FM 415-1	K7516	NB	NF 31.2, F 40.5 (11)
-2	K7516		F 41.6 (14)
-3	K7516		NF 35.0, NF 37.6, NF 40.0, F 43.6 (6)
-4	K7516		F 39.0 (13)
ST 309 1-5-9	K7516	NB	NF 39.9, F 46.4 (6)
1-2-11	K7516		F 37.0 (12)
1-2-8	K7516		NF 36.9, F 44.0 (13)
FM 415-5	K6586	NB	F 42.0 (9)
-6	K6586		NF 40.0, NF 40.5, NF 40.7
-7	K6586		F 40.9 (12)
-8	K6586		NF 38.0, NF 39.0, NF 40.0, F 42.0 (6)
FM 415-9	295377	SEN	NF 60.0, F 70.9 (3.2)
-10	295377		NF 65.0, F 74.8 (1)
-11	295377		NF 68.0, F 69.0 (3.5)

[a]NB Four-point, 0.480-in.-thick notched-bend specimen.
SEN 3- by 12-in. single-edge-notched 0.125-in.-thick specimen.

[b]NF No failure.
F Failure (time to failure in minutes).

3.3 Ti-6Al-4V EXTRUSIONS

Mechanical and fracture test data and metallurgical information as related to individual design properties are presented and discussed in this section. The effects of variations in chemical composition, microstructure, and crystallographic texture, K_A, are discussed for strength, fracture toughness, and stress-corrosion resistance.

3.3.1 Mechanical Properties

Tension and compression property test results of annealed Ti-6Al-4V extrusions varied significantly. TUS and TYS varied approximately 15% and 21%, respectively, based on the observed minimum values (table 34). Compression yield strength (CYS) varied 29%. The probable causes for these property variations are related to variations in alloy composition, microstructure, and crystallographic texture. Oxygen and aluminum content variations have been shown (ref. 4) to be particularly potent as related to titanium alloy property variations. For these data, the oxygen contents ranged from 0.12 to 0.20 weight percent and the aluminum contents ranged from 6.1 to 6.7 weight percent.

The morphology of the extrusion microstructures varied from the fully transformed beta-type (basketweave) shown in figure 57 to the alpha-beta type consisting of equiaxed or elongated primary alpha phase indicative of metal working below the beta transus (fig. 58). For analysis purposes each extrusion microstructure was rated on a scale from 1 to 10, with alpha-beta types receiving ratings as low as 1 and the basketweave types as high as 10 (microstructural rating, MR, table 34).

Crystallographic texture of the basal planes was generally of three types: (1) a "negative" texture with the majority of the basal planes normal to the extrusion direction (fig. 59), (2) a "positive" texture with the basal planes parallel to the extrusion direction and normal to the extrusion width direction (fig. 60), and (3) a random texture with the basal planes oriented relatively randomly (fig. 61). For quantitative purposes the K_A value (anisotropy factor) was calculated for each pole figure. Relatively random textures and textures that are strong in both the longitudinal and transverse directions can yield similar K_A values. This fact probably influences the correlation of K_A with mechanical properties.

In an attempt to determine quantitatively the effects of composition, microstructure, and texture on mechanical properties, the data were analyzed by linear regression analyses with the aid of a computer, resulting in the following equations for TUS, TYS, percent elongation, and CYS in the transverse direction:

$$\text{TUS} = 101 + 75.1(O_2) - 6.98(Al) + 16.1(V) + 45.4(Fe) - 0.69(MR) + 0.27(K_A)$$

$$R^2 = 0.69$$

$$\text{TYS} = 138 - 22.3(O_2) - 17.4(Al) + 24.3(V) + 62.7(Fe) - 1.5(MR) + 0.35(K_A)$$

$$R^2 = 0.84$$

TABLE 34.—Ti-6Al-4V ANNEALED EXTRUSION TEST RESULTS SUMMARY

Vendor	Heat	GD[a]	K_{Ic} (ksi$\sqrt{in.}$)	K_{Iscc} (ksi$\sqrt{in.}$)	Mechanical properties				Chemical composition (wt %)							MR[b]	K_A
					TUS (ksi)	TYS (ksi)	Elong (%)	CYS (%)	O_2	N_2	H_2	C	Al	V	Fe		
Harvey	BB-57	L			139.0	131.0	13.3	141.5	0.150	0.015	0.0054	0.023	6.2	4.0	0.21	7	29.4
	BB-57	T	74.0	34.0	142.4	133.0	14.0	143.4	0.150	0.015	0.0054	0.023	6.2	4.0	0.21	7	29.4
	BC-21	L			139.5	129.3	11.0	138.4	0.170	0.010	0.0043	0.042	6.58	4.07	0.25	8	21.6
	BC-21	T		43.5					0.170	0.010	0.0043	0.042	6.58	4.07	0.25	8	21.6
	BC-38	L			141.2	129.0	13.0	136.1	0.177	0.012	0.0041	0.018	6.50	4.1	0.16	8	8.42
	BC-38	T	117.0	34.9					0.177	0.012	0.0041	0.018	6.50	4.1	0.16	8	8.42
	BC-39	L		47.5	143.5	132.8	10.3	136.4	0.160	0.015	0.0050	0.029	6.40	4.0	0.23	8	0.64
	BC-39	T		48.0					0.160	0.015	0.0050	0.029	6.40	4.0	0.23	8	0.64
	BC-39A	L		51.5	143.5	132.8	10.7	136.4	0.160	0.015	0.0050	0.029	6.40	4.0	0.15	8	27.7
	BC-39A	T		45.0					0.160	0.015	0.0050	0.029	6.40	4.0	0.15	8	27.7
	BD-86	L			136.5	129.5	12.7	134.6	0.140	0.012	0.0056	0.030	6.40	4.2	0.26	4	16.6
	BD-86	T	80.3	49.5	137.0	130.4	12.5	138.2	0.140	0.012	0.0056	0.030	6.40	4.2	0.26	4	16.6
	BE-14	L			140.2	132.2	12.7	140.2	0.166	0.010	0.0052	0.029	6.4	4.2	0.18	7	7.2
	BE-14	T	122.4	44.3					0.166	0.010	0.0052	0.029	6.4	4.2	0.18	7	7.2
	BE-43	L			141.5	131.5	12.7	134.7	0.150	0.010	0.0029	0.032	6.4	4.1	0.24	7	7.0
	BE-43	T	76.6	48.5	145.1	128.2	11.5	141.4	0.150	0.010	0.0029	0.032	6.4	4.1	0.24	7	7.0
	BF-87-1	L	67.2	39.6	139.2	124.2	13.0	141.5	0.190	0.013	0.0054	0.025	6.3	4.11	0.25	6	35.8
	BF-87-1	T	71.8	39.7					0.190	0.013	0.0054	0.025	6.3	4.11	0.25	6	35.8
	BG-06	L			136.7	125.3	11.7	138.1	0.120	0.008	0.0042	0.015	6.4	4.2	0.21	9	5.5
	BG-06	T	75.9	34.0	137.9	126.9	12.0	139.3	0.120	0.008	0.0042	0.015	6.4	4.2	0.21	9	5.5
	BG-33-5	L	62.1	31.0	141.5	125.5	11.2	144.5	0.190	0.010	0.0065	0.020	6.59	4.27	0.21	7	3.5
	BG-33-5	T	65.6	42.3					0.190	0.010	0.0065	0.020	6.59	4.27	0.21	7	3.5
	BG-85	L	82.5	42.0	139.7	122.8	12.3	136.7	0.150	0.011	0.0050	0.023	6.42	4.07	0.21	8	17.8
	BG-85	T	81.5	43.4					0.150	0.011	0.0050	0.023	6.42	4.07	0.21	8	17.8
	BG-86-2	L	82.5	43.5	136.9	123.9	11.2	134.3	0.130	0.009	0.0053	0.027	6.55	4.08	0.23	4	16.6
	BG-86-2	T	81.5	51.5					0.130	0.009	0.0053	0.027	6.55	4.08	0.23	4	16.6
	BH-30	L	69.3	29.8	136.3	122.9	12.0	135.2	0.160	0.010	0.0024	0.031	6.44	4.11	0.20	7	29.2
Harvey	BH-30	T	72.4	38.0					0.160	0.010	0.0024	0.031	6.44	4.11	0.20	7	29.2

Note: Average data, usually two test values.

[a]For K_{Ic} and K_{Iscc} data, L = RW and RT, T = WR and WT, and ST = TR and TW test directions.

[b]Microstructural rating (1 = poor), 10 = excellent)

TABLE 34.—Continued

Vendor	Heat	GD[a]	K_{Ic} or K_Q (ksi$\sqrt{in.}$)	K_{Iscc} (ksi$\sqrt{in.}$)	Mechanical properties				Chemical composition (wt %)							MR[b]	K_A
					TUS (ksi)	TYS (ksi)	Elong (%)	CYS (%)	O_2	N_2	H_2	C	Al	V	Fe		
C-W	A1537	L		52.0	137.2	125.4	14.7	131.7	0.161		0.0082	0.016	6.12	4.10	0.19	9	- 8.1
	A1537	T	83.1	44.0	135.9	124.2	14.0	132.7	0.161		0.0082	0.016	6.12	4.10	0.19	9	- 8.1
	A1537B	L							0.161		0.0082	0.016	6.12	4.10	0.19	9	- 8.1
	A1537B	T	81.6	61.3					0.161		0.0082	0.016	6.12	4.10	0.19	10	1.0
	A1690	L			147.7	135.6	13.7	142.7	0.172		0.0072	0.025	6.20	4.18	0.17		
	A1690	T		30.0	155.9	148.5	16.0	169.9	0.172		0.0072	0.025	6.20	4.18	0.17		
	A1690B	T	70.9	47.5					0.172		0.0072	0.025	6.20	4.18	0.17	10	1.0
	A1701	L			138.3	127.9	13.5	133.8	0.176		0.0053	0.028	6.40	3.90	0.19		
	A1701	T	84.9	34.0	140.7	128.7	14.0	138.2	0.176		0.0053	0.028	6.40	3.90	0.19		
	A1701B	T	78.5	45.2					0.176		0.0053	0.028	6.40	3.90	0.19	10	1.0
	A1717	L			137.6	127.1	13.5	131.4	0.174		0.0089	0.015	6.23	4.22	0.18	2	-10.5
	A1717	T	86.9	34.0	140.7	129.9	13.5	138.1	0.174		0.0089	0.015	6.23	4.22	0.18	2	-10.5
	A1717B	T	79.8	44.0					0.174		0.0089	0.015	6.23	4.22	0.18	10	1.0
	A1757	L			135.5	125.5	13.8	132.7	0.185		0.0082	0.016	6.1	4.0	0.18	2	- 0.77
	A1757	T	74.0	31.0	150.3	138.2	13.5	148.8	0.185		0.0082	0.016	6.1	4.0	0.18	2	- 0.77
	A1757B	T	74.1	39.3					0.185		0.0082	0.016	6.1	4.0	0.18	10	1.0
	K3502	L		29.0	149.3	130.8	14.2	145.1	0.200		0.0067	0.015	6.3	4.3	0.20	1	77.0
	K3502	T		27.0					0.200		0.0067	0.015	6.3	4.3	0.20	1	77.0
	K6583	L			145.5	130.8	13.8	135.5	0.200		0.0074	0.026	6.2	4.3	0.18	1	92.9
	K6583	T		21.0					0.200		0.0074	0.026	6.2	4.3	0.18	1	92.9
	K6641	L			146.4	132.9	13.7	145.6	0.190		0.0082	0.026	6.2	4.2	0.18	1	
	K6641	T		21.5					0.190		0.0082	0.026	6.2	4.2	0.18	1	
	K6642	L			145.1	132.5	14.0	137.5	0.180		0.0089	0.026	6.2	4.1	0.16	1	141.9
	K6642	T		21.0					0.180		0.0089	0.026	6.2	4.1	0.16	1	141.9
	K6643	L			142.6	132.0	14.8	135.7	0.180		0.0091	0.022	6.3	4.3	0.17	2	
	K6643	T		22.0					0.180		0.0091	0.022	6.3	4.3	0.17	2	
	K6669	L			145.4	134.1	14.8	134.1	0.190		0.0067	0.022	6.2	4.1	0.18	2	55.0
	K6669	T		27.0					0.190		0.0067	0.022	6.2	4.1	0.18	2	55.0
	K6676	L			143.6	129.8	14.3	137.8	0.170		0.0067	0.026	6.3	4.1	0.14	2	58.5
	K6676	T		32.5					0.170		0.0067	0.026	6.3	4.1	0.14	2	58.5
	303876	L			144.3	134.3	13.5	136.4	0.196				6.5	4.3	0.19		
C-W	303876	T	69.8	29.3	144.5	132.5	14.5	149.1	0.196				6.5	4.3	0.19		

Note: Average data, usually two test values.

[a]For K_{Ic} and K_{Iscc} data, L = RW and RT, T = WR and WT, and ST = TR and TW test directions.

[b]Microstructural rating (1 = poor, 10 = excellent).

TABLE 34.—Concluded

Vendor	Heat	GD[a]	K_{Ic} (ksi$\sqrt{in.}$)	K_{Iscc} (ksi$\sqrt{in.}$)	Mechanical properties				Chemical composition (wt %)							MR[b]	K_A
					TUS (ksi)	TYS (ksi)	Elong (%)	CYS (%)	O_2	N_2	H_2	C	Al	V	Fe		
Timet	K4886	L		37.5	140.4	126.5	16.0	134.5	0.180	0.014	0.0070	0.022	6.1	4.2	0.16	9.5	-13.5
	K4886	T		38.0					0.180	0.014	0.0070	0.022	6.1	4.2	0.16	9.5	-13.5
	K6328	L		34.0	144.2	132.8	16.2	138.5	0.190	0.019	0.0060	0.026	6.3	4.1	0.16	8	-27.6
	K6328	T		34.5					0.190	0.019	0.0060	0.026	6.3	4.1	0.16	8	-27.6
	K6336	L		35.0	145.6	129.4	16.0	142.9	0.190	0.015	0.0080	0.026	6.4	4.1	0.22	8	-11.6
	K6336	T							0.190	0.015	0.0080	0.026	6.4	4.1	0.22	8	-11.6
	K6417	L		35.0	142.1	129.7	16.0	140.5	0.190	0.016	0.0050	0.026	6.3	4.0	0.15	9	-17.5
	K6417	T		37.5					0.190	0.016	0.0050	0.026	6.3	4.0	0.15	9	-17.5
	K6417A	L		35.0	142.1	127.9	16.0	140.3	0.190	0.016	0.0050	0.026	6.3	4.0	0.15	8	-16.9
	K6417A	T		43.5					0.190	0.016	0.0050	0.026	6.3	4.0	0.15	8	-16.9
	K5616	L		39.0	142.2	127.6	17.4	135.0	0.180	0.010	0.0060	0.026	6.3	4.1	0.17	10	-17.3
	K5616	T		35.0	142.2	127.6	17.4	135.0	0.180	0.010	0.0060	0.026	6.3	4.1	0.17	10	-17.3
	K5616A	L		35.5	142.2	127.6	17.4	135.0	0.180	0.010	0.0060	0.026	6.3	4.1	0.17	10	-15.3
Timet	K5616A	T		34.0	142.2	127.6	17.4	135.0	0.180	0.010	0.0060	0.026	6.3	4.1	0.17	10	-15.3

Note: Average data, usually two test values.

[a]For K_{Ic} and K_{Iscc} data, L = RW and RT, T = WR and WT, and ST = TR and TW test directions

[b]Microstructural rating (1 = poor, 10 = excellent)

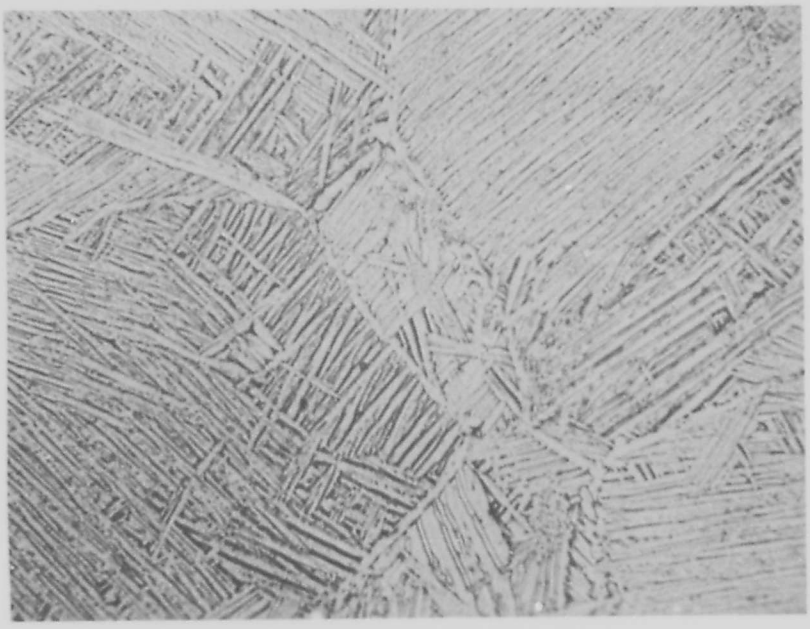

FIGURE 57.– Ti-6Al-4V EXTRUSION MICROSTRUCTURE REPRESENTATIVE OF A FULLY TRANSFORMED BETA MORPHOLOGY, MR=10 (X500)

FIGURE 58.– Ti-6Al-4V EXTRUSION MICROSTRUCTURE TYPICAL OF ALPHA-BETA-TYPE MORPHOLOGY, MR=1 (X500)

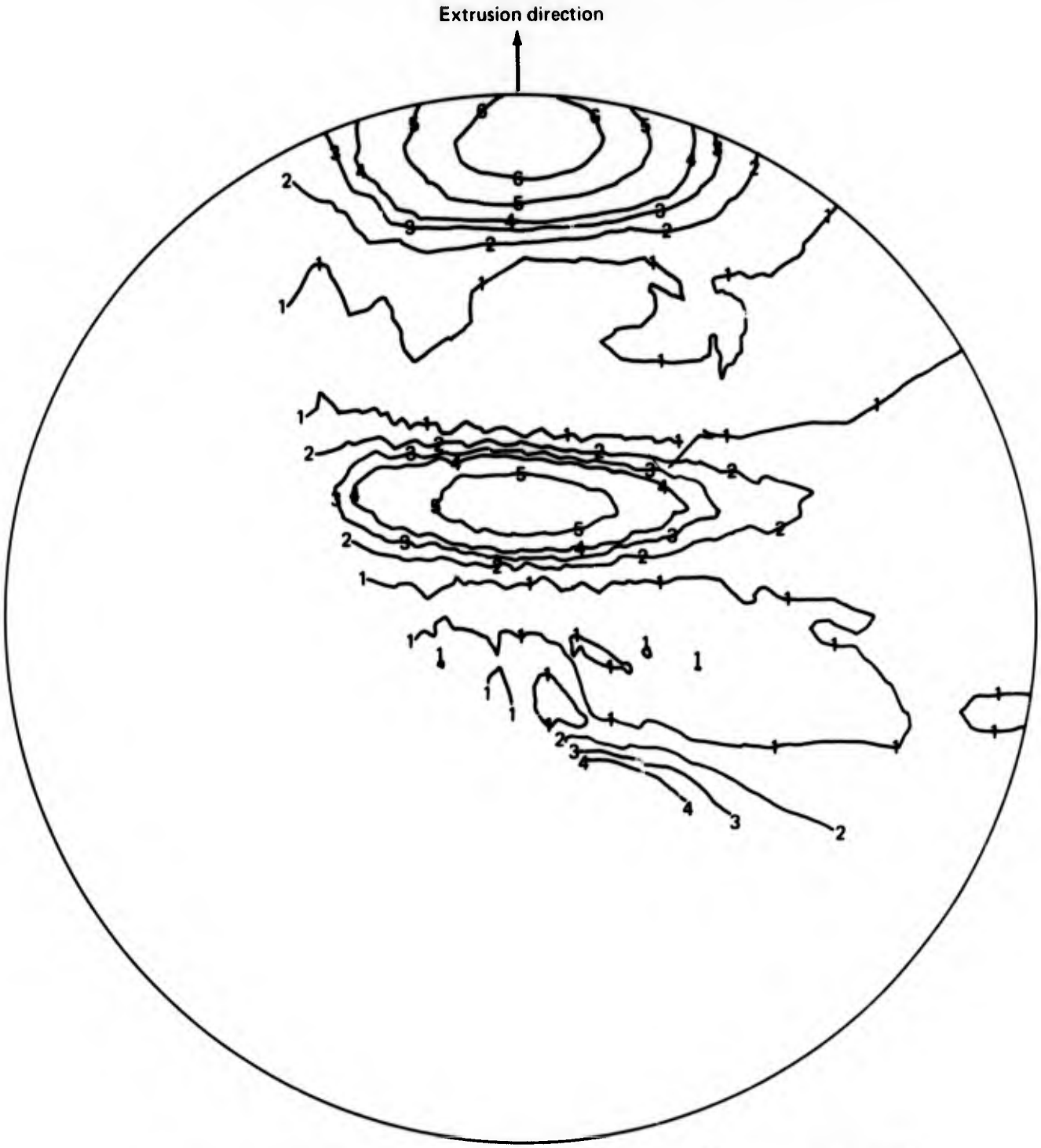

Contour lines	1	2	3	4	5	6
Times random intensity	0.5	1.0	1.5	2.0	4.0	8.0

$K_A = -56.8$

FIGURE 59.– POLE FIGURE FOR Ti-6Al-4V EXTRUSION WITH A HIGH NEGATIVE TEXTURE OF BASAL PLANES, SAMPLE 11M-1

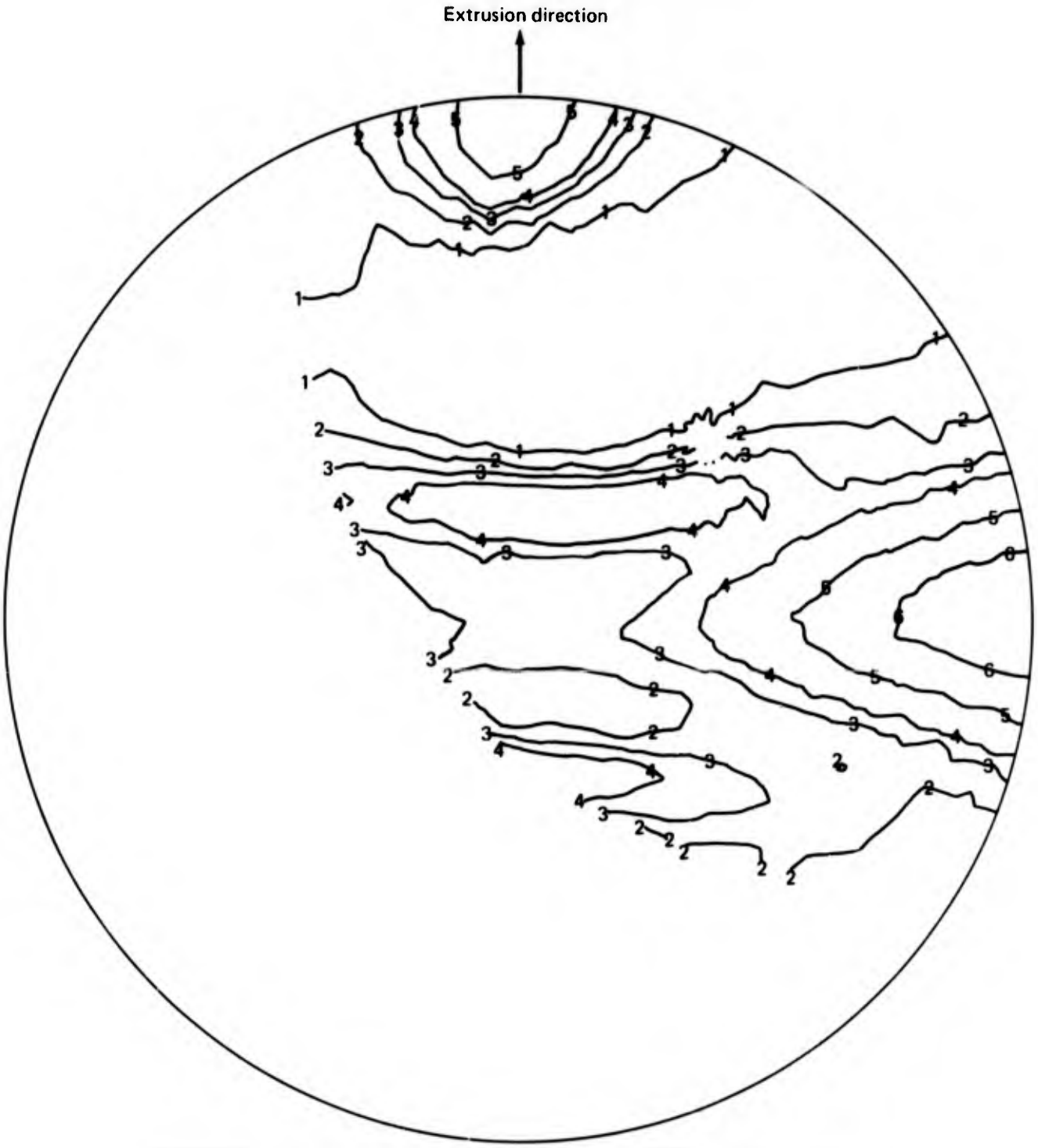

Contour lines	1	2	3	4	5	6
Times random intensity	0.5	1.0	1.5	2.0		3.0

$K_A = 141.9$

FIGURE 60.—POLE FIGURE FOR Ti-6Al-4V EXTRUSION WITH A HIGH POSITIVE TEXTURE OF BASAL PLANES, SAMPLE 6M-1

Contour lines	1	2	3	4	5	6
Times random intensity	0.5	1.0	1.5	2.0		

K_A = -5.99

FIGURE 61.– POLE FIGURE FOR Ti-6Al-4V EXTRUSION WITH A RELATIVELY RANDOM ORIENTATION OF BASAL PLANES, SAMPLE 8M-1

Percent elongation $= 40.2 + 8.9(O_2) - 4.7(Al) + 0.76(V) - 6.1(Fe) - 0.13(MR) + 0.038\ (K_A)$

$R^2 = 0.86$

CYS $= 116.5 + 12.6(O_2) - 23.1(Al) + 39.7(V) + 70.5(Fe) - 1.7(MR) + 0.51(K_A)$

$R^2 = 0.71$

where:

O^2 = oxygen content in wt %

Al = aluminum content in wt %

V = vanadium content in wt %

Fe = iron content in wt %

MR = microstructural rating (1 = alpha-plus-beta type and 10 = transformed beta type)

K_A = anisotropy factor

The similar equations for the longitudinal grain direction are as follows:

TUS $= 123 + 70.4(O_2) + 4.37(Al) - 5.8(V) - 5.2(Fe) + 0.34(MR) - 0.0083(K_A)$

$R^2 = 0.62$

TYS $= 168 + 12.5(O_2) + 3.06(Al) - 15.4(V) + 3.6(Fe) + 0.08(MR) - 0.05(K_A)$

$R^2 = 0.28$

Percent elongation $= 60.4 + 46.3(O_2) - 10(Al) + 1.98(V) + 0.44(Fe) + 0.13(MR) - 0.034(K_A)$

$R^2 = 0.68$

CYS $= 42.9 + 80.4(O_2) + 13.8(Al) - 1.13(V) - 11.4(Fe) + 0.14(MR) + 0.13(K_A)$

$R^2 = 0.65$

Detailed regression analysis information is contained in appendix F.

The mechanical property equations for the transverse grain direction show good correlation between properties and composition and microstructure. The multiple correlation coefficients (R^2) were remarkably high (0.69 to 0.86). The significant independent variables were microstructure (MR) and texture (K_A). The standard deviation of the coefficients for MR and K_A for all equations were less than 20% of the coefficient value. Except for the standard

deviation of the vanadium coefficient in the TYS equation, all the coefficients for oxygen, aluminum, vanadium, and iron had extremely high standard deviations and the coefficients can only be used to show trends. These high standard deviations are most likely the result of inaccurate chemical analyses and the small data population used to determine the equations (e.g., 10 sets of transverse data).

In general, higher transverse mechanical properties can be achieved with an alpha-beta type microstructure (low MR ratings) and high positive textures (high K_A values).

The regression analysis equations for the longitudinal mechanical properties are comparable to those for the transverse grain direction. The multiple correlation coefficients (R^2) were high (0.62 to 0.68) except for TYS (0.28). Again, microstructure (MR) and texture (K_A) were the significant parameters in that their respective standard deviations were low. However, the coefficients of MR and K_A for the longitudinal grain direction generally had signs opposite to those for the transverse grain direction. The lower correlations for the longitudinal grain direction are probably related to the fact that the longitudinal data were generated by various vendor laboratories and the transverse data were generated at one Boeing laboratory. Differences in test techniques between laboratories generally result in some data inconsistencies.

3.3.2 Fracture Properties

Extrusion fracture characteristics including K_{Ic} and K_{Iscc} varied greatly for the extrusions evaluated. Plane strain fracture toughness as measured by K_{Ic} or K_Q values varied from 6.21 to 122.4 ksi$\sqrt{in}$. Again, the probable causes of this wide range of data are associated with variations in alloy composition, microstructure, and crystallographic texture. In addition, the K_Q values can be depressed or increased by excessive plasticity encountered when the specimen is too thin to meet plane strain fracture validity requirements. Compositional variations were discussed in the previous section.

The effects of texture on K_Q values did not follow a consistent trend. Higher values of K_Q for the transverse grain direction than for the longitudinal direction were expected for high negative K_A values. This comparison, however, was based on only five data points, which were representative of narrow ranges of textures and K_Q values. No consistent trend was established for the relationship of fracture toughness and microstructure. However, transverse K_Q values for material with microstructures consisting of some equiaxed or elongated alpha grains and with a negative K_A value were reduced slightly after beta annealing. This effect is thought to be related more to the change in texture than to the changes in morphology of the microstructure.

The regression analysis for fracture toughness in the transverse grain direction is as follows:

$$K_Q = 86.2 - 180(O_2) + 24.2(Al) - 14.7(V) - 321(Fe) - 0.63(MR) - 0.12(K_A)$$

$$R^2 = 0.28$$

where:

alloying elements are in wt %

MR = microstructural rating

K_A = anisotropy factor

The equation shows a poor correlation of composition and microstructure to fracture toughness, as indicated by $R^2 = 0.28$. The coefficients for MR and K_A had low standard deviations and are considered significant. The effect of MR, however, is weak in that the maximum change in MR of 10 would only change K_Q by 6.3 ksi$\sqrt{in}$. The effect of texture is stronger in that a maximum change of 22 ksi$\sqrt{in}$. could be expected.

Stress-corrosion resistance, K_{Iscc}, was the property most sensitive to variations of composition, microstructure, and texture. Data varied nearly 300% as values ranged from 21 to 61 ksi$\sqrt{in}$. The data when analyzed by regression analysis resulted in the following equation for the transverse grain direction:

$$K_{Iscc}\,(trans) = 95 - 120(O_2) - 5.6(Al) - 5.0(V) + 76(Fe) + 0.94(MR) - 0.084(K_A)$$

$$R^2 = 0.69$$

For the longitudinal grain direction, the equation is as follows:

$$K_{Iscc}\,(long) = 237 - 390(O_2) - 4.3(Al) - 23.8(V) - 73(Fe) + 1.6(MR) - 0.31(K_A)$$

$$R^2 = 0.72$$

Both equations show a fair correlation of independent variables to K_{Iscc}. The significant coefficients are for the variables MR and K_A for both equations where the coefficient standard deviations are lower. Using the maximum variations typically observed for Ti-6Al-4V extrusion composition, microstructure, and texture, the maximum effect of each variable was determined for each equation. For both equations, K_A and oxygen content had the strongest effects on K_{Iscc}. The standard deviations for the oxygen coefficients were 769 for the transverse equation and 2209 for the longitudinal equation. These high values are again most probably related to the inaccuracies in oxygen analyses. The aluminum coefficients also had high standard deviations (11.5 transverse and 44.5 longitudinal). Although the standard deviations for oxygen and aluminum are high, both equations show a negative trend for these alloying elements, which verifies the results previously found for beta-processed plate.

Significant improvements in stress-corrosion resistance were observed after beta annealing at 1900° F. K_{Iscc} values increased as much as 58%. These improvements are related to both improved microstructures (increased MR ratings) and improved crystallographic texture. In the regression analysis, beta-annealed material was assumed to possess microstructures with an MR rating of 10 and a K_A value of 1.0. This was justified on the basis of previous experience with Ti-6Al-4V beta-annealed plate (ref. 3).

The most consistent test results for both fracture properties and mechanical properties were those for extrusions supplied by Timet. The associated compositions, microstructures, and textures were also very consistent (table 34).

3.4 Ti-6Al-4V BAR AND FORGINGS

The test results generated for Ti-6Al-4V bar material are presented and discussed as related to individual properties including strength, fracture toughness, and stress-corrosion resistance. Some data from previous evaluations (ref. 5) were included with the present data so as to provide an improved statistical sample for regression analyses.

3.4.1 Mechanical Properties

Major variations in the mechanical properties (table 35) of beta-processed bar including TUS, TYS, elongation, and reduction in area (RA) were observed in comparing different material heat lots and in comparing the various grain directions within a heat lot. The maximum variations between heat lots for TUS and TYS were 17% and 27%, respectively. Maximum directionality within a heat lot was 7% for TUS and 4.5% for TYS. Tensile ductility (i.e., elongation and RA) varied as much as 140% and 160%, respectively, in maximum differences between heat lots. Within a heat lot, variations of 63% and 55%, respectively, were observed.

The variations in chemical composition, microstructure, and crystallographic texture, (K_A) associated with the mechanical property variations of table 35 were significant. Oxygen contents ranged from 0.110 to 0.196 weight percent. Aluminum contents varied from 6.0 to 6.4 weight percent. Microstructures as denoted by MR ratings ranged from 1 to 7, and K_A values for texture ranged from -38 to +38.

Regression analyses of mechanical properties and the variables of oxygen, aluminum, microstructure (MR), and texture (K_A) resulted in poor correlations. The multiple correlation coefficients (R^2) for TUS, TYS, percent elongation, and RA were all less than 0.5. The analysis data are listed in appendix G. The lack of correlation is probably related to inaccuracies in chemical analyses, small data population representing relatively narrow ranges in composition, and to other independent variables not included in the regression analyses. Particularly, the varying degrees of forging or rolling applied to each bar can be a major factor governing mechanical properties. This variable can somewhat be accounted for by including "as-forged thickness" or "cross-sectional area" into regression analyses. Future analyses should include these variables.

3.4.2 Fracture Properties

The fracture properties of Ti-6Al-4V bar, including K_{Ic} (or K_Q) and K_{Iscc}, were found to be highly variable for the materials evaluated. While the data generated during the SST program emphasized K_{Iscc} testing, the emphasis of this evaluation was directed toward the generation of K_{Ic} or K_Q data.

TABLE 35.–Ti-6Al-4V ANNEALED BAR TEST RESULTS SUMMARY

Vendor	Heat	GD[a]	K_Q (ksi$\sqrt{in.}$)	K_{Iscc} (ksi$\sqrt{in.}$)	Mechanical properties				O_2 (wt %)	Al (wt %)	MR[b]	K_A
					TUS (ksi)	TYS (ksi)	Elong (%)	RA (%)				
Timet	K4474	L		34.2	137.6	123.2	14.1	30.1	0.150	6.4	4	17.9
	K4474	T		39.9					0.150	6.4	4	17.9
	K4474A	L		34.5	143.3	132.6	13.7	25.2	0.150	6.4	4	- 0.66
	K4474A	T		35.9					0.150	6.4	4	- 0.66
	K4504	L		34.5	141.0	126.6	13.1	26.3	0.160	6.2	3	- 2.83
	K4504	T		35.2					0.160	6.2	3	- 2.83
	K5528	L	64.1	36.9	146.8	139.4	17.0	34.9	0.177	6.2	1	5.3
	K5528	T	50.6	29.0	148.0	139.8	11.0	21.6	0.177	6.2	1	5.3
	K5528	ST	53.3	25.9	147.6	140.4	12.0	22.3	0.177	6.2	1	5.3
	K6348	L	132.0	57.0					0.110	6.3	7	- 6.3
	K6348	T	117.8	45.0					0.110	6.3	7	- 6.3
	K6348	ST	114.0	45.0					0.110	6.3	7	- 6.3
	K7174	L			138.4	128.8	7.0	15.0			2	- 9.8
	K7174	T	66.1	40.9	140.6	131.0	9.0	15.0			2	- 9.8
	K7533	L			139.7	130.0	11.0	22.0			3	8.6
	K7533	T	73.9	41.1	140.6	131.0	10.0	18.9			3	8.6
	K7758	L			128.7	115.1	13.0	21.0	0.140	6.4		
	K7758	T	71.0	38.5	137.7	115.1	9.0	27.3	0.140	6.4		
	K7758	ST			131.6	118.2	10.0	21.0	0.140	6.4		
	K7888	L			128.4	115.2	11.5	17.2	0.190	6.1	3	0.77
	K7888	T	75.7	42.6	125.9	110.6	8.0	19.5	0.190	6.1	3	0.77
Timet	K7888	ST			128.0	110.4	11.0	22.3	0.190	6.1	3	0.77

Note: Average data, usually two test values.

[a]For K_{Ic} and K_{Iscc} data, L = RW and RT, T = WR and WT, and ST = TR and TW test directions.

[b]Microstructural rating (1 = poor, 10 = excellent).

TABLE 35.—Concluded

Vendor	Heat	GD[a]	K_Q (ksi$\sqrt{in.}$)	K_{Iscc} (ksi$\sqrt{in.}$)	Mechanical properties				O_2 (wt %)	Al (wt %)	MR[b]	K_A
					TUS (ksi)	TYS (ksi)	Elong (%)	RA (%)				
RMI	301918	L			141.9	125.6	11.7	24.0	0.192	6.4		
	301918	T	67.0						0.192	6.4		
	302318	L			142.9	129.2	13.5	36.0	0.186	6.3	7	36.7
	302318	T	92.8	36.0	143.8	129.7	12.0	31.5	0.186	6.3	7	36.7
	302318A	L			142.3	126.6	14.0	32.5	0.179	6.3	7	-21.7
	302318A	T	91.0	36.0	141.8	128.8	12.5	32.8	0.179	6.3	7	-21.7
	704363	T	59.6	31.0							3	28.9
	704429	L			135.6	122.5	10.0	19.3	0.176	6.4	4	-37.7
	704429	T	85.3	51.0	139.9	125.9	9.5	19.7	0.176	6.4	4	-37.7
	704429	ST			138.4	123.9	9.0	19.3	0.176	6.4	4	-37.7
	704438	L			135.7	122.2	10.0	19.3	0.196	6.4	5	-13.1
	704438	T	79.2	52.0	135.9	123.0	9.3	19.7	0.196	6.4	5	-13.1
	704438	ST			137.6	122.3	9.0	19.3	0.196	6.4	5	-13.1
RMI	804445	T	69.3	41.0							2	-14.6
Armco	K00573C	T		64.5					0.170	6.0	5	-13.7
	K00573B	T		45.0					0.170	6.0		
Armco	K00573D	T		57.0					0.170	6.0	6	-69.4

Note: Average data, usually two test values.

[a]For K_{Ic} and K_{Iscc} data, L = RW and RT, T = WR and WT, and ST = TR and TW test directions.

[b]Microstructural rating (1 = poor, 10 = excellent).

3.4.2.1 Stress-Corrosion Resistance, K_{Iscc}

Stress-corrosion resistance for annealed bar was observed to range from 26 to 65 ksi $\sqrt{in}$. (table 35). The directionality of K_{Iscc} was at a maximum of only 11 ksi $\sqrt{in}$. The variations generally correlated with differences in texture, K_A, and variations in composition. Negative values of K_A were associated with relatively higher transverse K_{Iscc} values. Materials with lower oxygen content had higher K_{Iscc} values. Fully transformed beta-type microstructures (high MR ratings) generally could be linked to higher K_{Iscc} characteristics. Examples of the various types of bar microstructures and textures (basal plane pole figures) are shown in figures 62 through 67.

Regression analyses of the data from table 35 resulted in the following equation relating K_{Iscc} to oxygen and aluminum contents, microstructure, and texture, K_A, for the transverse grain direction. Sufficient data were not available for the longitudinal grain direction (RW plus RT) and the short transverse grain direction (TR plus TW) to conduct analyses.

$$K_{Iscc}\,(\text{trans}) = 181 - 112(O_2) - 20.3(Al) + 1.3(MR) - 0.15(K_A)$$

$$R^2 = 0.58$$

where:

Alloying elements are in weight percent

MR = microstructural rating (alpha-beta type = 1, and transformed beta type = 10)

K_A = anisotropy factor

The standard deviations for each of the coefficients are listed in appendix G. The independent variables of aluminum, MR, and K_A were significant with relatively low standard deviations. Again, the oxygen coefficient had a high standard deviation and can only be used to show the negative trend. The high standard deviation for the oxygen coefficient is most likely a result of inaccuracies in oxygen content determinations. The texture factor, K_A, produces the largest change in K_{Iscc} considering the range in K_A likely to occur for Ti-6Al-4V bar. The next stronger factor is aluminum, which with a likely change from 5.8% to 6.7% can affect K_{Iscc} by 18.3 ksi $\sqrt{in}$.

3.4.2.2 Fracture Toughness, K_{Ic} or K_Q

The fracture toughness of annealed Ti-6Al-4V bar varied from 51 to 132 ksi $\sqrt{in}$. The higher values observed were determined using 0.480-in.-thick, four-point-loaded, notched bend specimens that resulted in K_Q values rather than valid K_{Ic} values. In spite of this problem, fracture toughness variations generally correlated with variations in alloy composition, microstructure, and texture. A regression analysis was conducted for the transverse grain direction values of fracture toughness. The resulting equation is as follows:

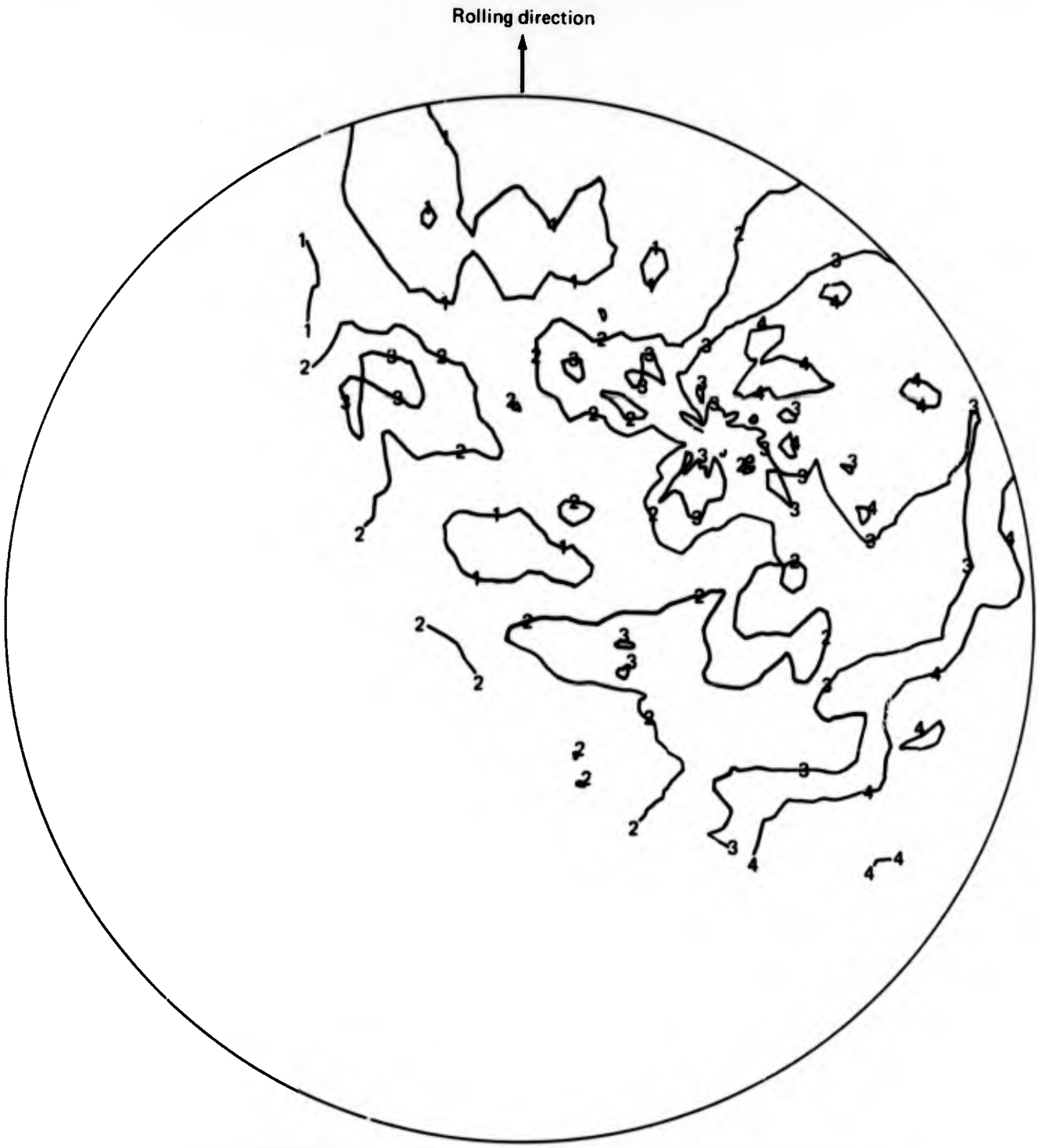

Contour lines	1	2	3	4	5	6
Times random intensity	0.5	1.0	1.5	2.0		

$K_A = 45.2$

FIGURE 62.– BASAL PLANE POLE FIGURE FOR Ti-6Al-4V BETA-ROLLED BAR, SAMPLE FM 931-1

Contour lines	1	2	3	4	5	6
Times random intensity	0.5	1.0	1.5	2.0		

$K_A = 5.28$

FIGURE 63.– BASAL PLANE POLE FIGURE FOR Ti-6Al-4V BAR, SAMPLE F 382-7

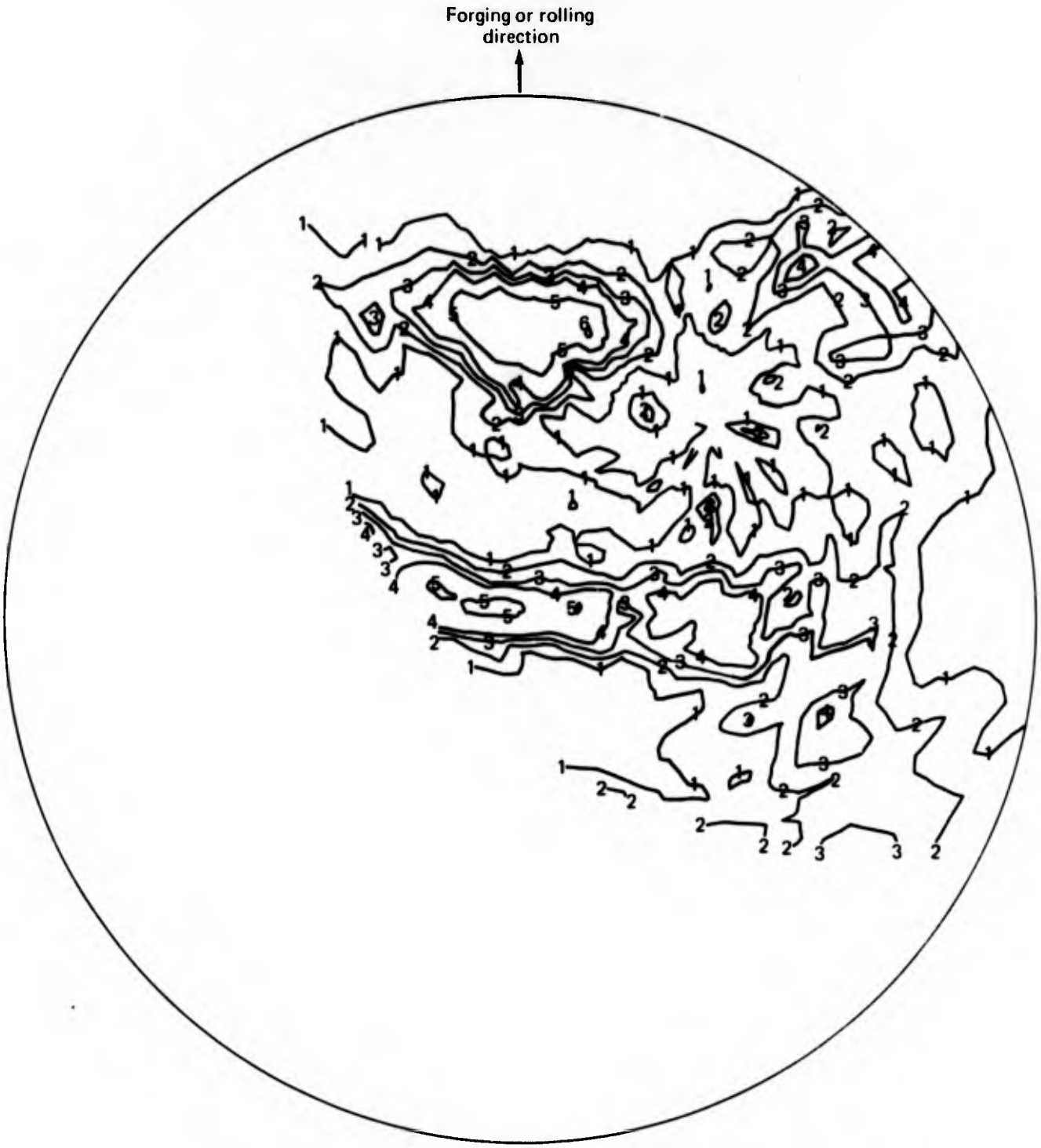

Contour lines	1	2	3	4	5	6
Times random intensity	0.5	1.0	1.5	2.0	4.0	8.0

$K_A = -14.6$

FIGURE 64.– BASAL PLANE POLE FIGURE FOR Ti-6Al-4V BAR, SAMPLE F 414-18

FIGURE 65.–MICROSTRUCTURE OF Ti-6Al-4V BETA-ROLLED BAR, SAMPLE FM 931-1 (X500)

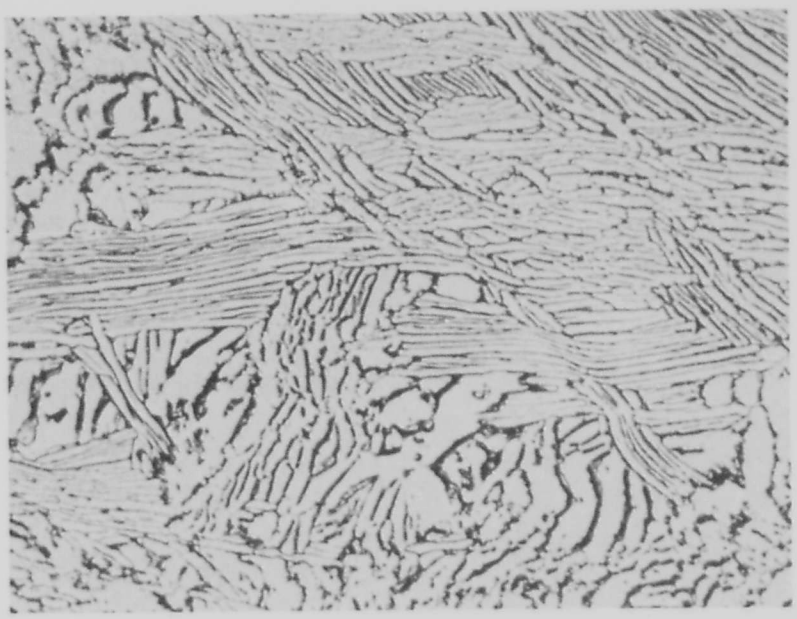

FIGURE 66.–MICROSTRUCTURE OF Ti-6Al-4V BAR, SAMPLE F382-7 (X500)

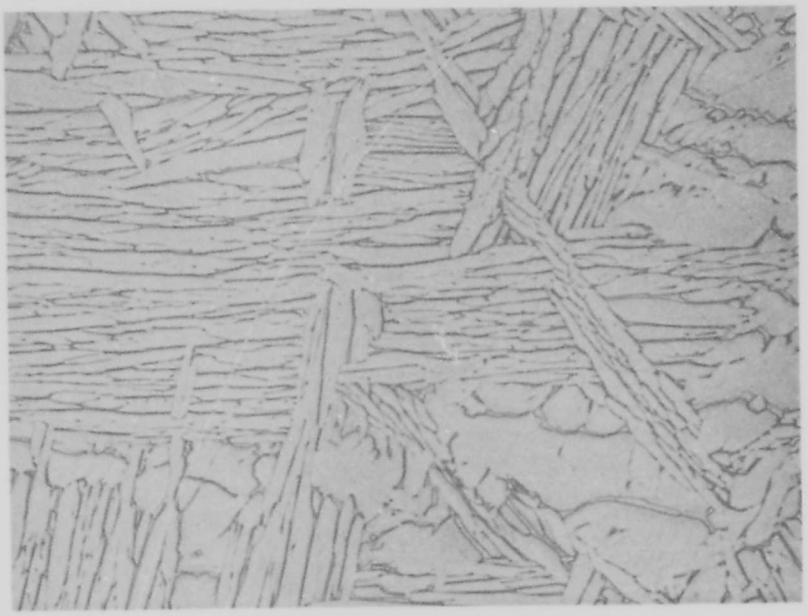

FIGURE 67.–MICROSTRUCTURE OF Ti-6Al-4V BAR, SAMPLE F414-18 (X500)

$$K_Q\,(\text{trans}) = 141 - 274(O_2) - 6.83(Al) + 6.42(MR) - 0.023(K_A)$$

$$R^2 = 0.91$$

This equation has the highest multiple correlation coefficient, R, determined for all of the regression analyses conducted on all Ti-6Al-4V forms included in this report. The coefficients for both MR and K_A are significant. Again, the oxygen and aluminum coefficients have high standard deviations and should be used only to show trends. The strongest factor affecting K_Q is microstructure in that as MR varies from an alpha-beta type to a fully transformed beta type, the K_Q can change by approximately 64 ksi$\sqrt{\text{in}}$.

4.0 CONCLUSIONS

The mechanical, fracture, and metallurgical evaluation conducted on titanium mill products procured for the SST prototype program has led to the following general conclusions, grouped by mill product form.

4.1 SHEET

Fracture toughness.—Fracture toughness, K_c, of Ti-6Al-4V hand-mill sheet is generally high (140-180 ksi$\sqrt{in.}$) for a wide variety of chemical compositions and textures.

Compression yield strength.—The compression yield strength of Ti-6Al-4V hand-mill sheet is markedly affected by texture such that large differences between the longitudinal and transverse CYS can occur for highly textured sheet.

Super ELI sheet.—Both continuously rolled and hand-mill super ELI sheet have very high toughness and stress-corrosion resistance. Higher K_c and K_{scc} values are associated with the transverse direction, which is perpendicular to the general alignment of basal planes.

Stress-corrosion resistance.—The K_{scc} of Ti-6Al-4V sheet is generally 40% lower for the STA 1000° F heat treatment than for the duplex-annealed heat treatment. However, unfavorable texture and relatively high oxygen and aluminum contents can reduce the K_{scc} more drastically than this STA 1000° F heat treatment.

Furnace cooling of textured sheet through the α_2 (Ti_3Al) region results in large reductions in K_{scc} compared to the as-received heat treatment condition.

The environmental stress-corrosion resistance is markedly affected by the salt concentration of the test environment. A higher K_{scc} was observed in distilled water, rain water, and 0.0035% salt water than in 0.35% and 3.5% salt water.

The following is a regression analysis equation for the transverse K_{scc} (ksi$\sqrt{in.}$) of hand-mill sheet.

$$K_{scc}\,(\text{trans}) = 182.5 - 0.95(\text{Al}) - 720(O_2) - 2.32(\alpha_2) - 1.91(\Delta\text{TYS}) - 0.090(K_A) - 122(\text{gage})$$

where:

Al = aluminum content (wt %)

O_2 = oxygen content (wt %)

α_2 = quantitative ordering parameter (0 to 10)

ΔTYS = transverse minus longitudinal yield strength (ksi)

K_A = anisotropy factor from pole figure

gage = sheet thickness (in.)

Crack growth rate correlation.—In Ti-6Al-4V sheet excellent correlation can be obtained between actual fatigue crack growth measurements and striation spacing measurements using electron microscopy replication techniques.

4.2 PLATE

Fracture toughness.—Valid tests using 2.5-in.-thick specimens showed the K_{Ic} for beta-annealed Ti-6Al-4V to be generally in the range of 91-104 ksi $\sqrt{in.}$

Stress-corrosion resistance.—For low-oxygen Ti-6Al-4V, a 25%-40% reduction in K_{Iscc} for the STA 1000° F heat treatment occurs compared to the beta-annealed condition. The reduction is much less for higher oxygen content material.

The effect of a high-temperature (1750° F) simulated diffusion bonding cycle on Ti-6Al-4V is to increase the fracture toughness for an alpha-beta-worked Ti-6Al-4V plate. However, a significant reduction in K_{Iscc} occurs with this treatment. For the beta-annealed condition, no increase in toughness was observed but a marked decrease in K_{Iscc} occurred after this high-temperature cycle.

A modified K_{Iscc} testing procedure in which the loads are sustained for shorter periods gave fairly good correlation when compared to the conventional 60-min sustained-load test.

4.3 EXTRUSIONS

Ti-6Al-4V extrusions procured for the SST prototype are characterized by wide variations in mechanical and fracture properties, which are primarily related to variations in alloy composition, microstructure, and texture. The variables of oxygen content, microstructure, and crystallographic texture cause the major variations in K_{Iscc} of Ti-6Al-4V extrusions. Low transverse grain direction values of K_{Iscc} are related to high oxygen contents, positive textures (high K_A values), and elongated or equiaxed alpha phase morphology. Low longitudinal K_{Iscc} properties are associated with high negative textures. Typical variations in iron and vanadium contents do not cause major variations in K_{Iscc} properties. Low aluminum contents appear to enhance fracture properties.

The effects of variations in alloy composition, microstructure, and texture on mechanical properties are less pronounced and opposing to those on fracture properties.

A greatly improved combination of mechanical, fracture toughness, and stress-corrosion properties can be achieved for Ti-6Al-4V extrusions by more stringent controls on composition, microstructure, and crystallographic texture.

4.4 BAR AND FORGINGS

The mechanical and fracture characteristics of beta-processed Ti-6Al-4V bar and forging material procured for the SST program were highly variable. These variations were related to test direction and variations in alloy composition, microstructure, and texture. Relatively high oxygen contents (0.19 weight percent) can be related to high strength, moderate fracture toughness, and low stress-corrosion resistance (K_{Iscc}). Regression analyses of the fracture toughness data resulted in the following equation, which explains nearly 92% of the variation in K_Q data:

$$K_Q \text{ (trans)} = 141 - 274(O_2) - 6.8(Al) + 6.42(MR) - 0.023(K_A)$$

where:

Alloying elements are in weight percent

MR = microstructure rating (alpha-beta type = 1, and transformed beta type = 10)

K_A = anisotropy factor relating the difference in basal plane orientation for both transverse and longitudinal grain directions.

5.0 RECOMMENDATIONS

The tests and analyses conducted as part of phase I of the SST Technology Follow-On program provide an excellent titanium technology base. The work in phase II includes the development of new titanium materials specifications based on the new technology generated in phase I. Materials procured to the new specifications will be evaluated to verify new specification requirements. The tests and analyses of phase I, however, present additional technical questions to be answered by future work. Additional investigative effort is recommended for the following areas.

5.1 HAND-MILL AND CONTINUOUSLY ROLLED SHEET

1. Further quantitative work is required to more fully evaluate the effect of α_2 formation on the stress-corrosion resistance of Ti-6Al-4V. The interrelated effects of texture, chemical composition, and microstructure must be determined.

2. To make regression analysis more meaningful, a complete range of chemistries for Ti-6Al-4V sheet should be evaluated. This would include oxygen (0.04%-0.20%), aluminum (5.5%-6.5%), vanadium (3.5%-4.5%), and iron (0.02%-0.50%).

3. Continued evaluation is required with respect to quantitative relationships between texture and material properties such as K_C, K_{SCC}, E_T, TYS, etc. Work should be centered around minimizing texture and hence property directionality as well as the development of specific textures to increase properties.

5.2 BETA-PROCESSED PLATE

1. Further work is required in determining the effects of texture, microstructure, and chemical composition on K_{Ic}. Welding additional material to the plates to be tested will prove useful in meeting valid K_{Ic} thickness requirements.

2. More work is required on the effect of mill processing on texture and hence on final properties. The relationship between beta annealing and mill processing must also be determined with respect to resulting texture and properties.

3. The effect of α_2 formation on the properties of beta-processed Ti-6Al-4V plate must be more quantitatively assessed, with special emphasis on K_{Iscc}.

5.3 EXTRUSIONS

Additional regression analyses of extrusion properties and metallurgical parameters should be conducted to determine more accurately the effects of metallurgical variables on properties. The analyses should include more extrusion data covering wider ranges in properties and alloy composition. The chemistries for existing extrusion data plus new data should be determined on a more accurate basis. Additional metallurgical factors such as grain size, extrusion shape and size, ordering (α_2) parameter, and an improved texture factor in lieu of K_A, should be included in the analyses.

5.4 BAR AND FORGINGS

1. Other metallurgical factors relating to bar and forging material should be added to those evaluated in this study and further analyzed by regression analyses. These should include nitrogen, carbon, iron, and vanadium contents; microstructural parameters of prior beta grain size and alpha phase morphology and size; and modified texture factors that are related to all three grain directions. Again, alloy chemical composition should be more accurately analyzed.

2. The relationships between hot working deformation and microstructure should be determined by a systemic study. The microstructural parameters should include grain size and shape of the alpha phase and the prior beta grains and crystallographic texture of the alpha basal planes.

APPENDIX A

FACTORS FOR K_{Iscc} OR K_{scc}

A method is presented here for calculating K_{scc} or K_{Iscc} for one or two specimens from data that give a sustained load in 3.5% NaCl with one no-failure after 60 min and one failure in less than 60 min.

The equation used is:

$$K_{scc} = K_{NF} + F\,(K_F - K_{NF})$$

where:

K_{NF} = highest no-failure K level

K_F = failure K level

F = factor based on time at K_F (see table)

Time to failure at K_F (min)	F
30-59	0.7
15-29	0.6
10-14	0.5
5-9	0.4
3-4	0.3
1-2	0.2
1	0.1

This equation is based on actual data from many K versus time-to-failure curves determined using four to eight specimens as demonstrated in the plot below.

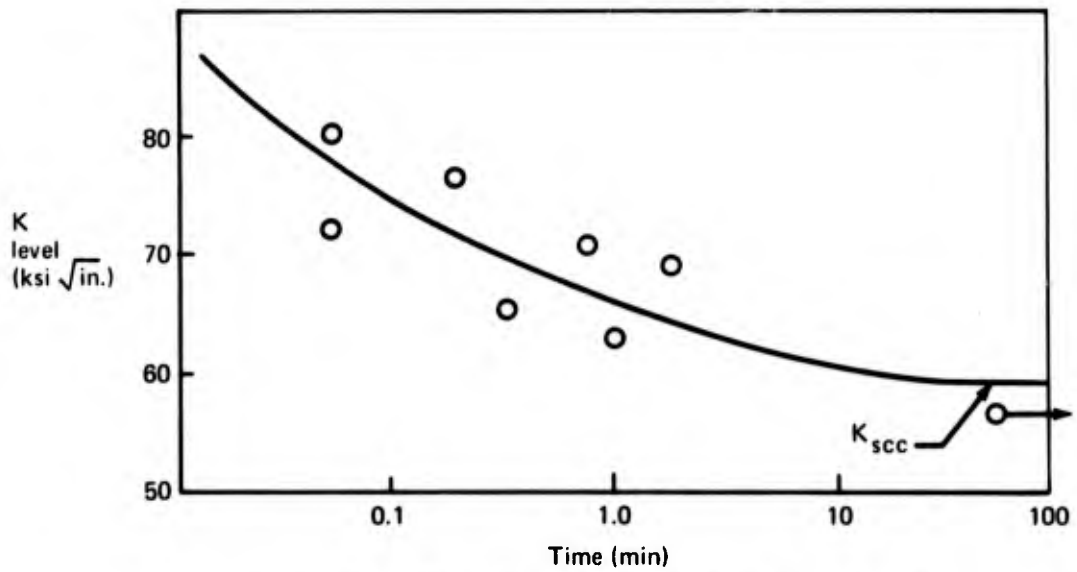

SHORT-TIME FAILURES DURING K_{scc} TESTING

The method is more appropriate for tests in which ($K_F - K_{NF}$) is relatively small compared with K_{NF}, i.e., $R = (K_F - K_{NF})/K_{NF} = 0.33$ maximum. That is, if $K_{NF} = 20$ the next load should be 30. If failure occurs at 30, $K_F = 30$. Thus:

$$R = \frac{K_F - K_{NF}}{K_{NF}} = \frac{10}{30} = 0.33$$

Examples at higher loads are:

$$K_F = 60;\ K_{NF} = 45 \quad R = 15/45 = 0.33$$

$$K_F = 75;\ K_{NF} = 60 \quad R = 15/60 = 0.25$$

If no failures occur at all the test levels and no further data are obtained at K levels of, say, 80 to 100, then 5 ksi$\sqrt{\text{in.}}$ is added to highest no-failure K level. Although this is *very* arbitrary it is more reasonable than using the highest no-failure K level.

If the first load fails and no no-failure data are gathered, other arbitrary factors must be used. For example, if the first load is 25 ksi$\sqrt{\text{in.}}$ and failure occurs, the following K_{scc} based on time to failure is used:

Time (min)	K_{scc} (ksi$\sqrt{\text{in.}}$)
1.0 min	18
1.1-1.5	19
1.6-4.0	20
4.1-10.0	21
11.0-20.0	22
21.0-59.9	23

APPENDIX B

TEST SPECIMEN FRACTURE FACES

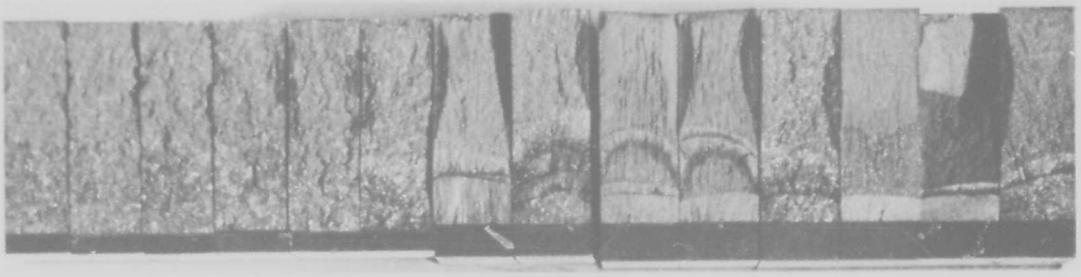

A1 A2 A3 A4 A5 A6 A7 A8 A9 A10 A11 A12 A13 A14

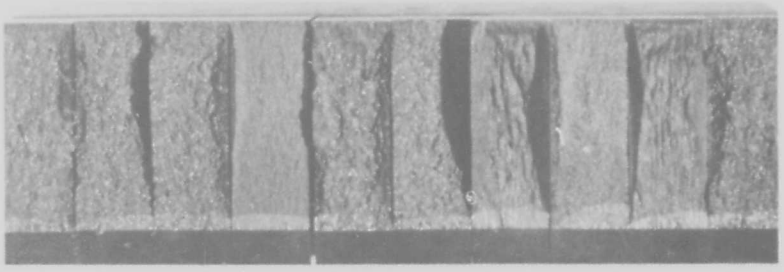

A15 A16 A17 A18 A19 A20 A21 A22 A23 A24

Code	Fracture specimen no.
A1	ST302–E1
A2	–E2
A3	–E3
A4	–E4
A5	–E5
A6	–E6
A7	–E7
A8	–E8
A9	–F1
A10	–F2
A11	–F4
A12	–F5
A13	–F6
A14	–F8
A15	–A2
A16	–A3
A17	–A5
A18	–B1
A19	–B3
A20	–B4
A21	–B6
A22	–C2
A23	–C3
A24	–C4

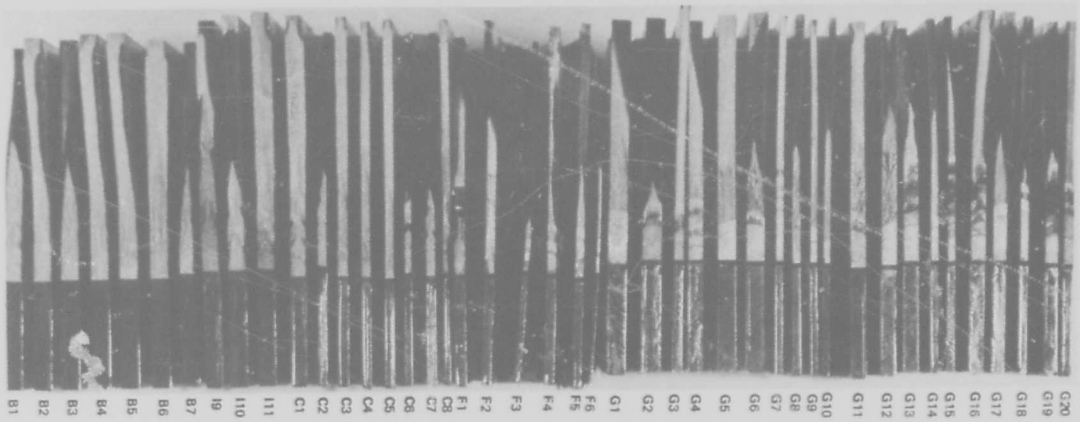

Code	Fracture specimen no.	Code	Fracture specimen no.
B1	ST303–FM986–10	G1	ST315–9233T
B2	–8	G2	–9233L
B3	–7	G3	–8144L
B4	–6	G4	–12177L
B5	–5	G5	–L3579–T
B6	–4	G6	–L3579–L
B7	–3	G7	–L4071–T
		G8	–L4071–L
I9	ST319–415 –9	G9	–L3914–T
I10	–10	G10	–L3914–L
I11	–11	G11	ST315 FM267 H–T
		G12	G–T
C1	ST305–69964–1L	G13	G–L
C2	–69914–1L	G14	B–T
C3	–20257–1L	G15	B–L
C4	–71480–14	G16	ST315–69954–L
C5	–20274–1L	G17	–20646–L
C6	–71689–1L	G18	–20620–L
C7	–20356–1L	G19	–20374–L
C8	–69741–1L	G20	–20044–L
F1	ST312–20233–1L		
F2	–20233–2T		
F3	–20182–2TL		
F4	–20182–2T		
F5	–20284–4L		
F6	–20284–4LT		

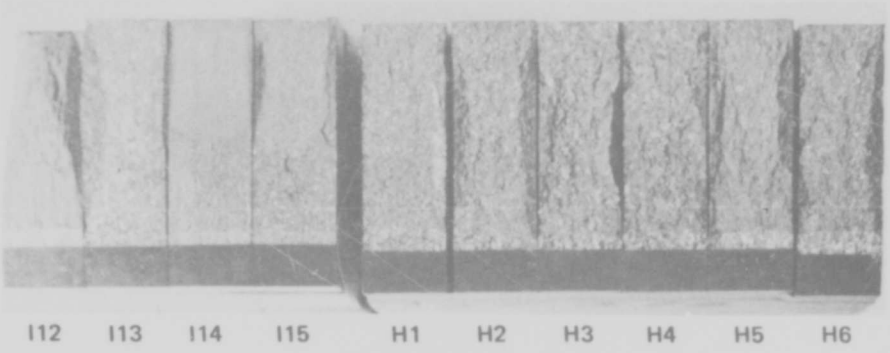

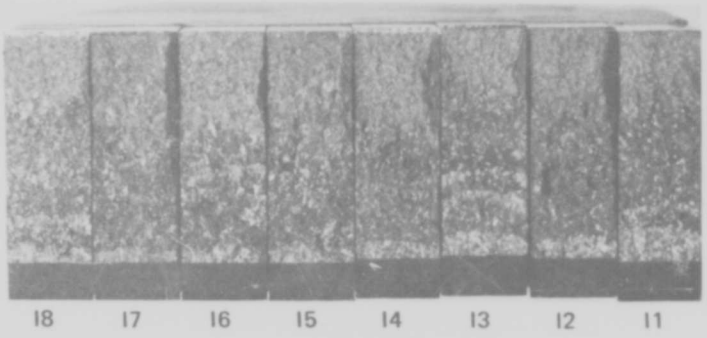

Code	Fracture specimen no.
I12	ST319–F1
I13	–F3
I14	–F5
I15	–F7
H1	ST316–K0759–1
H2	–K0759–2
H3	–295153–1
H4	–295153–2
H5	–K6087–1
H6	–K6087–2
I8	ST319–415–8
I7	–7
I6	–6
I5	–5
I4	–4
I3	–3
I2	–2
I1	–1

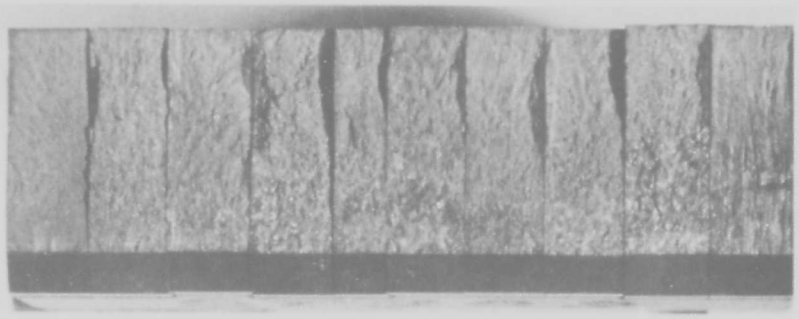

D1 D2 D3 D4 D5 D6 D7 D8 D9 D10

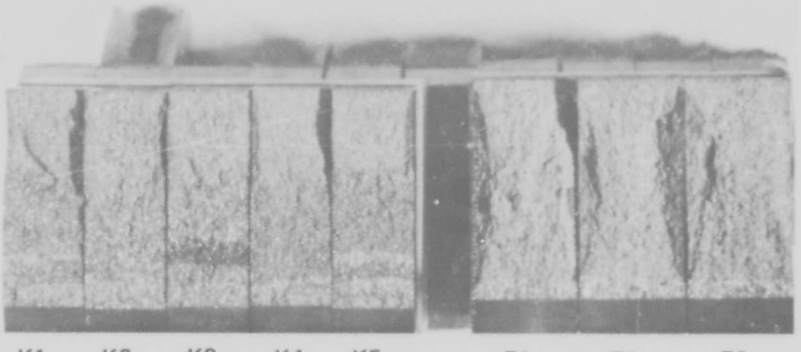

K1 K2 K3 K4 K5 E1 E2 E3

Code	Fracture specimen no.
D1	ST308–7918
D2	–8506
D3	–P2
D4	–SN1486
D5	–M
D6	–1944C
D7	–68316–2
D8	–2054
D9	–2054B
D10	–2502–1B
K1*	ST322–418–17
K2*	–13
K3*	–9
K4*	–6
K5*	–2
E1	ST309–1–2–2
E2	–1–5–3
E3	–1–2–4

*Extrusion

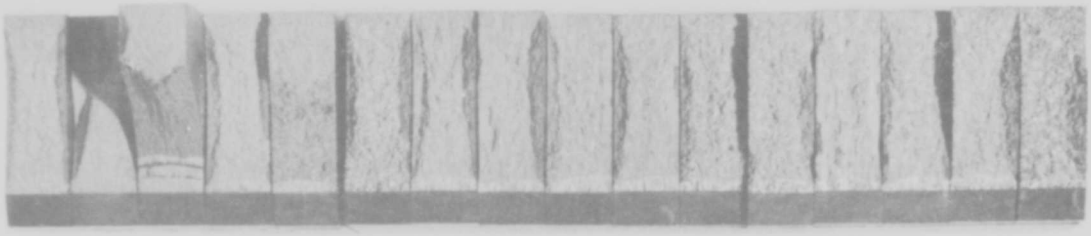

L1 L2 L3 L4 L5 L6 L7 L8 L9 L10 L11 L12 L13 L14 L15 L16

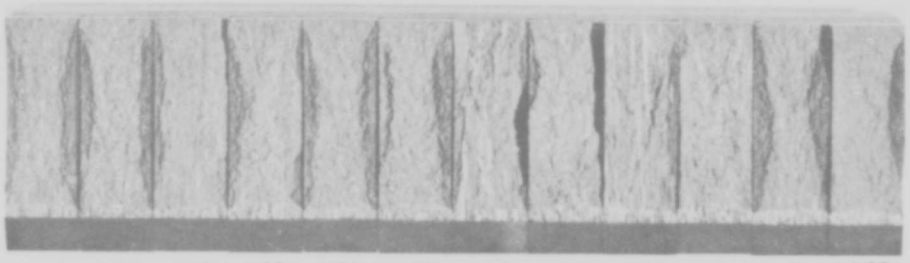

L17 L18 L19 L20 L21 L22 L23 L24 L25 L26 L27 L28

Code	Fracture specimen no.	Code	Fracture specimen no.
L1	ST324–DB11	L17	ST324–FM961–3T
L2	–DB12	L18	–3L
L3	–DB13	L19	–4T
L4	–DB14	L20	–4L
L5	–DB15	L21	–7T
L6	–A2B	L22	–7L
L7	–A2	L23	–10T
L8	–B1	L24	–10L
L9	–H1B	L25	–16T
L10	–H2B	L26	–16L
L11	–H3B	L27	–18T
L12	–H4B	L28	–18L
L13	–N1		
L14	–N1B		
L15	–X–2		
L16	–X–2B		

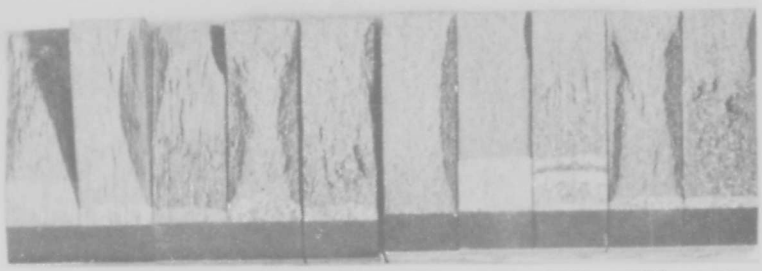

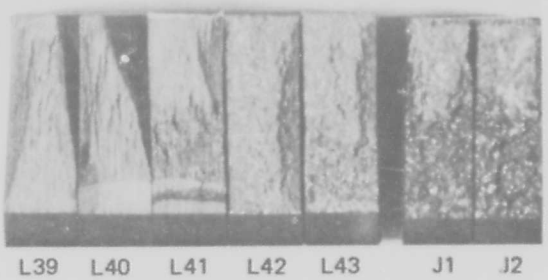

Code	Fracture specimen no.
L29	ST324–DB1
L30	–DB2
L31	–DB3
L32	–DB4
L33	–DB5
L34	–DB6
L35	–DB7
L36	–DB8
L37	–DB9
L38	–DB10
L39	–DB17
L40	–DB16
L41	–DB18
L42	–DB19
L43	–DB20
J1	ST320–416–3
J2	–416–4

APPENDIX C

Ti-6Al-4V SHEET K_{scc} REGRESSION ANALYSIS COEFFICIENTS

APPENDIX C—Ti-6Al-4V SHEET K_{scc} REGRESSION ANALYSES COEFFICIENTS[a]

K_{scc} grain Direction	Constant	Al	O_2	V	Fe	α_2	ΔTYS	K_A	Gage	Metallography: % Primary α	Metallography: α Grain size (x 10^{-4} in.)	Metallography: Elongation of α particles	H_2	Eq. No.	R^2 (b)
T	200 307	-0.95 0.23	-720 1456	+ 3.77 51.2	-212 554	-2.32 0.03	-1.91 0.02	-0.090 0.00017	-122 173					1	0.69
T	403 885	+0.15 0.22	-1215 2136	-47.9 54.9	+131 616			-0.19 0.00010						3	0.67
T	303 902	+0.24 0.27	-1037 1391	-21 57	- 90.8 60		-2.79 0.014	22 data points only						5	0.57
L	209 1169	+3.90 0.57	- 931 2058	-21.9 -72.0	+288 965		+1.19 0.024							19	0.42
T	200 818	-0.71 0.23	- 745 1464	+ 3.43 52.0	-190 552	-2.59 0.012	-2.51 0.03		-115 174					2	0.67
L	350 1156	+4.3 0.52	-1040 3132	-56.6 70.6	+410 1072			+0.096 0.00018						4	0.43
T	2180	+1.86 0.42	-1034 3182	-79.0 151	+409 1933		-2.01 0.016					-0.29 0.16		18	0.68
T	457 2007	2.11 0.39	- 949 3039	-77.6 139	+367 1790		-1.83 0.016		-168 256					20	0.73
T	447 452	2.38 0.30	-1035 3778	+325 1922	- 74.6 168	-1.48 0.053	-2.26 0.015							38	0.88
T	302 905	-1.26 0.506	-1036 1381	-18.4 57.4	- 94.3 599		-2.82 0.0147	Repeats eq. 5 with 78 data points						39	0.57
T	446 2127	-1.54 0.40	-1013 3141	-71.7 148	+396 1896		-2.04 0.016			-0.065 0.002				42	0.68
T	243 868	-1.63 0.475	- 955 1332	+ 0.074 55.8	-151 579		-2.60 0.014		-185 187					44	0.63
T	772 2630	-61.0 22.4	- 880 2880	-69.5 162	+593 1902			-0.139 0.0002			-6.48 0.70			43	0.77
T	321.9 659	-22.8 17.3	- 713 3925			-2.95 0.043	-2.73 0.015						-0.224 0.0009	49	0.87

[a]The standard deviation is given directly below the value for the coefficient.

[b]Multiple correlation coefficient.

APPENDIX C—Concluded

K_{scc} grain direction	Constant	Al	V	Fe	α_2	△TYS	K_A	Gage		Metallography			H_2	Eq. No.	R^2 (b)
										% Primary α	α Grain size $\times 10^4$ in.	Elongation of α particles			
T	630.6 2360	-60.5 24.4	-1015 2926	-33.8 1550	552 1983			-0.202 -0.00014		-0.123 -0.0025				48	0.74
T	772 2630	-61.0 22.4	- 880 2880	-69.5 162	+593 1902			-0.139 0.0002			-6.48 0.7			43	0.77
T	530.3 2455	-33.5 44.3	- 875 4302	-43.7 97.4	+275 2039	-2.32 0.067		-0.147 0.00017						45	0.82
T	454 1135	-26.1 20.2	-1101 2237	-21.0 61	+ 98.9 779			-0.215 0.00011	-111 273					46	0.71
T	622.5 2488	-58.4 25.5	- 989 2829	-38.1 154.1	+562 2109			-0.201 0.00015				-0.09 0.19		47	0.73
T	630.6 2360	-60.5 24.4	-1015 2926	-33.8 1550	552 1983			-0.202 0.00014		-0.123 0.0025				48	0.74
T	321.9 659	-22.8 17.3	- 713 3925			-2.95 0.043	-2.73 0.015						-0.224 0.0009	49	0.87
T	250.2 337	-8.45 8.19	-1003 1296				-2.80 0.010							50	0.53
T	116.6 386.5	-7.78 10.06					-3.05 0.013							51	0.29
T	284.7 665.9	-15.5 17.1	- 881 3582			-2.94 0.044	-2.58 0.015							52	0.85
L	138.6 1034	-1.10 28.5	- 363 5642			-5.64 0.07	+1.48 0.02							53	0.75

[a]The standard deviation is given directly below the value for the coefficient.
[b]Multiple correlation coefficient

APPENDIX D

FATIGUE CRACK LENGTH VERSUS CYCLE CURVES FOR ACTUAL MEASUREMENT AND STRIATION SPACING TECHNIQUE

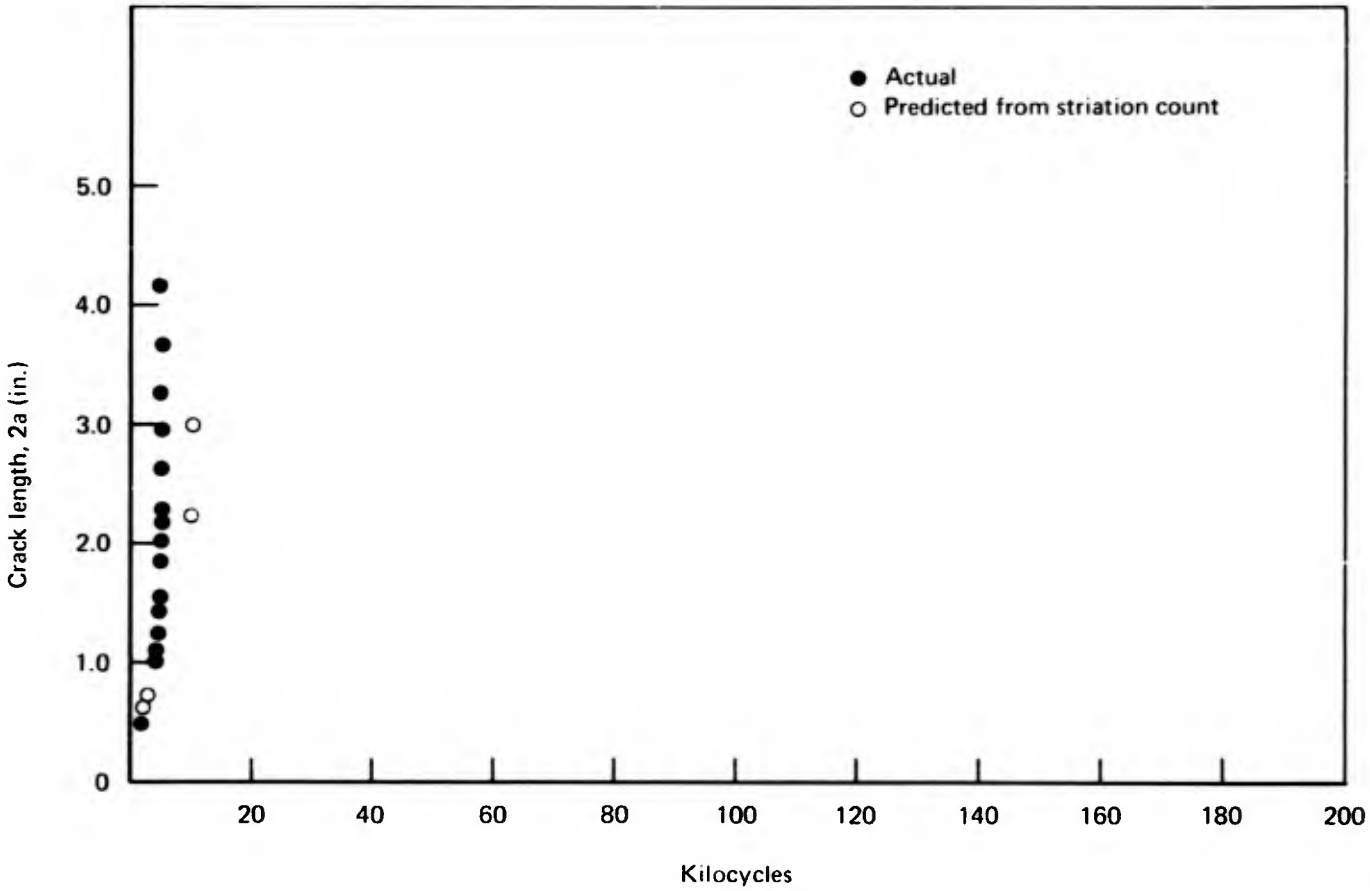

CRACK LENGTH VS FATIGUE CYCLES–FM 883-2-2

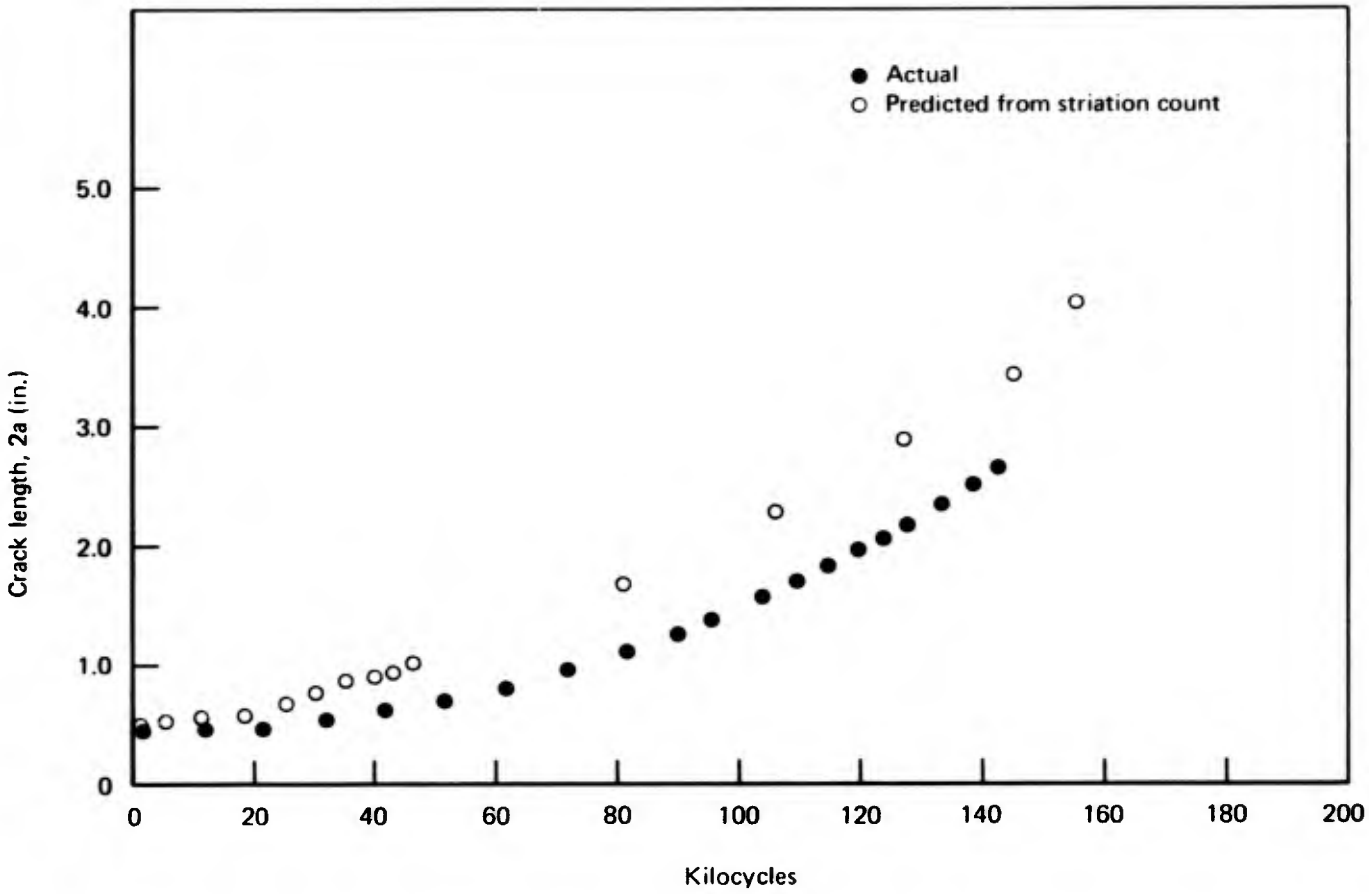

CRACK LENGTH VS FATIGUE CYCLES–FM 883-4-1

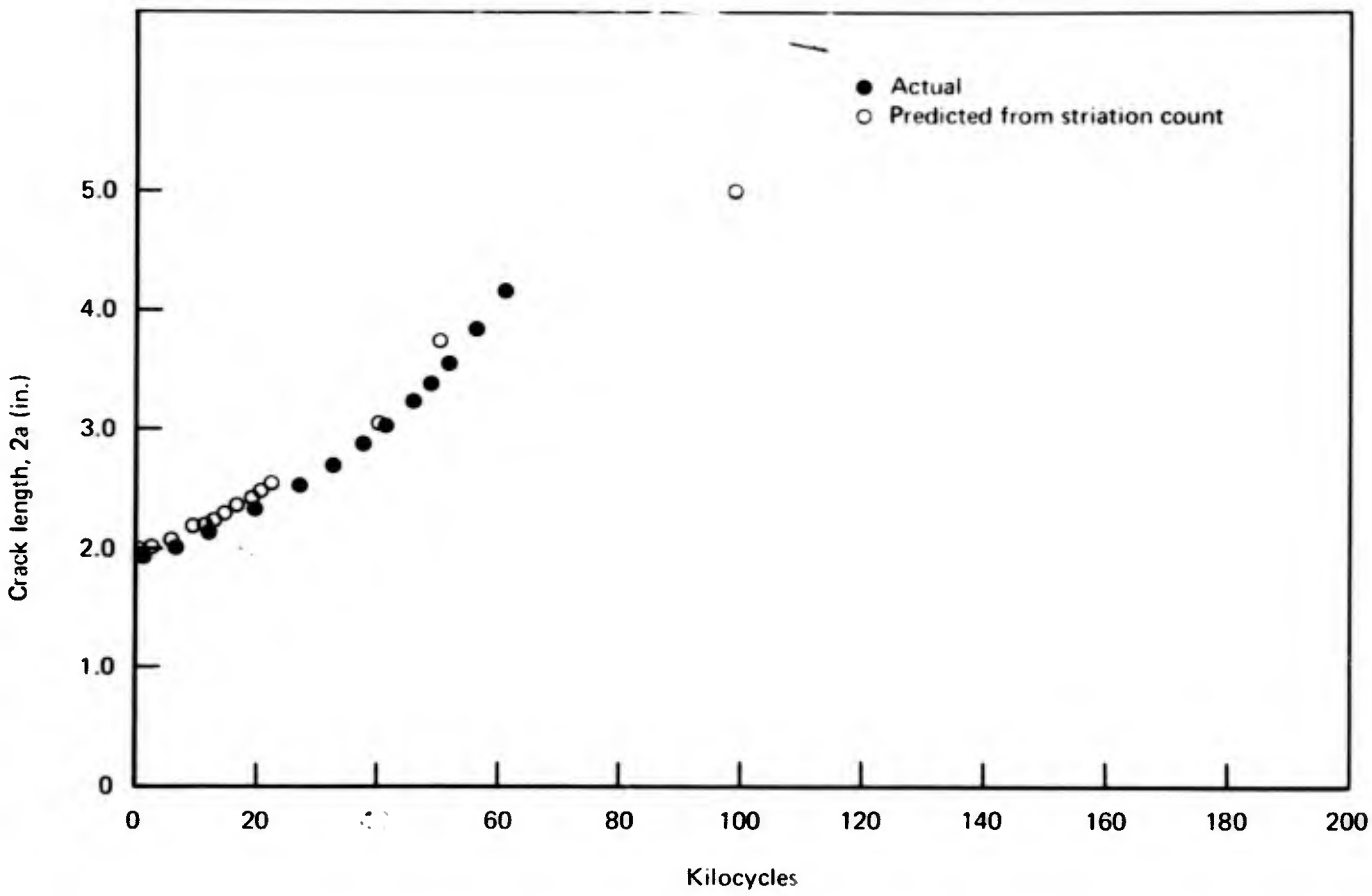

CRACK LENGTH VS FATIGUE CYCLES–FM 883-5-B1

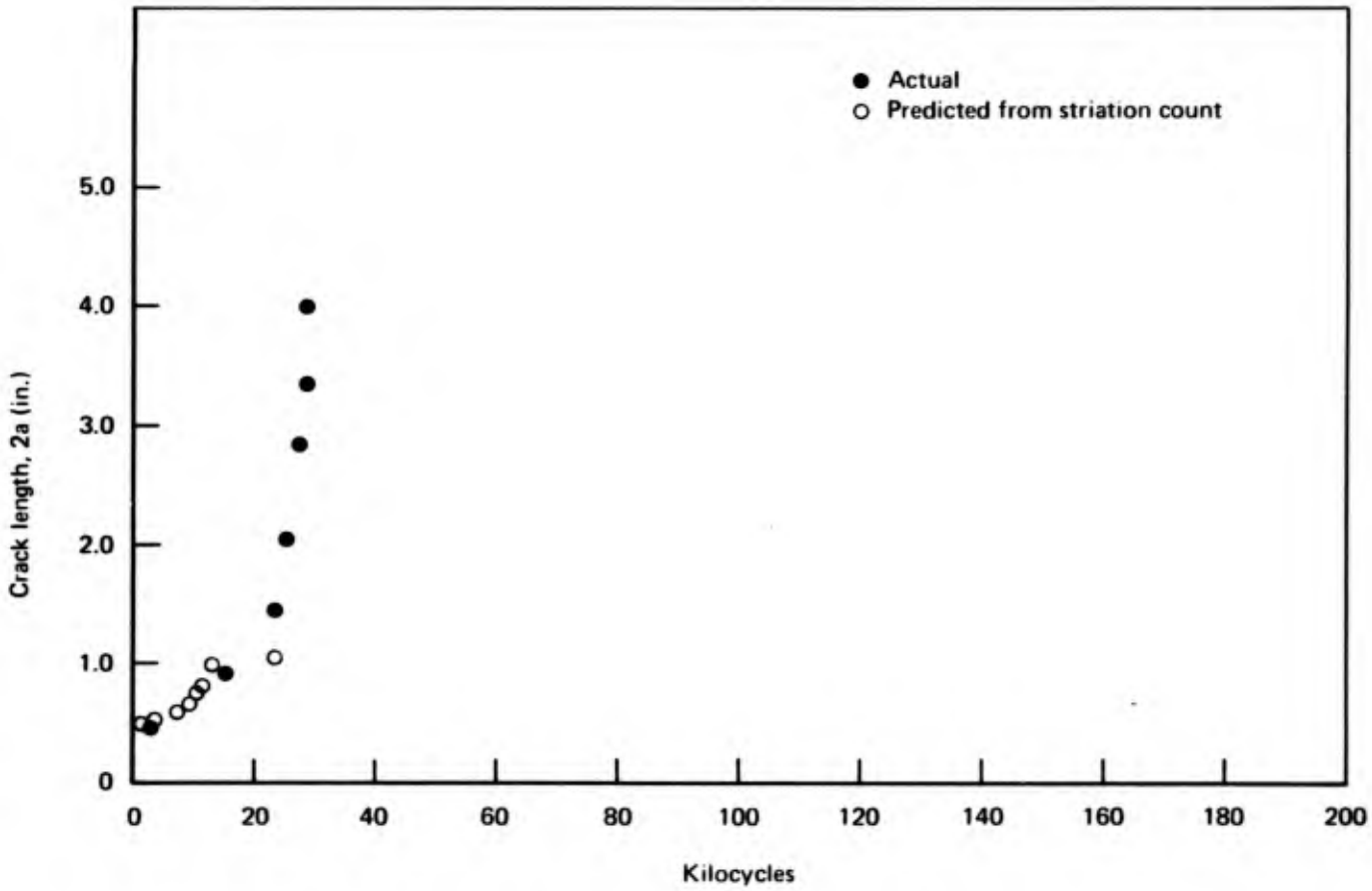

CRACK LENGTH VS FATIGUE CYCLES–FM 883-5-D1

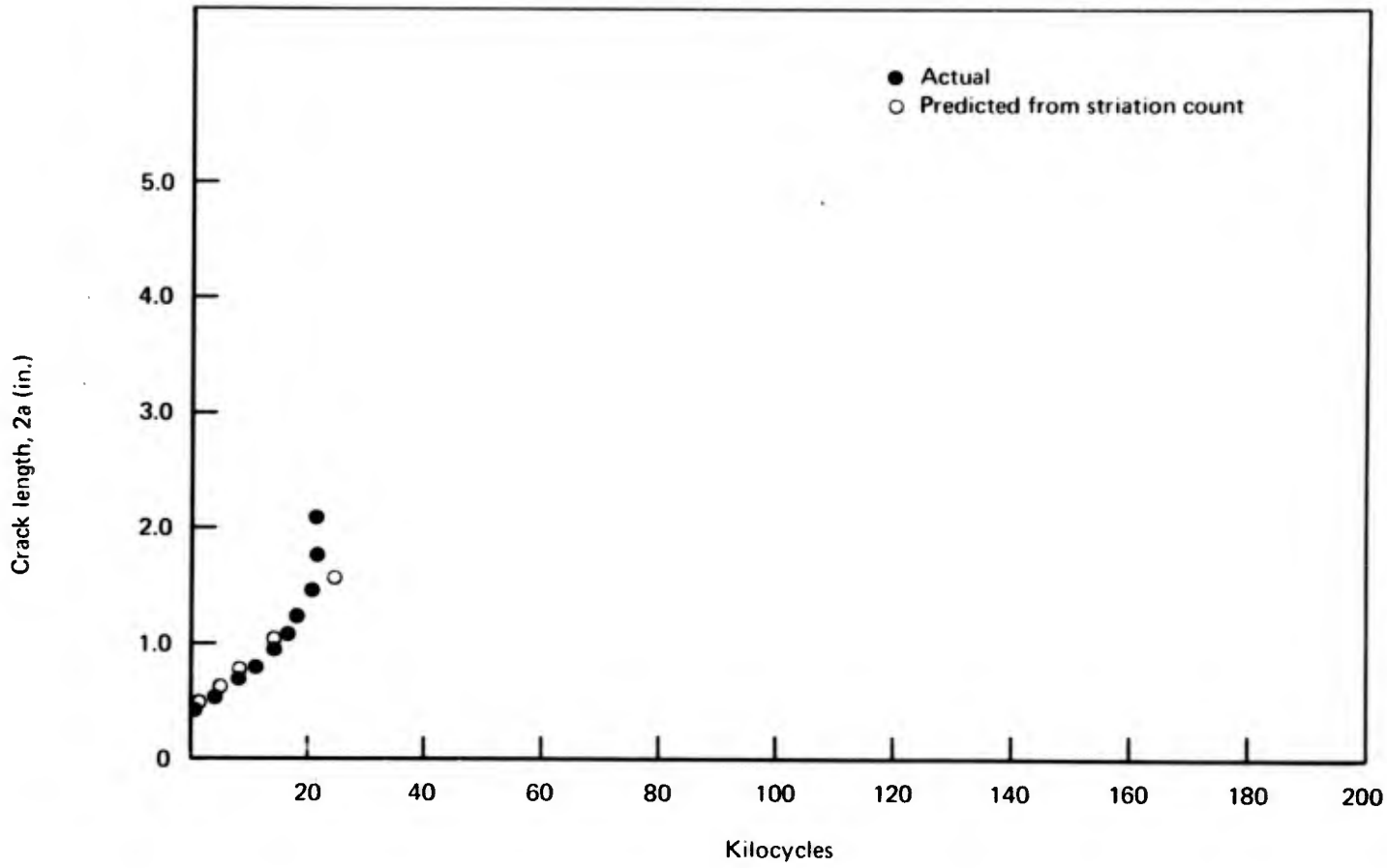

CRACK LENGTH VS FATIGUE CYCLES—FM 891-1

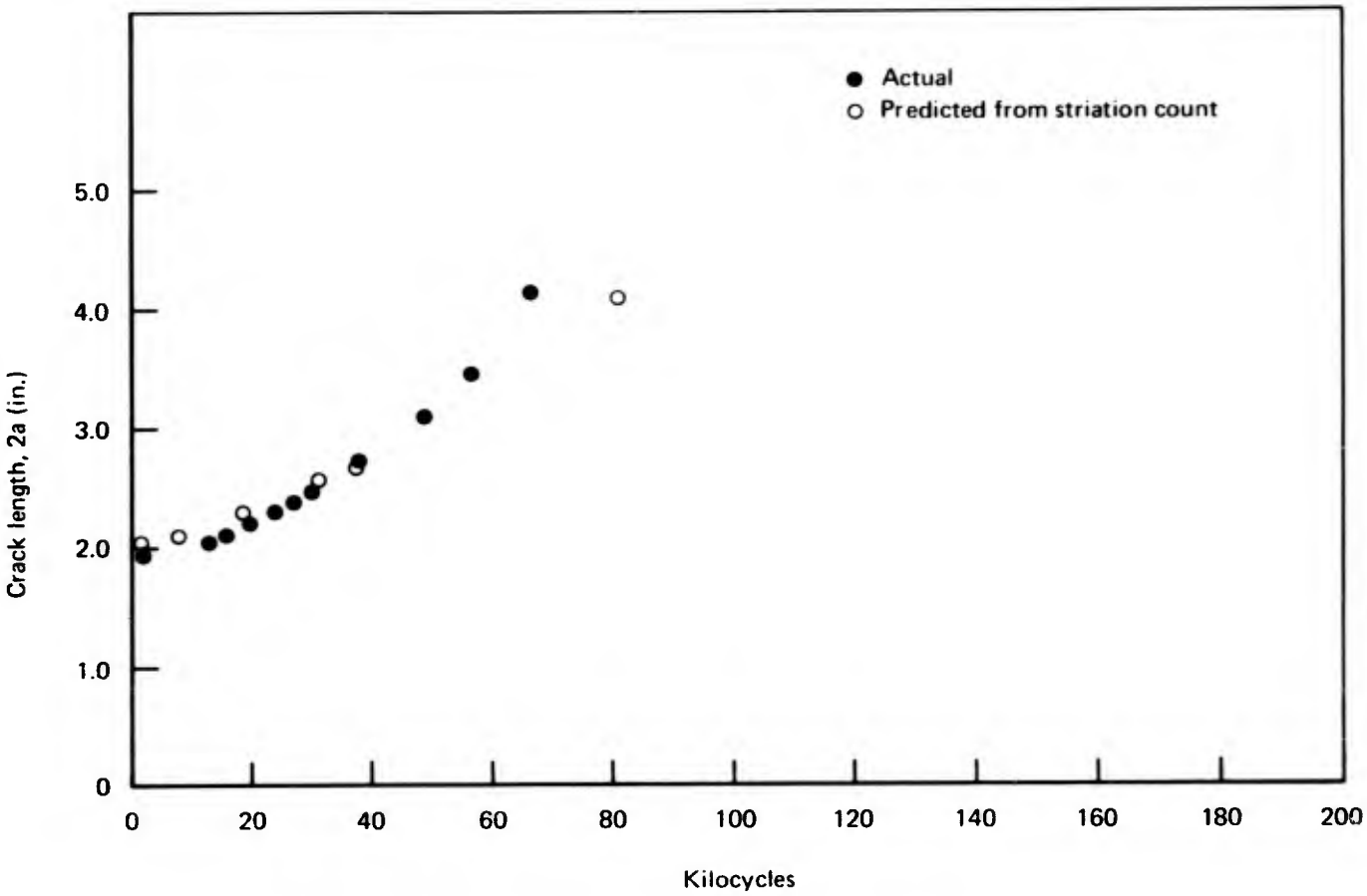

CRACK LENGTH VS FATIGUE CYCLES—FM 891-2

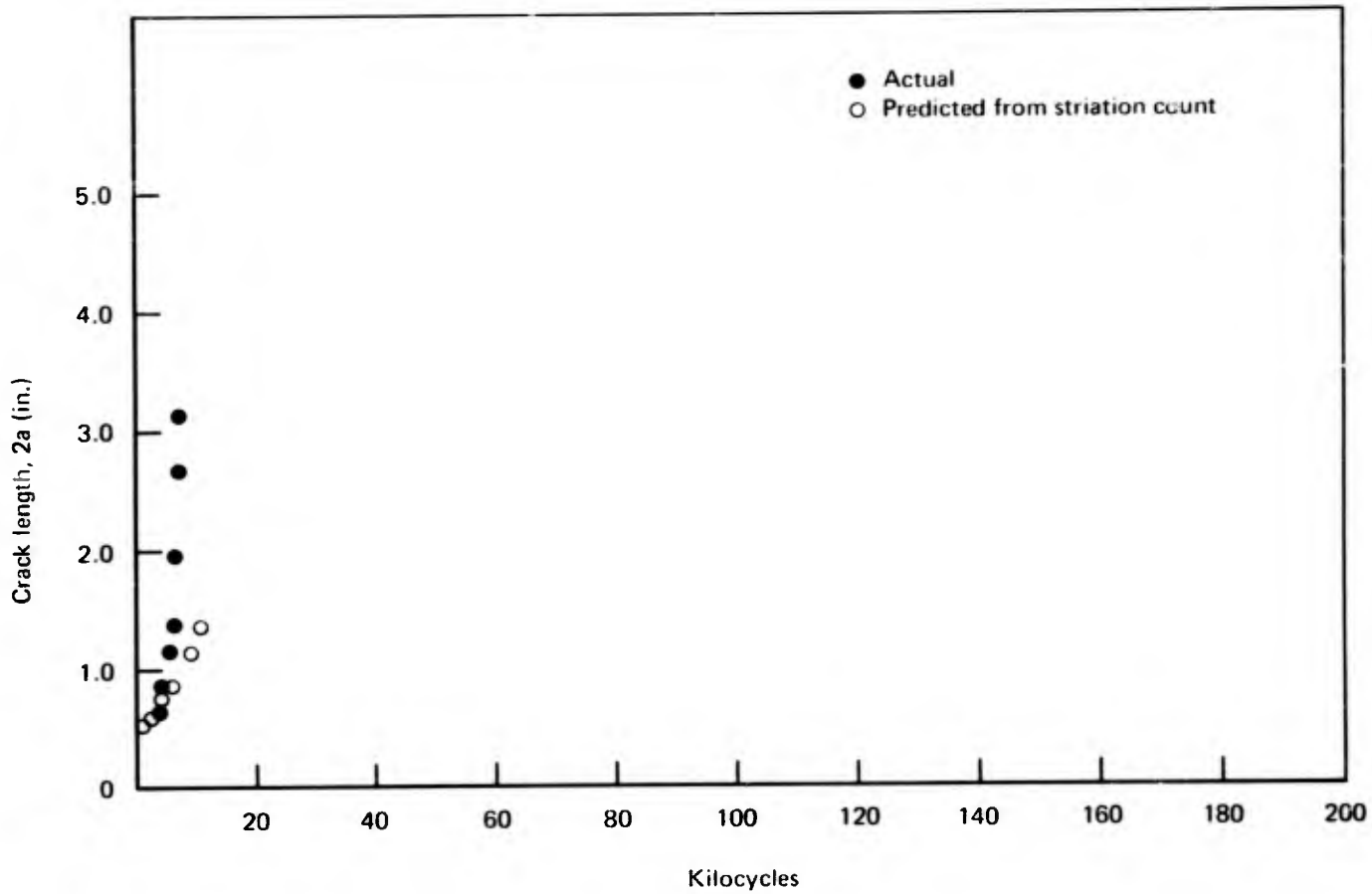

CRACK LENGTH VS FATIGUE CYCLES—FM 891-3

APPENDIX E

RECEIVING INSPECTION REGRESSION ANALYSIS

APPENDIX E—RECEIVING INSPECTION REGRESSION ANALYSIS[a]

Property	Dir	Material[b]	Eq. no.	R^2	Constant	Gage	O_2	N_2	H	C	Al	V	Fe	# coef[c]	Dependency $R^2 > 0.4$[d]
K_{salt}	T	Plate 174A	37	0.26	+179.0 138	+ 9.79 0.67	-279 223	-1093 8823	+86.1 17,440	-816 3786 +	-22.5 2.1	22.6 6.1	135 103	8	Gage · O_2 Gage · H_2 O_2 · N_2 O_2 · Al
Percent elongation	L	Sheet 174A	31	0.09	15.4 0.89	9.46 1.56	+7.80 7.42	+3.34 98.6	+53.3 607	-24.2 77.9	-0.372 0.014	-0.335 0.034	-1.57 1.57	6	H_2 · Fe
	T	Sheet 174A	32	0.24	+ 9.81 0.71	+21.7 1.4	+9.83 6.90	+ 21.7 91.8	+93.8 563	-12.4 69.8	+0.0709 0.0101	-0.0236 0.0169	-4.57 1.42	6	H_2 · Fe
	L	Plate 174A	33	0.09	14.08 2.93	- 0.651 0.0167	+3.26 7.80	+ 3.59 296	-79.0 729	+75.1 180	+0.024 0.060	0.254 0.043	11.8 4.3	4	–
	T	Plate 174A	34	0.13	22.46 3.12	-0.904 0.018	-3.02 8.37	+36.18 321	-46.05 754	+72.1 144	-0.886 0.066	1.01 0.048	6.85 4.74	5	–
	L	Cont. roll sheet 197, 197A	35	0.47	-1.91 22.38	+9.85 25.35	+11.43 49.61	-86.2 2139	186 6508	8.47 213	+2.07 0.67	0.395 1.36	6.67 22.6	1	Gage · O_2 N_2 · V Al · V Al · Fe
	T	Cont. roll sheet 197, 197A	36	0.53	-4.4 22.3	+15.32 22.98	+8.59 45.0	-34.63 1956	-242 6167	+4.79 211	+1.79 0.67	+1.19 1.33	8.61 20.6	1	Gage · O_2 Gage · N_2 N_2 · V Al · V, Al · Fe
TYS	L	Sheet 174A	21	0.34	101.6 3.0	80.1 5.4	+49.2 25.5	+62.4 338	+329 2080	245 265	0.437 0.04	+6.49 0.12	+13.4 5.39	6	H_2 · Fe
	T	Sheet 174A	22	0.26	93.5 2.58	+21.2 5.2	+86.7 25.2	+71.7 334	+807 2051	261 252	1.25 0.037	2.59 0.06	0.39 5.2	6	H_2 · Fe
	L	Cont. roll sheet 197, 197A	23	0.45	27.9 97.9	-74.5 110	+84.3 216	+296 9350	+271 28,400	+159 932	+13.5 2.93	1.43 5.93	40.3 98.8	1	Gage · O_2 N_2 · V Al · V, Al · Fe
	T	Cont. roll Sheet 197, 197A	24	0.35	95.9 154	52.6 159	+84.9 312	+460 13,570	+653 42,778	+365 1470	+6.82 4.68	7.28 9.27	+24.1 143	2	Gage · O_2 Gage · N_2 N_2 · V, Al · Fe
TUS	L	Sheet 174A	25	0.26	116.0 2.8	-45.4 4.9	+63.8 23.1	+ 79.1 306	+433 1880	+156 240	-0.70 0.043	+4.80 0.1	+9.55 4.89	6	H_2 · Fe, Al · V
	T	Sheet 174A	26	0.23	115.4 2.5	+24.1 5.2	+80.4 24.7	+50.0 328	+808 2015	+180 248	+0.67 0.036	+0.76 0.06	2.92 5.07	5	H_2 · Fe
	L	Plate 174A	27	0.26	113.4 7.7	4.70 0.044	+102 20.4	+235 775	+29.7 1910	+81.7 471	+1.64 0.158	+0.21 0.11	+8.93 11.3	4	–
	T	Plate 174A	28	0.20	142.9 8.2	4.58 0.048	+97.1 22	+44.2 847	+204 1990	+183 381	1.90 0.17	-1.07 0.13	+6.67 12.5	5	–
	L	Cont. roll Sheet 197, 197A	29	0.63	93.0 94.8	70.9 107.4	+82.1 210	-47.4 9063	+1229 27,573	+106 903	-2.40 2.84	+13.7 5.77	26.9 95.7	2	Gage · O_2 N_2 · V Al · V Al · Fe
	T	Cont. roll sheet 197, 197A	30	0.41	97.1 123	41.5 126	+113 248	+47.7 10,700	+985.5 34,000	+288 1169	+1.80 3.72	+ 4.31 7.37	12.5 113	0	Al · V, Gage · O_2 Al · Fe, Gage · N_2 N_2 · V
TYS	L	Plate 174A	40	0.27	112.9 8.8	6.94 0.050	+87.9 23.5	+409 890	144 2194	+132 542	+0.533 0.180	0.43 0.13	+38.9 13.0	6	–
	T	Plate 174A	41	0.24	157.5 9.1	6.48 0.05	+72.8 24.4	+211 936	+38.5 2198	242 421	4.90 0.19	2.54 0.14	12.4 13.8	5	–

[a]The standard deviation is given directly below the value for the coefficient.

The units are as follows K_{salt}—ksi · in.
TUS, TYS—ksi
Percent elongation—%
Gage—inches
O_2, N_2, H_2, C, Al, V, Fe—weight %

[b]Plate 174A—Beta processed, annealed Ti-6Al-4V Plate
Sheet 174A—Annealed hand-mill Ti-6Al-4V sheet
Cont. roll sheet 197, 197A—Continuously rolled and annealed sheet

[c]For nine terms

[d]Minus or plus independent variable

APPENDIX F

COEFFICIENTS FOR Ti-6Al-4V EXTRUSION REGRESSION ANALYSES

APPENDIX F—COEFFICIENTS[a] FOR Ti-6Al-4V EXTRUSION REGRESSION ANALYSES

Property	Grain direction	Constant	O_2	Al	V	Fe	MR	K_A	R^2 (b)	No. of data	Run No.
K_{Iscc}	T	95.0	-120.4	- 5.6	- 5.0	76.0	0.94	-0.084	0.687	38	3
		696	769	11.5	15.2	295	0.031	0.0002			
	L	236.7	-389.7	- 4.3	-23.8	-73.0	1.6	-0.31	0.717	15	1
		2160	2209	44.5	51.8	1462	0.39	0.005			
K_Q	T	86.2	-180.1	24.2	-14.7	-321.3	-0.63	-0.12	0.281	21	2
		2042	4631	39.5	43.7	2402	0.12	0.0036			
	L										
TUS	T	101.1	75.1	- 6.98	16.1	45.4	-0.69	0.27	0.688	10	2
		1614	4043	70.8	37.9	2700	0.179	0.0041			
	L	123.0	70.4	4.4	- 5.8	- 5.2	0.34	-0.0083	0.617	24	1
		395	286	7.2	12.6	145	0.0024	0.00051			
TYS	T	138.0	- 22.3	-17.4	24.3	62.7	-1.5	0.35	0.837	10	
		1295	3242	56.8	30.4	2165	0.144	0.0033			
	L	168.3	12.5	3.1	-15.4	3.6	0.08	-0.05	0.276	24	1
		608	440	11	19	223	0.037	0.0007			
Percent elongation	T	40.2	8.9	- 4.7	0.76	- 6.1	-0.13	0.038	0.859	10	
		226	567	9.9	5.3	379	0.025	0.0006			
	L	60.4	46.3	-10.0	2.0	0.44	0.13	-0.033	0.683	24	1
		279	202	5.1	8.9	103	0.017	0.00035			
CYS	T	116.5	12.6	-23.1	39.7	70.5	-1.7	0.51	0.713	10	1
		2890	6590	98.9	97.1	4410	0.282	0.007			
	L	42.9	80.4	13.8	-1.13	-11.4	.14	.13	0.65		

[a]The standard deviation is given directly below the value for the coefficient

[b]Multiple correlation coefficient

APPENDIX G

COEFFICIENTS FOR Ti-6Al-4V BETA-PROCESSED BAR REGRESSION ANALYSES

APPENDIX G—COEFFICIENTS[a] FOR Ti-6Al-4V BETA-PROCESSED BAR REGRESSION ANALYSES

Property	Grain direction	Constant	O_2	Al	MR	K_A	R^2 (b)	Number of data	Run no.
K_{Iscc}	T	181.3	-111.7	-20.3	1.3	-0.15	0.580	18	3
		912	1106	21.3	0.121	0.0009			
	L								
K_Q	T	141.2	-274.2	- 6.83	6.42	-0.023	0.915	13	3
		1955	1163	49.6	0.123	0.0017			
	L	-5.23	-843.4	24.1	26.1	-0.043	0.355	14	1
		21.6	4878	4.0	0.525	0.009			
TUS	T	43.5	- 71.1	17.2	0.096	0.086	0.165	9	2
		5276	3750	125	0.38	0.0029			
	L	130.9	-101.2	4.03	0.17	0.059	0.181	9	1
		5541	4556	121	0.376	0.0022			
TYS	T	155.2	- 34.5	- 3.7	0.12	0.059	0.030	9	2
		8226	5848	195	0.596	0.0045			
	L	63.6	- 55.8	12.2	-1.02	0.09	0.187	9	1
		6902	5674	151	0.47	0.0027			
Percent elongation	T	11.8	- 12.2	-22.3	0.47	0.015	0.439	9	1
		1059	753	25.2	0.077	0.0006			
RA	T	-144	18.5	24.9	1.8	0.126	0.485	9	1
		5643	4012	134	82.9	0.0031			
	L								

[a]Standard deviation is given directly below the value for the coefficient

[b]Multiple correlation coefficient

REFERENCES

1. W. F. Spurr, et al, *Titanium Alloy Selection Report*, D6-19729, The Boeing Company, October 1, 1965.

2. F. L. Parkinson, *Titanium Alloy 6Al-4V Sheet*, SST Technology Follow-On Program–Phase I, report FAA-SS-72-01 (Boeing document D6-60201), July 15, 1972.

3. F. L. Parkinson, *Beta Processed Titanium Alloy 6Al-4V Plate*, SST Technology Follow-On Program–Phase I, report FAA-SS-72-00 (Boeing document D6-60200), July 1972.

4. W. F. Spurr, *Titanium Alloy 6Al-4V Extrusions*, SST Technology Follow-On Program–Phase I, report FAA-SS-72-06 (Boeing document D6-60206), July 1972.

5. W. F. Spurr, *Titanium Alloy 6Al-4V Bar and Forging*, SST Technology Follow-On Program–Phase I, report FAA-SS-72-04 (Boeing document D6-60204), July 1972.

6. M. K. Gagnon, *Regression Analysis Technique*, report C/S-PS-1230, The Boeing Company, June 25, 1971.

7. R. H. Olsen, *Quantitative Texture Analysis by X-ray Diffraction*, D6-25265, The Boeing Company, October 1970.

8. R. R. Boyer, *CAG Metals Laboratory Report*, 6-8830-81-CS, The Boeing Company, December 15, 1971.

9. F. L. Parkinson, *Titanium Alloy 6Al-4V Hydrogen Effects*, SST Technology Follow-On Program–Phase I, report FAA-SS-72-07 (Boeing document D6-60207), July 1972.

10. W. F. Spurr, *Titanium Development Program*, D6A10065-1, FAA contract FA-SS-66-5, The Boeing Company, March 1966.

11. A. L. Wingert, *Effect of Oxygen on Ti_3Al Ordering*, Master's thesis in Metallurgical Engineering, University of Washington, March 1972.